NASA Contractor Report 3155

Design and Application of a Test Rig for Super-Critical Power Transmission Shafts

M. Darlow and A. Smalley

CONTRACT NAS3-16824
AUGUST 1979

NASA

NASA Contractor Report 3155

Design and Application of a Test Rig for Super-Critical Power Transmission Shafts

M. Darlow and A. Smalley
Mechanical Technology Incorporated
Latham, New York

Prepared for
Lewis Research Center
under Contract NAS3-16824

National Aeronautics
and Space Administration

**Scientific and Technical
Information Branch**

1979

TABLE OF CONTENTS

TABLE OF CONTENTS (cont'd)

SUMMARY

To demonstrate the feasibility of supercritical power transmission shafting, a test rig has been designed, built, and successfully operated. Shafts of up to 6.1 meters (20 ft) in length can be accommodated, and controlled speeds to 20,000 rpm can be achieved; a controlled torque of up to 900 N-m (8000 in.-lb) can be imposed on the test shaft; extensive vibration instrumentation is available and good display of vibration signals is possible; a computerized data acquisition system allows on-line balancing and vibration monitoring; the facility and test vehicle provide a very sensitive tool for technology investigation associated with supercritical shafting.

Initial tests of a 3.66 meter (12 ft) long, 7.62 cm (3 in.) diameter, thin-walled shaft demonstrated, as expected, that balancing of a hard mounted shaft without damping was difficult, and that once the first critical speed was negotiated, sustained subsynchronous vibrations at the frequency of the first critical speed dominated the dynamic motion of the shaft and led to an intolerable operating condition. A self-contained squeeze film damper was designed and built which successfully controlled subsynchronous and synchronous vibrations so that balancing through four bending critical speeds was possible.

Tests under torque revealed that the shaft can undergo temporary deterioration in its state of balance due, apparently, to change in orientation of mass eccentricity vectors which are self-cancelling under zero torque conditions. Investigations of nonsynchronous shaft vibration using a real time analyzer revealed significant forced vibrations at bearing cage rotational frequency and at twice rotational speed, and also showed that for operation beyond 12 times the first critical speed, subsynchronous vibration at the frequency corresponding to the first critical speed can be observed even with a well-designed damper.

I. INTRODUCTION

Past supercritical shaft studies include the shaft technology and evaluation programs conducted in part by Battelle Institute and in part by Boeing-Vertol (refs. 1-5). These programs had the objectives of:

- developing the required technical skills for designing supercritical shafts
- demonstrating supercritical shaft operation on a full-scale rig using these skills.

Shafts were designed and run during these programs, but the shaft whirl amplitudes and transmitted forces were excessive, particularly at the critical speeds. It was not possible either to balance out or to damp out these shaft motions using the technology available at that time.

A shaft is described as "supercritical" if it runs above one or more of its lateral flexural critical speeds.

The need for supercritical shafting arises because of increases in shaft speeds or reductions in lateral critical speeds. With higher rotational speeds, higher power levels can be transmitted and shaft torques can be reduced. Lower system lateral critical speeds are caused by increases in unsupported shaft lengths which allow reductions in system weight and number of parts.

Advanced shafting technology will help meet military needs to improve helicopter and STOL aircraft which provide close support of ground forces. Designers of such aircraft face requirements for such features as higher payloads, more severe hover or runway length requirements, and reduced vulnerability, in addition to the perennial goals of improved life, reliability and maintainability.

The primary requirement for helicopter and STOL aircraft is safe, reliable, quiet operation at low-speeds and altitude, which can most readily be met by gas turbine-driven propeller/rotor systems. In such aircraft, power must be transmitted through relatively long shafts from a central engine to the rotors (such as in the CH 47 helicopter). Alternatively, power must be produced at the rotors and phased for proper operation by interconnecting shafting designed for power levels which can occur when one or more engines is inoperative. In both cases, long shafting is required. While a number of other drive configurations (e.g., non-interconnected engines) have been considered, the physical system integrity provided by shafting offers a considerable advantage.

Supercritical power transmission shafts provide important benefits. During the aircraft/powertrain design stage, the designer can specify a lighter shaft which operates at higher speeds and carries a reduced torque. He can specify reduced fuselage volume to accommodate the smaller diameter shafts and couplings. He may also be able to specify curved shafts to interconnect gearboxes when both flexible couplings and gearboxes are impractical.

Lifetime benefits to the drive train of supercritical shafting technology include: fewer system failures because the number of components is reduced, higher payloads because the system weight is lower, and quieter aircraft interiors because of fewer points at which the shaft is attached to the aircraft.

Maintenance and overhaul procedures will be simpler for supercritical shafts because fewer system parts will be involved. Development of an effective and economical procedure for rebalancing at overhaul time may, of course, be crucial to the achievement of simpler overhaul procedures.

This report describes a five year program to design and develop a test facility for supercritical shafting and presents the initial results obtained using this facility. The report is structured, as far as possible, to reflect chronological developments in the program. The program has been highly successful in meeting the following goals:

- To provide an environment in which supercritical shafting of representative dimensions can be tested under realistic, controlled, conditions of speed and torque.
- To identify problems associated with supercritical shafting.
- To develop the technology needed for successful operation of supercritical power transmission shafting.

The feasibility of supercritical power transmission shafting has been clearly demonstrated. The basic tools for successful operation (balancing and a self-contained damper) have been demonstrated. The sensitivity and effectiveness of the test facility for investigating the phenomena of supercritical shafting have been demonstrated.

At the same time, a number of areas requiring careful attention have been identified: balancing must be executed with a verified method; an effective damper is essential; the effects of torque on balance must be carefully attended to; and optimum methods for handling the effects of torque must be developed; the presence of excitation sources at twice rotational speed and at bearing race frequency must be recognized; the precise nature of these nonsynchronous sources and the means to control shaft response to them require further quantification; and the potential for subsynchronous, self-excited vibrations which tend to occur at the first critical speed must also be recognized. The precise nature of this subsynchronous excitation source and the means to control these subsynchronous vibrations require further attention.

II. SUMMARY OF RESULTS

1. A test rig for evaluation and development of supercritical power transmission technology has been designed, built and successfully operated.

2. The test shaft was successfully balanced through one bending critical speed with no external damping.

3. A subsynchronous instability was observed in the response of the undamped test shaft above the first critical speed.

4. The test shaft was successfully balanced through two bending critical speeds with the aid of a simple Coulomb damper.

5. A more sophisticated damper was designed and built for the test shaft. This was an entirely self-contained squeeze film damper.

6. The squeeze film damper provided control of both synchronous and subsynchronous vibrations and allowed operation after balancing to over 12 times the first critical speed.

7. Tests were conducted to determine the effectiveness of two techniques for balancing the damped test shaft.

8. Using the influence coefficient balancing technique, the test shaft was successfully balanced through four bending critical speeds.

9. Using a variation on the modal balancing technique, the test shaft was also balanced successfully through four bending critical speeds.

10. Predictions of natural frequency and log decrement agreed satisfactorily with measured values.

11. Tests were conducted in which the test shaft was run with a locked-in torque of up to 900 N-m (8000 in.-lb).

12. The application of torque had no noticeable effect on the location of the critical speeds.

13. The application of 8000 in.-lb of torque to a shaft balanced without torque substantially increased vibration levels of the first critical speeds over those obtained with no torque.

14. The test shaft was successfully balanced with 900 N-m (8000 in.-lb) of torque applied.

15. Removal of the torque increased vibration levels at the first critical speed over those obtained after balancing with torque.

16. Subsynchronous vibrations of significant amplitudes at the first critical speed were observed, even with the squeeze film damper, when operating at 12000 rpm (12.6 times the first critical).

17. Subsynchronous forced excitation of the first and third critical speeds was observed at cage rotation frequency for the damper bearing.

18. Forced excitation of the first and the third critical speeds was observed at a frequency equal to two times running speed.

III. CONCLUSIONS

On the basis of the results presented in this report, the following conclusions are drawn:

1. Operation of supercritical power transmission shafting is feasible.

2. The application of some external damping is necessary in order to maintain a stable system.

3. At-speed, multiple-plane, flexible-rotor, balancing is necessary in order to operate safely through several bending critical speeds.

4. The squeeze film damper designed, built, and installed in this test rig was effective in eliminating subsynchronous instability in the test shaft for operating speeds to over 12 times the first critical speed.

5. This squeeze-film damper was also effective in controlling the test shaft response at the critical speeds so that successful flexible rotor balancing could be implemented.

6. The influence coefficient balancing technique is an effective method for the balancing of supercritical power transmission shafting.

7. The modified modal balancing technique as applied is also an effective method for the balancing of supercritical power transmission shafts.

8. A satisfactory prediction of natural frequency and log decrement can be made and applied successfully in rotordynamics design using damped critical speed analysis.

IV. RECOMMENDATIONS

For the application of supercritical shafting and for future investigations, the following recommendations are made:

1. The use of supercritical power transmission shafting should be considered in applications where shaft weight, complexity and/or fabrication and maintenance costs are important.

2. Some external damping should be used to aid in the control of vibrations in supercritical power transmission shafts.

3. Supercritical shafts should be balanced to account for the variation in unbalance excitation over the operating torque range.

4. Alternative damper designs should be evaluated for use with supercritical power transmission shafting. These alternatives should seek to further simplify the design while maintaining good vibration control.

5. Alternative methods of correction weight addition should also be evaluated for use with supercritical power transmission shafts. One possibility is the use of metallic tape that will adhere to the outside of the shaft.

6. Sources of nonsynchronous vibration excitation should be quantified as a function of bearing conditions, coupling type, and applied torque and misalignment.

7. Means of effectively controlling nonsynchronous vibrations should be developed and reduced to quantitative design practice.

8. Development of advanced bearings, couplings, dampers and balancing methods should be undertaken with a view to allow operation of supercritical shafting which is even lighter, larger and faster.

V. BRIEF PROGRAM HISTORY

The history of the supercritical shaft test facility and associated test program is illustrated schematically in the milestone chart in Figure V.1. The following discussion is related to the various tasks of the program begun in October, 1972. Details on each task are presented in later sections of the report.

Task 1 - Acquire Shaft Steady-State and Dynamic Performance Data for Planning Supercritical Model Shaft Test Rig

In October, 1972, Boeing-Vertol was awarded a subcontract to provide engineering data for the CH-47 and HLH power transmission shaft systems. A preliminary design data package was prepared by MTI (see Figures V.2, V.3), and in December, 1972, a meeting was held between MTI and Boeing-Vertol to review this package and the Boeing-Vertol subcontract report. Recommendations made by Boeing-Vertol were incorporated in the final design and led to some changes from Figure V.3. Task 1 was completed in January, 1973.

Task 2 - Formulate Test Rig Concept and Plan Test Program

Task 2 was begun in October, 1972. Model shafts were to be used to simulate full-size shafts which run up to 15,000 rpm, and/or up to 18 m (60 ft) in length. The model shafts were designed to run up to 20,000 rpm, and to handle as yet unspecified high torque and be up to 4.3 m (14 ft) in length. Recommendations were received from Boeing-Vertol concerning the concepts of the full-size shafts and the model shaft to be designed. The synchronization shaft of a CH-47C helicopter has a maximum operating shaft speed of 8018 rpm and an operating torque of 3500 N-m (30,400 in.-lb). The synchronization shaft of an HLH helicopter has a maximum operating shaft speed of 9100 rpm and an operating shaft torque of 9400 N-m (84,000 in.-lb). This task was completed in February, 1973.

Task 3 - Prepare Initial Design of Test Rig

Task 3 was begun in October, 1972 and was based on the results of Task 2. Recommendations from Boeing-Vertol formed a substantial portion of the background for this design effort. Task 3 was completed in January, 1973.

Task 4 - Perform Dynamic Analysis of Test Rig to Establish Shaft Performance

In Task 4, initiated in October, 1972 and completed in March, 1973, a dynamic analysis of the original test rig was performed to establish expected shaft performance and to ensure safe operation of the test rig. Unbalance response and analytical balancing calculations were performed (see Reference 12).

Task 5 - Finalize Test Rig Hardware and Instrumentation Design, Prepare Test Rig Layout and Detail Drawings

Philadelphia Gear Corporation was awarded the pre-engineering contract in March, 1973 to provide a conceptual design of the gearboxes required for this test rig. The initial design was received in May, 1973 and reviewed by MTI. The power losses in the gearboxes were expected to be high due to unnecessarily high safety factors which were included in the initial gearbox designs. These designs were modified by Philadelphia Gear Corporation to the satisfaction of

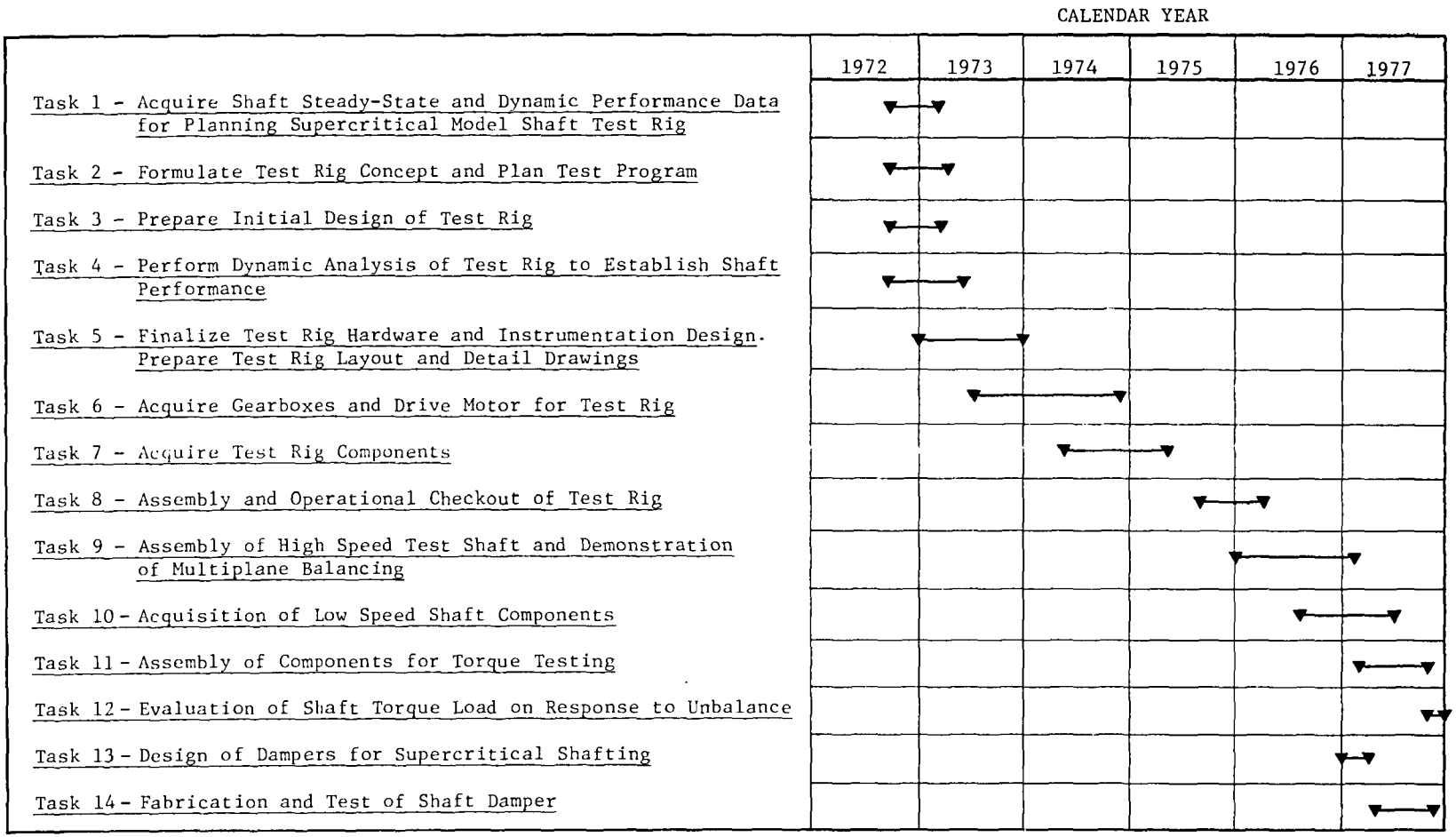

Fig. V.1 Contract Milestone Chart

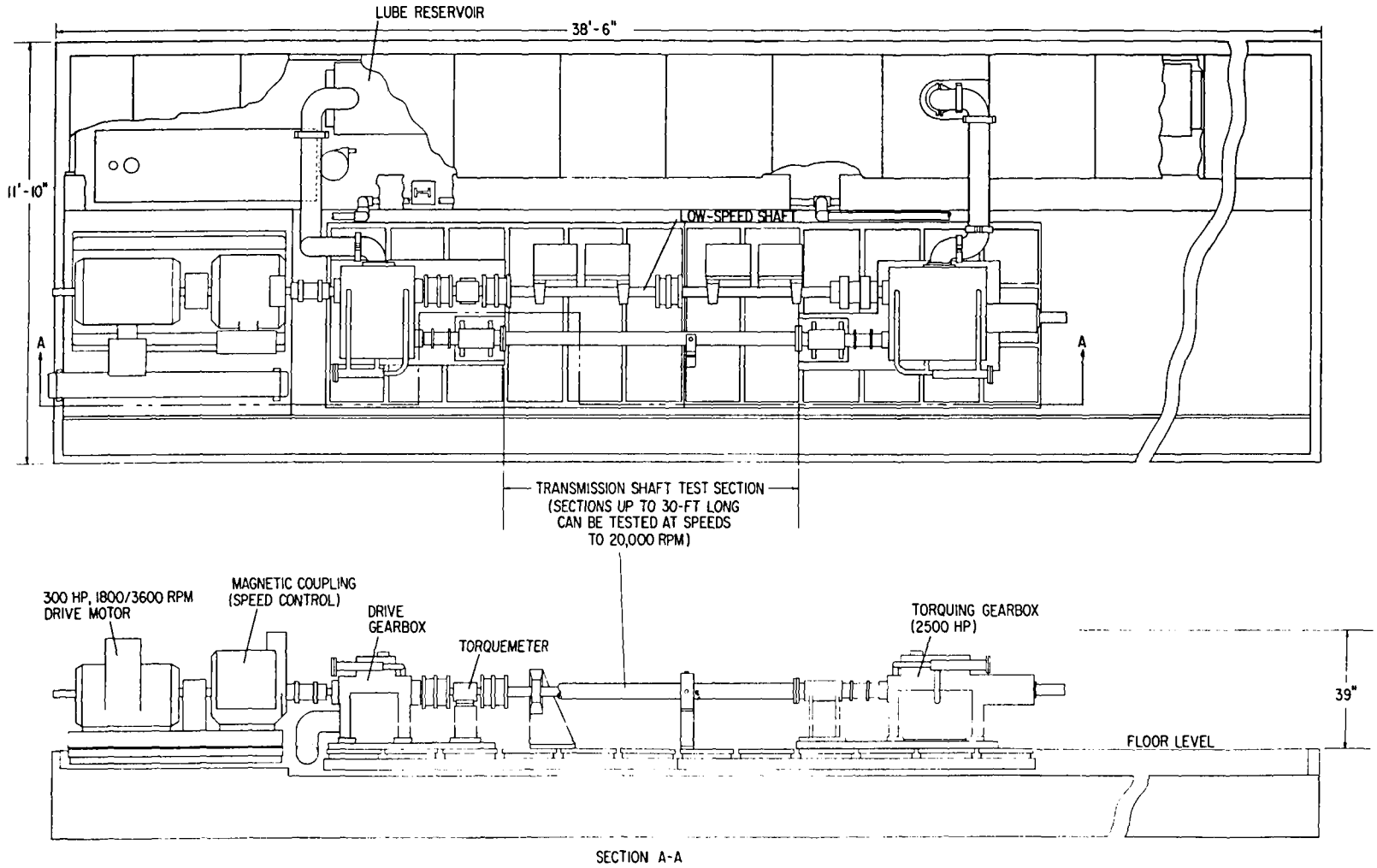

ARMY/NASA TEST FACILITY FOR DEVELOPMENT OF SUPERCRITICAL POWER-TRANSMISSION-SHAFTING TECHNOLOGY AND COMPONENTS
(Designed and Constructed by MTI Under NASA Contract NAS3-16824)

Fig. V.2 Preliminary Design of Supercritical Shaft Test Rig

MTI-15185

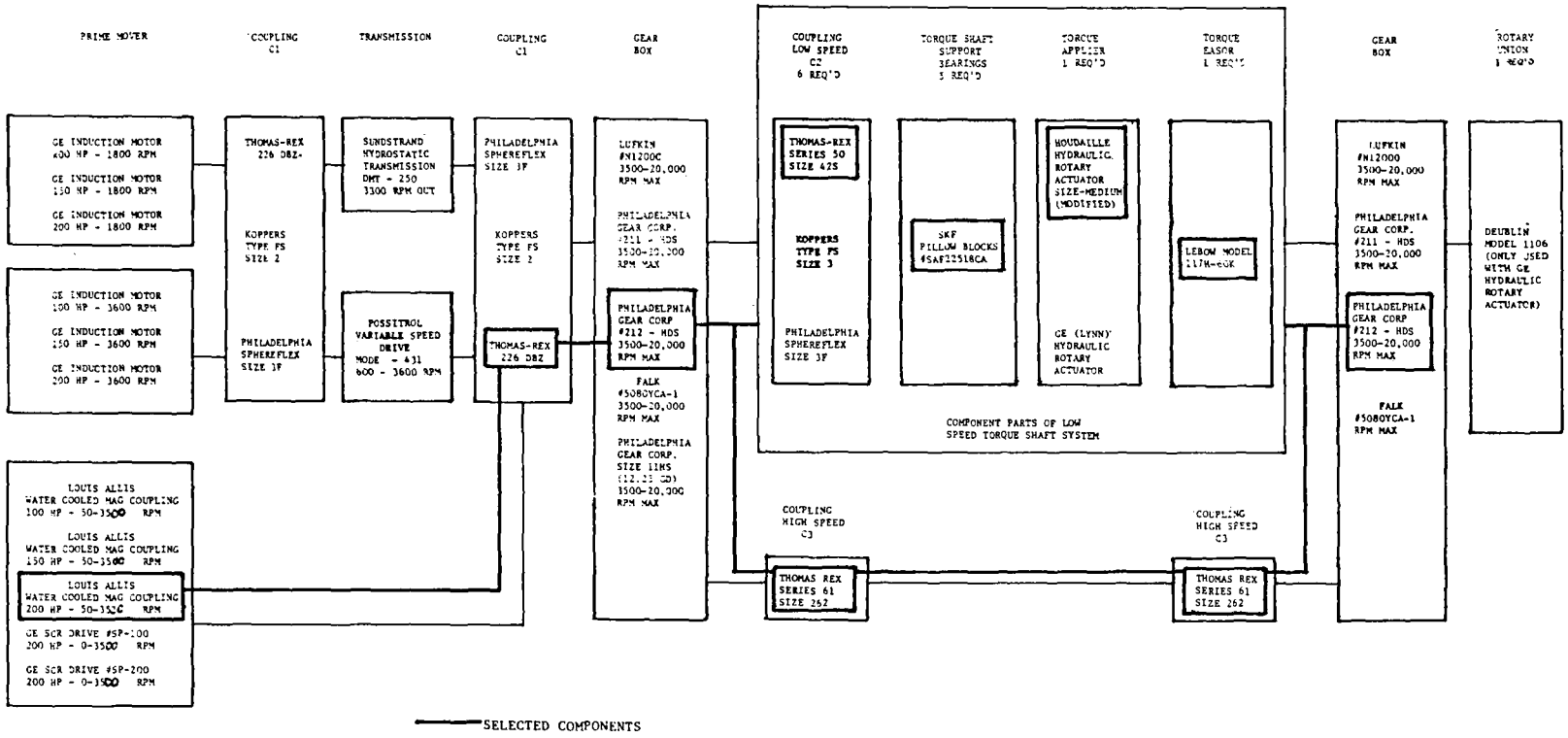

Fig. V.3 Component Parts Schematic as Selected for Preliminary Design Package

MTI. A Louis-Allis drive motor and magnetic coupling set was chosen as the prime mover for the supercritical shaft test rig in early 1973. The design of the test rig was completed and submitted to NASA in November, 1973. Task 5 was initiated in January, 1973 and completed in December, 1973.

Task 6 - Acquire Gearboxes and Drive Motor for Test Rig

For Task 6, initiated in July, 1973 and completed in November, 1974, the gearboxes were ordered from and delivered by Philadelphia Gear. Before the gearboxes left the Philadelphia Gear Plant, they underwent a thorough operational check-out under MTI supervision. The results of this operational check-out are presented in a later section of this report. The motor and magnetic coupling were ordered in July, 1973 and delivered in April, 1974.

Task 7 - Acquire Test Rig Components

The majority of the test rig components were acquired, including the machine floor plates (on which the test components were mounted) and all high-speed components (with the exception of the test shaft itself). Also, architectural work for the test rig base was performed. Task 7 was initiated in May, 1974 and completed in May, 1975.

Task 8 - Assembly and Operational Check-out of Test Rig

For Task 8, MTI built a separate dedicated facility to house the test rig. Mechanical and electrical hardware was assembled and necessary plumbing was installed. The drive motor and drive gearbox were run to 10,000 rpm. This task was initiated in September, 1975 and completed in March, 1976.

Task 9 - Assembly of High-Speed Test Shaft and Demonstration of Multiplane Balancing

Task 9 was begun in January, 1976 at which time an order was placed for the balance rings for the test shaft. In March, 1976, an order was placed for assembly and straightening of the test shaft. The straightened test shaft assembly was delivered in April, 1976. In May, 1976, the motor and gearbox were run to 90 percent of full speed. While initial unbalance of the high-speed pinion of the drive gearbox prevented running over 18,000 rpm, the shaft was subsequently balanced and the motor and drive gearbox were run to 20,000 rpm in June, 1976. The high-speed test shaft was assembled and aligned to the test rig in June, 1976. Undamped balancing tests were begun in August, 1976 and completed in January, 1977. Balancing with Coulomb dampers was performed in October, 1976. Task 9 was completed in January, 1977.

Task 10 - Acquisition of Low-Speed Components

Task 10 involved the acquisition of final components for the test rig, and in particular, the low-speed shaft components. Some final modifications to the test rig design were made in September, 1976. Orders for the low-speed shaft purchased parts were placed in October, 1976, and for the fabricated hardware in February, 1977. All hardware was delivered to complete Task 10 in April, 1977.

Task 11 - Assembly of Components for Torque Testing

In Task 11, begun in March, 1977, the components required for torque testing were assembled. The new floor plate was aligned and grouted in place in April,

1977. Assembly of the torque testing components began in May, 1977 and was completed in November, 1977.

Task 12 - Evaluation of Shaft Torque Load on Response to Unbalance

Task 12 involved the evaluation of the effect of shaft torque load on the response of the test shaft to unbalance. The tests were conducted and completed in December, 1977.

Task 13 - Design of Damper for Supercritical Shafting

In January, 1977 the design of the damper for the supercritical shaft test rig was selected. Actual design of the damper was begun in February, 1977, and completed in March, 1977.

Task 14 - Fabrication and Test of Shaft Damper

In Task 14, the shaft damper was fabricated and tested. In April, 1977 orders were placed for the fabrication of hardware and components for the shaft damper, designed under Task 13.

Delivery of the fabricated hardware and components began in May, 1977, and the balance was delivered in June, 1977. The remainder of the damper components were delivered in July, 1977. Assembly of the damper began in July, 1977 and was completed in August, 1977; and its installation was completed in September, 1977. The damped balancing tests were begun in September, 1977 and completed in November, 1977.

VI. TEST FACILITY

PURPOSE

The test facility was designed to evaluate supercritical power transmission shafting. Tests were performed to identify any problems, needed technology, or limitations inherent in the use of such shafting. One of the principal areas of interest involved the demonstration of balancing of supercritical shafts. The tests included the balancing of a very flexible shaft with both damped and undamped supports and with test shaft loads ranging from 0 to 900 N-m (8000 in.-lb) of torque.

COMPONENT DESIGN

Figure VI.1 shows the four-square rig used for testing full scale and model supercritical power transmission shafts and components. Table 1 presents the major components of the test facility, the vendors that supplied the components, and their principal specifications.

A four-square test rig has a closed-loop consisting of two gearboxes, a high-speed shaft and a low-speed shaft, as shown in Figure VI.1. Both the low-speed and high-speed shafts, are driven by the drive gearbox. A torque is introduced by applying an axial force to the intermediate helical gear of the torquing gearbox. The resultant axial motion of this gear imparts an angular displacement to the pinion on each shaft. As a result, each shaft develops a reaction torque.

In this way only a small portion of the applied torque will be provided by the prime mover. Whereas, for a dynamometer-type test rig, the entire torque must be provided by the prime mover.

Prime Mover

The prime mover for the test rig is a Louis-Allis two-speed motor which drives a Louis-Allis variable speed magnetic coupling, shown in a photograph in Figure VI.2. The motor runs at either 1800 or 3600 rpm; it delivers 112 kw (150 hp) at 1800 rpm and 224 kw (300 hp) at 3600 rpm. The magnetic coupling is designed to have continuous variable speed from 50 to 3600 rpm and to deliver up to 224 kw (300 hp).

Gearboxes

The drive and torquing gearboxes were specially designed and fabricated by the Philadelphia Gear Corporation. The driving gearbox, shown in the photograph in Figure VI.3, has a gear ratio between high-speed and low-speed shafts of 5.6997 to 1 and both ends of the low-speed shaft are exposed. One end of this shaft is driven by the motor/magnetic coupling set, and the other end is connected through a series of shafts to the torquing gearbox. Only one end of the high-speed pinion shaft is exposed from the drive gearbox; it is connected through the high-speed test shaft and spindles to the torquing gearbox. The drive gearbox is a Philadelphia Gear special double reduction high-speed gear increaser, designed to transmit 1860 kw (2500 hp) at 3500 rpm input speed and approximately 20,000 rpm output speed. The pinion shafts are case-hardened and precision ground, and the gears are through-hardened and shaved. The input and output shafts have double-acting, tilting pad Kingsbury thrust bearings. The intermediate shaft gear thrust was designed to oppose pinion thrust and, thus, eliminate the need for one tilting pad thrust bearing. The housing of the gearbox is made of reinforced welded steel.

TABLE 1

VENDORS OF MAJOR COMPONENTS FOR SUPERCRITICAL SHAFT TEST FACILITY

Component	Vendor	Main Specifications
Gearboxes	Philadelphia Gear	2500 hp capacity 5.7 to 1 ratio
Motor/Clutch	Louis-Allis	300 hp; 1800/3600 rpm
Couplings	Thomas	2500 hp
Floor Plates	Patch-Wegner	10' x 5' x 7"
Pillow Blocks	Seal Master	3600 rpm
Torque Sensor	LeBow	60,000 in.-lb; 3600 rpm
Test Shaft	Nashua Industrial Machine Co.	12' x 3" dia x 0.12" wall
Spindles, Probe Brackets	Turbonetics	
Test Rig Enclosures/Base	Hartheimer, Bender and Estey, Architects Lyons, Pappa Construction	

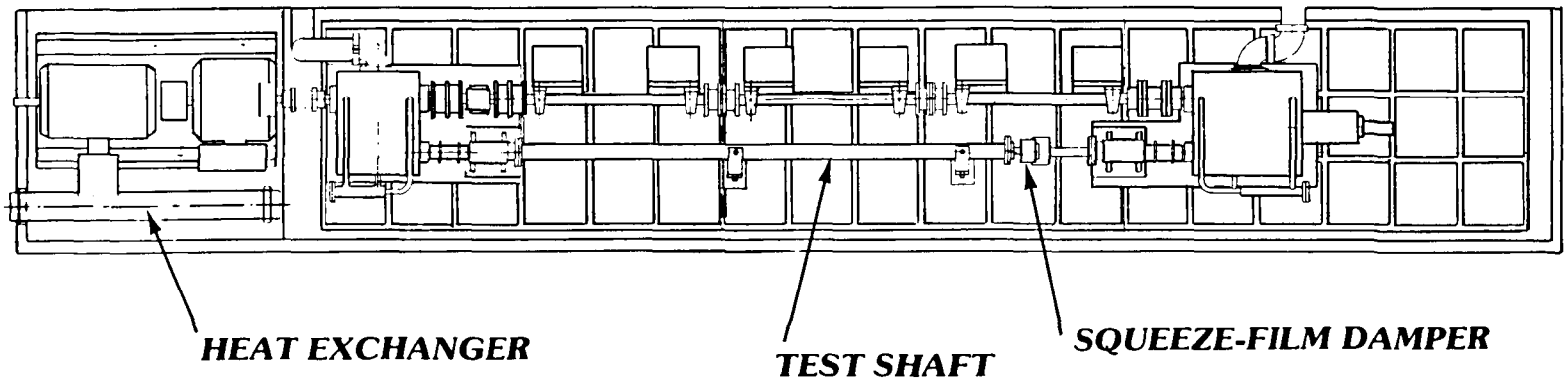

Fig. VI.1 Sketch of Supercritical Power Transmission Shaft Test Rig with Squeeze - Film Damper

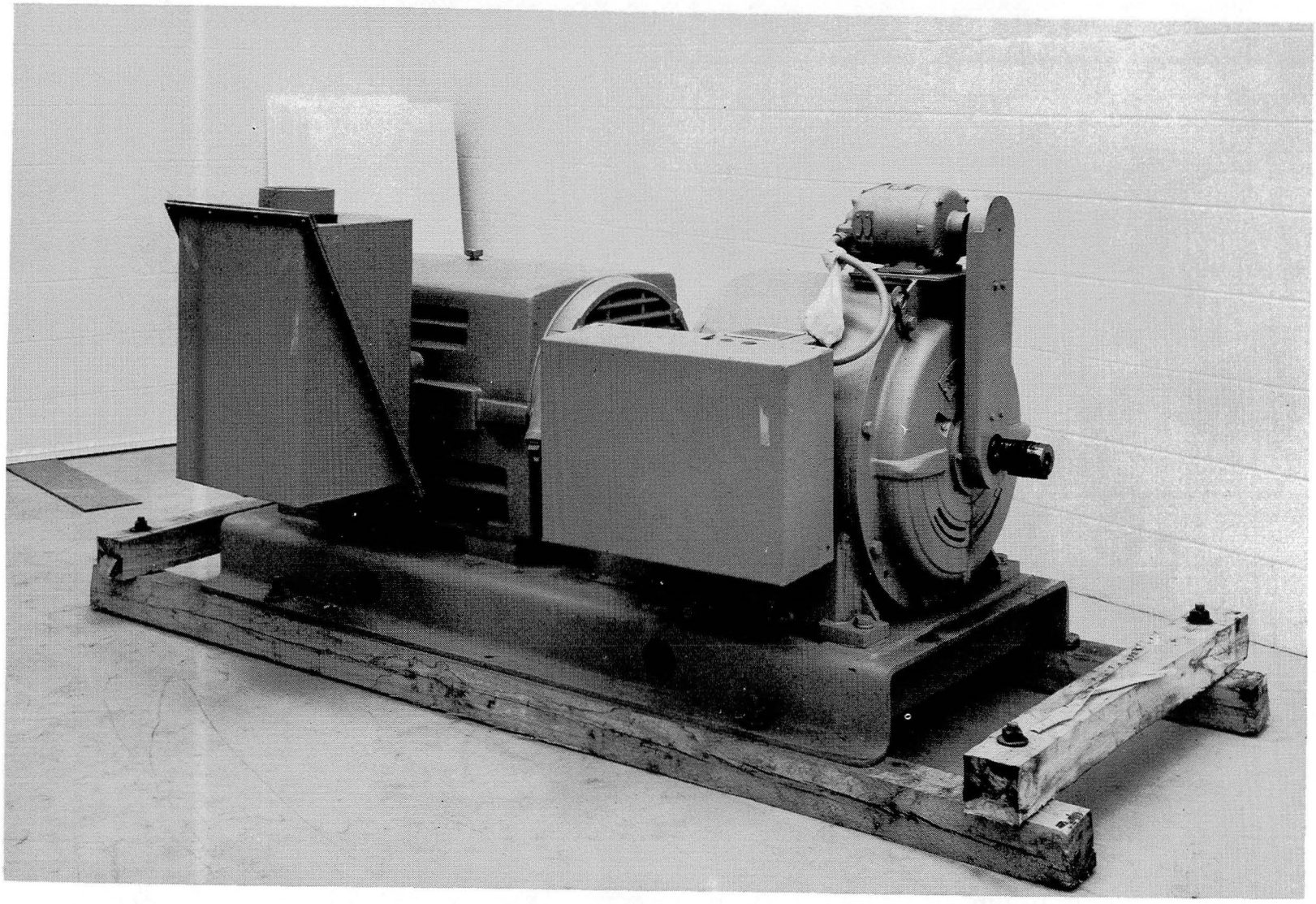

Fig. VI.2 150/300 hp Drive Set for Supercritical Shaft Test Rig

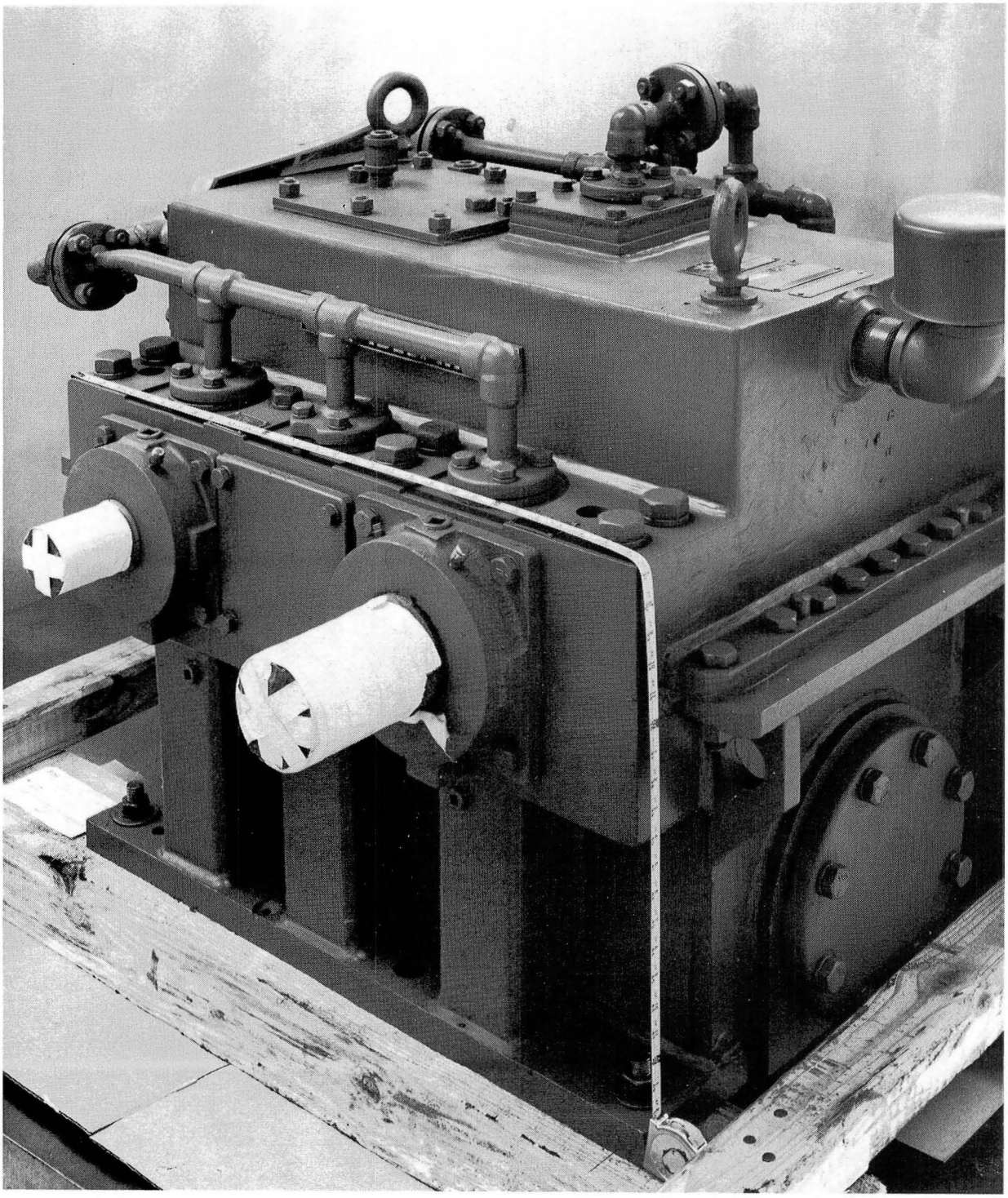

Fig. VI.3 Drive Gearbox for Supercritical Shaft Test Rig

The torquing gearbox, in Figure VI.4, is similar to the drive gearbox, except that it includes a torque applier, and has only a single input shaft and a single output shaft. The torque applier is a hydraulically operated device which can impose from 0 to 900 N-m (8000 in.-lb) of torque to the high-speed side of the test rig, (this is equivalent to almost 5600 N-m (50,000 in.-lb) on the low-speed side of the test rig). Torque is applied by moving the intermediate gear and pinion axially, thus utilizing the tooth helix angle to impose opposite moments about the input and output shaft axes. The torque applier was supplied with hydraulic system and controls. Both gearboxes were provided with drains at convenient locations to allow for free drainage of lubricant under the action of gravity.

Also delivered with the gearboxes was a self-contained lubrication system: sump, motor, oil pump, coupling guard, heat exchanger, filter, by-pass valve, sump strainer, and pressure gage. The oil sump for the gearboxes was made from a Link-Belt conveyer trough, sized to permit adequate dwell time for return oil, and equipped with a liquid level gage, thermometer, and filler cap with vent and strainer. All outside surfaces of the sump were completely primed and painted. The motor and oil pump were sized to supply the necessary pressure and flow to lubricate and cool the fluid film journal and thrust bearings and all gear meshes within each of the gearboxes. The heat exchanger was sized to remove the gearbox system power losses using cooling water with a maximum inlet temperature of 29°C (85°F). (The actual inlet temperature of the cooling water was generally well below this temperature.) The maximum allowable temperature rise in the water was 11°C (20°F), and the maximum allowable pressure drop was 34 kPa (5 psi). An inlet fouling factor of .001 was assumed on the water side for the heat exchanger. The oil filter is a single 10 micron replaceable cartridge type with minimal pressure loss, and has an integral differential pressure gage. The oil bypass relief valve is adjustable from 140 to 690 kPa (20 to 100 psi), and is capable of handling 100 percent of the design flow. The relief valve was set to approximately 400 kPa (60 psi). The sump strainer is 100 mesh and sized to handle the maximum system flow rates.

The high-speed shafts in both gearboxes were modified to permit attachment of balancing correction weights, if needed, in three planes of each shaft. Provisions were made in both gearboxes for mounting vibration monitoring probes on the low-speed shaft using existing through caps, and in three locations along the high-speed shaft. Some changes were made in the final design of the gearboxes, principally bearing diameter reductions to reduce the power requirements of the gearboxes.

The drive gearbox was spin tested at Philadelphia Gear Corporation under MTI supervision. The box was mounted on a test stand and driven by a diesel engine through two intermediate speed and position changing boxes. The drive gearbox operated with no external load. Since the shaft ends had single keyways, to prevent introducing unbalance, dummy coupling ends were fitted to retain dummy keys which filled the keyways. Bently probes and thermocouples at each bearing were in place, and data from each was recorded. A spin test was run until the bearing temperatures stabilized. The vibration amplitudes for all Bently probes were less than 38 microns (1.5 mils), and it was established that the box ran well under no load.

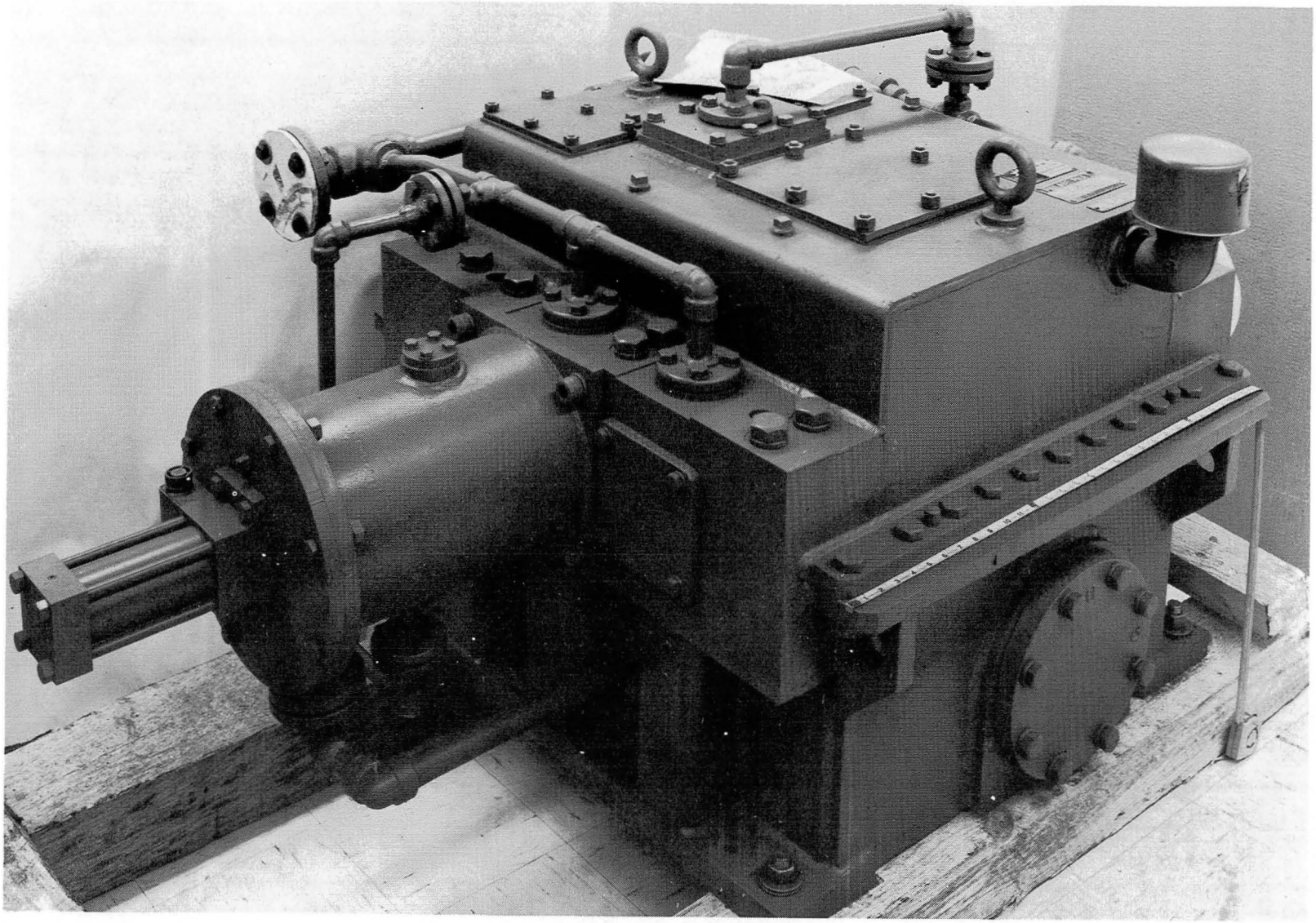

Fig. VI.4 Torquing Gearbox for Supercritical Shaft Test Rig

The torquing gearbox was spin tested at Philadelphia Gear Corporation, also under MTI supervision. The box was set up for a no-load spin test on a motor driven test stand. As in the tests of the drive unit, the shafts had dummy couplings to retain dummy keys. The hydraulic unit was not operational at this time; therefore, shop air was used to retain the sliding cluster gear at each end of its stroke during the run. The torquing gearbox also appeared to run well.

High-Speed Spindles

The test rig has two high-speed spindles, one at each end of the high-speed test shaft. These spindles support the high-speed test shaft and prevent excessive lateral excitations from being transmitted, either from the gearboxes to the test shaft, or from the test shaft to the gearboxes. The high-speed spindles also prevent any moment loading on the gearbox high-speed pinion since the pinion shaft bearings were not designed to handle any significant overhung moment loading. A drawing of one of the high-speed spindles in its final configuration is shown in Figure VI.5 and in a photograph in Figure VI.6.

Each high-speed spindle has a hollow shaft supported by two angular contact ball bearings preloaded against each other with wave spring washers. The bearings are oil jet lubricated and are actively scavenged. The hollow shafts were designed to accept alignment targets in each end which were used with an optical alignment telescope. In this way, the high-speed spindles could be precisely aligned over a distance of nearly 14 ft.

Oil sealing, in the original design of the high-speed spindles, was accomplished by a single labyrinth seal at each end of the spindle shaft with no additional containment of the oil. The high-speed spindles were fabricated, assembled, and used for the undamped balancing tests as originally designed. However, a significant oil leakage occurred from the ends of the spindles whether or not the spindles were rotating. The design of the high-speed spindles was modified to eliminate this problem (see Figure VI.5). Each of the single labyrinth seals on the spindle shafts was replaced by a double air buffer labyrinth seal and the spindle end caps were replaced by close clearance caps designed to trap any oil which might leak by the labyrinth seals. A valve was installed which could bleed air to the central cavity of the high-speed spindles and ensure that the spindle bearings would be exposed to atmospheric pressure on both sides. The hardware for these modifications was fabricated and installed in the spindles. The damped balancing and torque tests were conducted with the modified spindles and no oil leakage was detected from either of them.

High-Speed Test Shaft

A high-speed test shaft was fabricated from stock aluminum tubing as shown in Figure VI.7. Standard aluminum tubing, 7.6 cm (3 in.) in diameter, with a 0.3 cm (1/8 in.) wall thickness and length of 3.66 m (12 ft) was specified. End adapters were designed to be assembled to the tubing with an interference fit and rivets, and to substitute for one hub of a modified Rexnord 52X coupling. The 52X coupling was modified by increasing the size of the mounting bolt holes to match shoulder bolts with a very small clearance, and by adding a circumferential pattern of threaded holes for balancing correction weights, if needed.

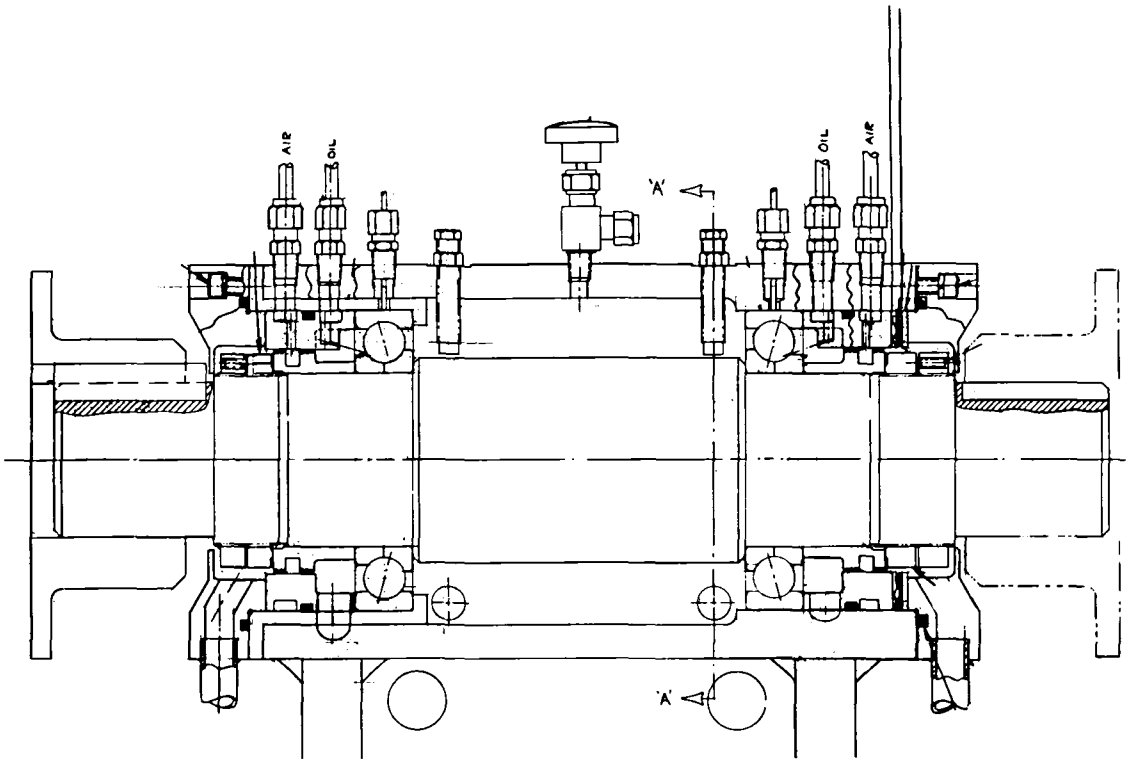

Fig. VI.5 High-Speed Spindle

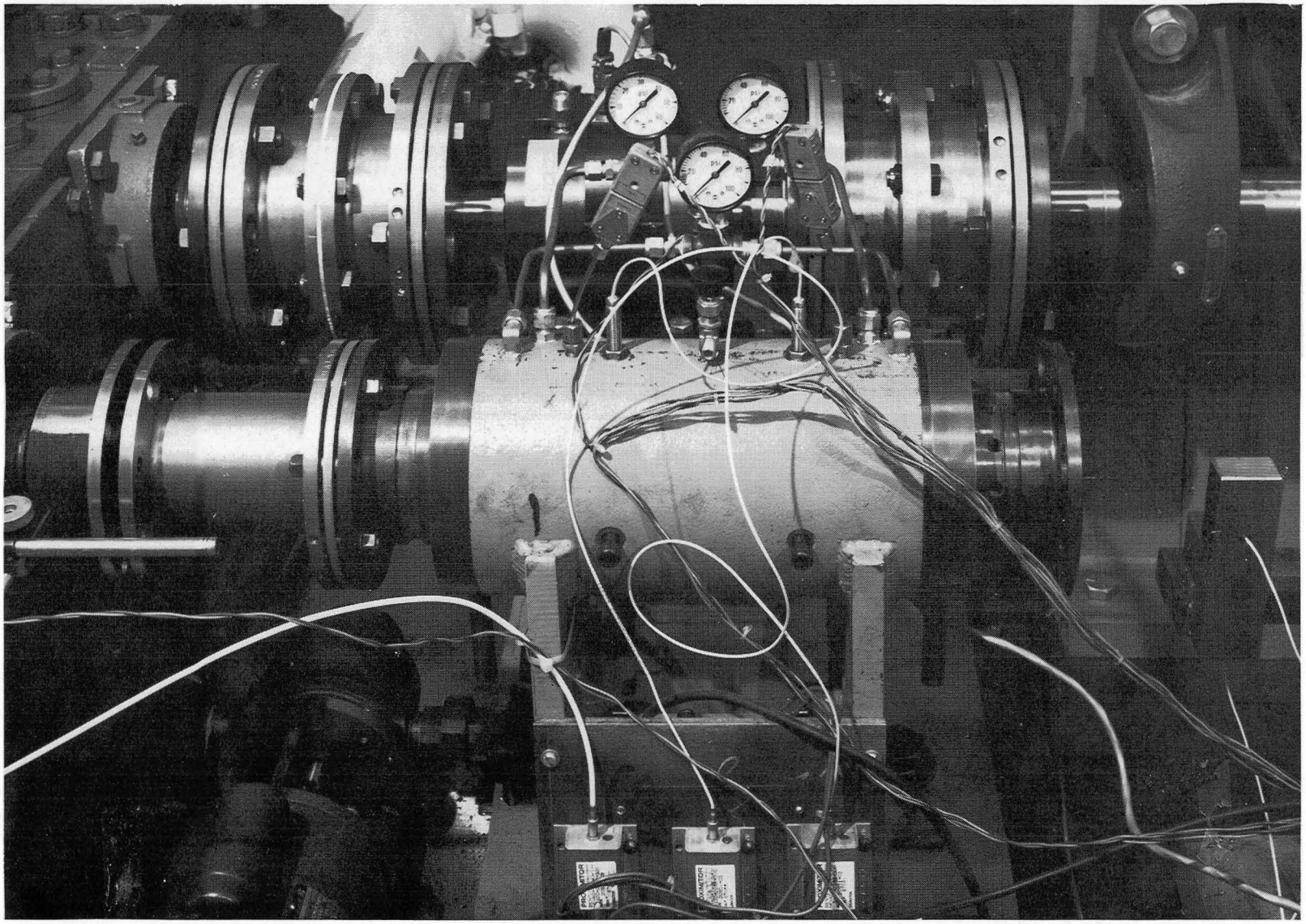

Fig. VI.6 Assembled High-Speed Spindle in Final Modified Configuration

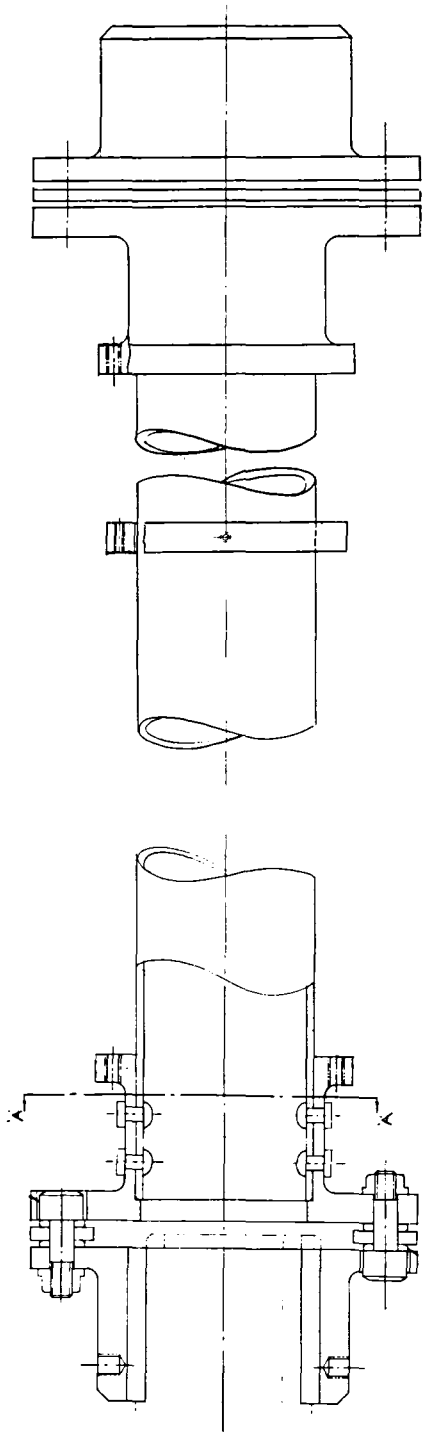

Fig. VI.7 Assembly Drawing of High-Speed Test Shaft

Aluminum balance rings were also designed to be assembled on the high-speed test shaft. Each ring has an inside diameter of 8.9 cm (3-1/2 in.), an outside diameter of 10.2 cm (4 in.), and a width of 1.3 cm (1/2 in.), with a series of axial threaded holes. These balance rings were attached to the tube by three radial set screws which applied pressure against steel pads cemented to the aluminum tube. The set screws are located in blind holes in the balance rings to prevent expulsion by centrifugal force. The optimum preload at each set screw was determined to be 8 mils to ensure solid mounting of the balance rings without deforming the tube; the maximum net eccentric weight that can safely be added to one balance ring while maintaining positive pressure at all 3 contact points was calculated, and is shown as a function of speed in Figure VI.8.

The assembly procedure for the test shaft was designed to be as follows:

- Machine the outside surfaces of the ends of the aluminum tubing to be circular and to have the specified diameter for interference assembly into the end adapters.

- Mount the seven balance rings on the tubing so that their outside surfaces are concentric with the machined surfaces at the ends of the tube and their balance hole patterns are in line.

- Assemble the end adapters on the aluminum tube so that the ends of the adapters are square with the machined surface of the aluminum tubing.

- Rivet the end adapters to the aluminum tubing and check that they maintain their proper assembly position.

A photograph of the assembled high-speed test shaft is presented in Figure VI.9.

High-Speed Shaft Couplings

The high-speed spindles are connected to the high-speed pinion shafts of the gearboxes by Rexnord Model #52X, size 262. flexible disc couplings. These couplings are rated for 1070 N-m (9500 in.-lb) at 20,400 rpm, which exceeds the requirements of this test rig. These couplings can also accommodate up to one-third of a degree angular misalignment which exceeds the misalignment inherent in the test rig assembly. A photograph of one high-speed coupling is presented in Figure VI.10. Similar couplings are used to connect the high-speed test shaft to the high-speed spindles.

Low-Speed Hardware

The low-speed side of the test rig used both fabricated hardware and standard components. Fabricated hardware includes the low-speed shafts and bearing supports shown in Figure VI.11, the torque sensor stand shown in Figure VI.12, and assorted mounting hardware. Standard components include bearing pillow blocks, shaft couplings shown in Figure VI.11, and the torque sensor shown in Figure VI.12. The pillow blocks are Sealmaster models #MP-51 and #EMP-51. The couplings are Rexnord models #52 and #54, size 425, and the torque sensor is LeBow model #1107H-60K.

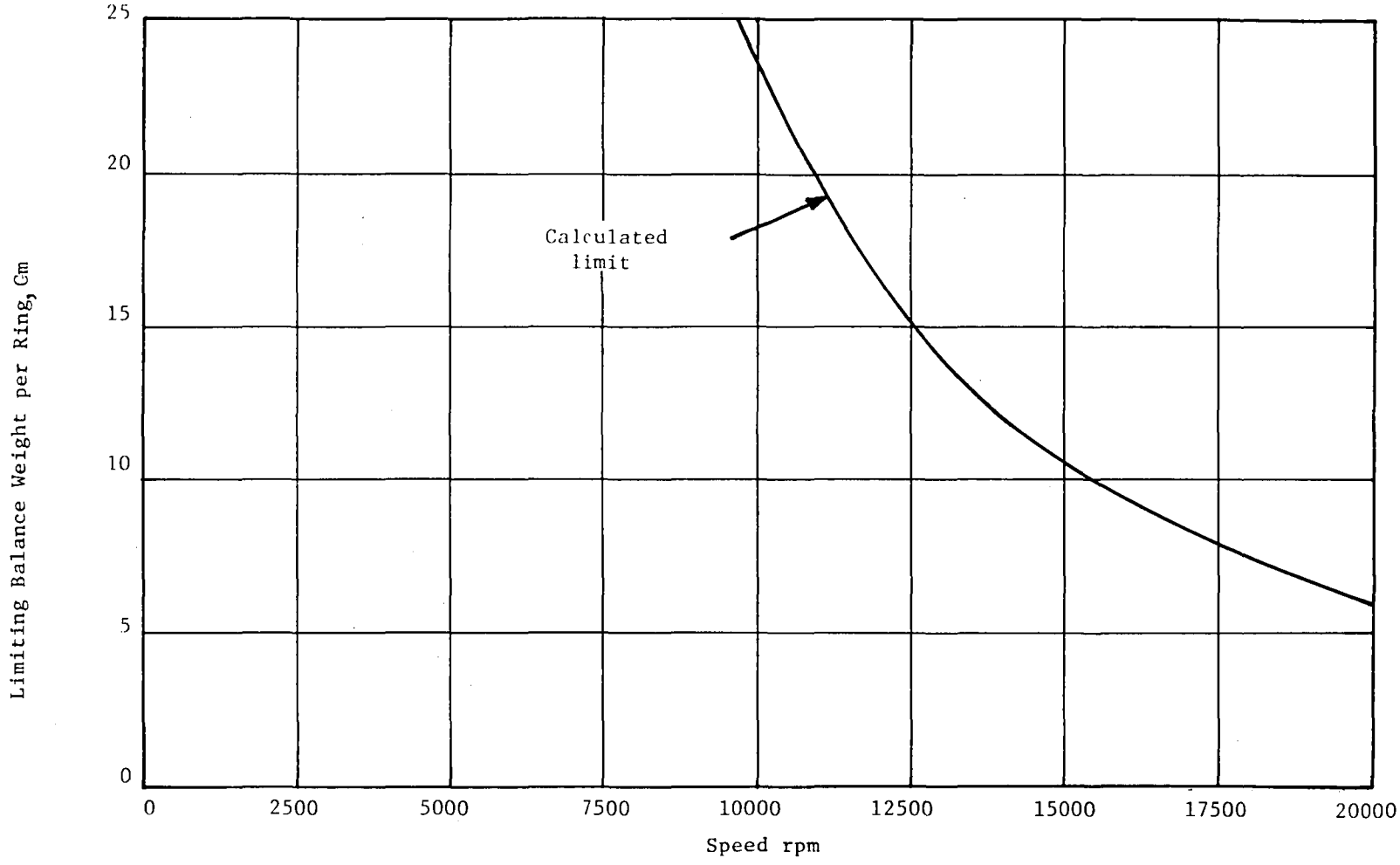

Fig. VI.8 Maximum Net Eccentric Weight in Any One Balance Ring as a Function of Speed

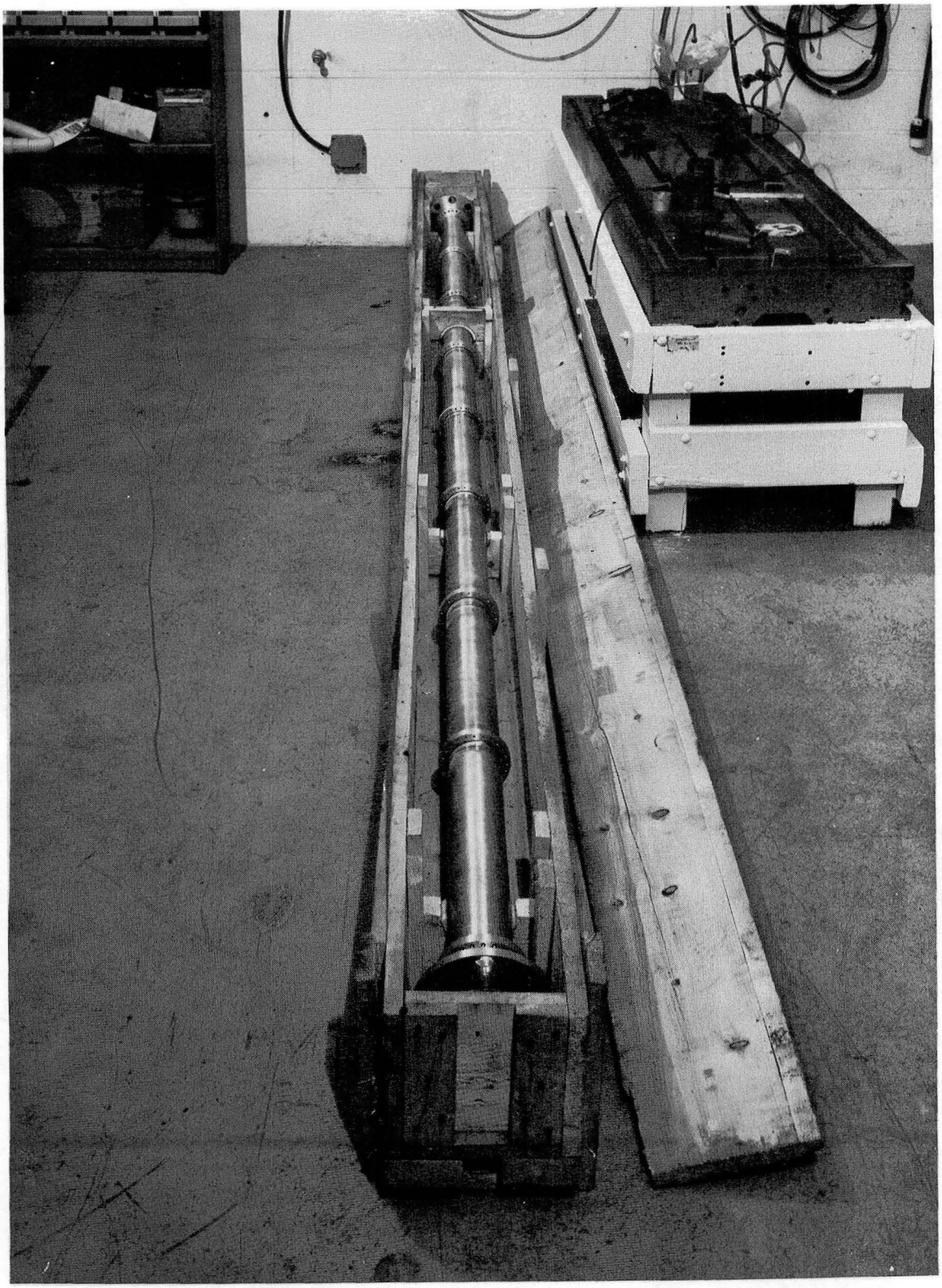

Fig. VI.9 Assembled High-Speed Test Shaft for Supercritical Shaft Test Rig

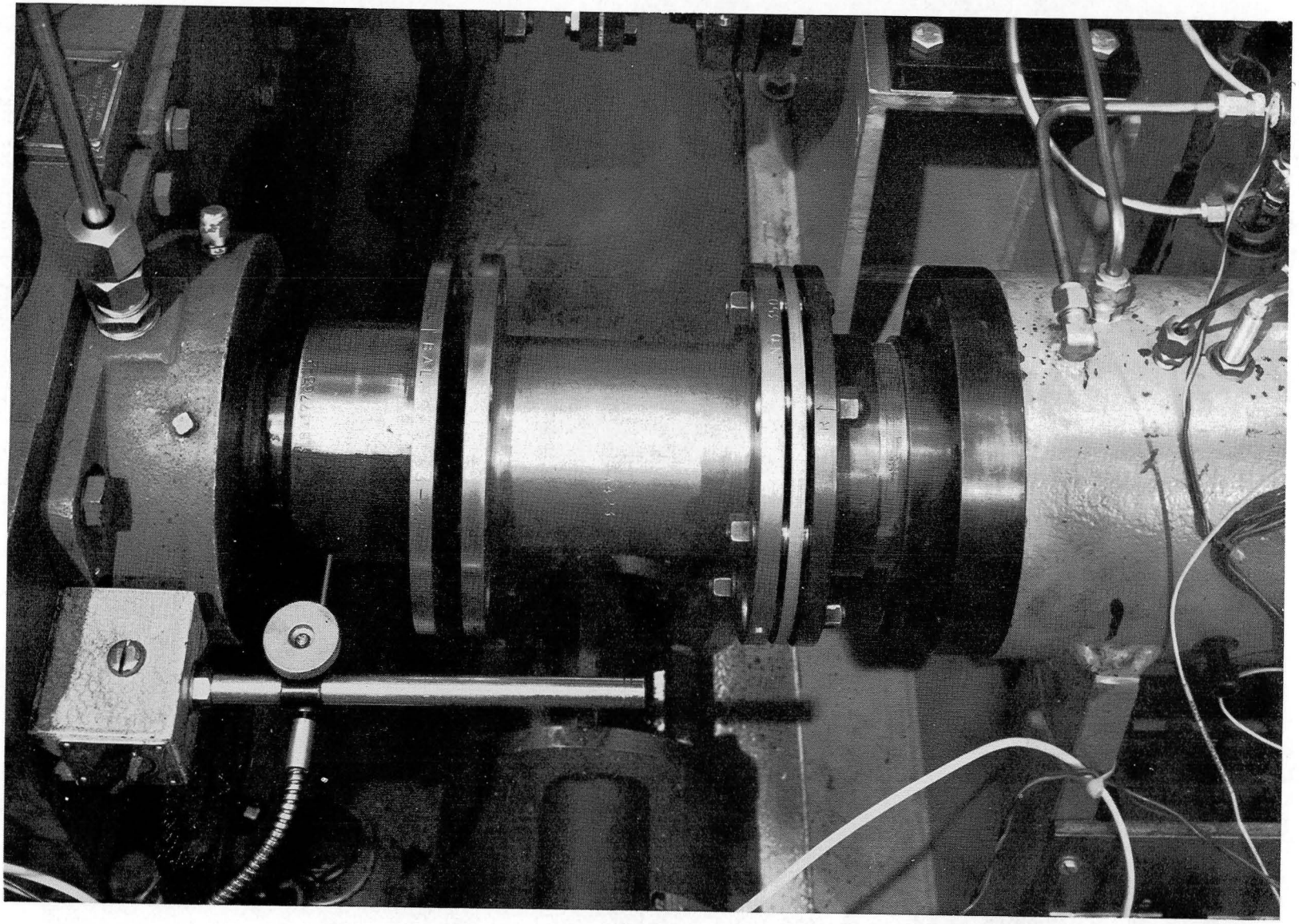

Fig. VI.10 Partially Assembled High-Speed Coupling Connecting Drive Gear-box with Drive-End Speed Spindle

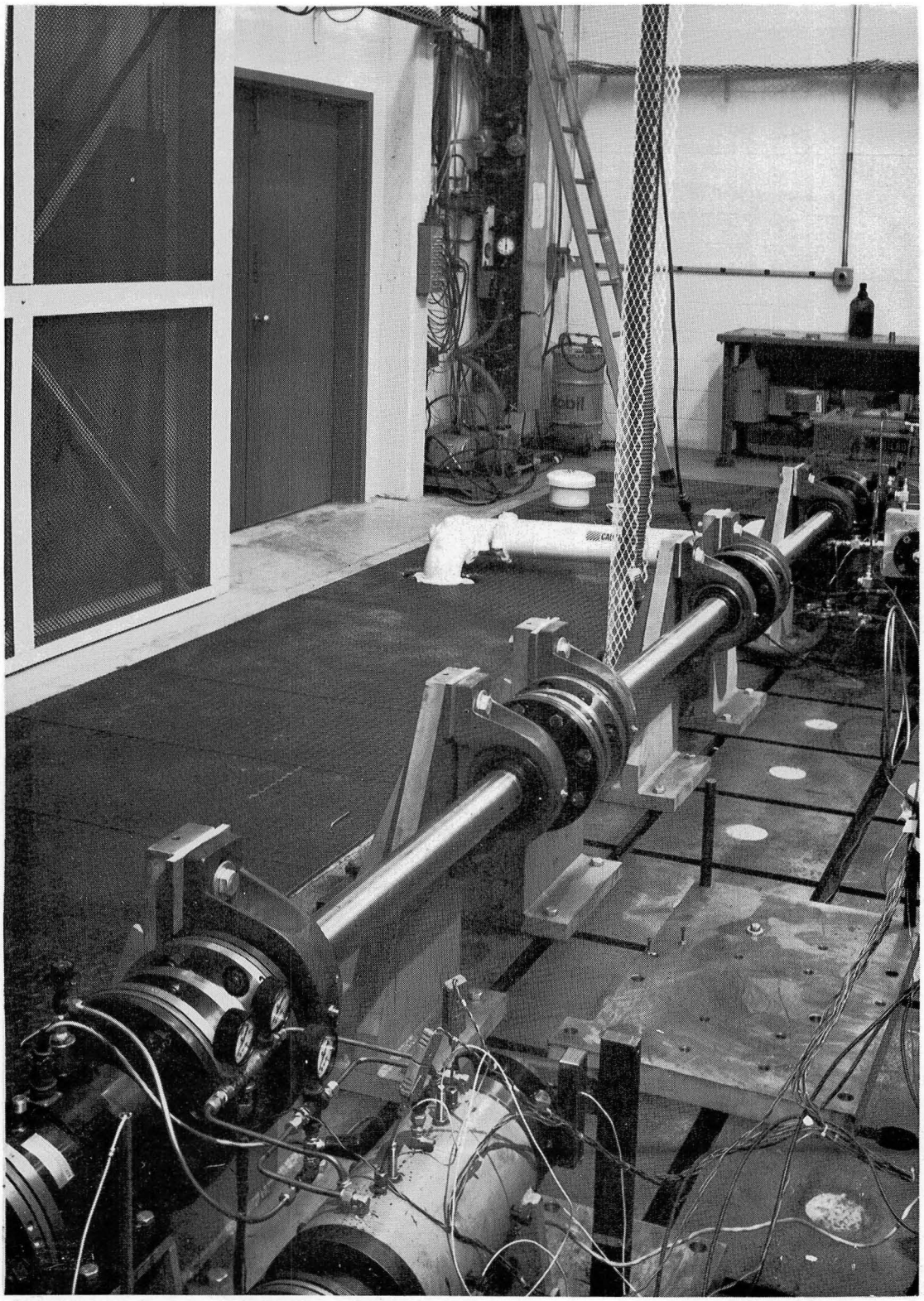

Fig. VI.11 Low-Speed Shafting and Supports

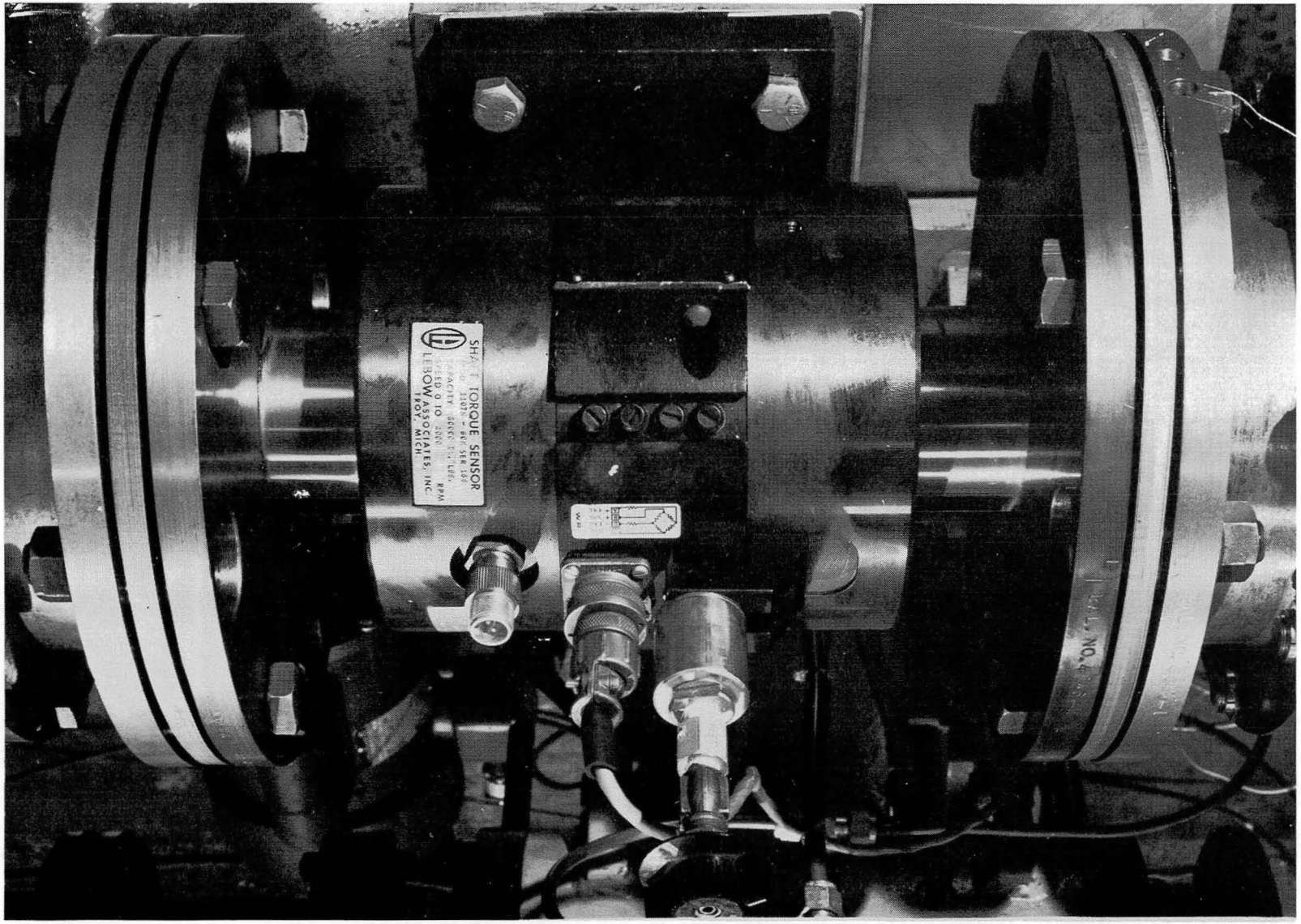

Fig. VI.12 Torque Sensor for Supercritical Shaft Test Rig

Floor Plates

The test rig is mounted on standard, cast iron floor plates, 1.5 m (5 ft) wide by 3 m (10 ft) long by 18 cm (7 in.) thick. Each floor plate is machined at its ends for mating, and has several transverse and longitudinal T-slots for mounting hardware. One of the longitudinal T-slots was ground so the floor plates could be accurately aligned with each other.

Miscellaneous Hardware - The remainder of the fabricated hardware for the test rig comprises gearbox and drive motor mounting plates, probe brackets, and assorted mounting hardware such as T-nuts and shims.

Plumbing

The coolant for the magnetic coupling is a mixture of distilled water and ethylene-glycol with rust inhibitors. It is circulated between a 570 liter (150 gallon) tank and the magnetic coupling, through a heat exchanger, for cooling. Line water is run through this heat exchanger, and its flow is controlled by a temperature control valve which senses the temperature of coolant flowing to the magnetic coupling.

Lubricating oil is supplied to the gearbox meshes and bearings from a 1500 liter (400 gallon) sump tank through a heat exchanger. The oil is returned to the sump by gravity flow through 15 cm (6 in.) return pipes. The heat exchanger is cooled by line water and a temperature control valve holds the lubricating oil supply to a temperature below 60°C (140°F).

The torquing gearbox was plumbed to a hydraulic oil dispenser which controls the torque through axial displacement of a piston carrying the intermediate gear wheel. There is a limit switch which indicates when the piston is at the end of its travel.

Another oil dispenser provides lubricating oil for the high-speed spindles. Scavenge pumps on each spindle return this oil through a heat exchanger to the oil dispenser sump. The heat exchanger is cooled by line water, the flow of which is controlled by a temperature control valve.

Electrical Components

Three phase electrical power at 480 volts is supplied to the test cell for the drive motor and the pump motors for some of the oil dispensers. Also provided to the test cell is 220 volt and 110 volt power for the remainder of the oil dispenser pump motors, and a variety of other electrical and electronic hardware.

Initially, the drive motor was started by means of a General Electric across-the-line starter. The starting current required was about 2000 amps and the temporary power requirement disrupted other electrical and electronic equipment operating on the same site. A silicon controlled rectifier stepping circuit was added to the starter circuit, reducing starting current to 600 amps and eliminating disturbance to other equipment. This SCR stepping circuit starter is a Robistat model #SS300-480-1, manufactured by Robicon Corporation.

Transducers

A large variety of transducers have been built into the test rig for monitoring of the test facility. The gearboxes are instrumented with Bently displacement probes observing the lateral motion of the high-speed pinion shafts, thermocouples in the lubrication oil supply pipes and on the surface of the scavenge pipes, and pressure sensors in the lubrication oil supply lines. The gearbox thermocouples, and all thermocouples associated with the supercritical shaft test rig, are copper constantan which has the greatest sensitivity for the temperature range of interest (below 200°C (400°F)).

A variety of transducers (pressure, temperature, etc.) are located in several of the test rig components to monitor critical parameters and to cause partial or complete shutdown in emergencies. For example, if the lube oil pressure for either of the gearboxes were to fall below a specified safe limit, the magnetic coupling in the drive system would be immediately disengaged. The specific trip-out sensors, which are built into the test rig, are described in more detail in a later section of this report.

Looking at the test shaft itself is a Fotonic Sensor® (photo-optical pickup) for tachometer input and phase reference, and a number of Bently eddy current type displacement probes, which measure dynamic displacement at several locations along the shaft axis.

Dynamic displacements of high-speed spindles are monitored by eddy current displacement probes, and spindle bearing oil temperatures are monitored by copper-constantan thermocouples.

Control Room

The supercritical shaft test facility includes a control room separated from the test cell by a concrete wall and a bullet proof glass window. The control room is equipped with electronics and instrumentation for test rig control, monitoring, and measurement. The test rig is controlled through a panel of electronic and pneumatic devices, including the motor starter, motor speed controls, and a row of trip-out lights which indicate the cause of an automatic shut-down. There are switches to regulate the lubrication oil, scavenge and hydraulic pumps, and an air regulator for pneumatic control of the torquing system. Displacement probe outputs are displayed on a panel of oscilloscopes and thermocouple outputs are displayed on a digital temperature readout. The various lubrication and hydraulic oil pressures are displayed on pressure gages, and drive motor current is displayed on an ammeter. Additional details of the electronics and the instrumentation used for control and observation of the test rig are provided later in this report.

The control room instrumentation includes a computerized system which automatically takes data from the displacement probes. The acquired data is used for balancing calculations, for recording and plotting test rig response, and for detecting trends in the response. The data acquisition system has a number of analog components including a twenty channel scanner, a tachometer, a dual-channel tracking filter, a phase meter, and a digital voltmeter. It also includes specially designed analog components which perform various functions such as reference signal conditioning and AC coupling of the data signals. During the operation of the data acquisition system, one of the displacement

probe signals is chosen by the scanner and is fed into channel "B" of the tracking filter. The reference signal from the Fotonic Sensor is conditioned and fed into the tachometer, the reference channel, and channel "A" of the tracking filter. The dual-channel tracking filter filters out all but the synchronous component of the data signal, and converts the reference signal from a square wave into a sine wave. The filtered outputs from the two channels of the tracking filter are then fed into the phase meter, which measures the phase angle between the two signals. The tracking filter also supplies a DC signal proportional to the amplitude of the synchronous component of the data signal. This DC signal is fed into the digital voltmeter.

The minicomputer sets the channel of the scanner and reads data from the phase meter, digital voltmeter, and tachometer. The minicomputer both automates the acquisition of data and performs sophisticated analyses upon this data. In particular, the computer calculates correction weights for reduction of synchronous amplitudes of vibration using the multiplane balancing algorithm and using a variation upon the modal balancing algorithm.

Test Facility Operation

To operate the test rig, the drive motor must first be started. It is started in either low-speed (1800 rpm) or high-speed (3600 rpm), as required. Before the drive system magnetic coupling can be engaged, the lubricating oil pumps for the gearboxes, the high-speed spindles, and the cooling water pump for the magnetic coupling must be started. After the magnetic coupling has been engaged, the speed of the test rig is controlled by means of a ten turn potentiometer mounted on the test rig control panel. The only test rig operating parameter that needs to be controlled by the test operator during operation (other than the speed of rotation) is the level of torque. An air regulator on the control panel controls the torque by pneumatically controlling a remote pressure relief valve on the hydraulic oil dispenser. This pressure relief valve controls the hydraulic pressure behind the torquing piston in the torquing gearbox, which, in turn, controls the position of the sliding gear that establishes the level of torque. In this way, the supercritical shaft test rig can be completely controlled by an operator in the control room, who is at the same time qualitatively observing the response of the test rig by means of the oscilloscopes, and quantitatively monitoring that response through the use of the data acquisition system.

VII. ASSEMBLY OF TEST RIG AND FACILITY

TEST RIG ENCLOSURE

The first step in the assembly of the test facility was the installation of the major components, including the test rig enclosure. The test rig enclosure is a concrete test cell constructed adjacent to, and sharing a wall with, an existing structure. The location of the test cell and control room, in relation to the existing structure, is illustrated in the drawing in Figure VII.1. The wall shared by the test cell and the existing structure is of reinforced concrete construction, as are the foundation, hardware pit, test bed, and floor of the test cell. The test bed is vibrationally isolated from the remainder of the test cell floor. The new walls of the test cell are of concrete block construction and the roof is composed of prestressed, reinforced concrete double T-beams. The outside walls of the test cell are shown during construction in the photograph in Figure VII.2. The foundation hardware pit, test bed, and floor are shown during construction in the photograph in Figure VII.3. The photograph in Figure VII.4 shows the inside of the test cell after the completion of construction, but before any hardware was installed.

The control room is located in the existing structure. It is separated from the test cell by an existing reinforced concrete wall, a steel door, and a bullet-proof glass window. A safety screen was constructed and attached to the test cell side of the existing reinforced concrete wall for additional protection in the unlikely event that a severe test rig failure were to cause airborne debris.

After the test rig enclosure was completed, fresh and waste water pipes and electrical lines were brought into the test cell. Overhead lights, a large exhaust fan, and a gas space heater were installed. A bridge crane and a chain hoist, shown in the photograph in Figure VII.5, were also installed for lifting and moving heavy equipment.

The monitoring instrumentation installed in the control room included the oscilloscopes and the multi-point temperature recorder, later replaced by a digital temperature display, shown in the photograph in Figure VII.6. The data acquisition system is shown in the photograph in Figure VII.7. The minicomputer shown in the photograph in Figure VII.8 was later moved to a room adjacent to the control room, and connected to the data acquisition system.

TEST RIG BASE

The baseplate for the drive motor was positioned, leveled, and grouted in place on the test bed with anchoring J-bolts. Next, the first two floorplates were installed on the test bed as follows:

- The floor plates were located in their approximate positions on large set screws with anchoring J-bolts hanging into the holes in the test bed; these holes had been formed by metal tubes cast into the test bed.

- The holes in the test bed were filled with grout to secure the J-bolts.

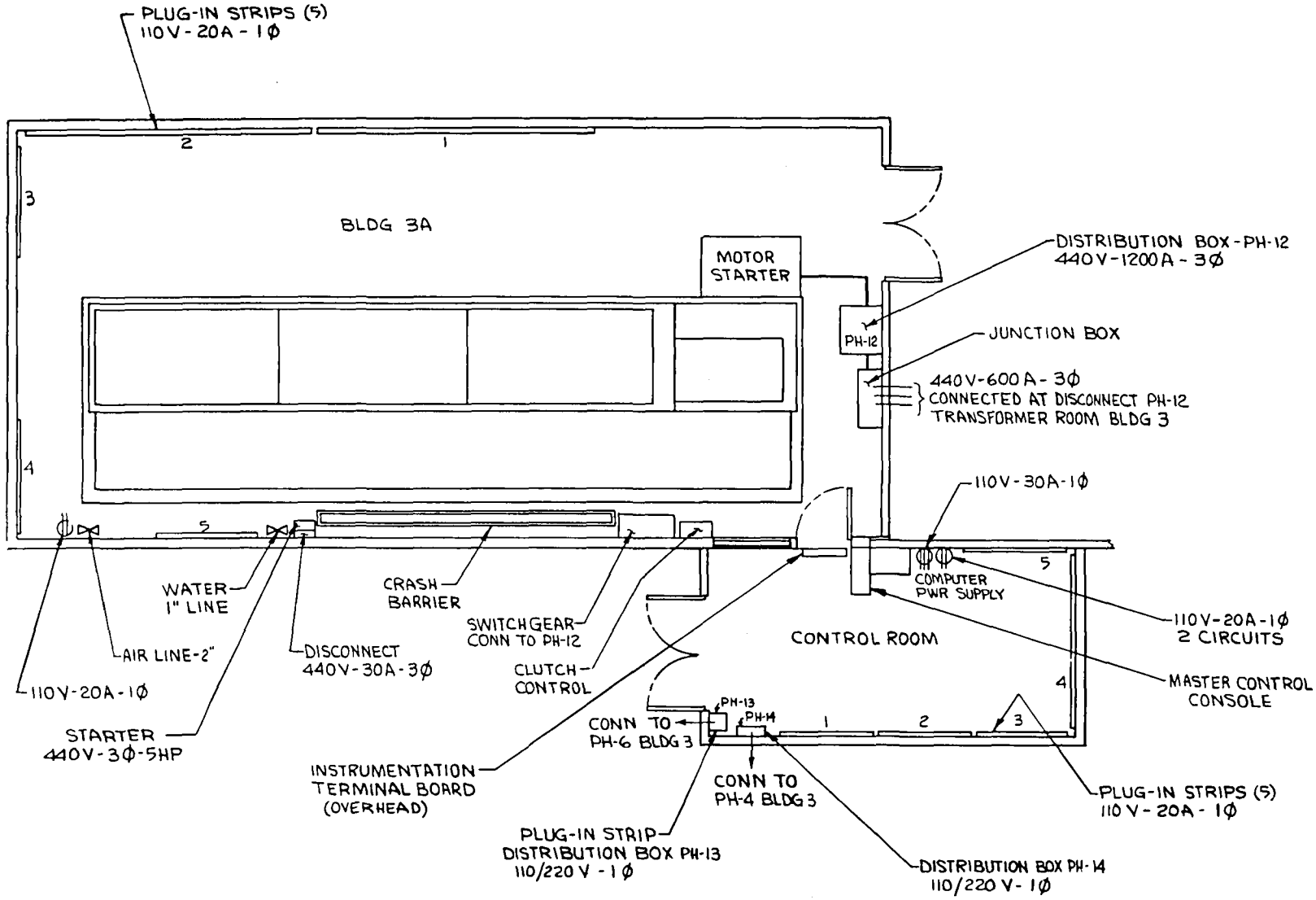

Fig. VII.1 Layout of Test Rig Enclosure for Supercritical Shaft Test Rig

MTI-18129

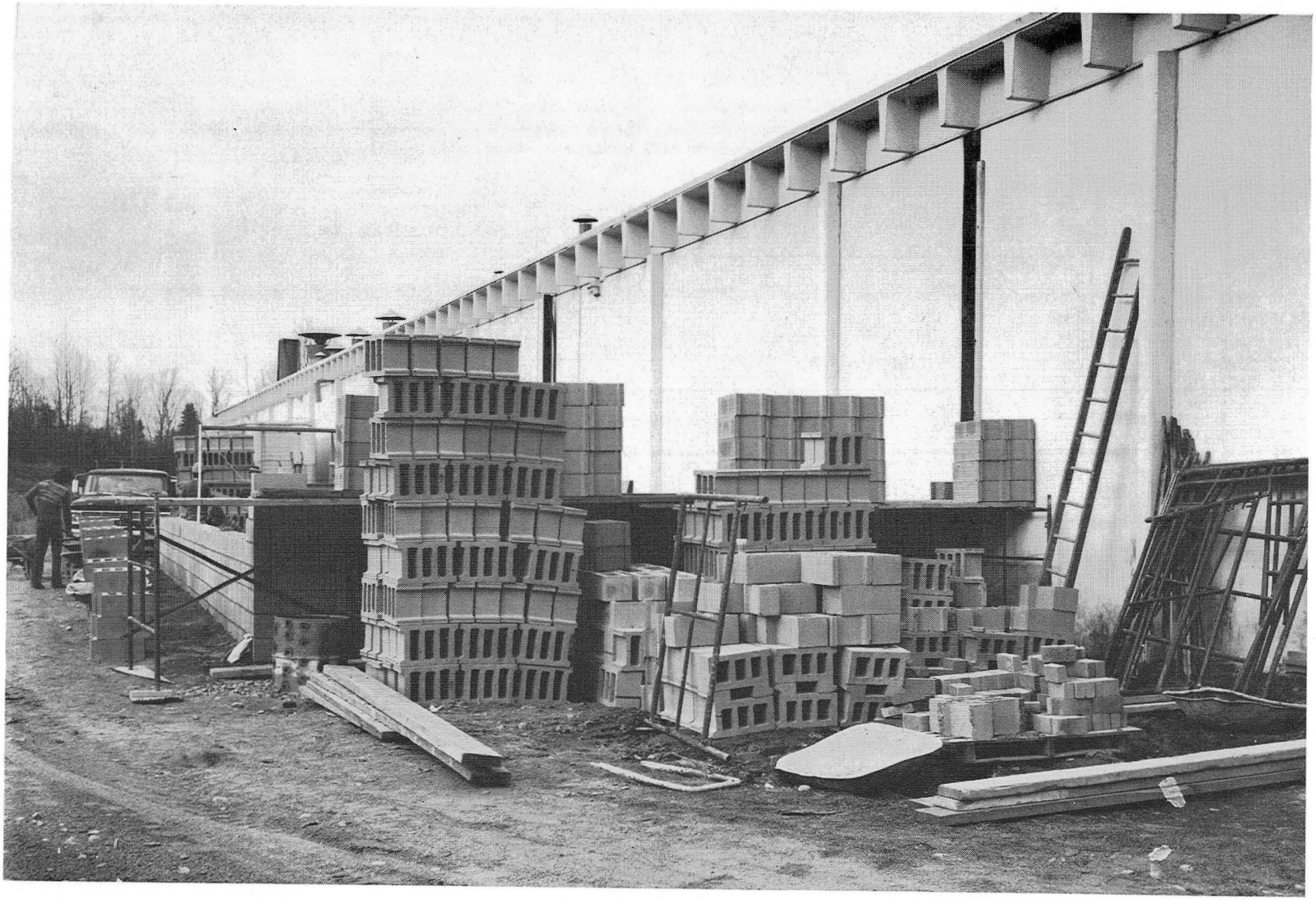

Fig. VII.2 Early in Construction of Walls of Test Enclosure for Supercritical Shaft Test Facility

Fig. VII.3 Preparations for Pouring Concrete for Test Bed of Supercritical Shaft Test Facility

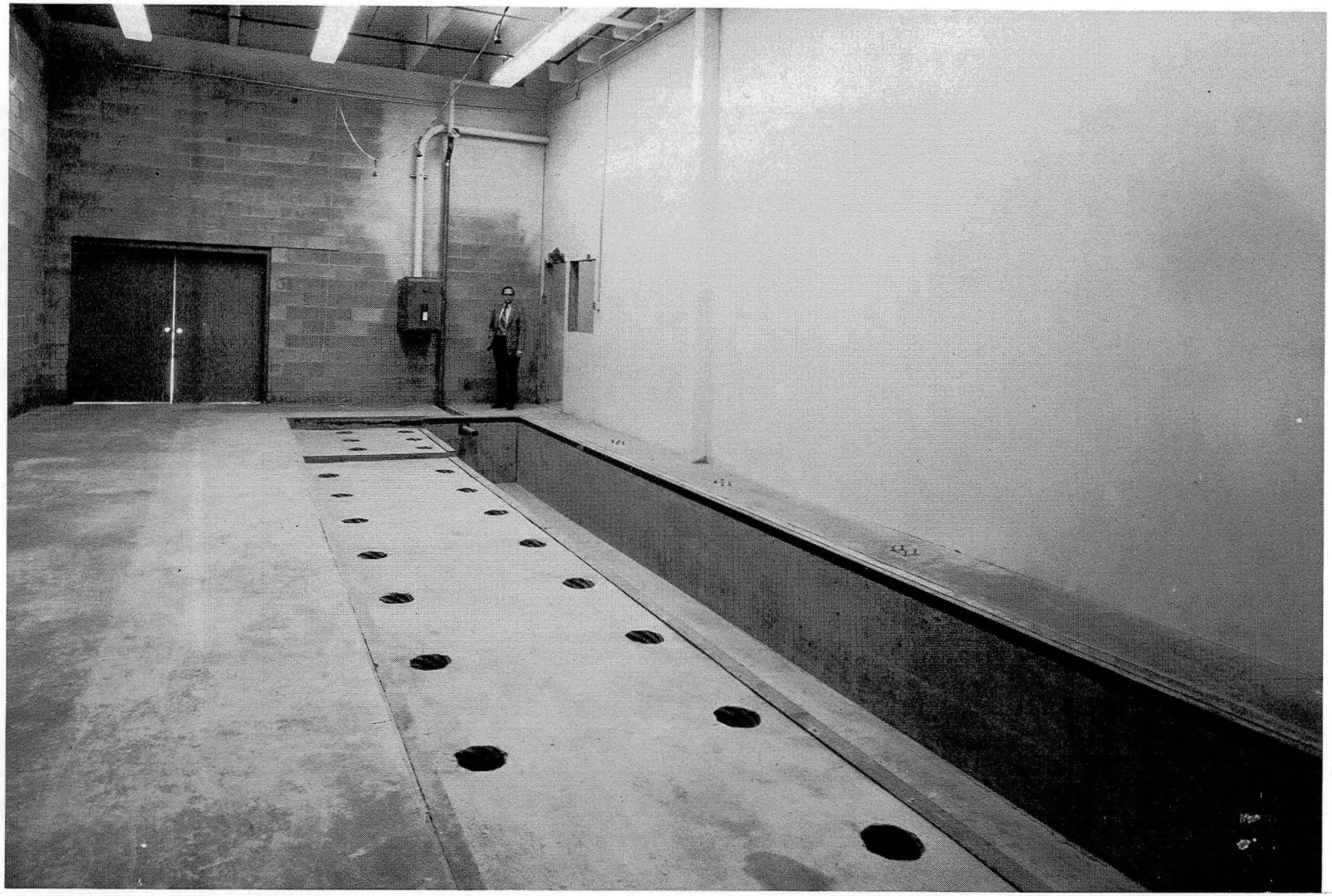

Fig. VII.4 Interior of Test Enclosure Showing Completed Test Rig Floor and Hardware Pit

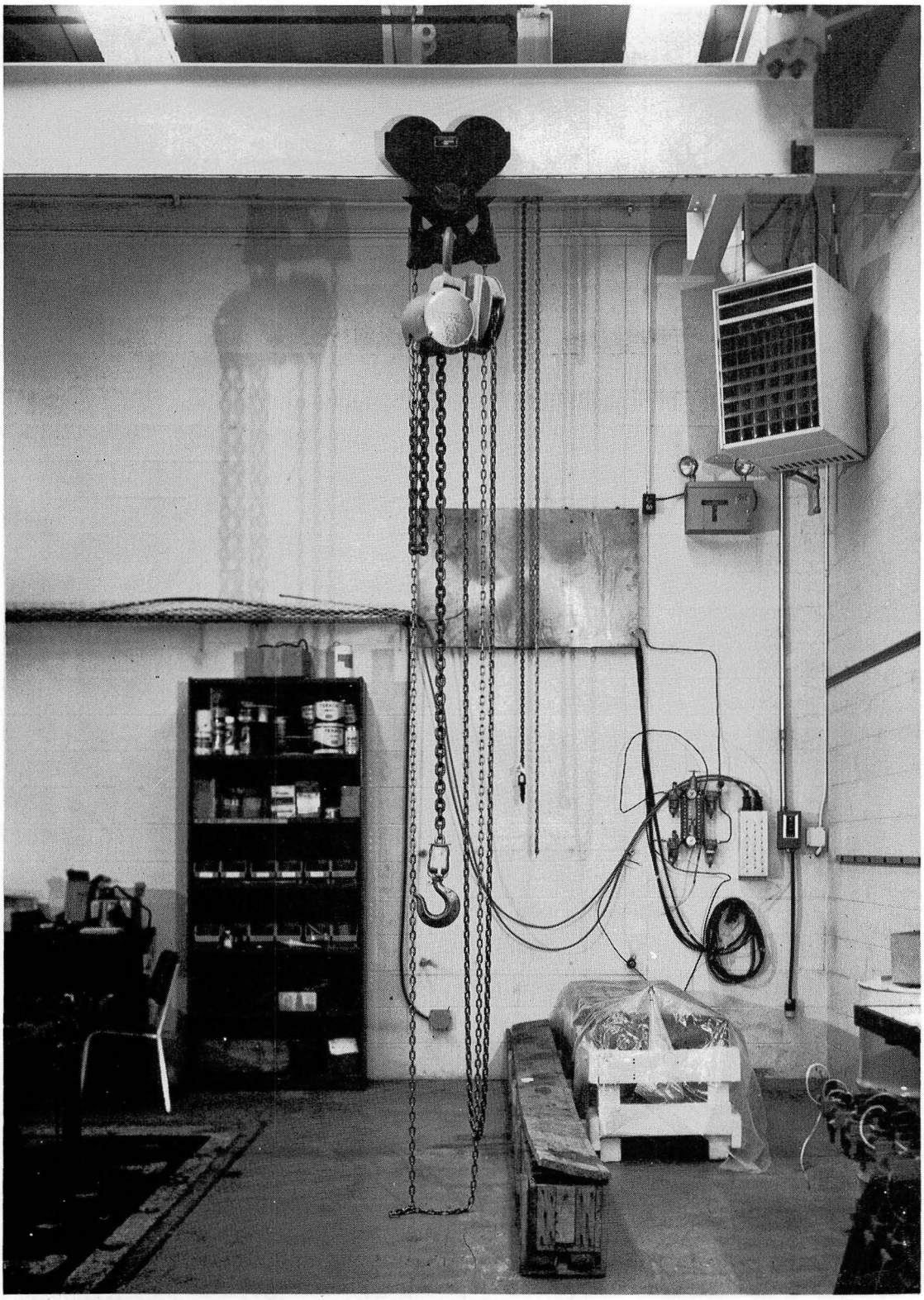

Fig. VII.5 Bridge Crane for Moving Heavy Hardware in Test Facility

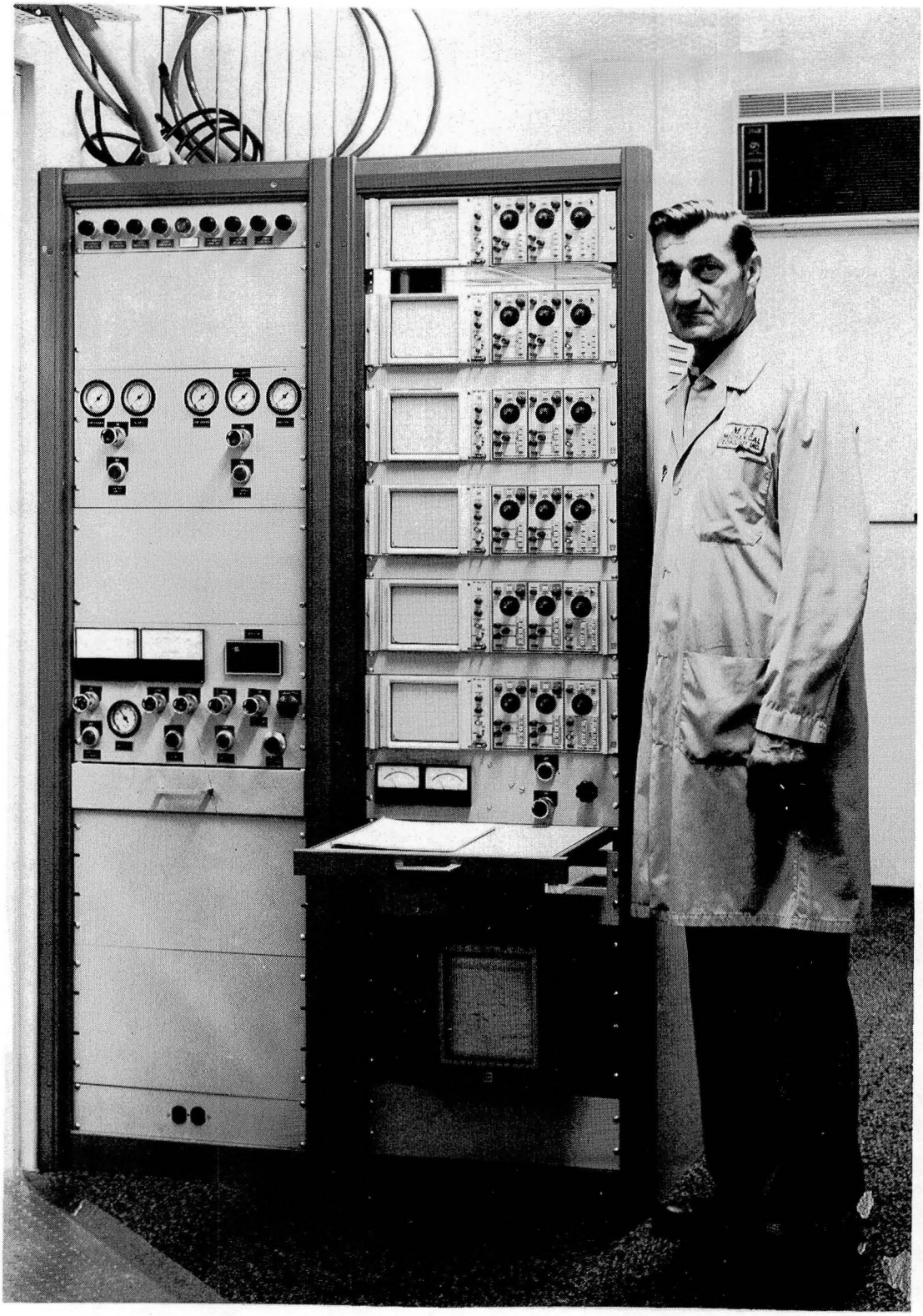

Fig. VII.6 Control Panel and Oscilloscope Panel for Supercritical Shaft Test Rig Prior to Installation of Torquing System

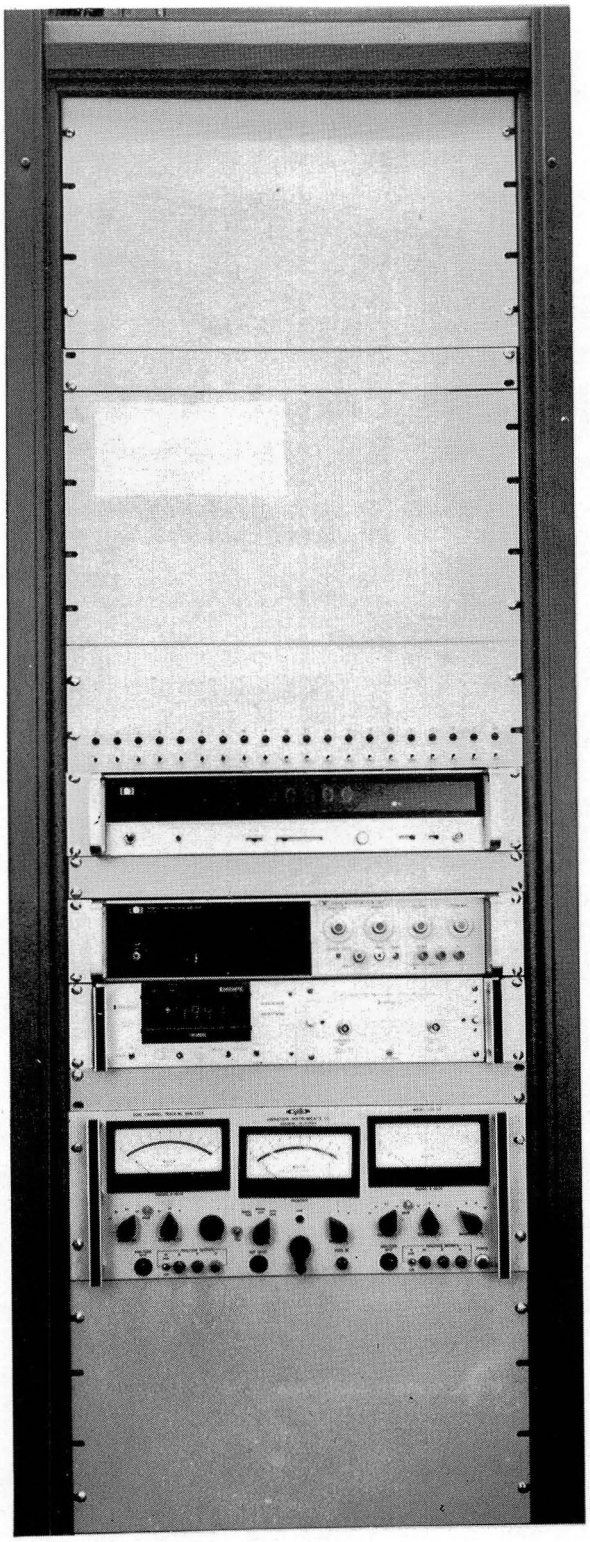

Fig. VII.7 Computer Controlled Data Acquisition System for Monitoring of Dynamic Test Rig Response

Fig. VII.8 PDP 11/34T Minicomputer Which Controls and Receives Data from Acquisition System

- The floorplates were accurately leveled and aligned with each other, and with the motor baseplate using a transit and adjusting the large set screws; the J-bolts were loosened during this operation.

- The J-bolts were secured to the floorplates with nuts.

- The test bed was filled with grout to a point just below the surface of the floorplates.

At a later date, a third floorplate was leveled, aligned and grouted into place in a similar fashion, to carry the torquing gearbox. Photographs of the motor baseplate and the first two floorplates are shown in Figure VII.9.

DRIVE SYSTEM

The drive motor was mounted on its baseplate, leveled, and aligned with the plane of the test bed. A photograph of the drive motor in place is shown in Figure VII.10. The 480 volt power box and the original starter box were mounted in their appropriate locations in the test cell and electrically connected to the motor. The original starter box is the large grey box in the center of Figure VII.11. The starter and motor controls on the control panel, along with the drive motor electronics, were electrically connected to the drive motor, starter, and magnetic coupling.

The solid state SCR stepping starter also shown in the photograph in Figure VII.11 was added at a later date, together with the running time clock which indicates the motor's total running time.

Next, the cooling water sump and heat exchanger for the magnetic coupling were installed in the hardware pit and plumbed in with the appropriate valves. The cooling water sump was filled with a mixture of distilled water and ethylene glycol with rust inhibitors.

The drive gearbox baseplate was then mounted to the floorplate nearest the drive motor. The drive gearbox was set down on its baseplate and roughly aligned with the drive motor. The locations of the mounting holes for the gearbox were marked on the baseplate, and the drive gearbox was removed so that these holes could be drilled and tapped. The drive gearbox was then returned to the baseplate and accurately aligned with the output shaft of the magnetic coupling. After the two halves of the flexible disc coupling were installed on the output shaft of the magnetic coupling and the input shaft of the drive gearbox, the drive gearbox was securely mounted to its baseplate and the coupling was joined.

The lubricating oil dispenser and sump for the gearboxes were installed in the hardware pit along with the appropriate heat exchanger. The lubricating oil supply and scavenge lines for the drive gearbox were fully plumbed, while the lines for the torquing gearbox were run part way and temporarily dead-ended (to be completed prior to the installation of the torquing gearbox). Next, the oil dispenser pump was wired to the appropriate power line and to the control panel switches. Displacement probes and thermocouples were installed

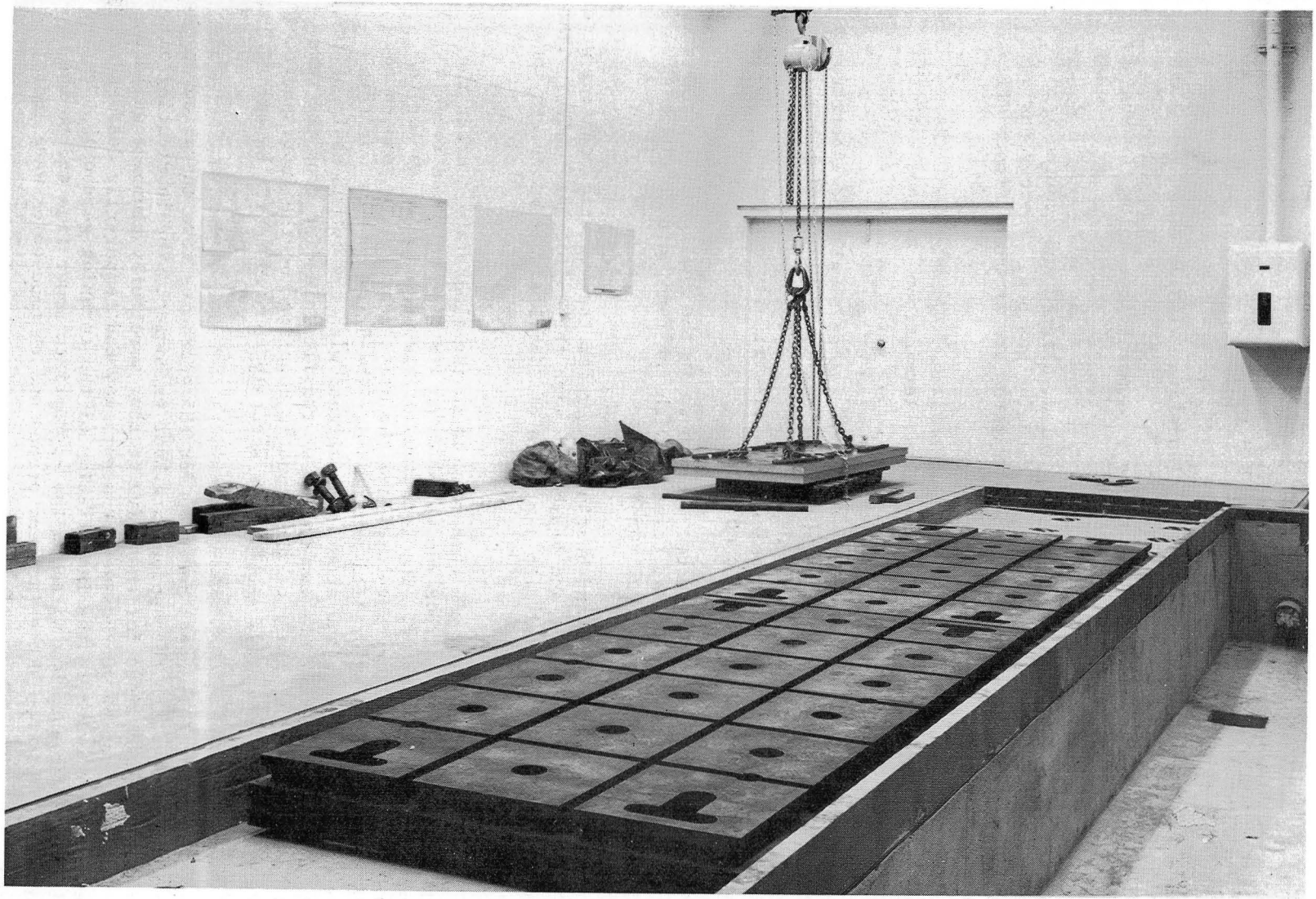

Fig. VII.9 Interior of Test Enclosure Showing Motor Plate and Floorplate Before Grouting

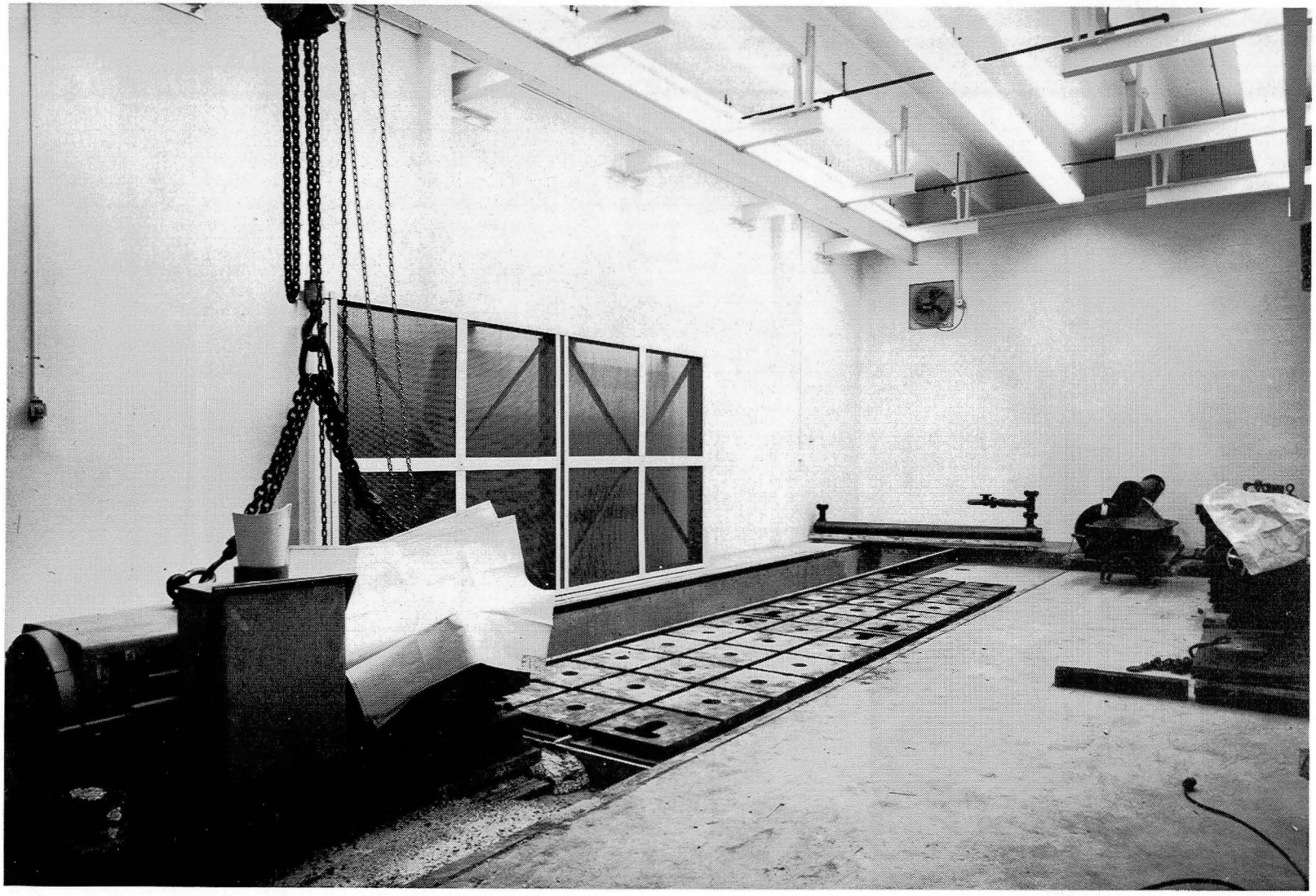

Fig. VII.10 View of Motor Baseplate Grouted in Place Before Grouting of Floorplate

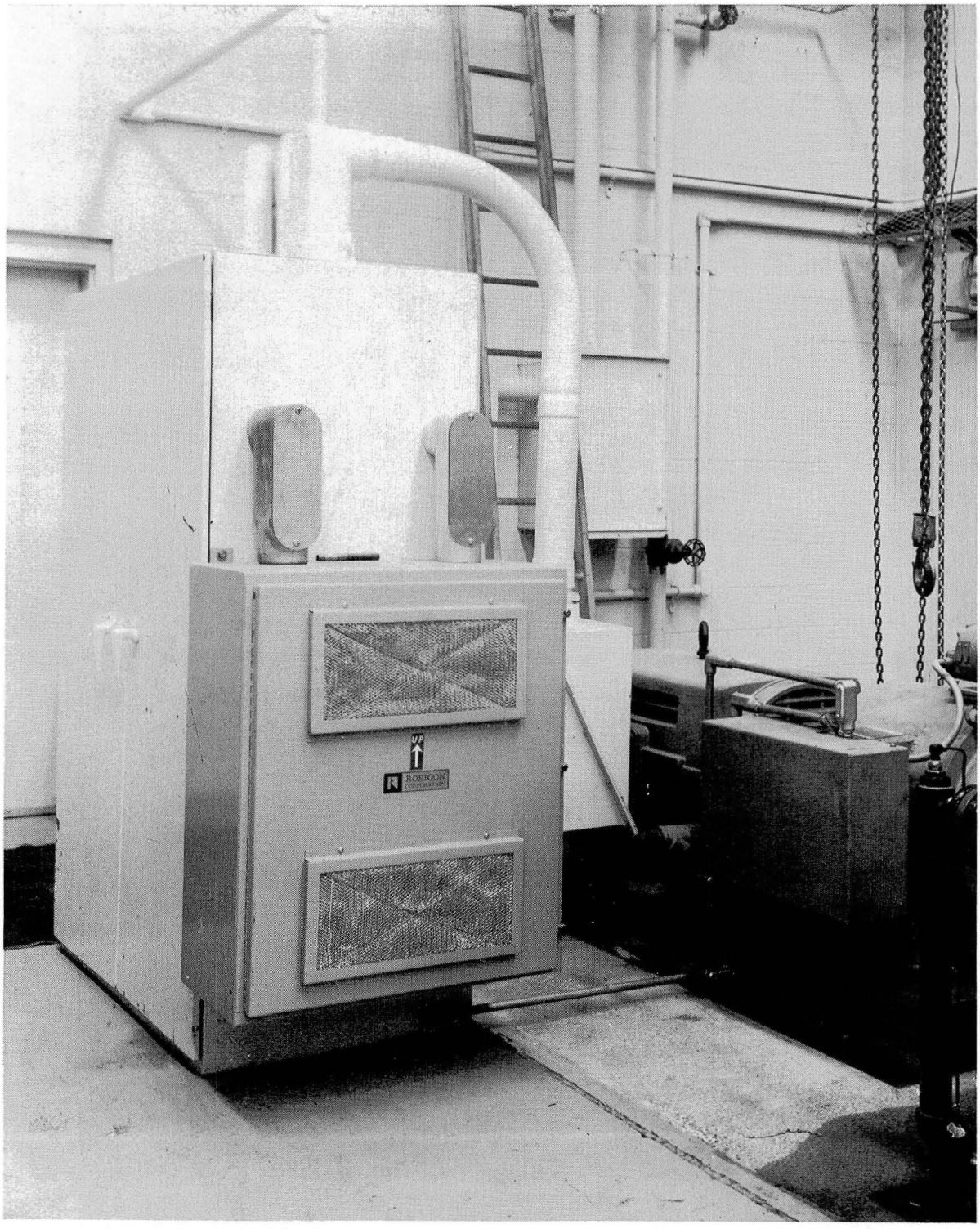

Fig. VII.11 Original Across-The-Line Starter and Solid State Starter for Drive-Motor of Supercritical Shaft Test Rig

in the drive gearbox, and the top cover of the gearbox replaced with a clear plastic cover, to permit viewing of the inside of the gearbox during low-speed operation. (During high-speed operation, no one is permitted to be in the test cell.) The oil pressure and sump level trip-outs for the magnetic coupling were installed in the drive gearbox lubricating oil supply line and in the gearbox lubricating oil sump, respectively. An additional pressure trip-out was installed in the oil supply line for use by the torquing gearbox at a later date. The torquing gearbox was actually mounted and plumbed at the time of assembly of the low speed shafting, approximately two years later. Photographs of the test cell during the plumbing of the drive gearbox are presented in Figures VII.12 through VII.14.

OPERATIONAL CHECKOUT OF DRIVE SYSTEM

The operation of the test rig drive system and drive gearbox was very carefully checked. First, the drive motor was started in low-speed mode; it ran smoothly with no problems. The drive motor was then run in the high-speed mode with the same results. The magnetic coupling was coupled to the drive gearbox and the drive system was run to the full low range speed limit of the motor, which is 1800 rpm and corresponds to 10,000 rpm on the high-speed side of the drive gearbox. The drive motor and magnetic coupling ran without any problem, and no significant vibration or dynamic response of the drive gearbox was observed.

The drive system and drive gearbox were then run in the high-speed mode to 18,000 rpm on the high-speed side of the drive gearbox, at which point significant dynamic runout was observed on the drive gearbox high-speed pinion shaft. A one-plane balance of the drive gearbox high-speed pinion shaft was conducted using the balancing holes located in the end of that shaft. Balancing data was taken at 18,000 rpm and a correction of approximately 28 grams (1 oz) was installed in the correction holes on the end of the shaft. The dynamic runout of the pinion shaft at 18,000 rpm was reduced from more than 100 microns (4 mils) peak-to-peak to less than 8 microns (0.3 mil) peak-to-peak. This unbalance was due to the use of a shaft key that did not precisely fit the keyway on the end of the drive gearbox high-speed pinion shaft when mounting the high-speed coupling. After this balancing operation, the test rig drive motor and drive gearbox were run to full speed (20,000 rpm on the high-speed pinion shaft) with smooth operation of the drive motor, magnetic coupling, and drive gearbox. At 20,000 rpm, the amplitude of vibration of the drive gearbox high-speed pinion shaft was still less than 50 microns (2 mils) peak-to-peak.

HIGH-SPEED TEST COMPONENTS

After the drive system was checked out, the remainder of the high-speed test hardware was assembled. First, the drive end high-speed spindle was assembled and aligned with the drive gearbox to less than 25 microns (1 mil) total indicator reading (TIR) using a dial indicator. This misalignment was well within the capacity of the disc-type flexible coupling between the gearbox and the spindle.

Second, the driven end high-speed spindle was assembled and installed in the test rig. Although this spindle was designed to be installed on the same baseplate as the torquing gearbox, a temporary baseplate just for the spindle was used at this time, since the torquing gearbox was not needed. The two high-

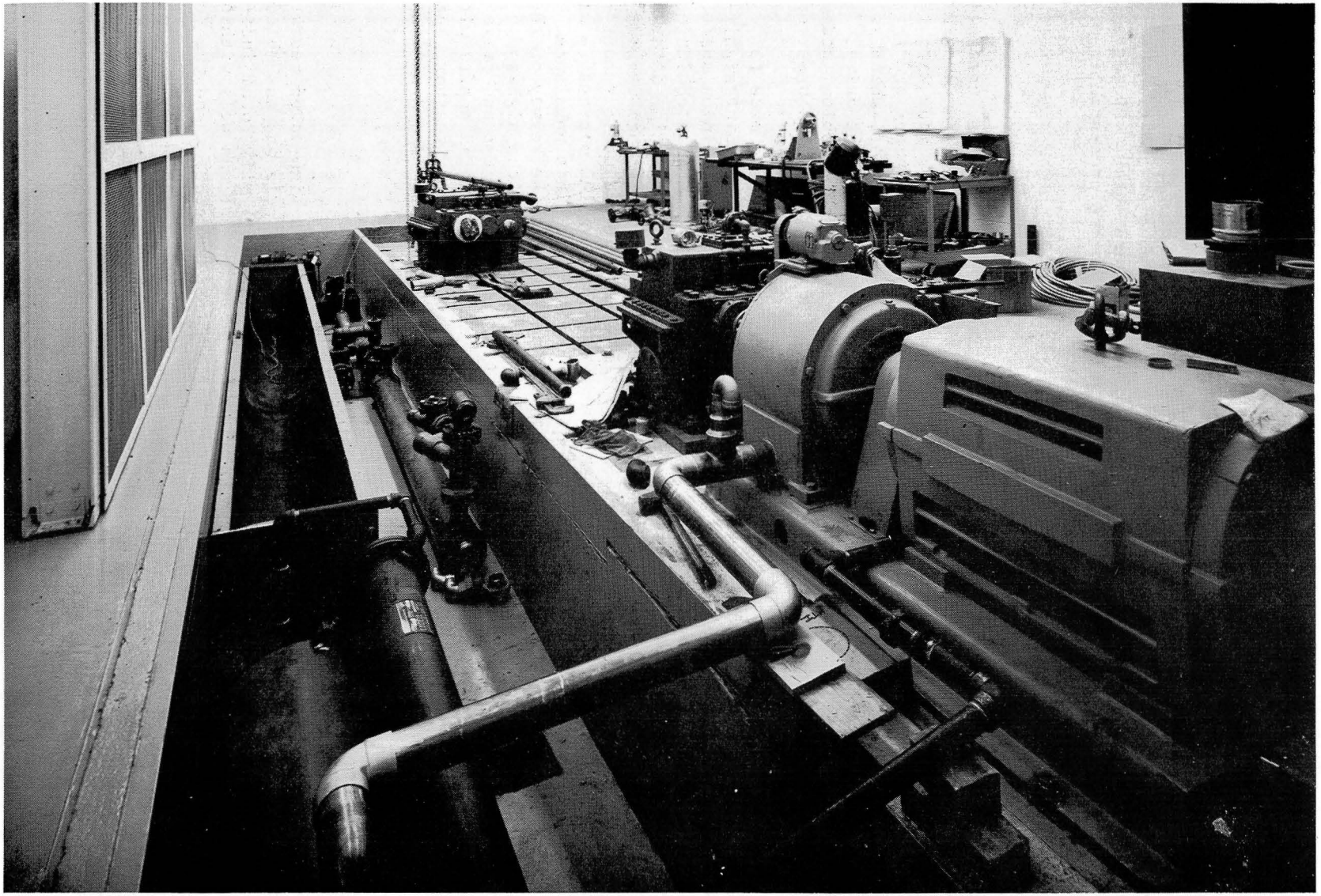

Fig. VII.12 View of Hardware Pit and Completed Plumbing of Magnetic Coupling Cooling System

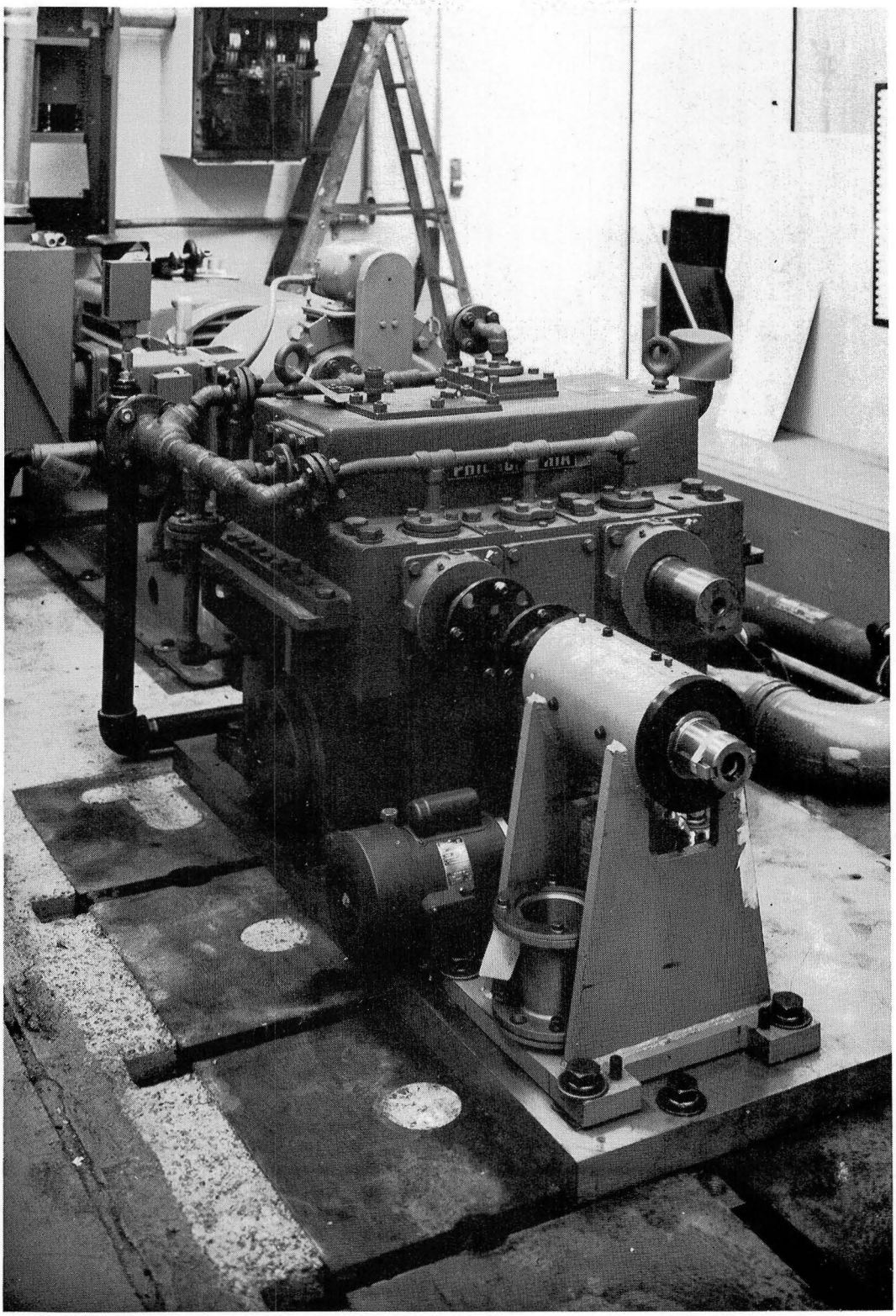

Fig. VII.13 Drive Gearbox and High-Speed Spindle Mounted on Drive Gearbox Baseplate

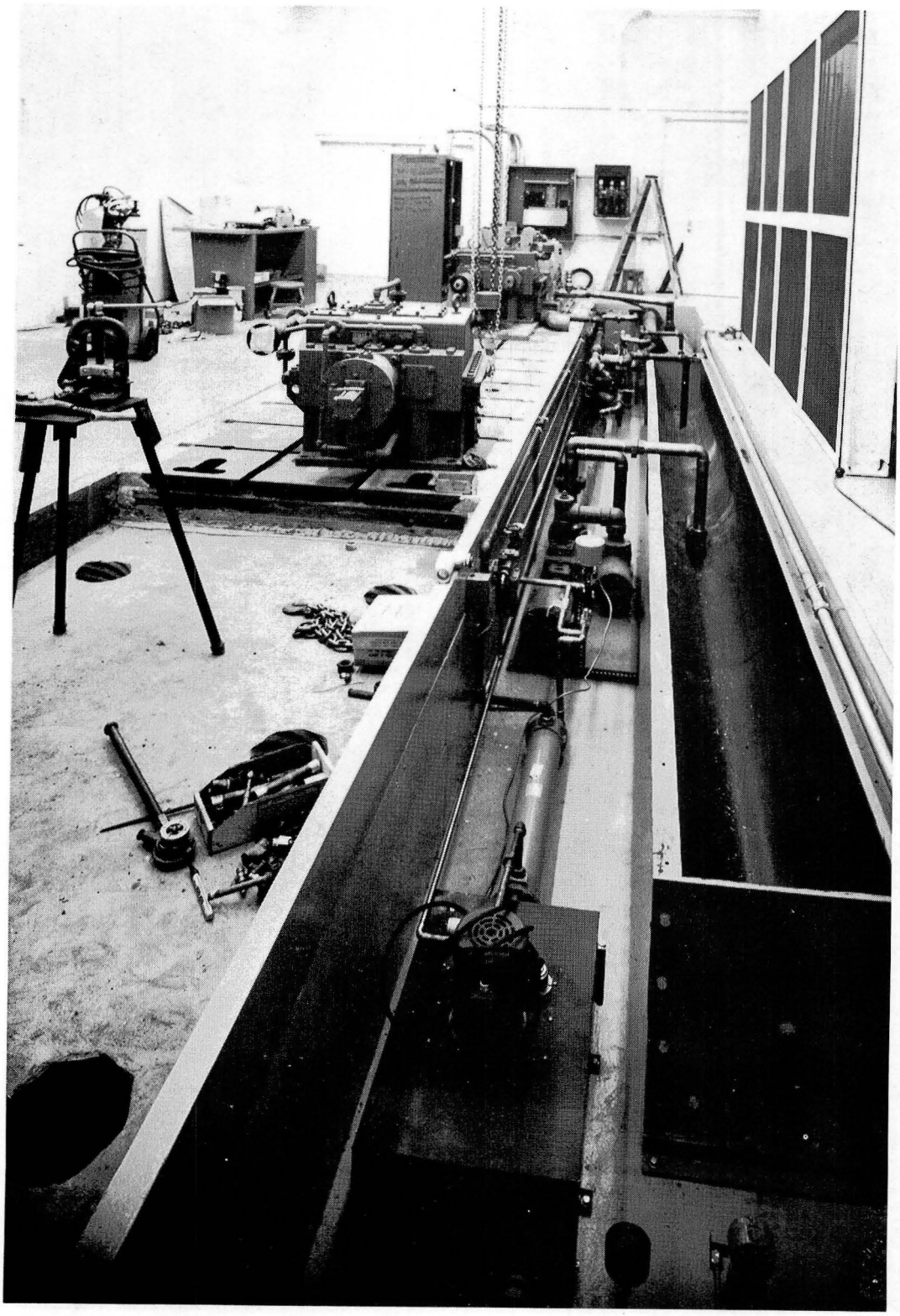

Fig. VII.14 View of Hardware Pit Showing Oil Dispensers for Gearbox and High-Speed Spindle Lubrication

speed spindles were aligned with each other by means of an optical alignment target in both ends of each spindle. The manufacturing tolerances of the targets in the spindle shafts were such that the intersection of the crosshairs on the targets was within 25 microns (1 mil) of the center of rotation of the high-speed spindles. An optical alignment telescope was then mounted to the far side of the driven end high-speed spindle such that its line of sight passed through the center of both spindles. The telescope was aligned such that its crosshairs were precisely aligned with the crosshairs from both targets in the drive end high-speed spindle. The position of the driven end spindle was adjusted until the crosshairs of both targets in that spindle also coincided with the crosshairs in the optical alignment telescope. At that point, it was estimated that tne two high-speed spindles were aligned with each other within 250 microns (10 mils) on the center line of the spindle shafts. This misalignment is eqivalent to less than 1 micron per cm (0.1 mil per in.) of distance between the spindles.

The oil dispenser and heat exchanger for the lubrication oil supply for the high-speed spindles were installed in the hardware pit. A scavenge pump was installed next to each high-speed spindle. The components of the system were then properly plumbed together. A cartridge-type oil filter was installed in the high-speed spindle lubrication oil system. A spindle oil pressure trip-out was set to disengage the magnetic coupling if the pressure of the lubrication oil supply from the spindles fell below 140 kPa (20 psi), and a spindle filter pressure trip-out was set to disengage the magnetic coupling if the pressure drop across the oil filter was high enough to cause the filter to bypass.

After the test shaft components were fabricated, the ends of the aluminum tubing were machined to be circular, straight, and within the proper diameter tolerance to provide for the designed interference with the end adapters. The tube was straightened by mounting the ends in specially fabricated teflon supports and pressing the center of the tube in the direction opposite the initial bow with a specially designed teflon-lined press. In this way, the bow in the shaft was reduced from about 1.65 mm (65 mils) total indicator reading in the center of the shaft to about 0.5 mm (20 mils). Seven balance rings and the two end adaptors were mounted on the tube while maintaining proper alignment of these components with the tube and with each other. Two Rexnord Model 52X coupling hubs were modified to match the end adaptors and special minimum clearance shoulder bolts were fabricated for assembly of the couplings.

The test shaft was initially installed in the test rig before the high-speed spindles were aligned to determine the proper axial spacing of the high-speed spindles. It was found, however, that the high-speed spindles could not be aligned with the test shaft installed due to reflection of the light through the slightly curved test shaft. The test shaft was, therefore, removed before the high-speed spindles were optically aligned. The optical alignment targets were then removed from the high-speed spindles and the test shaft was reinstalled (the alignment targets were not designed to be rotated at high speeds).

INSTRUMENTATION

Seven probe brackets were installed in the test rig, one adjacent to each of the balancing rings on the test shaft. The probes were installed in the probe brackets, which were then accurately lined up with the test shaft, and bolted to the floorplates.

A displacement probe was installed at the output end of the high-speed pinion of the drive gearbox and properly gapped from the pinion shaft. Two displacement probes were installed in each of the high-speed spindles for observing the vertical shaft motion just inboard of the spindle bearings. Initially, seven vertical probes and two horizontal probes were installed in the shaft probe brackets, one vertical probe adjacent to each of the balancing rings and the horizontal probes adjacent to one of the end planes and to the center plane. During some tests, as many as fourteen probes were installed.

A number of thermocouples were installed in the test rig. Initially, two iron-constantan thermocouples were put directly inside the drive gearbox to monitor the temperature of the oil in the drive gearbox during the checkout of the drive system. However, after these temperatures were found to be consistently low, these thermocouples were dropped from use since the remainder of the thermocouples used were copper-constantan. Strap-type thermocouples were installed on the 15 cm (6 in.) drain pipe from the drive gearbox. Thermocouples were installed near each of the high-speed spindle bearings to monitor spindle oil temperature. Later, we put a thermocouple in the magnetic coupling to measure the magnetic coupling cooling water temperature and a thermocouple in the inlet lubrication oil pipe for the drive gearbox. Additional thermocouples were installed when the torquing gearbox and low-speed side of the test rig were assembled.

A Fotonic Sensor® (photo-optical pickup) was installed for use as a speed and phase reference. The high-speed coupling hub attached to the drive gearbox was polished and painted half black as a target for the Fotonic Sensor. The output of the Fotonic Sensor is a square wave with which the data acquisition system measures the speed and determines the phase angle of each of the data signals in relation to a coordinate system rotating with the test shaft.

Figure VII.15 is a photograph showing the drive end high-speed spindle and the associated instrumentation, as well as the displacement probe that is installed in the drive box. Part of a test shaft probe bracket can also be seen in this photograph. (The hardware attached to the low-speed side of the drive gearbox in Figure VII.15 was an automobile transmission that was undergoing testing for the Energy Research and Development Administration). The photograph in Figure VII.16 shows the test rig with the probe brackets in place adjacent to the test shaft (additional hardware associated with the transmission test can also be seen in Figure VII.16.) The photograph in Figure VII.17 shows the test rig with the test shaft probes aligned and properly gapped, as well as showing the Fotonic Sensor installed.

The sketch in Figure VII.18 shows the relationship of the phase angle between the displacement probes and the Fotonic Sensor. Indicated in this diagram are the direction of rotation, the location of the Fotonic Sensor, and the relative location of the balancing holes to the Fotonic Sensor target and of the displacement probes to the Fotonic Sensor. Figure VII.19 is a sketch of the actual location of the displacement probes and the numbering system that was used to identify these displacement probes. These probe numbers are used in this report to identify the test shaft response plots presented in later sections.

CONTROL ROOM INSTRUMENTATION

The instrumentation in the control room includes control instrumentation (used for operating the test rig), sensor readout instrumentation (used for observing

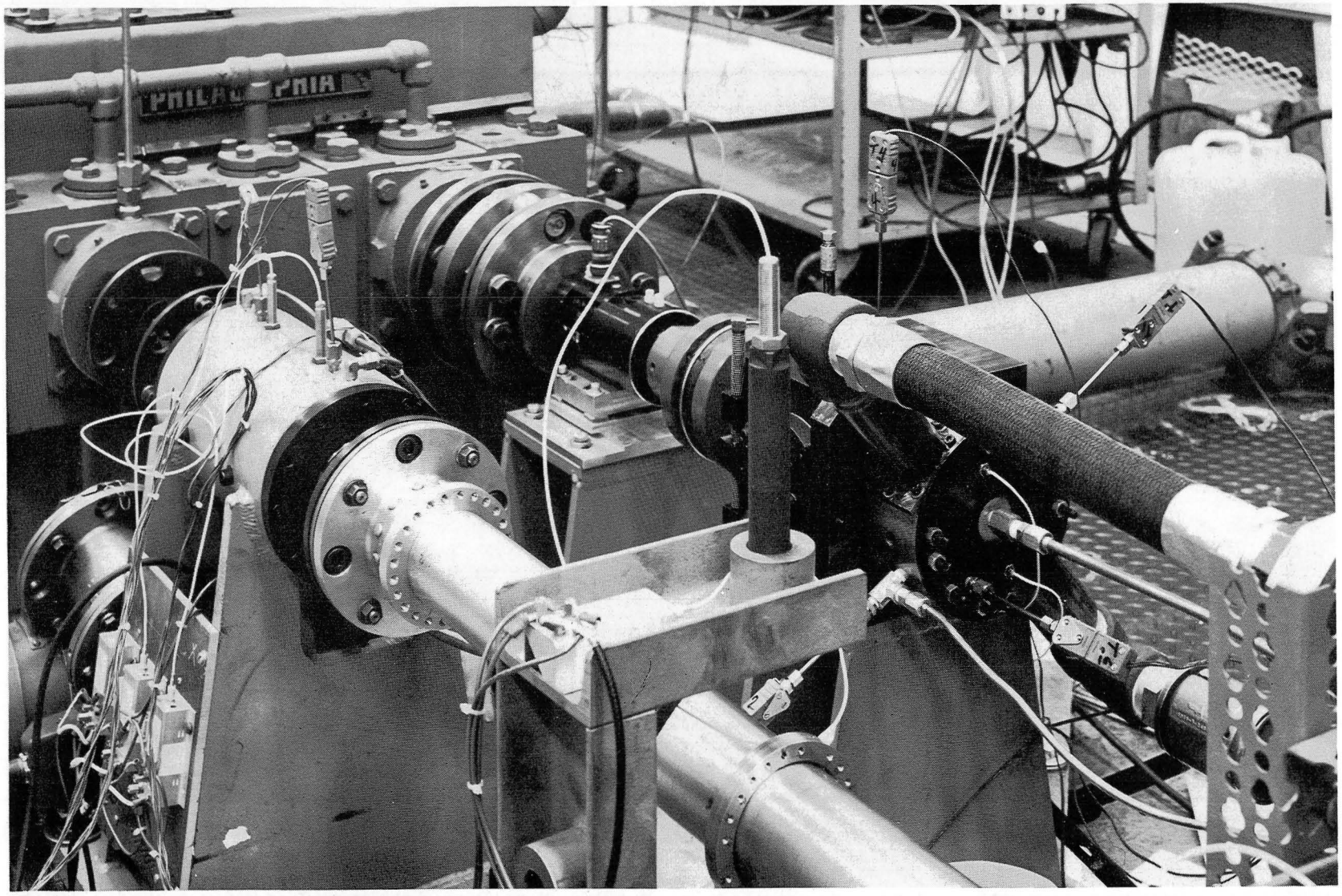

Fig. VII.15 Drive End of Assembled Supercritical Shaft Test Rig

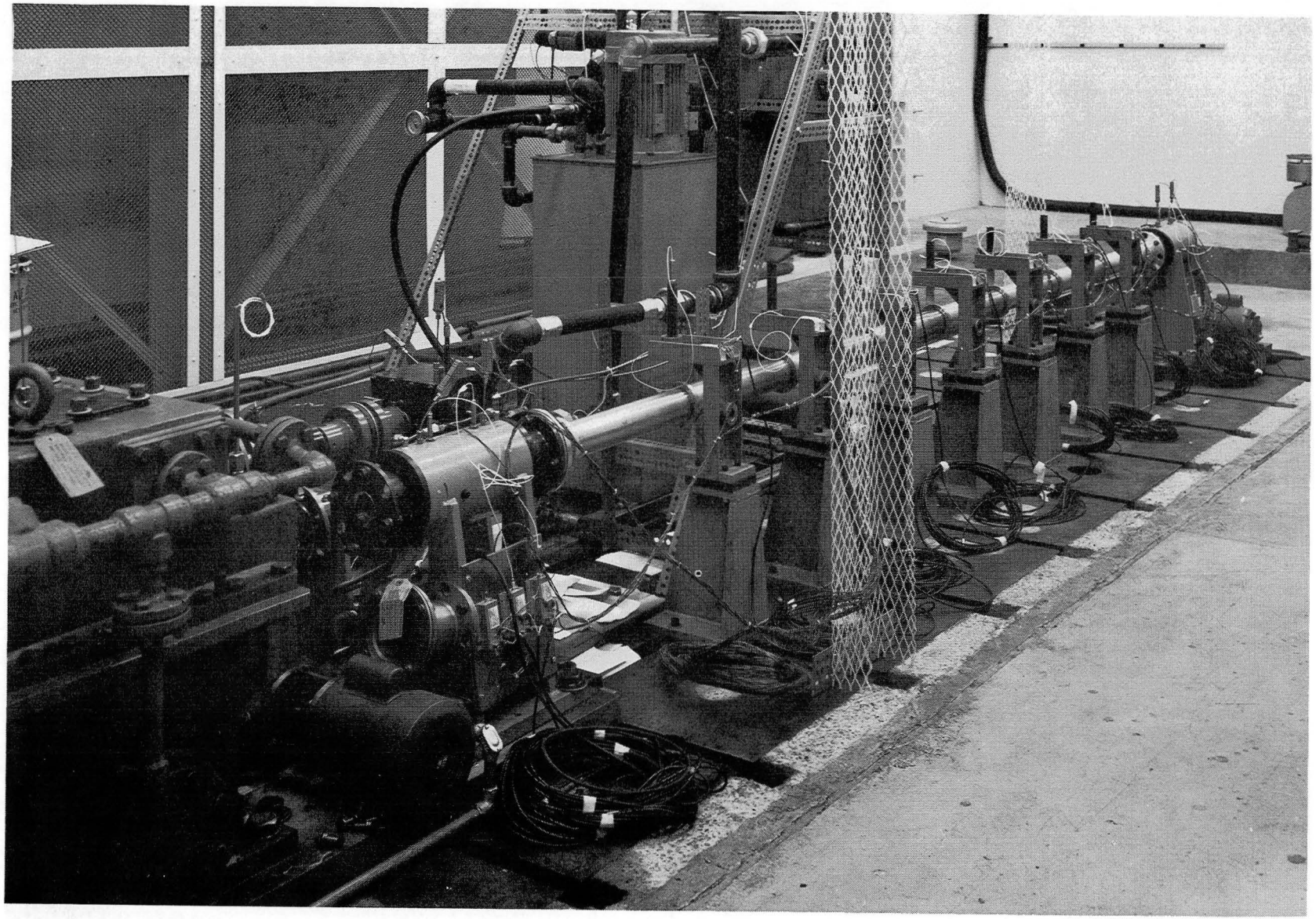

Fig. VII.16 Test Rig with Test Shaft Displacement Probe Brackets Mounted in Place

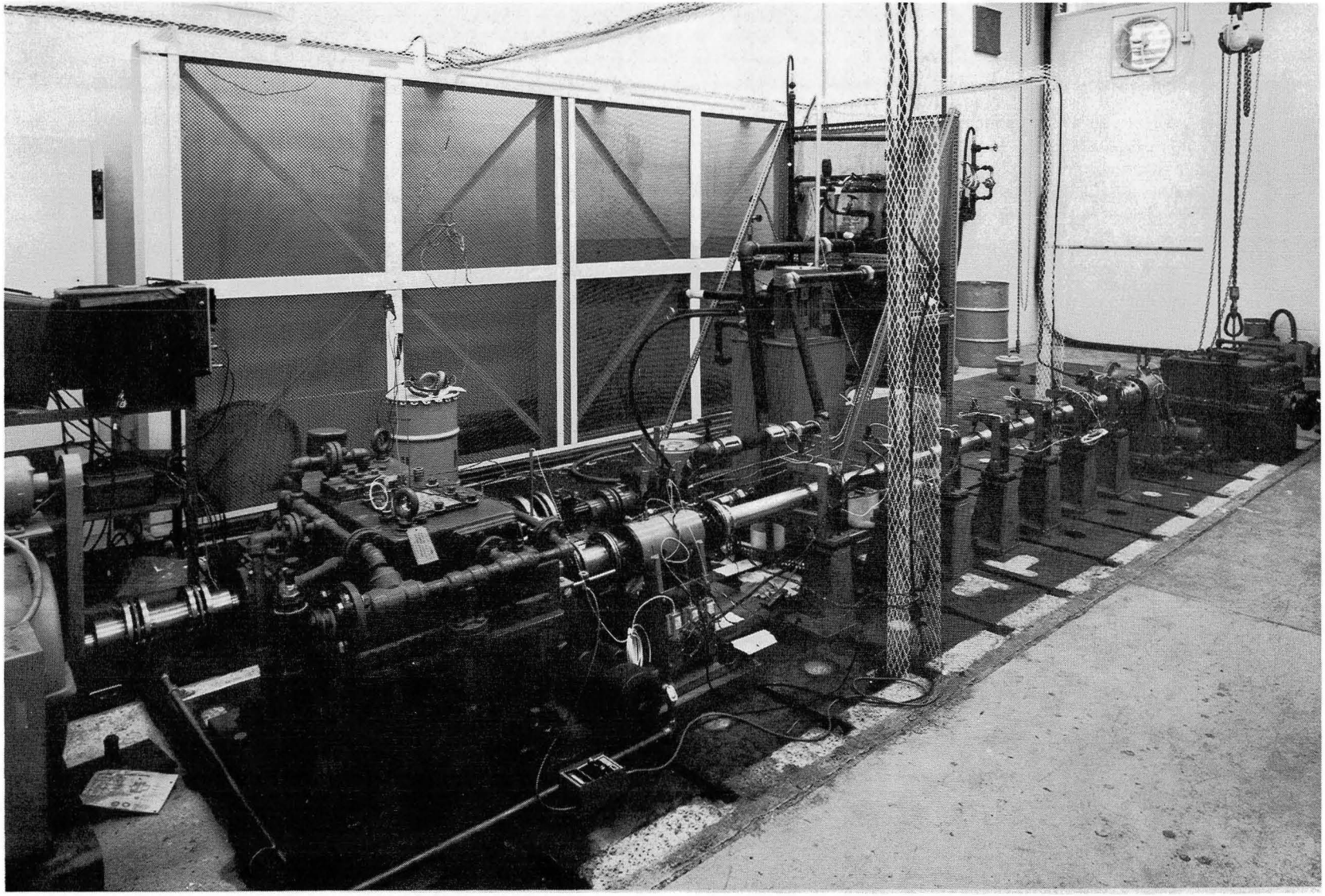

Fig. VII.17 Test Rig with Test Shaft Displacement Probes Installed

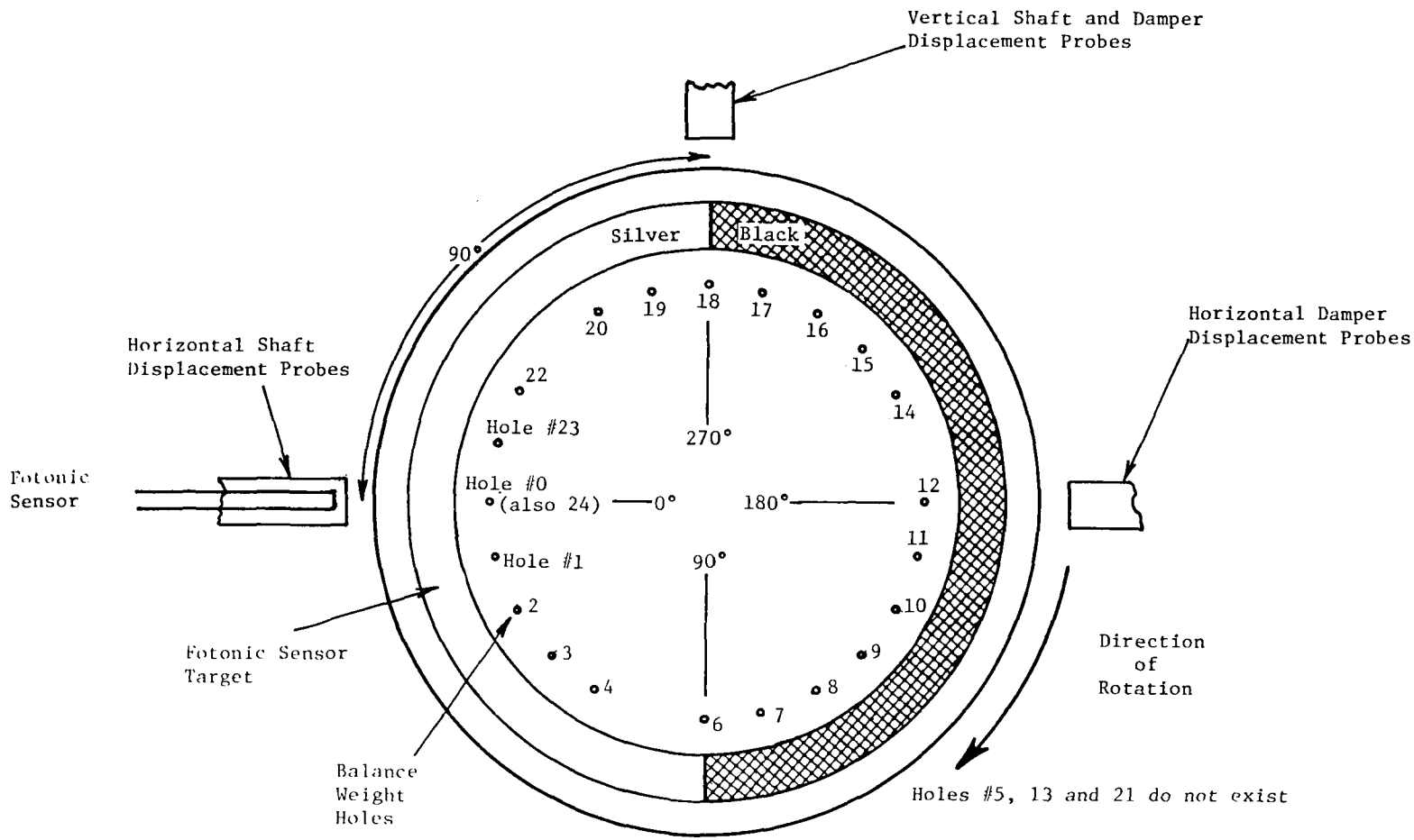

Fig. VII.18 Sketch Showing Phase Angle Reference of Displacement Probes, Fotonic Sensor and Correction Weight Holes with Test Shaft in Zero Degree Position

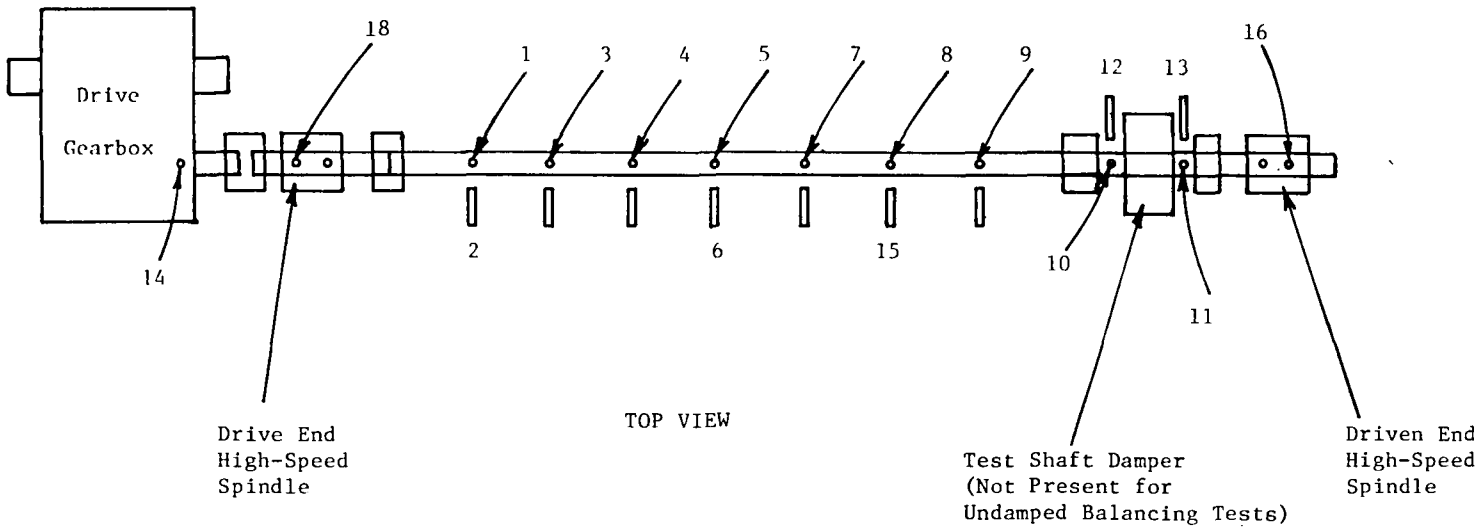

Fig. VII. 19 Displacement Probe Locations as Referred to by Probe Numbers

the operation of the test rig), and a computerized data acquisition system used to acquire quantitative data relating to the vibration of the test rig.

Figure VII.20 is a photograph of the control panel for the supercritical shatt test rig. The console power switch controls the power to all of the other control switches on the panel. The large red emergency stop button shuts off all the power to the control panel and rig. The drive motor is started and run by means of the motor speed switches, the motor start switch (which was added when the new starter was added), the magnetic coupling engage switch, and the speed control potentiometer. The main clutch cooling water switch starts the pump which circulates cooling water through the magnetic coupling. A water pressure guage indicates the line water pressure to the test rig downstream from pressure control valve which regulates the water flow to the test rig. The ammeter on the control panel indicates the drive motor current; the drive system is being overloaded if this current is higher than 320 amps. A meter is also provided on the control panel which indicates the speed of the high-speed test shaft. This speed meter actually operates off the magnetic coupling tachometer with a multiplication factor to take into account the gear ratio in the gearbox. Therefore, this speed meter will register regardless of whether or not the test shaft is actually connected to the drive gearbox. Lubrication oil for the gearboxes is controlled by a switch on the control panel which starts the oil dispenser pump. A pressure gauge on the control panel indicates the discharge pressure of the gearbox lubrication oil pump. Another pressure gauge on the control panel indicates the actual lubrication oil supply pressure to the gearboxes.

On the control panel, another switch starts the lubrication oil pump for the high-speed spindles. The discharge pressure of this pump is indicated by a pressure gauge on the control panel, while two other pressure gauges on the panel indicate the oil supply pressure to each of the high-speed spindles.

At the top of the control panel is a row of warning lights which indicate the reason for a trip-out of the magnetic coupling if such a trip-out does, in fact, occur. This row of trip-out lights includes warning lights for:

1. Low oil pressure in high-speed spindle
2. Low oil pressure in gearbox
3. Low water pressure in clutch
4. High water temperature in clutch
5. Low sump oil level in gearbox
6. High filter pressure drop in high-speed spindle
7. Torquing/gearbox piston at end of stroke

Additionally, a limit switch controlling the torquing gearbox stroke limit was installed with the torquing gearbox just piror to the torque tests.

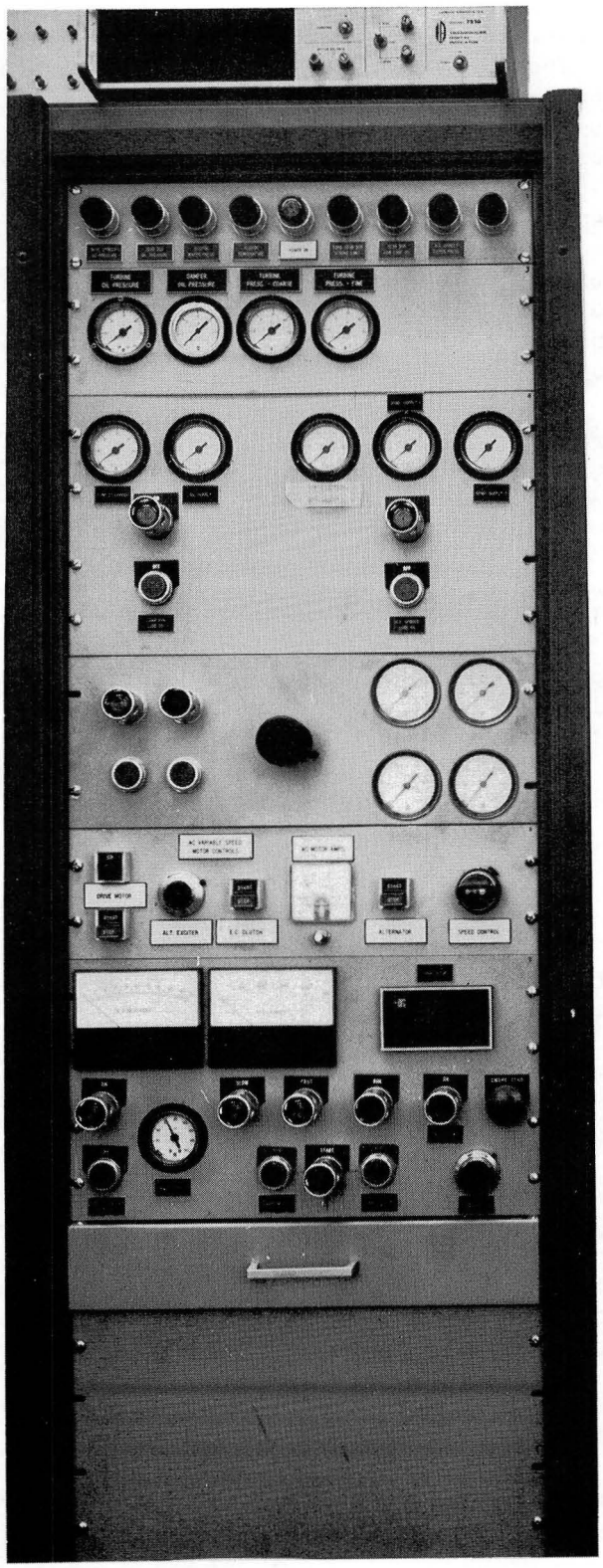

Fig. VII.20 Control Panel for Supercritical Shaft Test Rig

The torquing gearbox controls and gauges were installed at the same time as the torquing gearbox. These controls include a switch to start the hydraulic oil pump, a switch to engage the solenoid that controls oil flow to the torquing piston and an air regulator to control the level of torque being applied in the torquing gearbox. Pressure gauges register the discharge pressure of the hydraulic oil pump, the pressure on each side of the torquing piston, and the air pressure downstream of the air regulator.

There are six rack-mounted, dual-channel oscilloscopes in the panel, shown in Figure VII.21, which display test rig vibrations. These oscilloscopes have differential input amplifiers to eliminate the common problem of ground loops in the sensor circuits.

During initial operation, test rig temperatures were displayed on the multipoint temperature recorder shown in Figure VII.6. Later, digital readout with a 20-position switch, shown in Figure VII.21, was installed for monitoring temperatures.

An analog tape recorder was used for recording dynamic behavior of the test rig. The CEC Datatape model VR-3300 records 14 channels of information on standard 1-inch magnetic tape. Signals from most of the displacement probes, output from the Fotonic Sensor, and a voice track were recorded. Preamplifiers on the recorder were calibrated to attenuate displacement probe signals by a factor of 10 because the Bently displacement probe output usually exceeds the 1 volt rms saturation of the tape recorder.

The computerized data acquisition system discussed previously and shown in Figure VII.11 has the following major components:

- Hewlett-Packard model 5323A tachometer
- Vibration Instruments Corporation model 235DS dual-channel tracking filter
- Dranatz model 305 phase meter
- Hewlett-Packard model 3480D digital volt meter
- 20 channel computer-controllable scanner, designed and built by MTI.

Within the cabinet shown in Figure VII.7 are some specialized MTI electronics including decoupler boards, a reference signal conditioning board, and scanner control boards. The data acquisition system is controlled and monitored by a PDP 11/34T minicomputer, previously shown in Figure VII.8.

The tachometer, voltmeter and phase meters of the data acquisition system provide Binary Coded Decimal (BCD) outputs. The minicomputer sets the scanner channel, monitors the digital outputs, converts the BCD data into binary form, stores the data (in large volume) and anlayzes the data in a variety of ways.

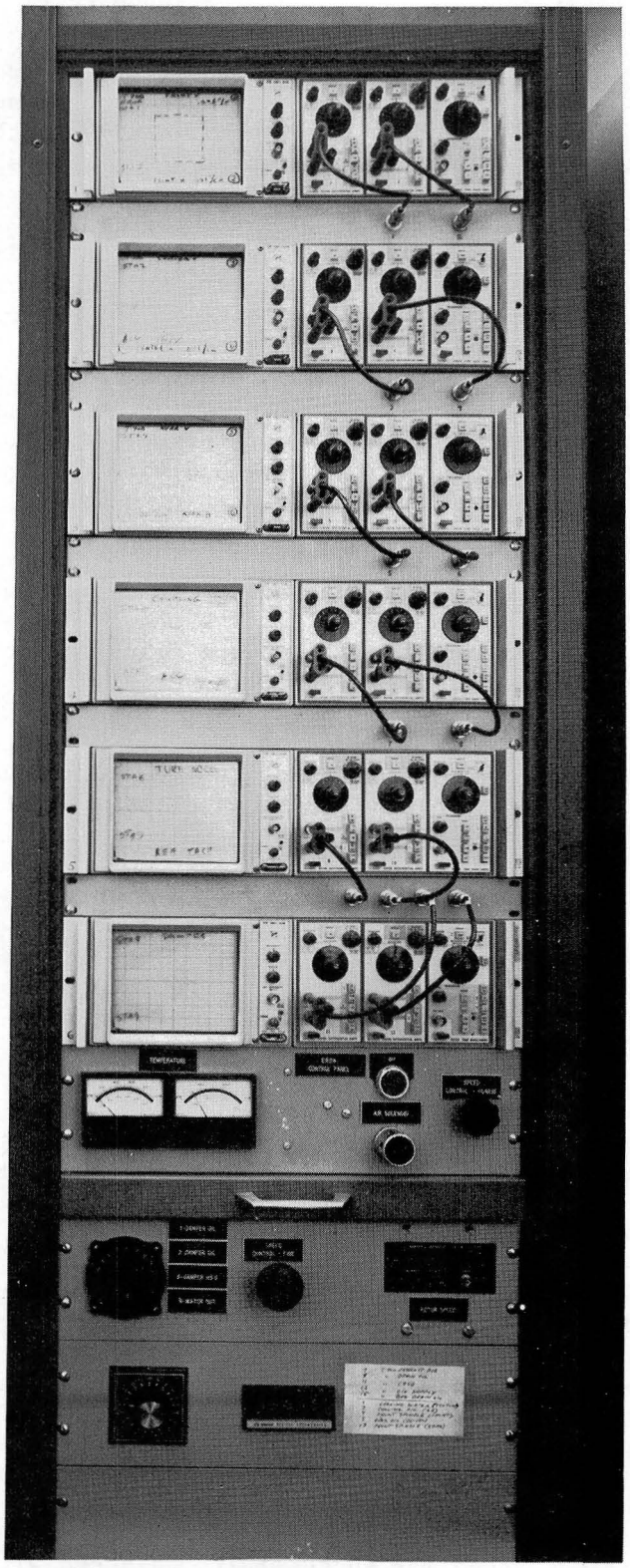

Fig. VII.21 Oscilloscopes and Digital Temperature Readout for Monitoring of Supercritical Shaft Test Rig Operation

VIII. PRELIMINARY TEST RESULTS - UNDAMPED SHAFT

An important purpose of this test program was to evaluate the relative significance of balancing and damping in the effective operation of supercritical shafts. While it was not considered likely that balancing, without explicitly designed damping, could ensure long-term operation with acceptable vibration, a baseline reference was sought for which minimum damping was present. This section covers an initial series of tests in which the minimum amount of damping was allowed to influence the running of the shaft. A preliminary rotordynamic analysis of the undamped test rig is documented in Reference (12). For the rig as finally configured, the predicted critical speeds were 800, 3400, 7000, and 14000 rpm, for the mode shapes shown in Figure VIII.1

"Pre-balancing" of the test shaft was performed by placing in the seven balance planes a correction weight to approximately counteract the mass eccentricity due to shaft bow. Computerized balancing proceeded with the initial purpose of negotiating the first critical speed. A number of balancing runs were performed, to the point that the estimated residual unbalance was of the order of 0.4 gm-cm in the center plane. At this point, it became clear that the extremely low level of damping was a severe handicap in achieving the necessary level of balance to negotiate the first critical speed. While the speed of the test rig could be held constant within two rpm, fluctuation of two rpm was sufficient to cause 30 degrees of phase angle variation in the vicinity of the first critical speed.

To minimize the impact of these speed fluctuations, an active data acquisition scheme was implemented which continuously sampled data, rejecting all data points until the required speed was met within a very small tolerance ($\pm$0.1 rpm). This allowed a much clearer indication of the rotordynamic behavior of the test shaft. By careful interpretation of the data obtained, and by use of a final correction weight of 20 mg, unbalance in the rotor was reduced sufficiently to allow negotiation of the first critical speed without the use of any type of shaft dampers. Plots of the synchronous response of the test shaft at the vertical probe at the center of the shaft, before and after balancing of the first critical speed, are presented in Figure VIII.2.

Photographs of the test shaft orbits at three different probe locations for two different speeds are presented in Figure VIII.3. All of these orbits reflect the shape of the test shaft surface and this shape was quite irregular with four high spots. The orbits at 800 rpm show very little response at the first critical speed and essentially reflect the static runout of the test shaft. The orbits at 484 rpm reflect the effect of a gravitational critical of the test shaft. A gravitational critical occurs when asymmetric shaft stiffness parametically excites a critical speed at twice running speed.

Near the first critical speed, the response of the test shaft at a particular speed varied with time, even though the speed acquired was held constant within 0.1 rpm. The time dependence is demonstrated by the polar plots presented in Figures VIII.4 and VIII.5 The time dependent response appears to be caused by a time variation in the critical speed.

Although the first critical speed was successfully balanced with no external damping, once above the first critical speed, vibrations of significant amplitude persisted. The principal vibration component was nonsynchronous and

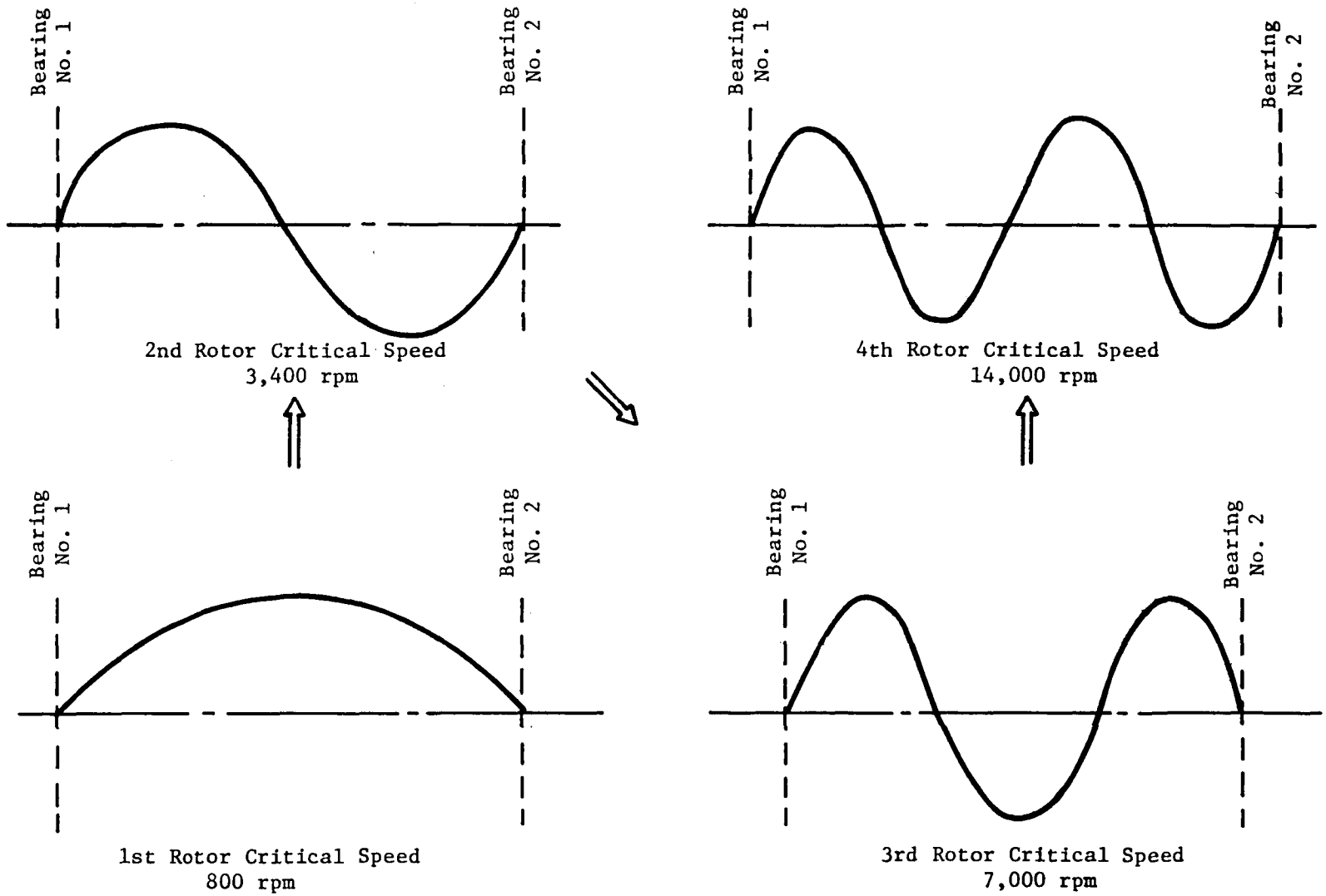

Fig. VIII.1 Mode Shapes of First Four Critical Speeds for Undamped Test Shaft

791013

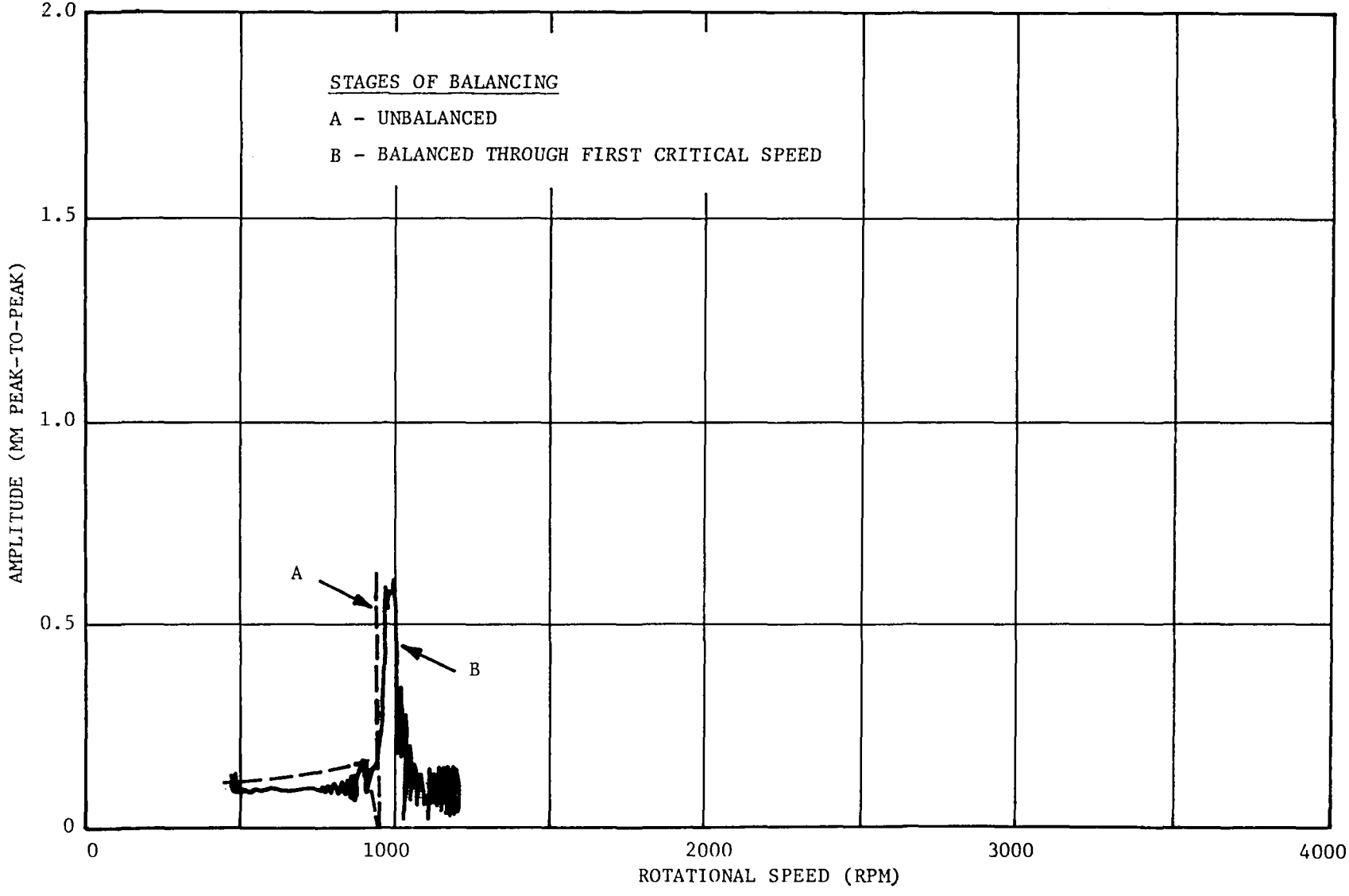

Fig. VIII.2 Synchronous Response of Test Shaft with No Damper as a Function of Speed at Each Stage of Balancing (at Probe No. 5)

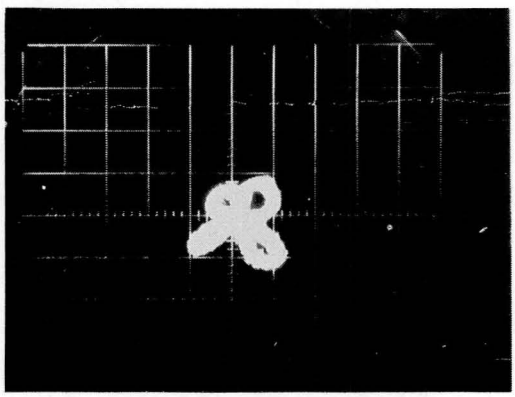

#1 Vert., #2 Horz., 800 rpm

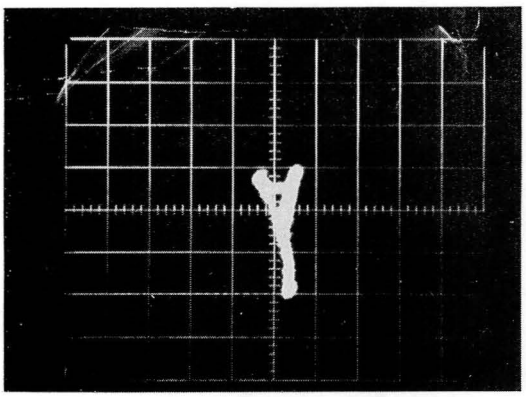

#8 Vert., #15 Horz., 484 rpm

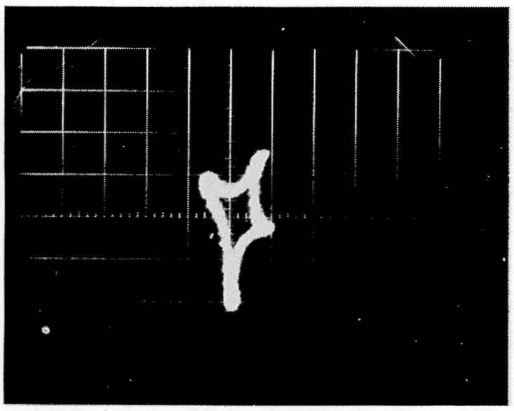

#5 Vert., #6 Horz., 800 rpm

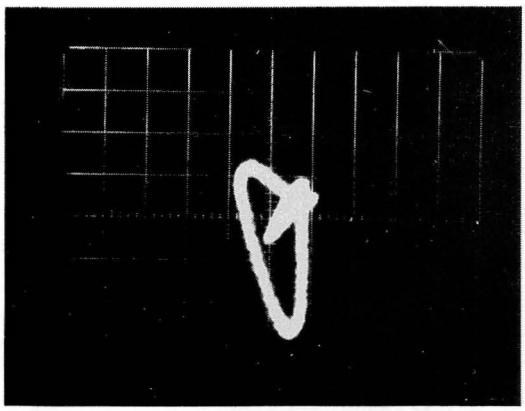

#5 Vert., #6 Horz., 484 rpm

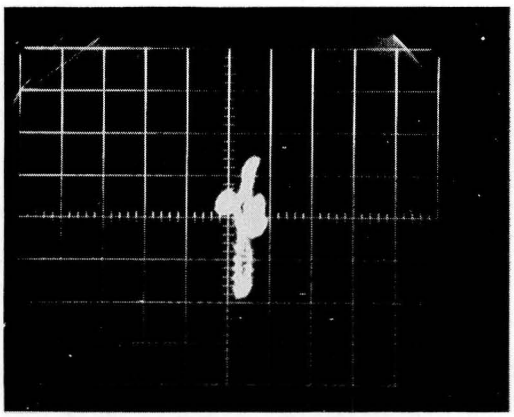

#8 Vert., #15 Horz., 800 rpm

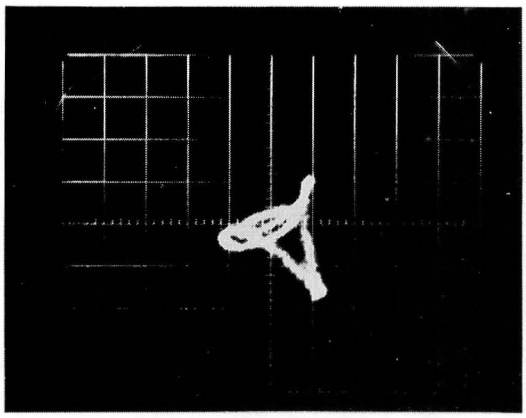

#1 Vert., #2 Horz., 484 rpm

Fig. VIII.3 Photographs of Undamped Test Shaft Orbits

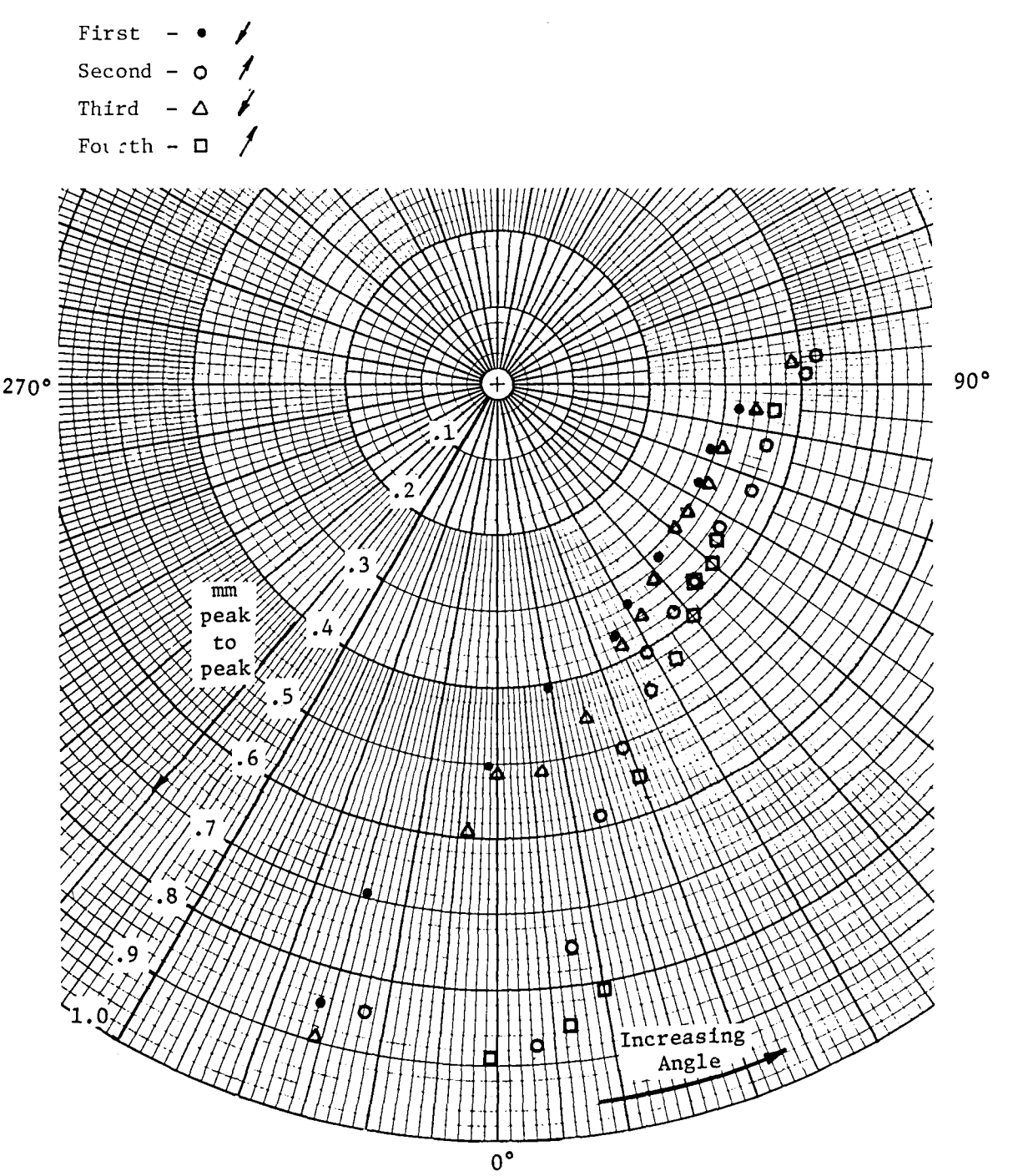

Fig. VIII. 4 Polar Plot of Undamped Test Shaft Response for Run #30A

Order of Data (Increasing Time in Direction of Arrow)

First - • ↗

Second - o ↗

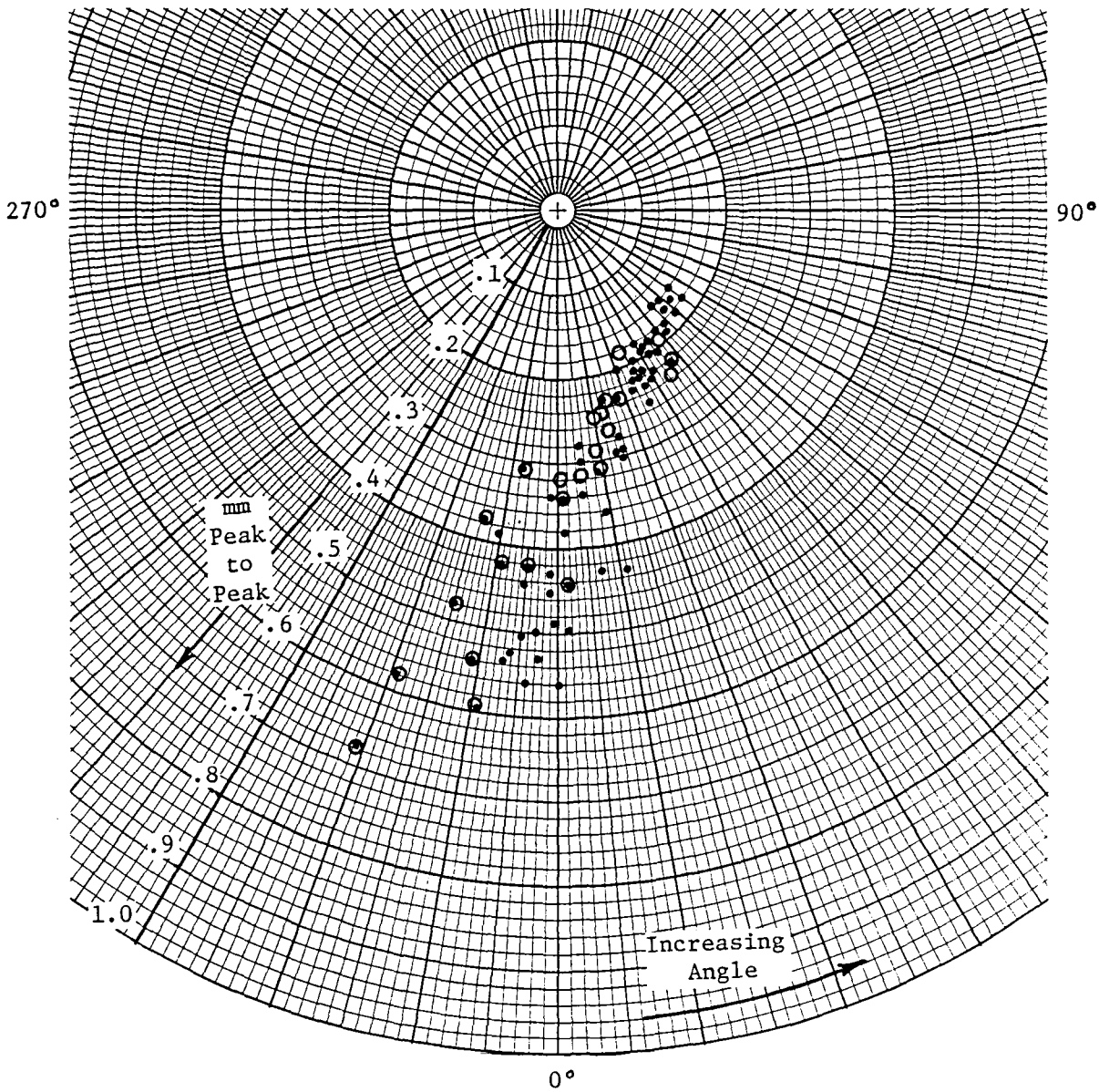

Fig. VIII.5 Polar Plot of Undamped Test Shaft Response for Run #30B (After Addition of 330 mg Weight)

of the first critical speed frequency, shown in Figure VIII.7. This indicate the presence of an incipient instability whose source may be internal fricti in the shaft, or in the disc packs of the high-speed couplings. Figures VII and VIII.7 are frequency spectrum plots of the test shaft vibration at speed below and above the first critical speed. Figure VIII.6 shows that the test shaft vibration below the first critical speed was primarily synchronous.

Results of the undamped tests indicate that some external damping would be necessary to control synchronous and nonsynchronous test shaft vibrations. To this end, tests were conducted to evaluate the effect of external damping on the response of the test shaft.

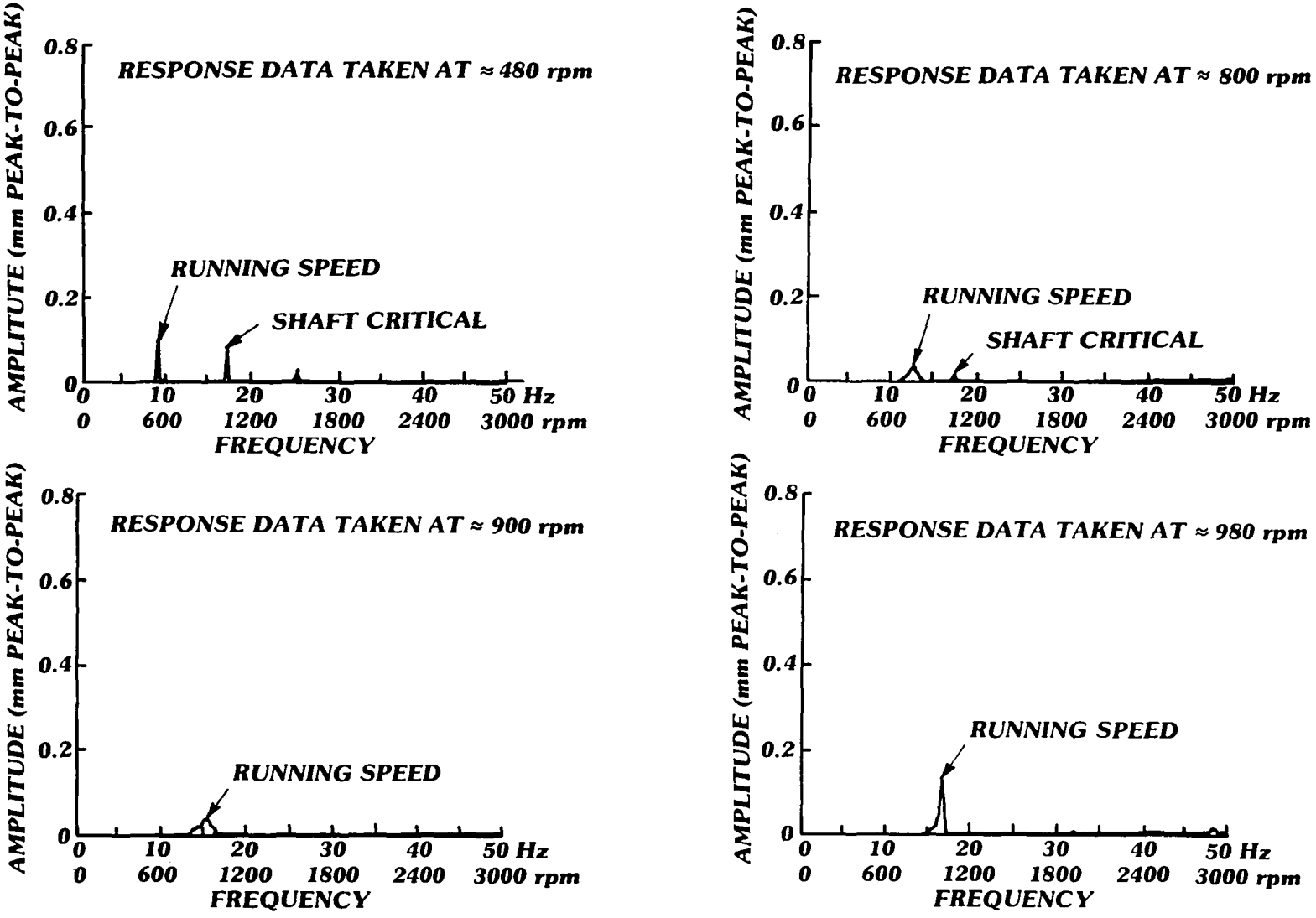

Fig. VIII.6 Frequency Spectrum Plots of Test Shaft Vibration With No Damper Running Below First Critical Speed

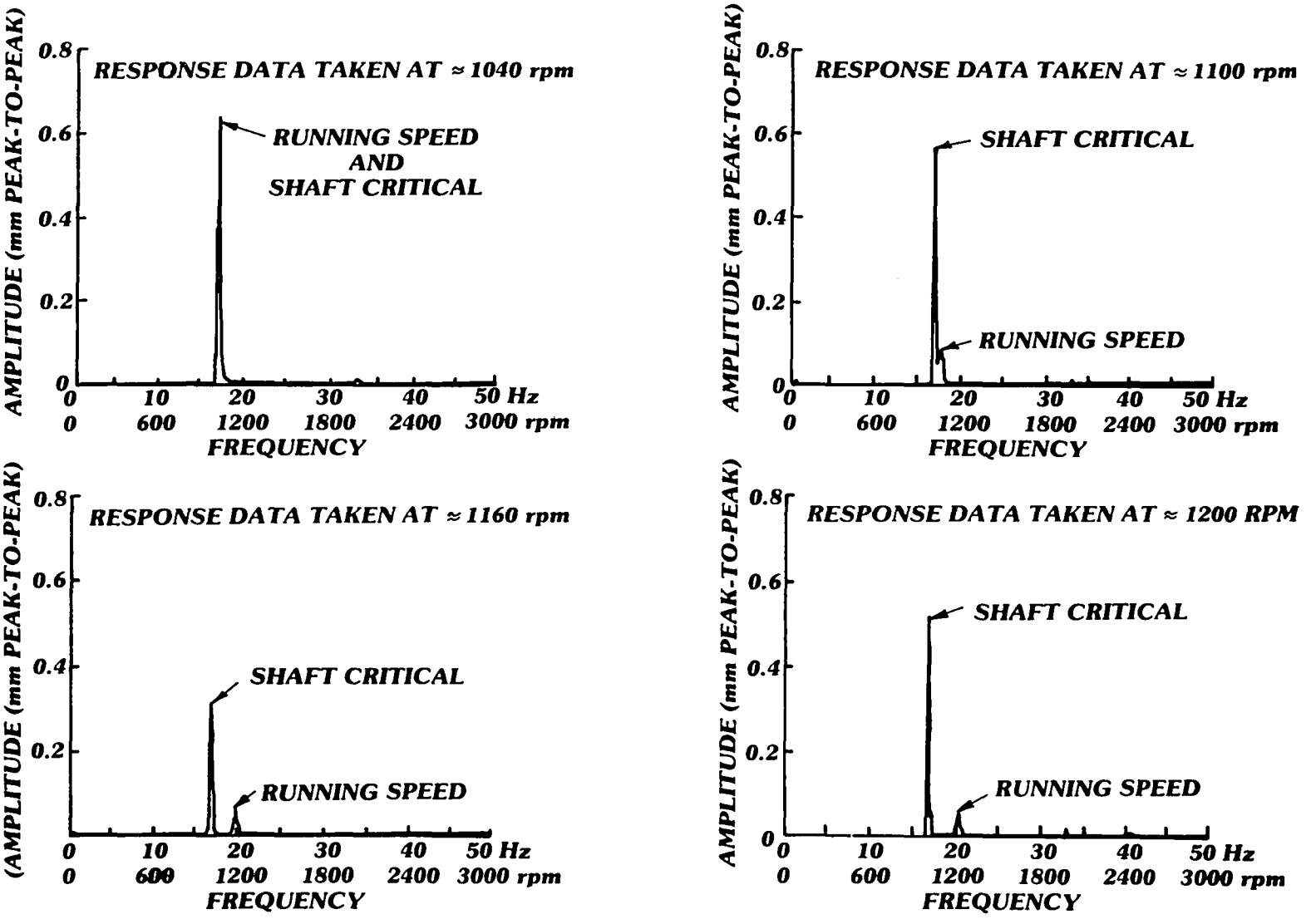

Fig. VIII.7 Frequency Spectrum Plot of Test Shaft Vibration with No Damper Running Above First Critical Speed

IX. SUPERCRITICAL SHAFT VIBRATION CONTROL BY DAMPING

It was established from the undamped tests that some form of external damping, in addition to balancing, would be required for control of synchronous and non-synchronous vibrations. Several methods for applying external damping were investigated, and two of these methods were employed during tests. This section provides a discussion of these methods and the results of these tests.

COULOMB FRICTION DAMPERS

It was decided to design, build, and install simple Coulomb friction dampers to help control the test shaft vibration. Initial design of these Coulomb dampers involved the use of a wooden plunger sliding in an abrasive holder with a leather runner glued to the end of the wood. The wooden plunger, or piston, was spring-loaded and the leather at the end of the piston ran against the shaft while the other end slid in a close clearance against an abrasive surface in its holder. Energy was dissipated by the rubbing of the wooden piston on the abrasive surface. As the tests progressed, the wooden and leather piston was replaced with a single element piston made of teflon. Four of these simple Coulomb dampers were used, one horizontal and one vertical at the two quarter points of the shaft. Two of these dampers are shown in the photograph in Figure IX.1.

The test shaft was easily balanced through the first critical speed, at about 970 rpm, and through the second critical speed, at about 3510 rpm. The Coulomb dampers clearly provided some control of the test shaft vibrations. The test rig was run to 5000 rpm with the Coulomb dampers and at that speed, the damper pistons were having difficulty following the shaft and it was decided not to run the test rig any faster. Although the dampers helped to control the test rig vibration, they did not operate consistently, and the effect of the dampers seemed to change with time. This type of damper, therefore, seems to be a good short-term solution for balancing a supercritical shaft at low speed, but would not be a practical method for providing external damping for continuous high-speed running. Plots of the test shaft response with the Coulomb dampers at each of the six probe locations for various stages of balancing are presented in Figures IX.2 through IX.7.

In these figures, Curve A shows the response prior to negotiation of the first critical. Curve B shows the response after balancing to negotiate the first critical and Curve C shows the response after balancing to negotiate the second critical, while keeping the first critical response acceptable. The peaks in Curve C, when compared for different probes, reflect the mode shapes of the first and second criticals. For example, probes 5 and 6 at the shaft midpoint show substantial amplitude at the first critical and negligible amplitude at the second critical. Probes 4 and 7, at the 3/8 and 5/8 points, participate strongly in both criticals.

The first critical was balanced by adding weight at the central balance ring. The second critical was balanced by adding weight at each of the two quarter points as an equal and opposite pair. The values to be added were determined by the influence coefficient method.

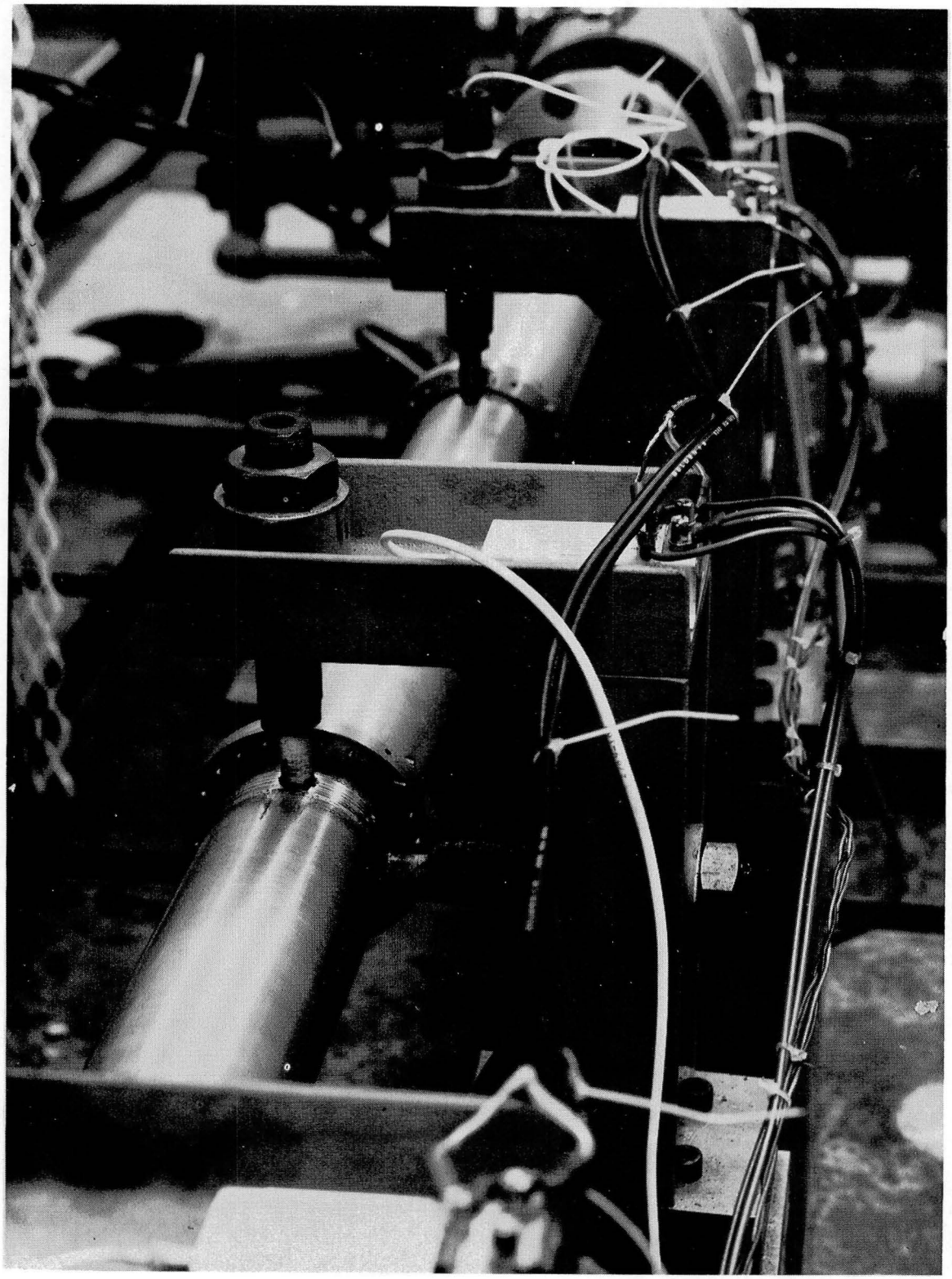

Fig. IX.1 Final Configuration Coulomb Dampers (Teflon) Used During Balancing Tests

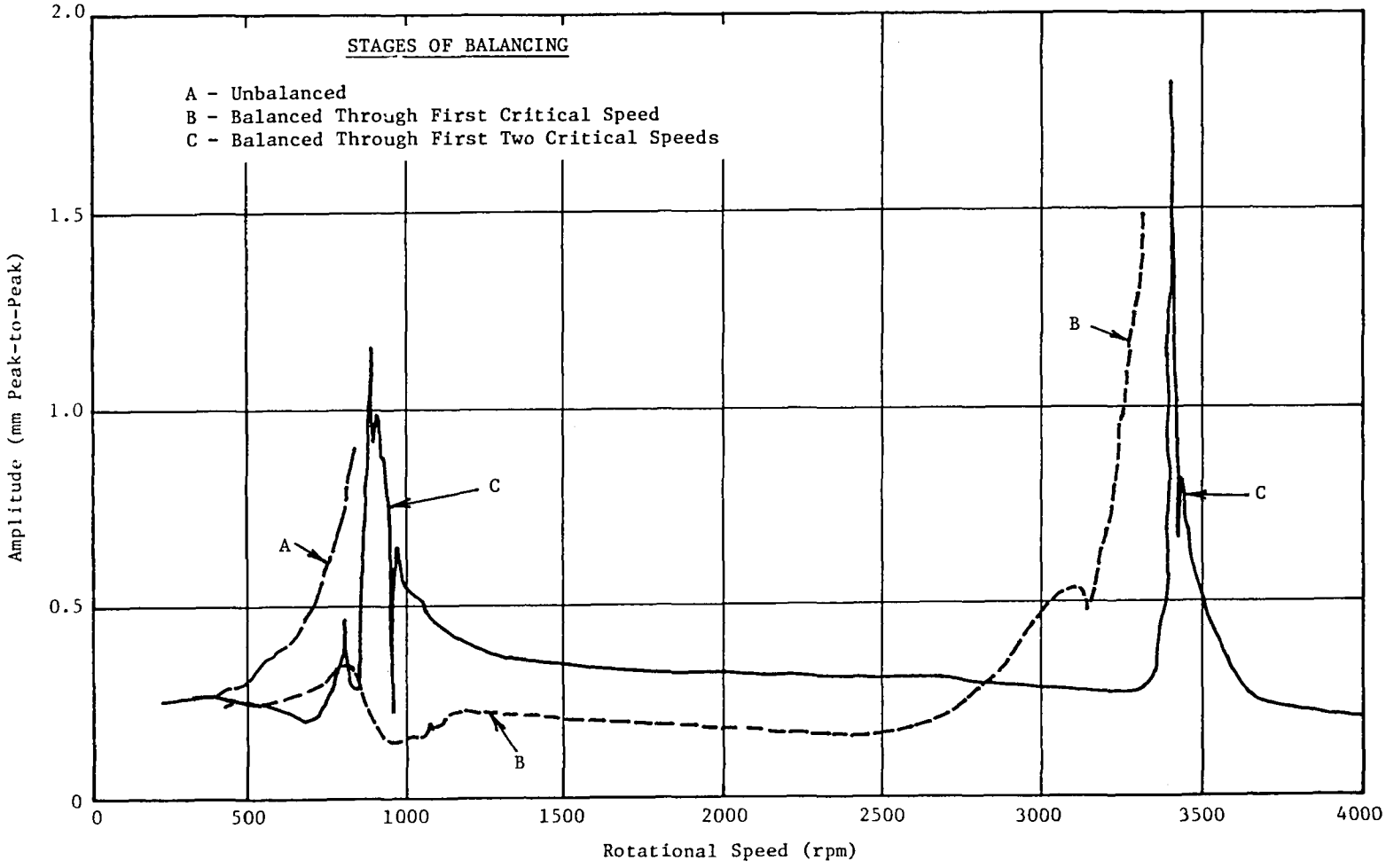

Fig. IX.2 Synchronous Response at Probe No. 1 with Coulomb Dampers as a Function of Speed at Each Stage of Balancing

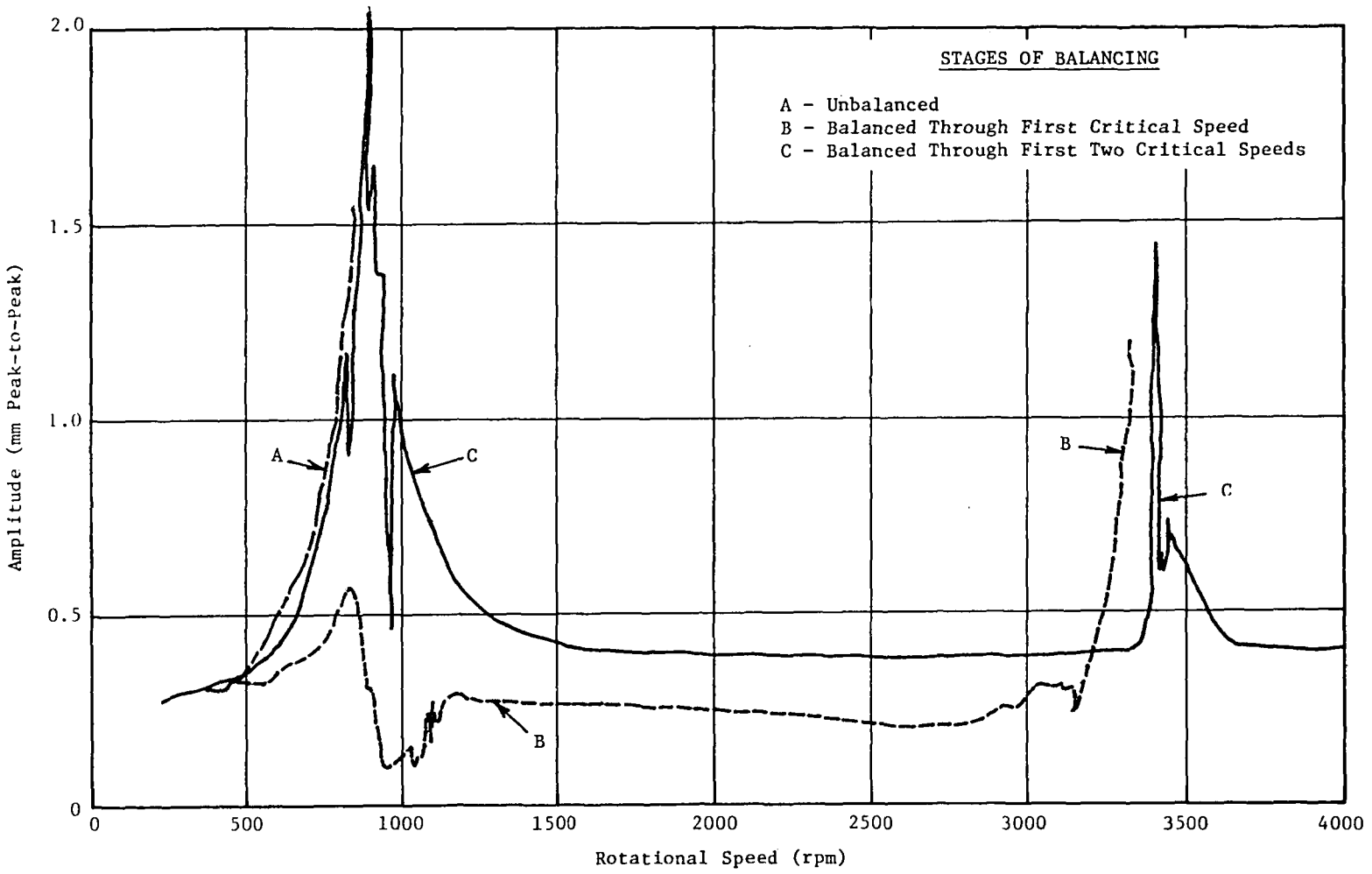

Fig. IX.3 Synchronous Response at Probe No. 4 with Coulomb Dampers as a Function of Speed at Each Stage of Balancing

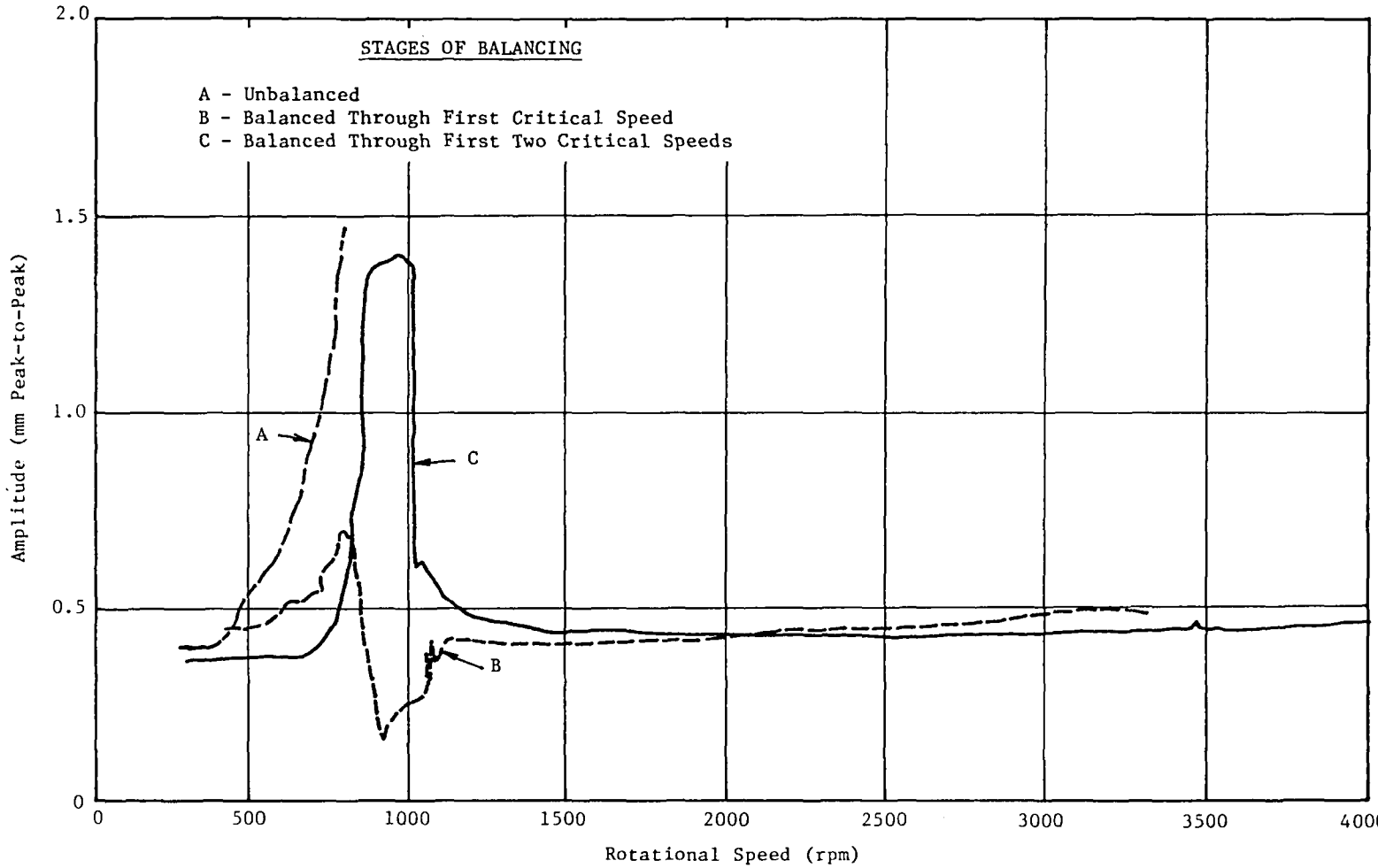

Fig. IX.4 Synchronous Response at Probe No. 5 with Coulomb Dampers as a Function of Speed at Each Stage of Balancing

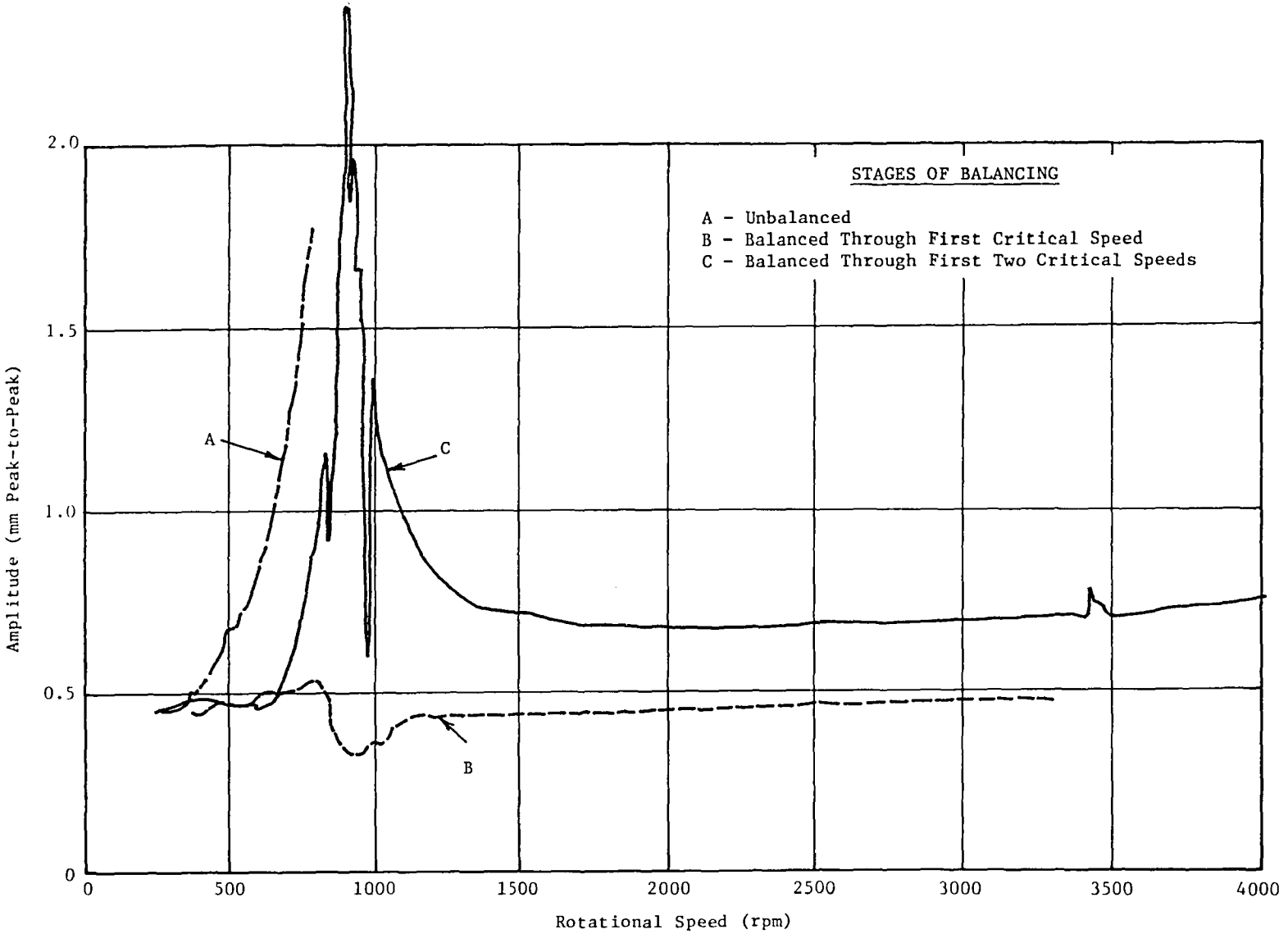

Fig. IX.5 Synchronous Response at Probe No. 6 with Coulomb Dampers as a Function of Speed at Each Stage of Balancing

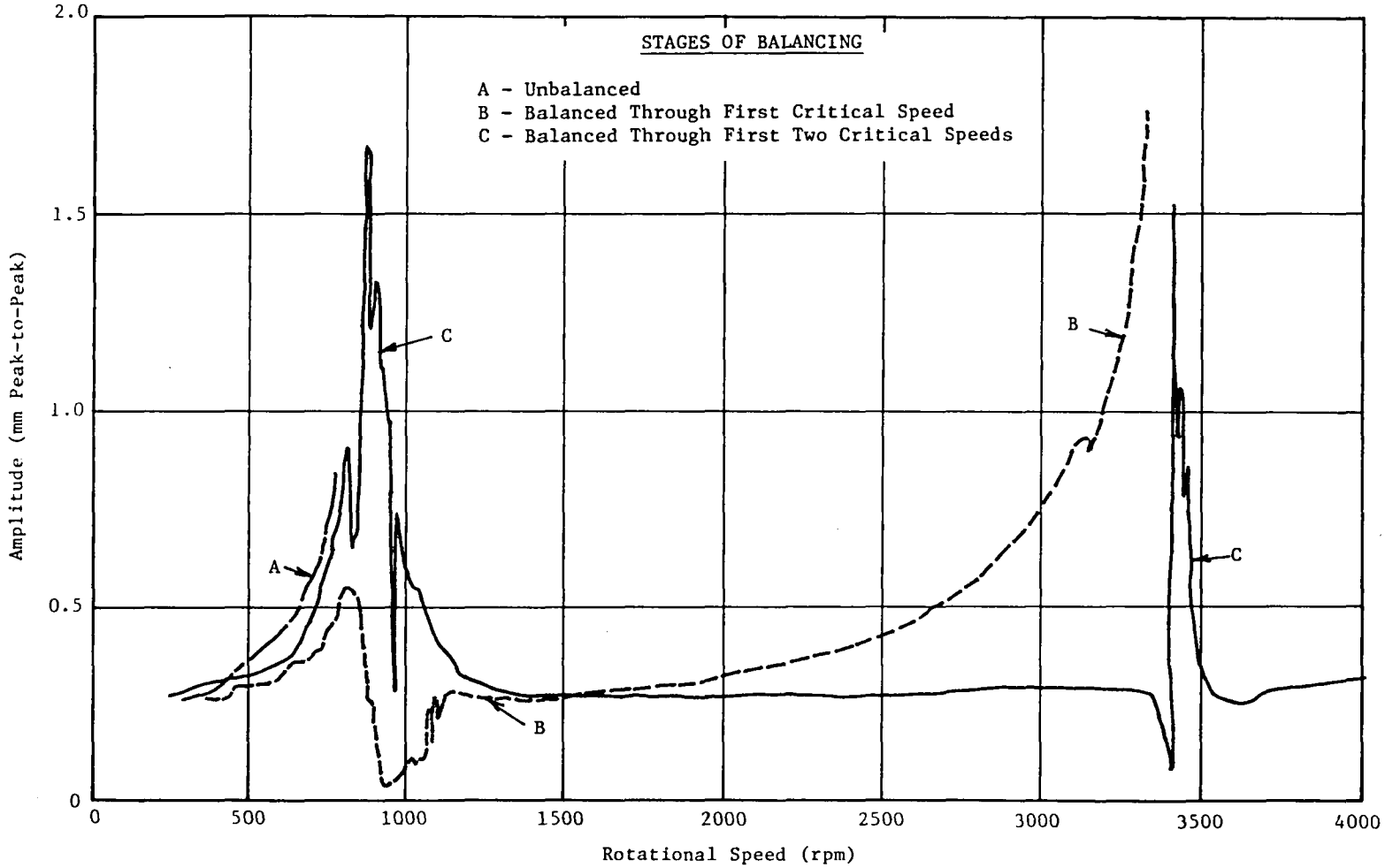

Fig. IX.6 Synchronous Response at Probe No. 7 with Coulomb Dampers as a Function of Speed at Each Stage of Balancing

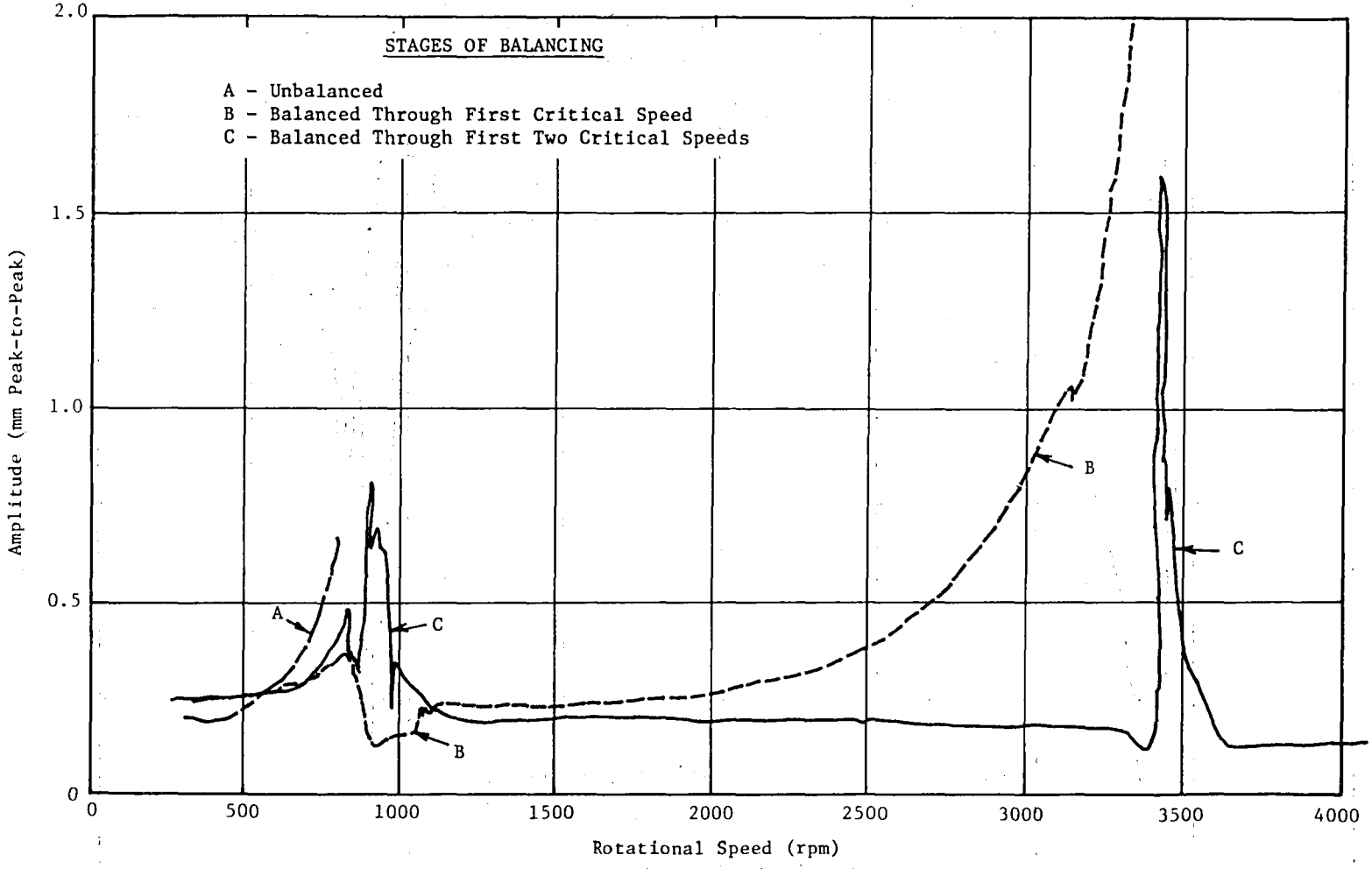

Fig. IX.7 Synchronous Response at Probe No. 9 with Coulomb Dampers as a Function of Speed at Each Stage of Balancing

SQUEEZE-FILM DAMPER DESIGN ANALYSIS

Following the encouraging feasibility results with the Coulomb friction dampers, a more comprehensive damper design analysis was undertaken. Use of a damper is a proven and effective method to control flexible rotor vibration. A number of conflicting factors, however, must be given due weight in the design of a damper application. Some of these factors are:

- The damper must be located at a point which participates, to a significant extent, in all critical speeds where resonance is to be controlled.
- The dynamic characteristics (stiffness, damping, and added mass) of the damper itself must allow similar participation in the critical speeds after installation.
- The damper must, at the same time, provide damping levels which will cause significant reductions in amplitude response at all critical speeds to be controlled.
- The damper must be able to tolerate the amplitudes to which it will be exposed, without failure due to overheating or over-stressing the components.
- The damper must be connected to the shaft by a bearing which can survive the imposed loads and speeds.

For this particular application, additional considerations for the design of the damper arise. They are as follows:

- The damper must be easily added to the existing test rig.
- The damper must be compact and self-contained to be practical in helicopter drive shaft applications.
- The damper must provide support stiffness as well as damping.

Consideration of these factors requires: 1) a good analysis of the rotor's dynamic characteristics with and without the damper, and 2) interaction of this analysis with parameter studies to find the damper configuration which provides both required dynamic characteristics and strength.

The approach selected was to flexibly couple an extension shaft with a damper to the present test shaft. An undamped critical speed analysis of the extended shaft was conducted. Figure IX.8 shows the predicted mode shapes and critical speeds for the first five modes. It should be noted that for all of these modes, there is some significant amplitude at the location of the damper as represented by bearing number 2. This is important to achieve the necessary dissipation of vibration energy at the damper.

Next, a damped natural frequency analysis was used to optimize the damping, at each critical speed, as measured by the system log decrement. The objective was to find realizable support properties (stiffness and damping) which maximize the

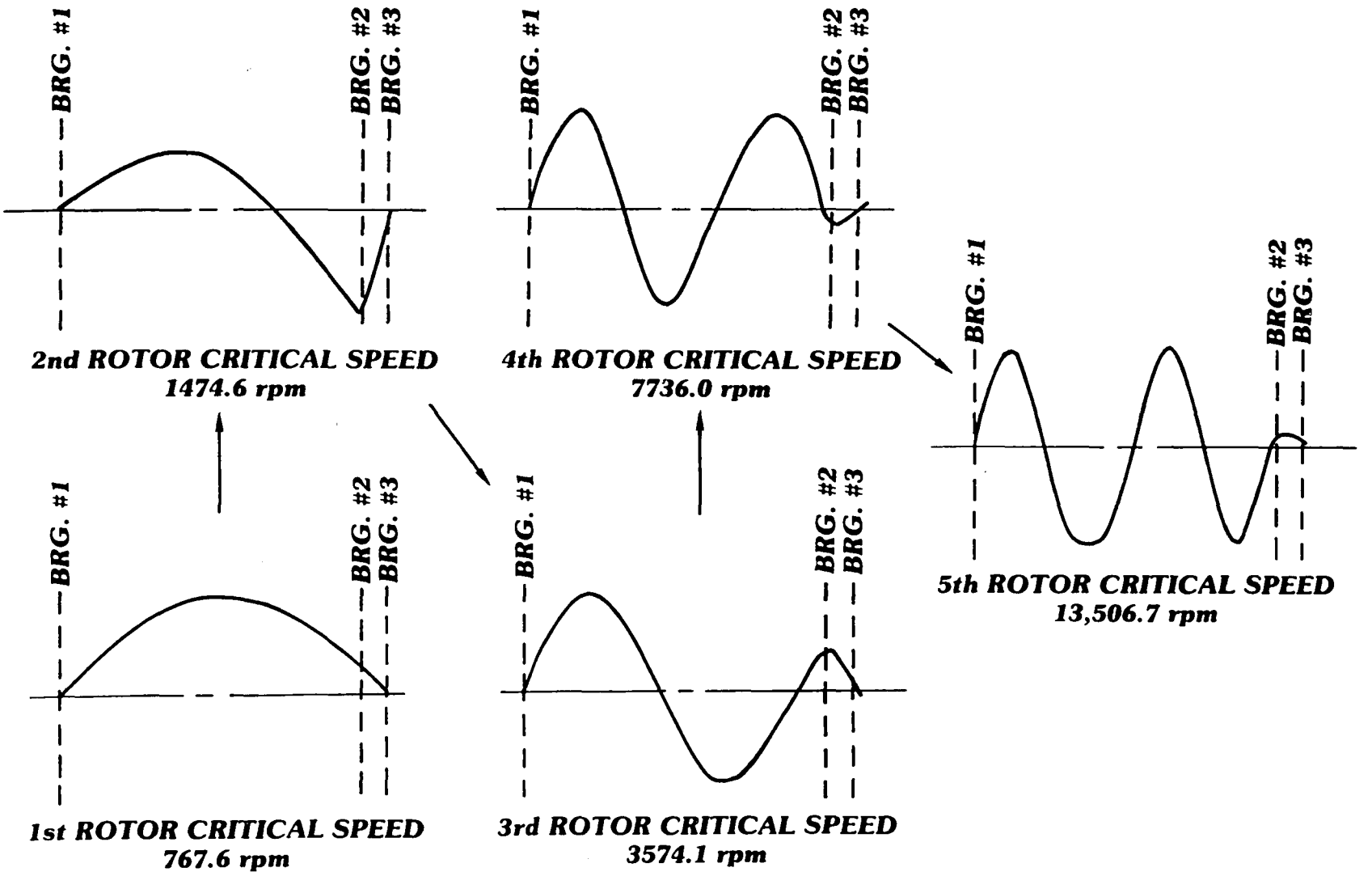

Fig. IX.8 Mode Shapes of the First Five Critical Speeds-Original Shaft With Extension to Carry Squeeze Film Damper

minimum value of log decrement at any critical speed. The initial model of the test rig included a support of 1.75 x 10^5 newtons/meter (1000 lb/in.). A series of damping values from 875 to 10,500 newton-seconds/meter (5-60 lb-sec/in.) were analyzed with this stiffness. The second critical speed was found to be critically damped. Log decrement for the other four critical speeds is plotted against damping in Figure IX.9. The value of damping which gives the best system damping for all criticals is about 8750 newton-seconds/meter (50 lb-sec/in.).

A series of support stiffness values from 1.75 x 10^5 to 2.63 x 10^6 newtons/meter (1000 to 15,000 lb/in.) were then analyzed with a constant damping value of 8750 newton-seconds/meter (50 lb-sec/in.). Again, the second critical speed was critically damped in all cases. Log decrement for the other four critical speeds is plotted against stiffness in Figure IX.10. The only critical speed for which there was a substantial detrimental effect from increase in support stiffness was the first critical speed. However, this effect was serious enough to require that the support stiffness be kept below 8.8 x 10^5 newtons/meter (5000 lb/in.).

Several types of dampers were considered, some of which were Coulomb friction, elastomer, and squeeze-film oil dampers. The Coulomb friction damper concept was not used because of the uncertainity involved in predicting the level of damping in such a damper and the difficulty of modeling Coulomb friction damping in a standard rotordynamic analysis. A squeeze-film oil damper was chosen because it allows a maximum amount of flexibility and predictability in the level of damping that can be achieved. The technical literature which exists for elastomer dampers in this application is limited (e.g. ref. 6); while that for squeeze-film dampers is quite extensive (e.g. refs. 7, 8, 9, and 10).

Based on the rotordynamic analysis, a support stiffness of 7 x 10^5 newtons/meter (4000 lb/in.) was selected and an O-ring was selected as the spring member. Based on studies recently performed by Smalley, Darlow, and Mehta[6], this is about as low as can be practically achieved with continous O-rings of this size. With this stiffness it is possible to take advantage of the use of O-rings in the design, while maintaining the maximum possible stability margin for the first critical speed. The squeeze-film damper was designed to be a sealed damper with no circulation of the oil. In this way, the damper would require no support hardware (such as an oil supply pump) which would prohibit its use in helicopter (or other space and weight limited) applications.

To determine the approximate shaft amplitudes that could be expected at the critical speeds, the response of the test shaft to unbalance was calculated. Total unbalance magnitude is based on the amount of correction required during the undamped balancing of the test shaft and is expected to be initially present in the shaft after a first coarse balance to offset the bow. A random distribution of the unbalance was used based on the work of Little[11]. Figure IX.11 shows the maximum response amplitude along the test shaft as a function of speed, with peaks which represent the first, third, fourth, and fifth critical speeds. As previously predicted, the second critical speed is critically damped and does not show up at all in the analysis. The predicted peak amplitudes are all below .66 mm (26 mils) single amplitude, which is actually below the limit imposed by the probe standoff, and indicates that the expected level of damping will be

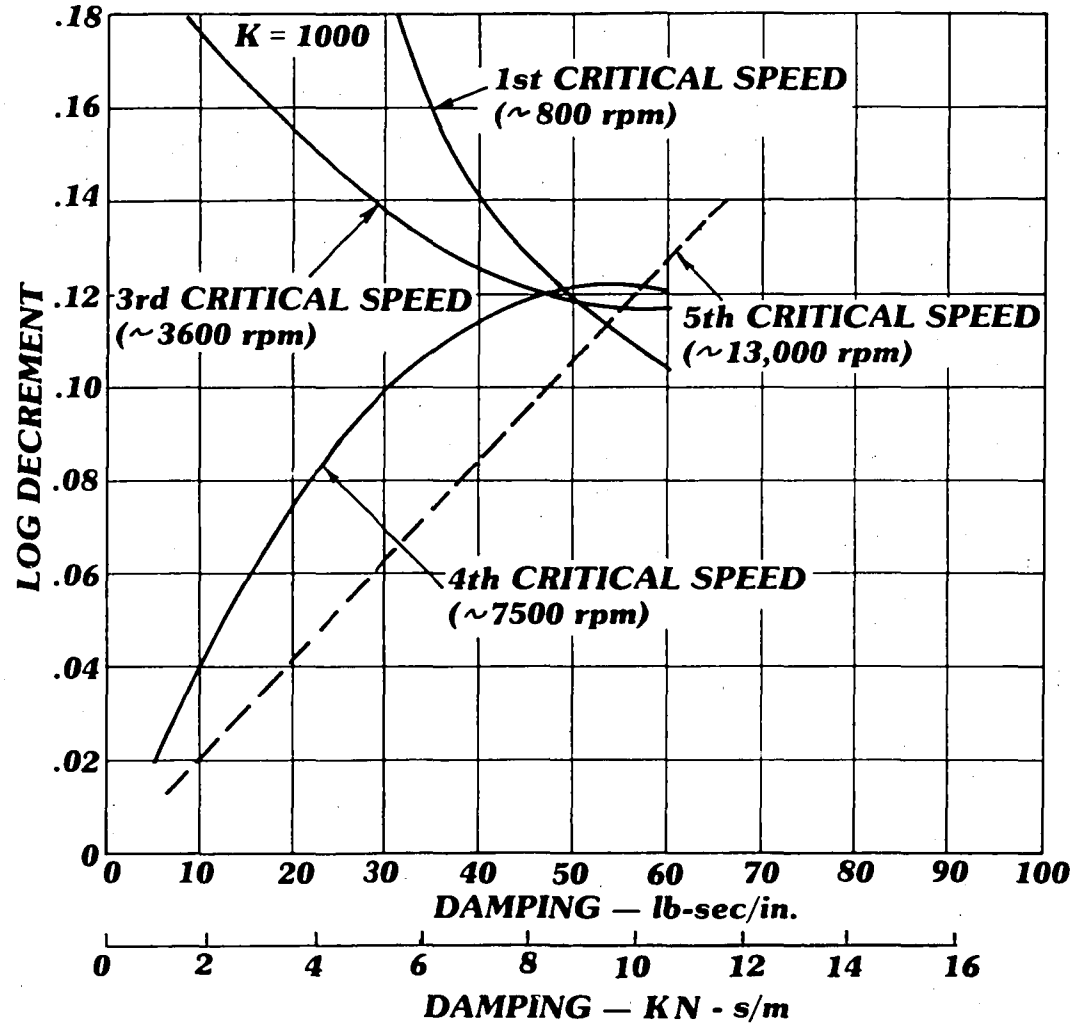

Fig. IX.9 Log Decrement as a Function of Damping
(Stiffness = 1.75 x 10^5 N/m {1000 lb/in.})

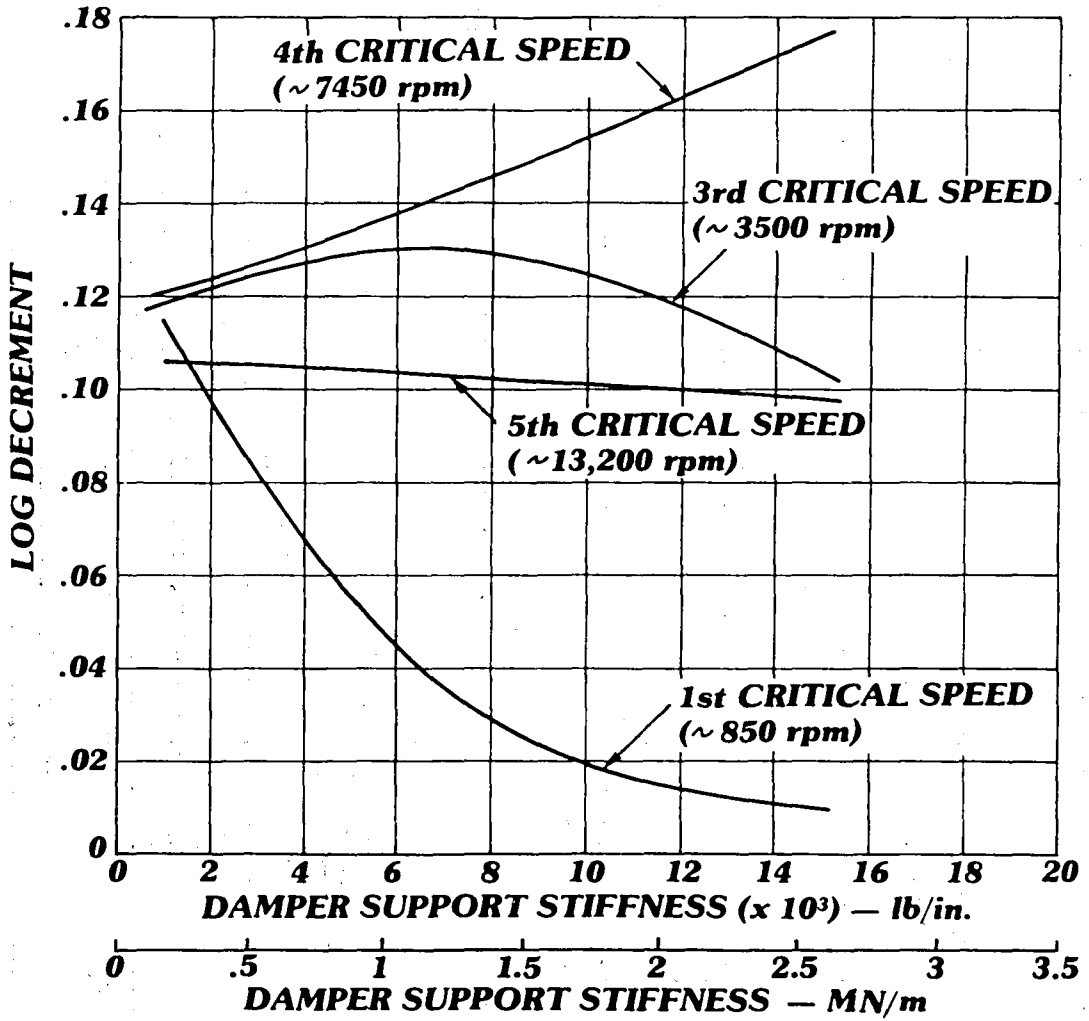

Fig. IX.10 Log Decrement as a Function of Support Stiffness (Damping = 8750 N-s/m {50 lb-sec/in})

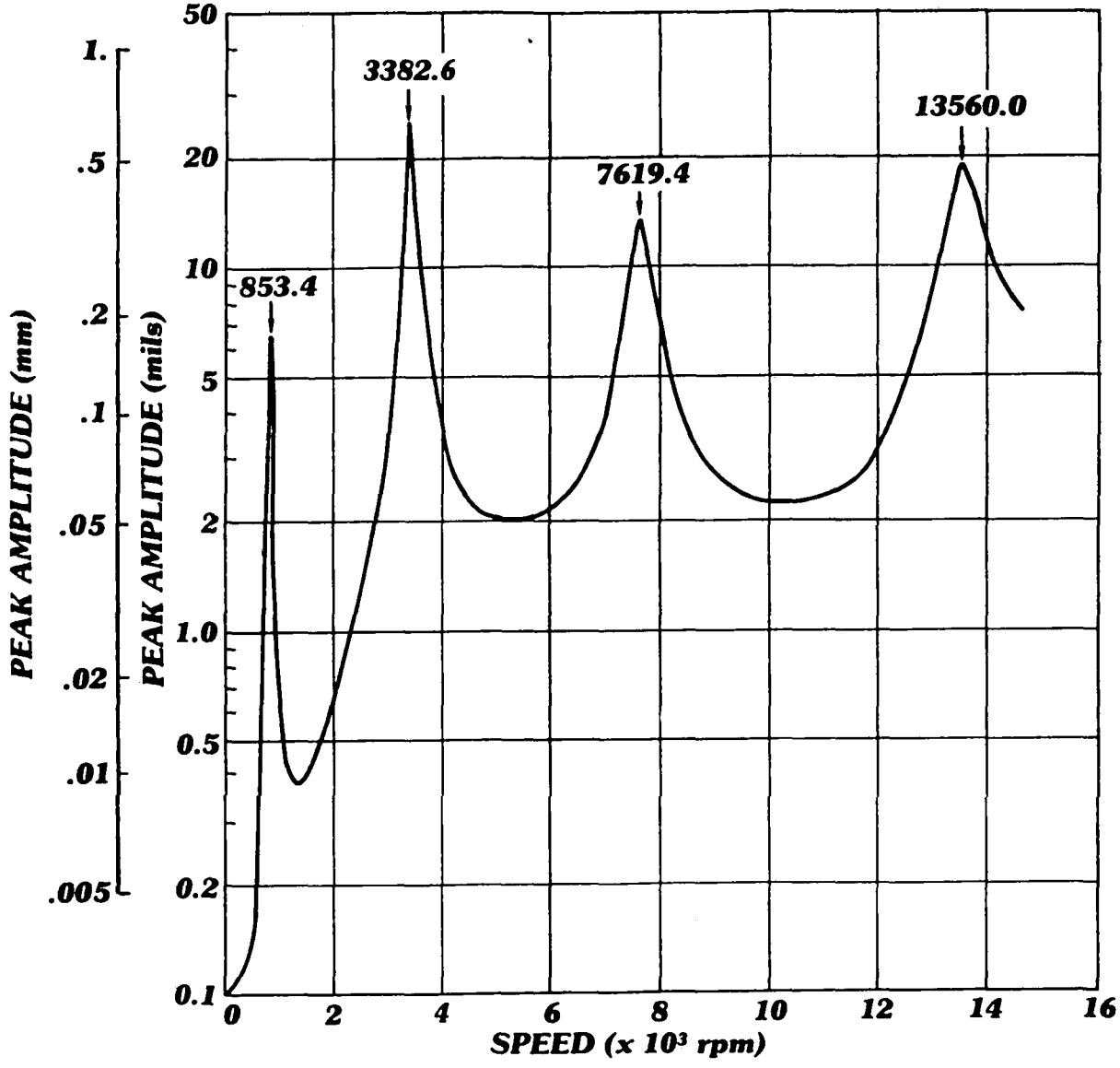

Fig. IX.11 Predicted Response of Test Rig with Damper.
Damping = 8750 N-s/m {50 lb-sec/in.}
Stiffness = 7 x 10^5 N/m {4000 lb/in.}

sufficient to control vibrations. Balancing should significantly reduce these amplitudes. Bearing force was also calculated as a function of speed for the same unbalance distribution and plotted in Figure IX.12. Of particular interest is the force at the damper bearing. The peak force occurs at the fifth critical speed (900 newtons (200 lb) at 13,500 rpm). Since there is a pair of bearings, each of which will give 500 hours design life under a 1560 newton (350 lb) load at 19,000 rpm, this force is not a problem.

The amount of damper pressure required to prevent cavitation can be estimated by dividing the maximum damper bearing force by the projected area of the damper (about 77 square centimeters, 12 sq in.). From this calculation, less than 14 newtons per square centimeter (20 psi) will be required. Figure IX.13 is a plot of predicted damper amplitude as a function of speed. The peak amplitudes on this plot have been shown to be large enough for the damper to provide sufficient energy dissipation, but small enough that there would be no danger of exceeding the .64 mm (25 mils) radial clearance of the damper.

SQUEEZE-FILM DAMPER DESIGN

The layout drawing for the test shaft damper is presented in Figure IX.14. The damper is evacuated, filled, sealed, and then pressurized by the use of a bladder. The damper was predicted to generate less heat than the bearings, so the dissipation of heat was not expected to be a serious problem. The bearings are grease-packed, sealed bearings, so that no oil supply is required. The O-ring retainers are radially adjustable and the damper may be centered manually to compensate for static deflection of the O-rings. The damper was designed to achieve a level of damping in the range of 8750 newton-seconds/meter (50 lb-sec/in.) for silicone oil with a viscosity of about 80 centistokes, using the short bearing theory and assuming no cavitation. The radial clearance is .635 mm (25 mils), the length is 7.6 mm (3 in.) and the diameter is 10 cm (4 in.), respectively. Although the damper was designed to allow for two O-rings, it was used initially with just one O-ring to obtain a low parallel support stiffness of 7×10^5 newtons/meter (4000 lb/in.) for a continuously supported O-ring. Although heating of the damper was not expected to be a problem, the damper housing was finned to provide additional heat dissipation capability.

The damper with its own .43 meter (17 in.) long shaft was assembled as an extension to the test shaft by means of disc-type flexible couplings at its ends. In this way, it was possible to provide a damper that was external to the test shaft, without having to modify the shaft. The damper shaft and rotating components of the damper are made of steel, while most of the housing components are aluminum. Non-rotating, moving components of the damper are made of aluminum to minimize the mass carried by the shaft.

The damper was designed for easy assembly and disassembly. All rotating parts were designed to be assembled with an interference fit and most of the housing components were designed to be assembled with a light press fit. Jacking holes were provided for disassembling most of the press fits. One of the damper shaft coupling flanges is welded to the damper shaft while the other is assembled with an interference polygon fit to maximize torque-carrying capability of the damper shaft. A set of balance weight holes was designed into each of the damper shaft flanges to provide for balance weight addition capability if

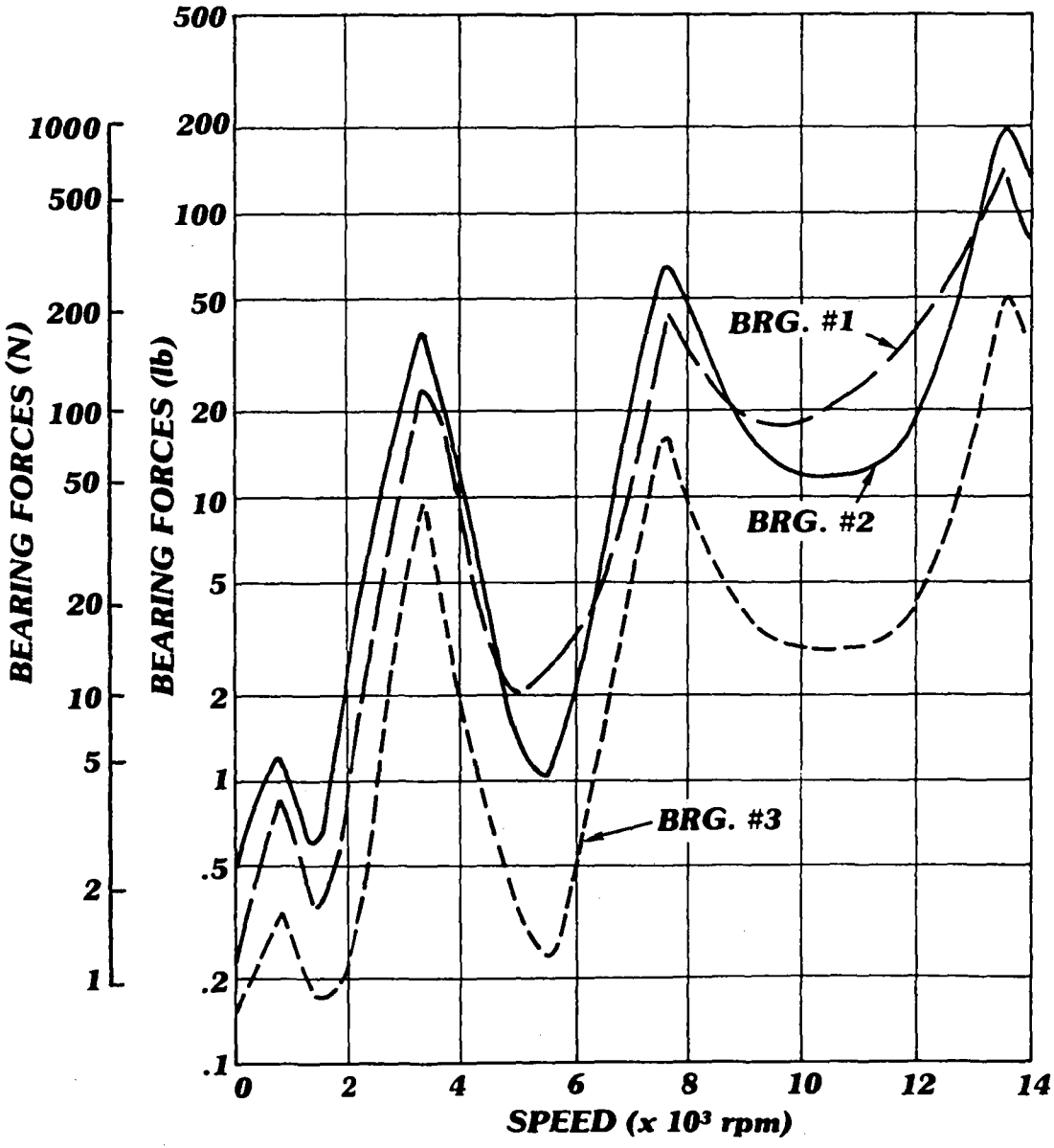

Fig. IX.12 Predicted Bearing Forces as a Function of Speed for Test Rig with Damper

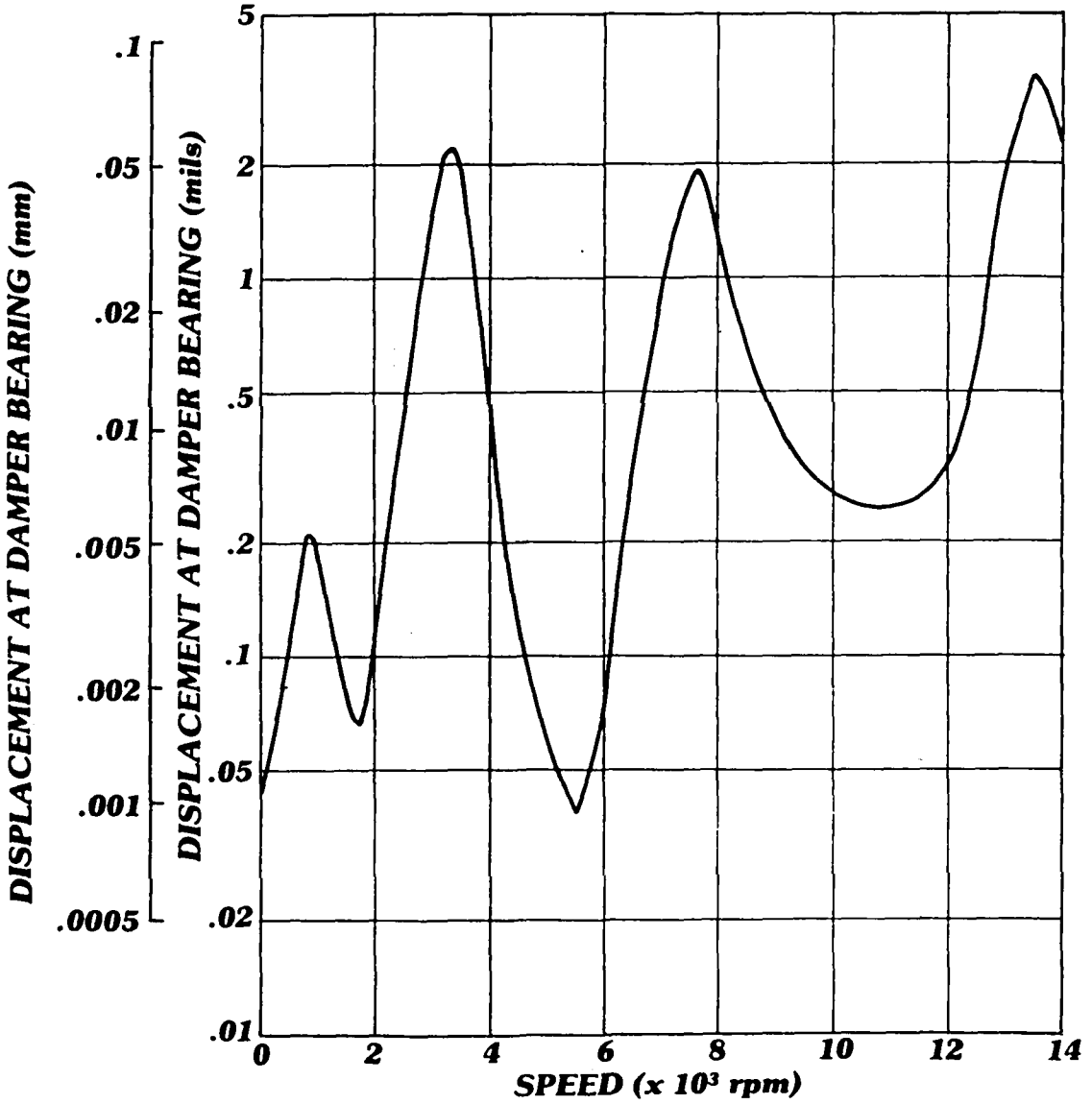

Fig. IX.13 Predicted Damper Amplitude as a Function of Speed for Test Rig with Damper

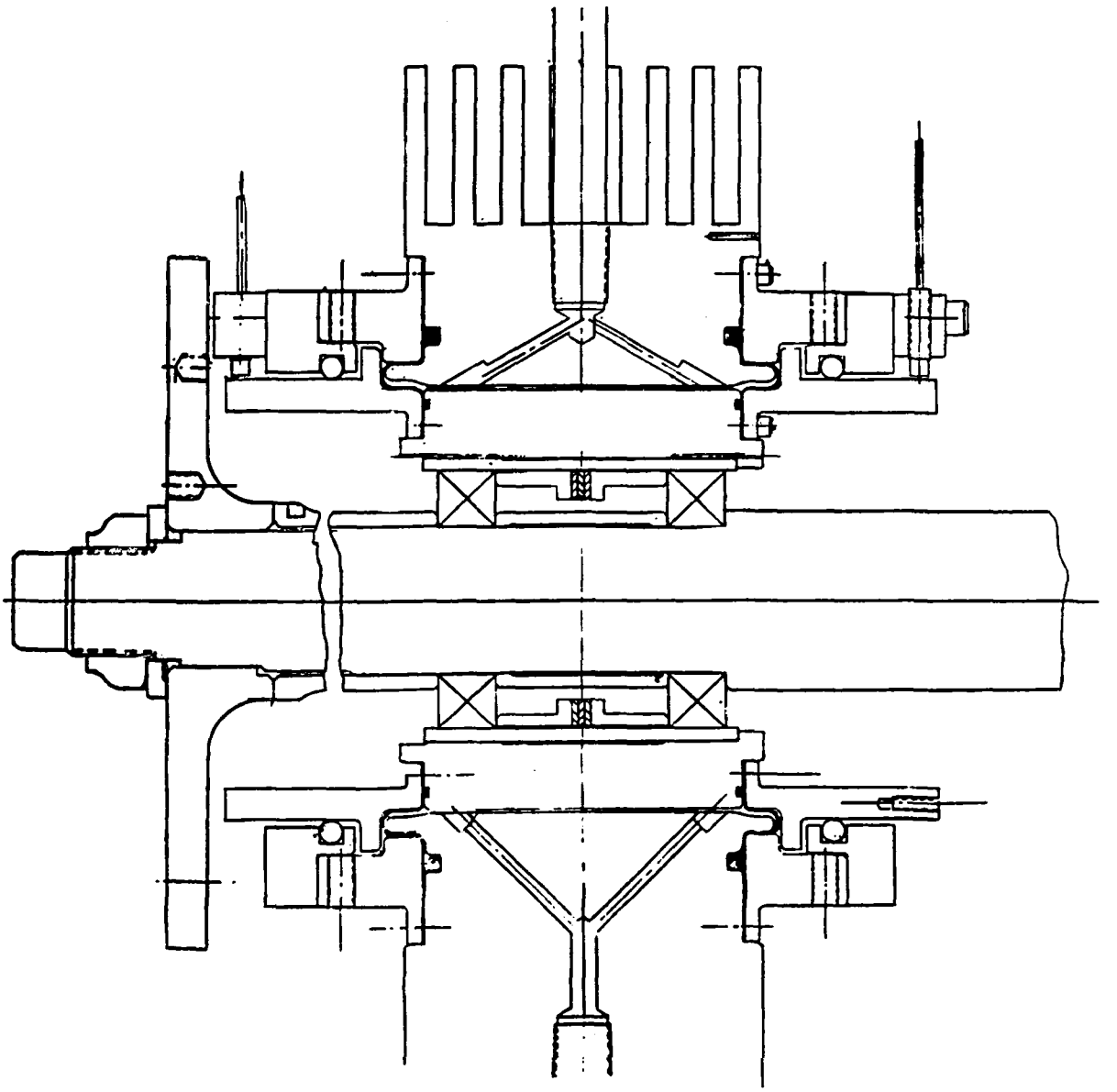

Fig. IX.14 Layout Drawing of Test Shaft Damper

needed. The damper shaft was designed to couple through disc-packs to the test shaft on one end, and to the previously modified hub of the driven end high-speed spindle on the other end. Specially designed minimum clearance shoulder bolts were used for attaching the couplings at both ends of the damper shaft.

The damper was designed to be mounted on a stand with slotted mounting holes to allow for adjustment during assembly. The damper housing O-ring holders were split and held together with dowel pins so that the O-rings and/or the O-ring holders could be changed without having to disassemble the damper. To change O-rings, it would only be necessary to remove the O-ring holder from the damper housing, cut the existing O-ring, splice in a new O-ring, and re-assemble the O-ring holder with the new O-ring. To accommodate an O-ring with different cross-sections, or to change the radial squeeze, it would only be necessary to replace the split housing.

The damper was designed to allow monitoring of dynamic motion, temperature and pressure. There are four mounting brackets for displacement probes, one horizontal and one vertical on each side of the damper housing; four thermocouples, one installed directly into the oil, and the other three at different points in the damper housing; and a pressure gauge to monitor the pressure of the damper oil.

SQUEEZE-FILM DAMPER AND TORQUING SYSTEMS ASSEMBLY AND INSTALLATION

Damper Assembly

The squeeze-film damper was almost completely assembled on a work bench, and installed as a unit in the test rig. The first operation was the assembly of the bearings and spacers on the damper shaft, all with interference fits. Sealed, grease-packed bearings were used. The components of the damper and damper housing were then assembled, including the moving and stationary parts and the specially designed Bellofram seals, shown in Figure IX.15, for encapsulating the damper oil. The damper housing was installed on its mounting bracket and stand. Several thermocouples were installed to monitor damper oil and damper housing temperatures.

The support O-rings were installed, making use of the split O-ring housings shown in the photograph in Figure IX.16. Initially, two O-rings were installed to simplify damper alignment, but one O-ring was removed before the operation of the damper to reduce the support stiffness to the design value. The damper shaft on its bearings was assembled into the damper housing by sliding the bearings into the small clearance bearing housing. The coupling flange was installed on the damper shaft with an interference polygon fit. A compression washer and retaining nut were then assembled onto the end of the damper shaft, and the retaining nut was torqued to 400 N-m (300 ft-lb).

Damper Installation

Since the test shaft damper was to be installed between the test shaft and the driven end high-speed spindle, it was necessary to increase the spacing between the high-speed spindles. The test shaft and damper were temporarily installed to determine the proper axial spacing of the spindles and the driven end spindle was mounted on the newly fabricated torquing gearbox baseplate. The test shaft and test shaft damper were then removed and the spindles were optically aligned, as previously described.

Fig. IX. 15 Bellofram Seals and Bladder for Test Shaft Damper

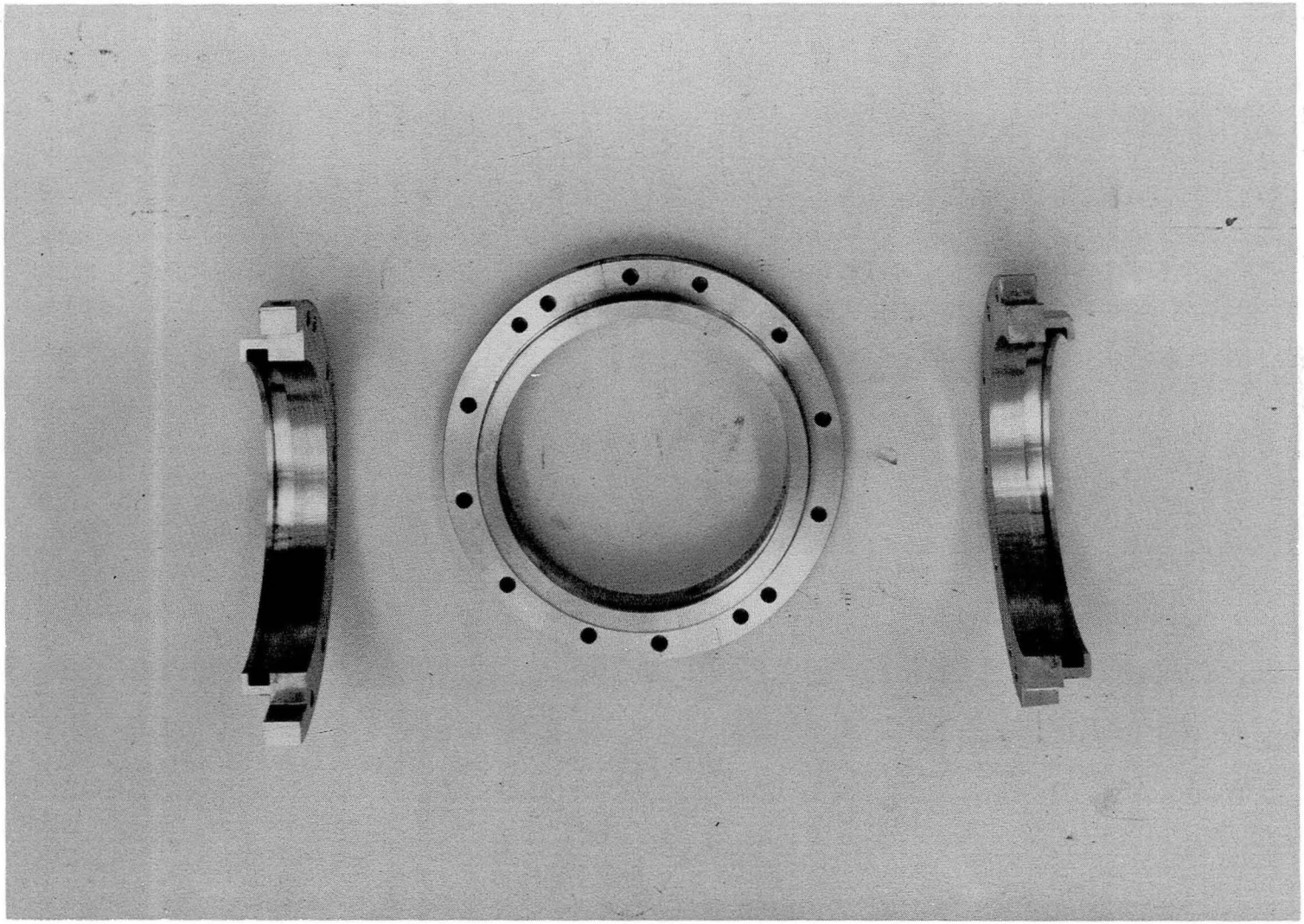

Fig. IX.16 Split Support O-Ring Holders for Test Shaft Damper

Since the damper had a solid shaft, each end of the damper shaft had to be aligned separately, requiring both a transit and an optical alignment telescope. The transit was set up approximately halfway between the spindles, and its line of sight was aligned with the crosshairs on both targets of the driven end spindle. The optical alignment telescope remained in position on the other end of this spindle with the same line of sight and then the damper was set in place. An alignment target was mounted on the end of the damper shaft facing the transit. The machined center on the other end of the damper shaft formed a target for the telescope. The damper was positioned so that the targets were lined up with the crosshairs on the transit and the telescope.

The test shaft was installed and the couplings on both ends of the damper shaft were assembled. The damper was plumbed for oil, air, and vacuum. The components installed during this plumbing procedure included valves, gauges, an oil flask, a sight glass, vacuum and air lines.

At this point, the support O-ring furthest from the test shaft was removed from the damper to reduce the support stiffness of the damper to the design value. The static stiffness of the remaining O-ring was checked with a spring scale and a dial indicator and found to be slightly over 175,000 N/m (1000 lb/in.). It has been shown in ref. (9) that the dynamic stiffness of an O-ring composed of Buna-N might be expected to be a factor of three to four higher than the static stiffness. Applying this factor to the measured static stiffness of the O-ring in the test shaft damper results in an expected dynamic stiffness very near the design value of support stiffness for the test shaft damper (4000 lb/in.).

The displacement probes for the test shaft damper were then calibrated, installed, and the gaps were properly set. The proximeters were mounted on the damper mounting stand, connected to the displacement probes, wired to power supplies and wired back to the control room. The thermocouples were also wired back to the control panel, and to the newly installed multiplexer switch and digital readout. This operation completed the installation of the test shaft damper. A photograph of the damper is presented in Figure IX.17.

The assembly, disassembly, and installation of the damper was straightforward. It is noted that the assembly of the test rig was such that the test shaft could be installed or removed without moving the damper. Once the test shaft damper was installed and aligned, it could remain in place even if a temporary removal of the test shaft was necessary.

Modification of High-Speed Spindles

Before the damper tests were conducted, modified parts for the high-speed spindles were installed to eliminate oil leaking and spraying. As described in an earlier section, these modifications included: air buffer labyrinth seals in place of the original labyrinth seals, leak trapping end caps, an air bleed valve for the center cavity, and O-ring sealing around the oil spray ring.

During many hours of modified high-speed spindle operation, no leakage was detected from either spindle, and it was unnecessary to provide air to the labyrinths or to open the air bleed valve to the central cavity of either of the spindles. It is concluded that the modifications to the high-speed spindles were entirely successful.

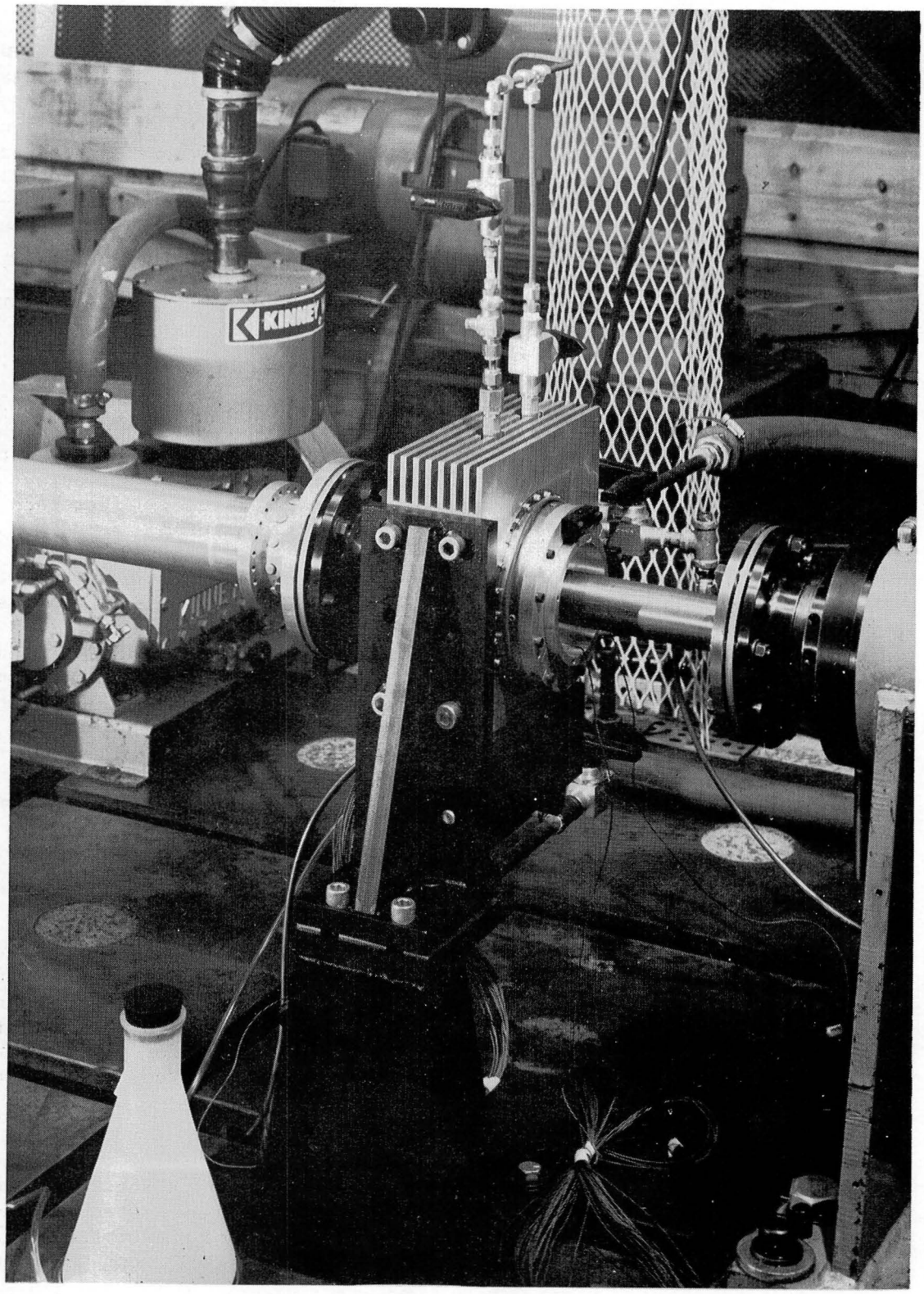

Fig. IX.17 Squeeze-Film Damper for Supercritical Shaft Test Rig

Torquing Hardware Assembly

The low-speed and torquing hardware was then assembled to complete the four square test rig. The third floor plate had been grouted in place, as described earlier for the first two floor plates, prior to the installation of the test shaft damper. The torque sensor was mounted on the mounting stand, aligned with the low-speed output shaft of the drive gearbox, and dowel-pinned in place to maintain the alignment. The torque sensor was then removed and coupling hubs were installed on the torque sensor shaft and the drive gearbox low-speed output shaft for coupling the two together. These coupling hubs were mounted such that when the torque sensor was reinstalled, a 3.3 mm (0.12 in.) gap remained between the coupling hubs. A dropout spacer, shown in Figure IX.23, was fabricated and installed to fill this gap so that when operation of the low-speed shafting was not desired, this spacer could be easily removed.

The pillow blocks for the low-speed shafting were mounted on the appropriate bearing pedestals, and the low-speed shafts were mounted in the pillow blocks.

The couplings for the low-speed shafts were disassembled and the hubs were mounted on the appropriate shafts. Starting at the torque sensor output shaft, the low-speed shafts were aligned end to end, one at a time. After each of the shafts was aligned, the appropriate couplings were connected.

The torquing gearbox was set in place on the baseplate and aligned with the driven end high-speed spindle. The axial spacing of the low-speed shafts with the torquing gearbox was checked and the coupling hub supplied by the gearbox manufacturer, on the low-speed shaft of the torquing gearbox, was removed. The proper coupling hub was assembled onto the low-speed shaft of the torquing gearbox to mate with the coupling hub on the end of the adjacent low-speed shaft.

Locations of the mounting holes for the torquing gearbox were marked on the mounting baseplate. The torquing gearbox was then removed so that these mounting holes could be drilled and tapped and then replaced and realigned with the high-speed spindle. The alignment of the torquing gearbox with the low-speed shafting was checked and found to be satisfactory. At that point, the torquing gearbox was mounted to the torquing gearbox baseplate.

The lubrication oil supply and drain lines for the torquing gearbox were then installed. The appropriate thermocouples were installed and wired to the thermocouple multiplexer switch on the control panel. The steel cover on the top of the torquing gearbox was replaced with a clear plastic cover for observation during low-speed operation. An oil pressure trip-out for the magnetic coupling was installed in the lubrication oil supply line for the torquing gearbox. The torquing gearbox end of the fully assembled test rig is shown in the photograph in Figure IX.18.

Torquing System Controls

The hardware used for controlling the operation of the torquing system was assembled and the hydraulic oil dispenser for the torquing system was installed in the hardware pit. Electrical power was wired in for the hydraulic oil dispenser pump motor and high-pressure solenoid switch along with the appro-

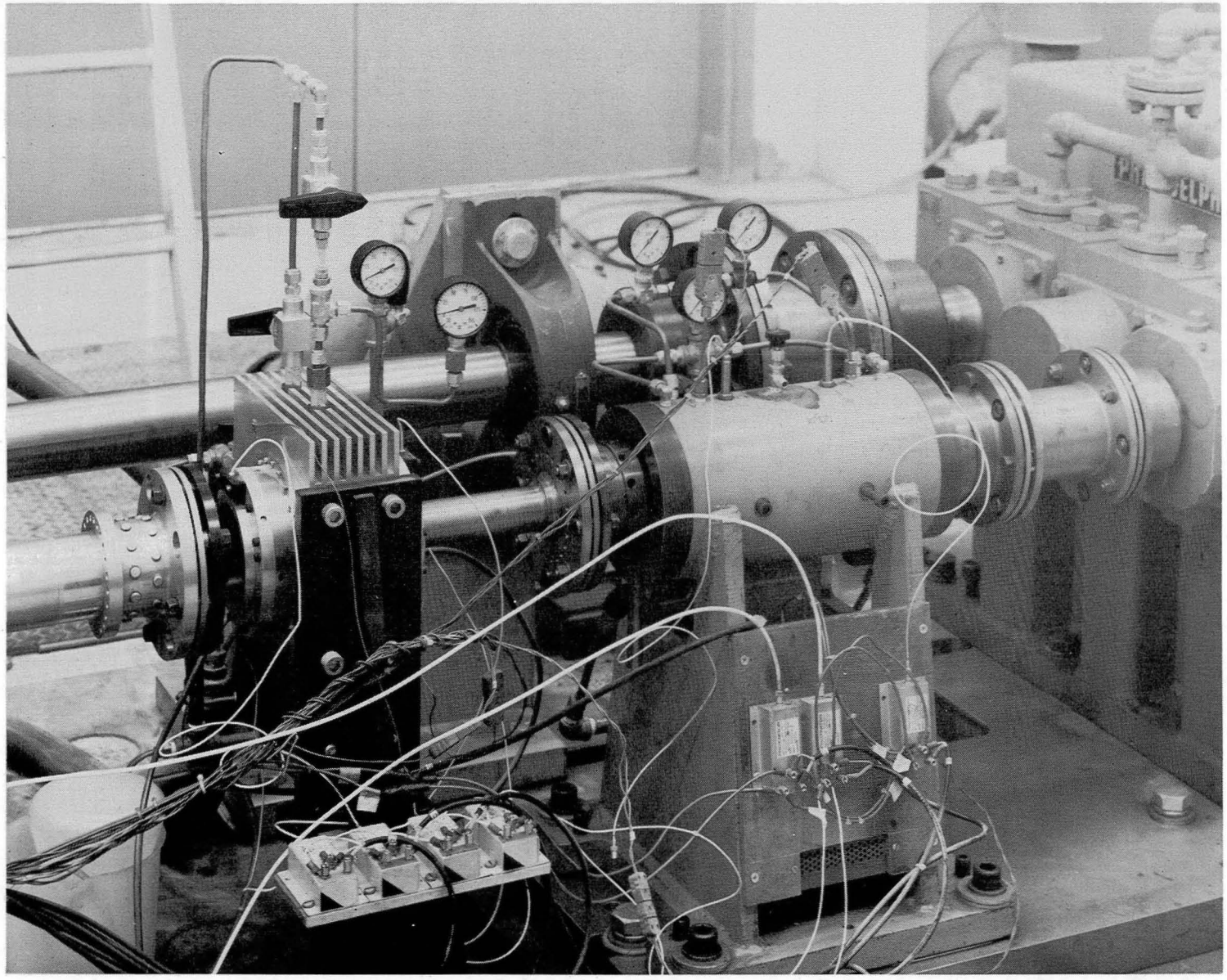

Fig. IX.18 Torquing Gearbox End of Completed Four-Square Test Rig

priate control panel switches in the control room. An air-operated control valve was substituted for the piston pressure relief valve supplied with the hydraulic oil dispenser. Plumbing was installed between pressure gauges and air regulator in the control panel, the hydraulic oil dispenser and the air-operated control valve. The hydraulic oil lines between the oil dispenser and the torquing piston on the torquing gearbox were installed, and all of the air was bled from these lines. The torquing piston limit switch was wired to the magnetic coupling trip-out and the trip-out indicator light on the control panel.

Two views of the completely assembled supercritical shaft test rig are presented in the photographs in Figures IX.19 and IX.20. The hydraulic oil dispenser was installed in the hardware pit and plumbed.

Checkout of Torquing System

Before the completely assembled test rig was rotated, the shafting was decoupled in two places and the movement of the torquing piston and gear was checked out. The air regulator on the control panel was used to control the movement of the torquing piston and gear, in and out, resulting in a relative rotation between the high- and low-speed shafts of the torquing gearbox. This demonstrated that the torquing system was operating satisfactorily. During the subsequent running of the test rig under a torque load, the torquing system controls were tuned.

Before actually applying the torque load to the test shaft, the two gearboxes were run with only the low-speed shafting connected. The drive motor was run in the low-speed mode and the magnetic coupling was run up to full speed, which is 1800 rpm at the low-speed shaft of the test rig. No problems with response of the low-speed shafting were observed (the first critical speed is predicted to be well out of the operating range). Some problems were encountered when attempting to run the rotor in high-speed mode when loaded by both gearboxes. These problems are attributed to high gearbox losses, greatly aggravated by low temperatures (about 100°F) in the lubricating oil. A potential solution to this problem was to heat the gearbox oil, but this was not pursued since immediate needs called only for operation in the low mode of the motor.

Both the low- and high-speed sides of the test rig were then connected, resulting in a complete four-square system. At this point, torque was applied using the torquing system, without rotating the test shaft, to observe the action of the torquing system and the operation of the torque sensor. It was found difficult to release the torque without rotating the test shaft. Also, if the test rig was already torqued, it was difficult to engage the clutch without overloading the magnetic coupling. When the test rig was rotating, however, there was no problem in applying or releasing the torque.

The torquing system was adjusted for proper operation and the high pressure output of the hydraulic oil dispenser was initially set very low to avoid over-torquing the test shaft. After establishing that the torque sensor was operating properly, torque was applied and the high pressure output was raised until it was just possible to apply the full torque of 900 N-m (8000 in.-lb) to the test shaft.

The torquing system was tuned for good control: the orifice in the remotely-operated control valve was replaced with a smaller orifice; the flow-control valve on the hydraulic oil dispenser was properly adjusted; the pressure con-

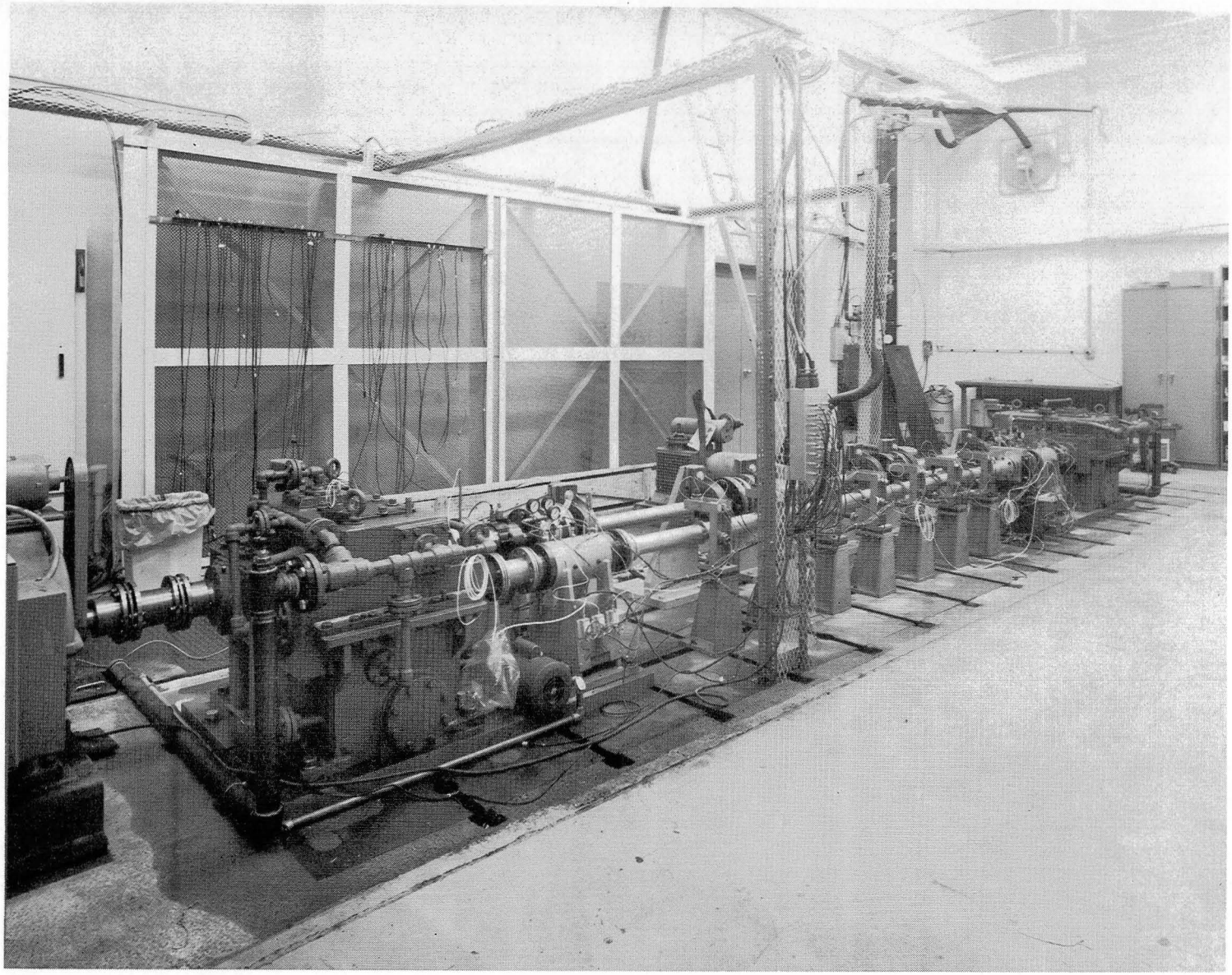

Fig. IX.19 View of Completely Assembled Four-Square Test Rig Showing High-Speed Side from Drive Gearbox End

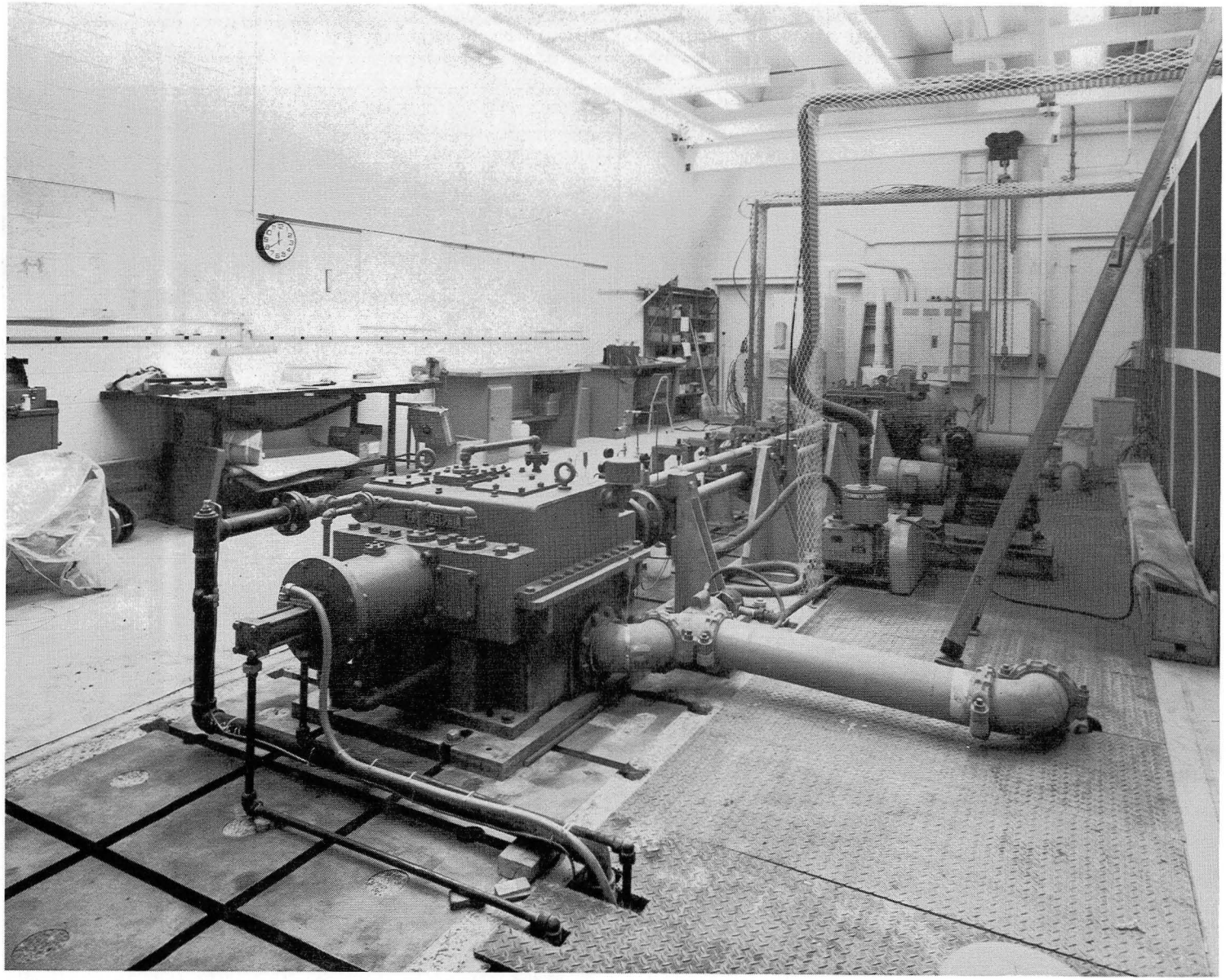

Fig. IX.20 View of Completely Assembled Four-Square Test Rig Showing Low-Speed Side

trol valves on the hydraulic oil dispenser were also adjusted. Based on the helix angle of the torquing gear and the bore of the torquing piston, a series of torque versus forward pressure curves were calculated and plotted for various values of return pressure of the torquing piston. This set of curves is presented in Figure IX.21.

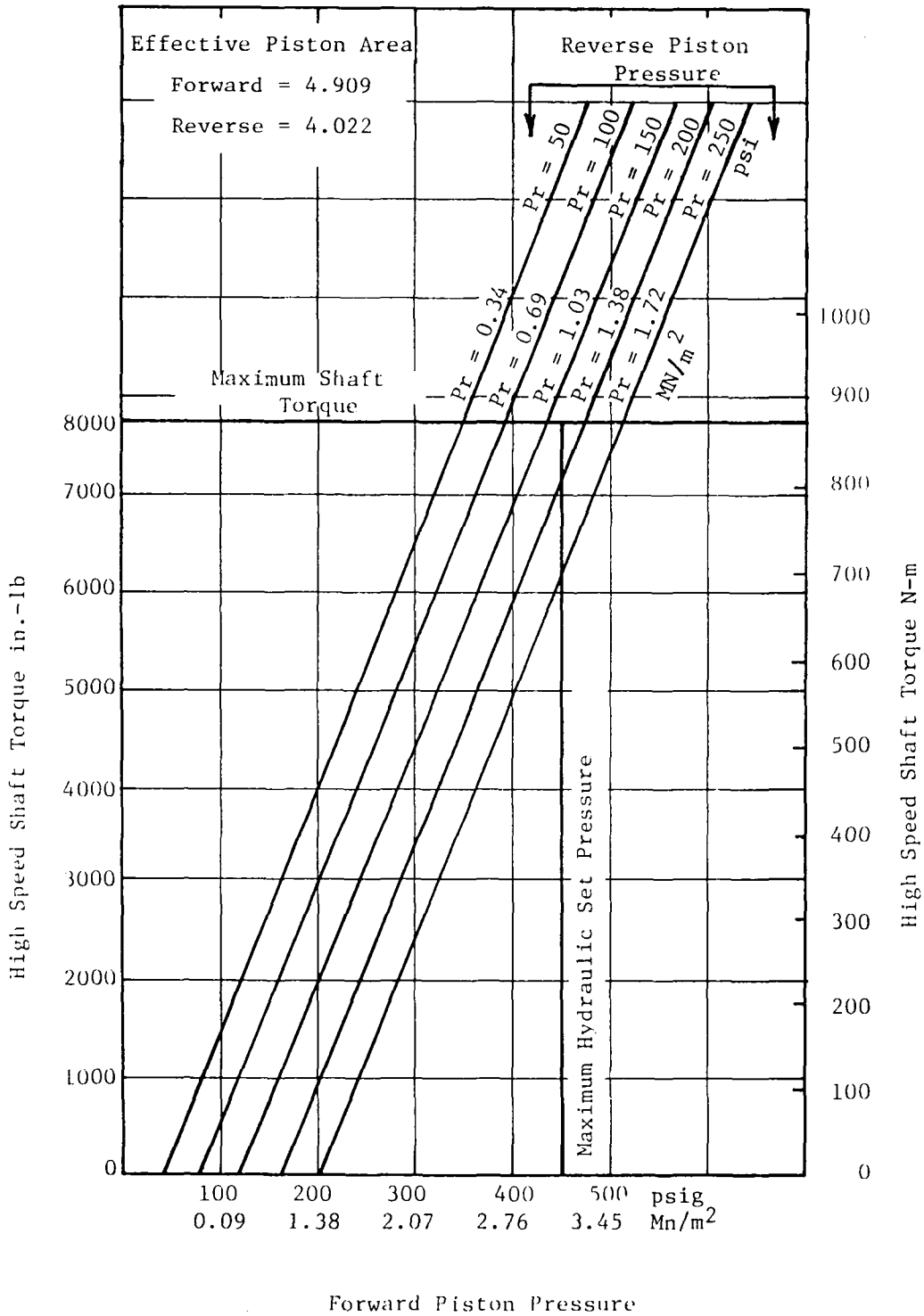

Fig. IX.21 High-Speed Shaft Torque as a Function of Forward and Reverse Piston Pressure

X. VIBRATION CONTROL BY BALANCING

After the installation of the test shaft damper, balancing tests were conducted with the damped test shaft. During the first series of tests, the test rig was run in an unloaded configuration with the torquing gearbox disconnected. Balancing tests were conducted using two different methods of flexible rotor balancing: the influence coefficient balancing method, as described in Reference 12, and a modified modal balancing technique which incorporates some of the features of influence coefficient balancing. A further series of tests was run to investigate the effects of torque load.

SUMMARY OF SQUEEZE-FILM DAMPER RESULTS

The following tests demonstrated tremendous improvement in dynamic stability of the test rig as a result of the squeeze-film damper. However, the addition of external damping alone could not provide complete control of all test shaft vibrations. The test shaft also had to be balanced to achieve safe operation throughout its speed range.

Through the combined use of external damping and balancing, the rig was run to over 12,000 rpm while negotiating the first four flexural critical speeds of the test shaft. This speed was over 12 times that which could be achieved without external damping. In addition, the test shaft was run under various levels of torque, to over 7000 rpm, and was successfully balanced while subjected to about 900 N-m (8000 in.-lb) of torque.

INFLUENCE COEFFICIENT BALANCING

First, the influence coefficient balancing tests were conducted. In its initial condition, the test shaft could not be run safely above 890 rpm, which was below the first critical speed. The first critical speed now built up gradually over a broader speed range than without the damper.

For balancing the first critical speed, only one balancing plane and one displacement probe near the shaft center were used. Balancing data for the first run was taken at 850 rpm, and for later runs at 887 rpm and 901 rpm. Three correction weights totaling about 5 gm were calculated and added as a result of these successive runs, and each improved the balance of the test shaft. After the third correction, the first critical speed was negotiated easily and the test shaft was run to 3300 rpm. The test shaft was run at a variety of speeds below 3300 rpm and data was taken for extended periods of time. There was no variation of data with time, as there had been for the undamped test shaft, there was no significant subsynchronous component of response above the first critical speed, and there was no incipient instability. It was concluded that the damper eliminated the instability and related problems that existed with the undamped test shaft.

When the test rig was assembled with the test shaft damper in place, the alignment targets were unintentionally left in the ends of the high-speed spindle shafts. This was not considered to be a problem for low-speed operation of the test rig (below 5000 rpm). However, it was anticipated that high-speed operation might disturb the centering of the crosshairs in the alignment targets. Therefore, the test shaft was removed after the first critical speed had been balanced and the alignment targets were removed. After the test shaft had been reinstalled in the test rig, even though match marks were used to ensure the

same angular orientation of the test shaft and spindle, the first critical speed was not as well balanced as it had been before the removal of the test shaft. This change in the balance condition of the test shaft was attributed to a shift of the test shaft in its couplings; the clearance between the coupling shoulder bolts and mounting holes was of the order of 0.025 mm (1 mil). The first critical speed was successfully rebalanced using previously obtained influence coefficients and indicated that the change in balance of the test shaft was not accompanied by a change in the influence coefficients.

When running at 3300 rpm, the test shaft assumed the whirl mode shape predicted for the third critical speed. As predicted, the second critical speed was critically damped and was not observed.

Three balance planes were used to balance the third critical speed: the center plane (No. 4), which had been used for balancing the first critical speed, and two additional planes (No. 2 and 6), located approximately at the quarter points of the test shaft (plane numbers run from 1 to 7). The three probes located adjacent to these three planes were used during the balancing of the third critical speed. Although the probe and plane located in the center of the test shaft (plane 4) were very near a node of the third critical speed, they helped suppress the vibration at the first critical speed induced by weights added to balance the third critical speed. During the balancing of the third critical speed, balancing data was taken at two speeds: 917 rpm and 3200 rpm. The third critical speed was balanced very well in just two successive balancing steps. In spite of the plane selection, the addition of these correction weights for the third critical speed caused deterioration in response at the first critical speed. However, it was still possible to safely negotiate the first critical speed.

After balancing through the third critical speed, it was noticed that response at both first and third critical speeds was deteriorating, although no further balancing weights were added. The damper was examined and the oil leakage around the thermocouple was discovered. An unsuccessful attempt was made to seal the leak without removing the thermocouple, so the thermocouple was removed and the hole was plugged, successfully sealing the leak. When the damper was refilled with oil, response of the test shaft significantly improved and approximated that observed immediately after balancing the third critical speed (with no change in balancing weights).

Since the center balance plane is near a node for the third critical speed, a trim correction for the first critical speed was applied in the center plane, with the expectation that the third critical speed response would be little affected. As a result, the response at the first critical speed was greatly reduced and, as expected, response at the third critical speed was not noticeably affected. At this point, the test shaft was very well balanced through the first and third critical speeds.

The test rig was then run up to 7300 rpm at which point there was significant response to the fourth critical speed. Due to a rapid increase in the amplitude of test shaft vibration, there was momentary contact between the shaft and a number of the displacement probes. This had an apparent effect on the unbalance of the test shaft as the first and third critical speeds could no longer be negotiated. (It should be mentioned here that the test rig was stopped by rapidly decelerating through the first and third critical speeds. These critical speeds were negotiated so quickly that there was no opportunity for the response of the test shaft to grow to a destructive level.)

The first critical speed was subsequently rebalanced. At this point, the response of the test shaft appeared to be somewhat less sensitive to unbalance at the first critical speed than it had during the previous balancing runs. This change was attributed to the "breaking in" of the test shaft damper, resulting in more efficient operation. No substantial changes were noted in the sensitivity of the response of the test shaft during the remainder of the tests, except when the cracks developed in the tubing and pipe nipple of the test shaft damper. Three successive correction weights were added to balance the first critical speed and a good balance condition was achieved.

The third critical speed was then rebalanced using previously obtained influence coefficients. After the addition of only one correction weight set, the response at both the first and third critical speeds was improved significantly and the third critical speed was easily negotiated.

Balancing operations were then performed for the fourth critical speed. The same planes and probes were used for the fourth critical speed as for balancing the third critical speed. Balancing data was taken at three speeds: 922 rpm, 3400 rpm and 6800 rpm. The largest trial weight that could be used to excite the fourth critical speed, and still permit negotiation of the first and third critical speeds, was .35 grams and the resultant change in the response of the fourth critical speed at 6800 rpm was only a small percentage of the initial response. However, a set of correction weights was calculated from this data and installed in the test shaft. Subsequently, the response of the test shaft at both the first and third critical speeds was made significantly worse. In fact, as a result, the third critical speed could no longer be negotiated. Instead of removing the correction weights for the fourth critical speed, it was decided to apply additional balance weights to improve the response of the test shaft at the first and third critical speeds. The influence coefficients determined during earlier balancing of the third critical speed were used. Two sequential correction weight sets were added, based on data taken at 917 and 3200 rpm, and the response of the test shaft at the first and third critical speeds was significantly improved. The response of these critical speeds was nearly as good as it had been prior to the balancing of the fourth critical speed.

When run up to the fourth critical speed, an 80 percent reduction in amplitude was observed. The fourth critical speed, however, could still not be negotiated and another balancing correction weight set was calculated using the previously obtained influence coefficients. When these weights were added, there was a slight degradation in balance of the first and third critical speeds, but both critical speeds were still easily negotiable. A great improvement was observed at the easily negotiated fourth critical speed.

Another correction weight set was calculated and installed based on data taken at 917 and 3200 rpm, using the influence coefficients established during the earlier balancing of the third critical speed. After this correction weight set was installed, the response of the test shaft at the first and third critical speeds was improved, while the response at the fourth critical speed was essentially unaffected. At this point, the test shaft was very well balanced through the first four critical speeds.

Plots of the synchronous amplitude versus speed at several displacement probe locations during the course of influence coefficient balancing are presented in Figures X.1 through X.6. A phase plane plot of the response at one of the dis-

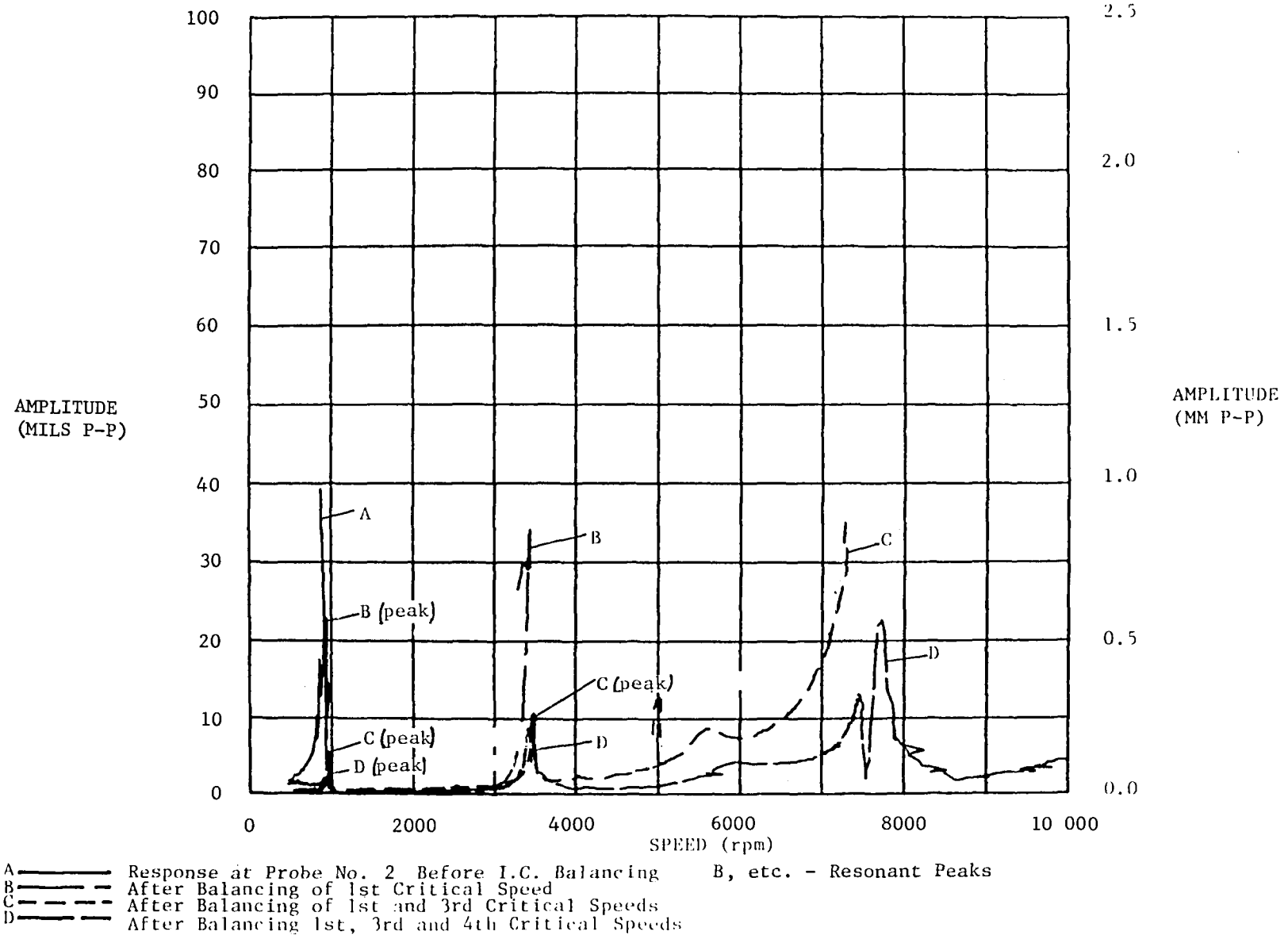

Fig. X.1 Response at Probe No. 2 During Influence Coefficient Balancing

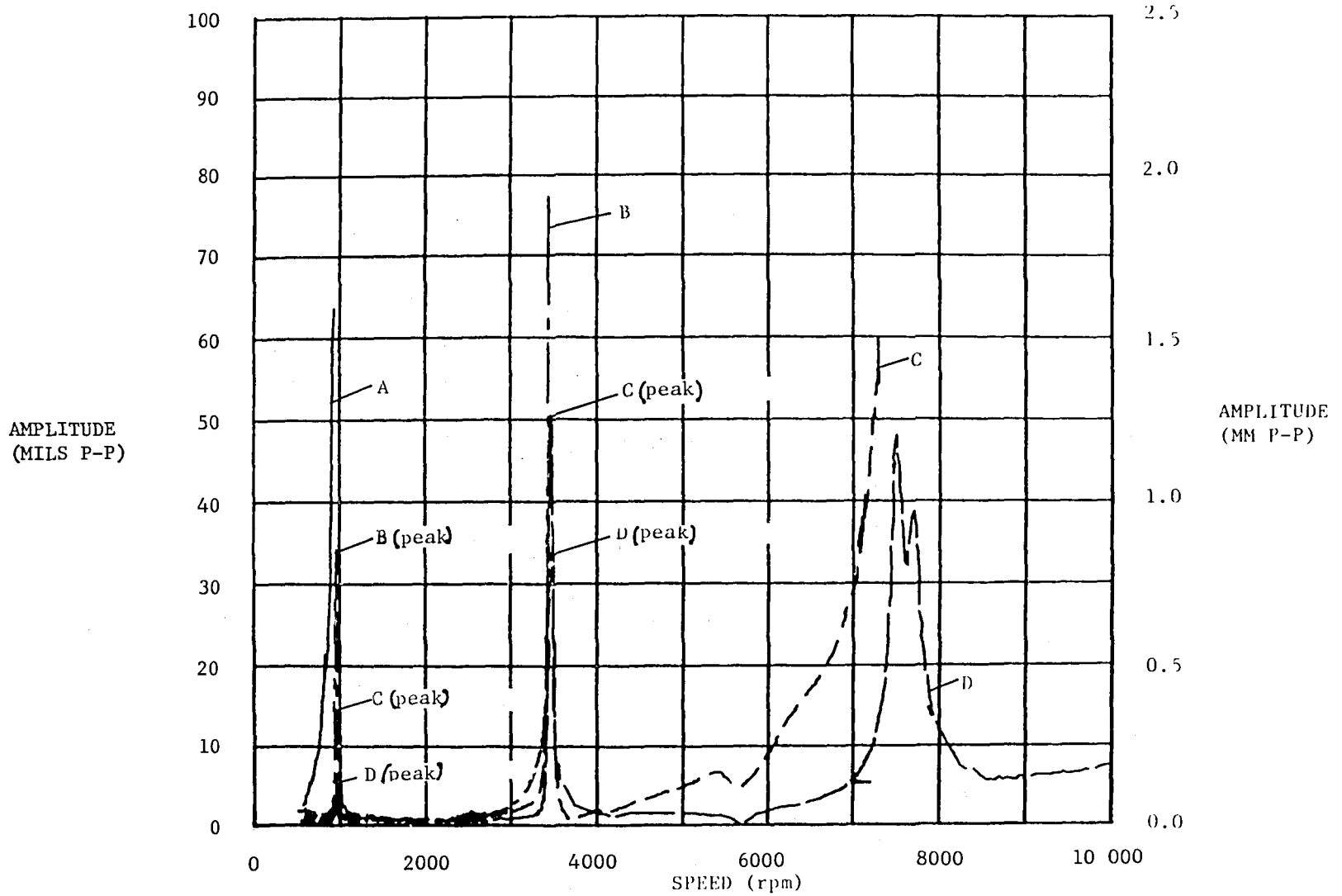

Fig. X.2 Response at Probe No. 3 During Influence Coefficient Balancing (Shaft Quarter Point)

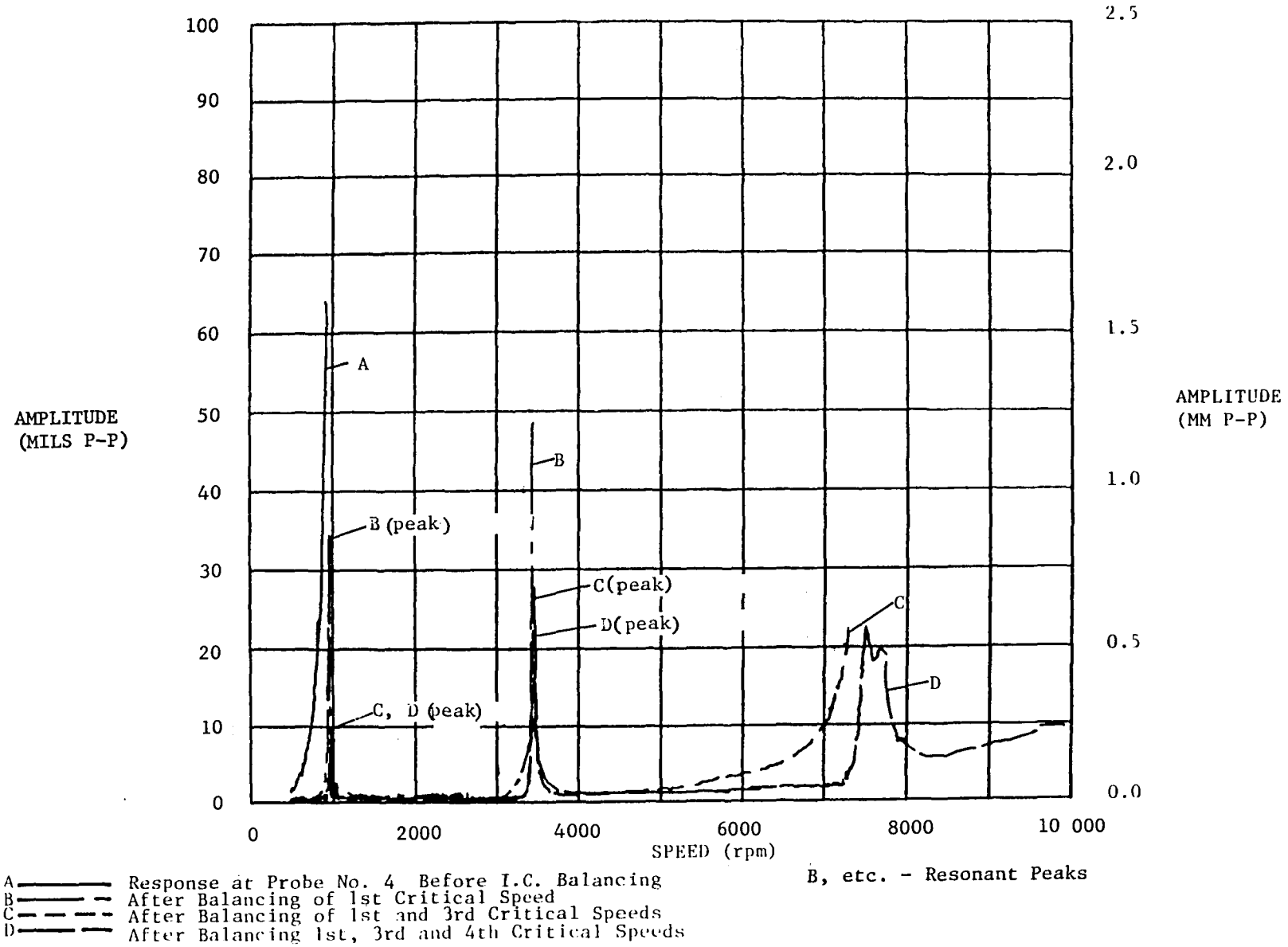

Fig. X.3 Response at Probe No. 4 During Influence Coefficient Balancing

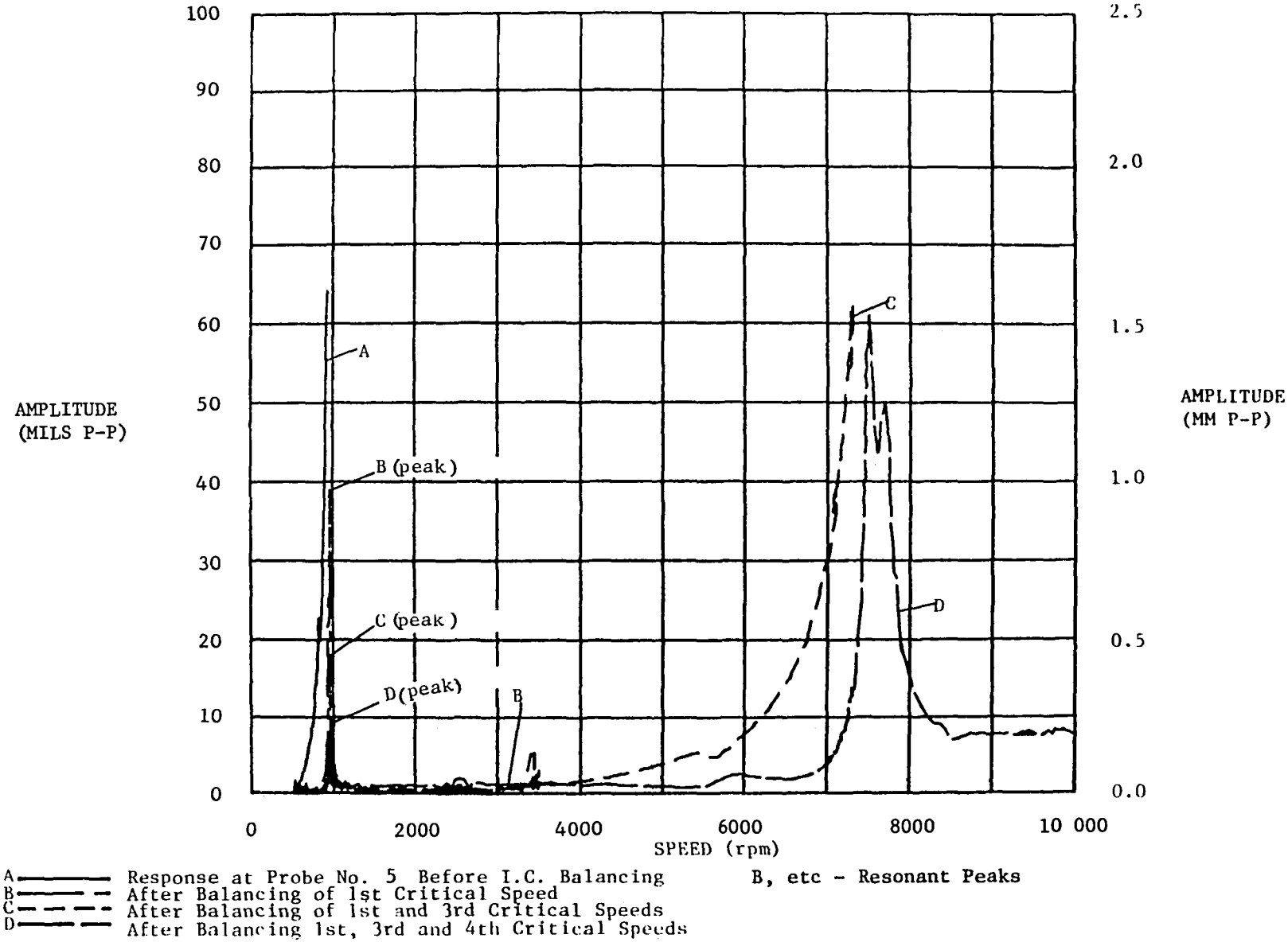

Fig. X.4 Response at Probe No. 5 During Influence Coefficient Balancing (Shaft Mid-Point)

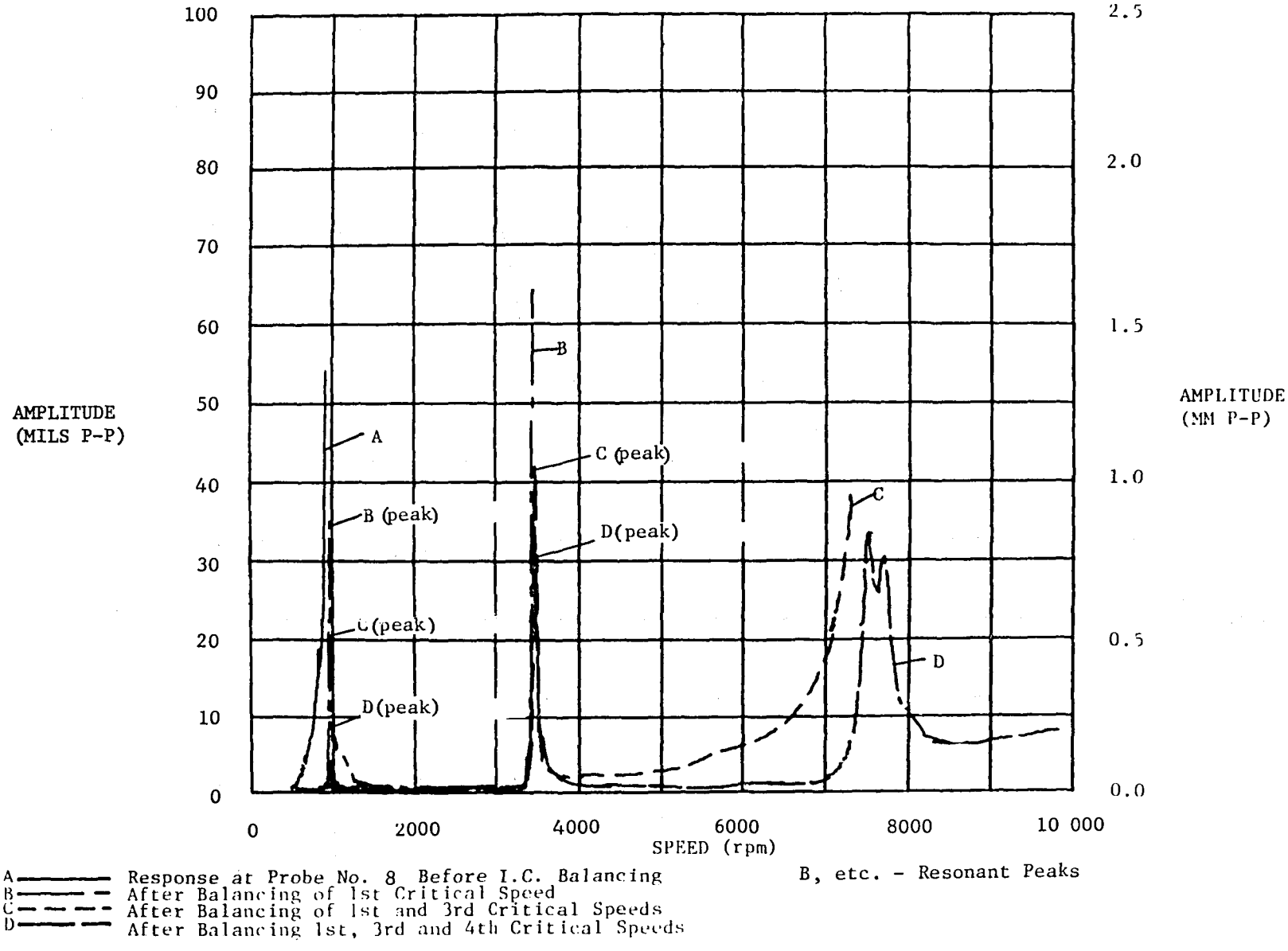

Fig. X.5 Response at Probe No. 8 During Influence Coefficient Balancing

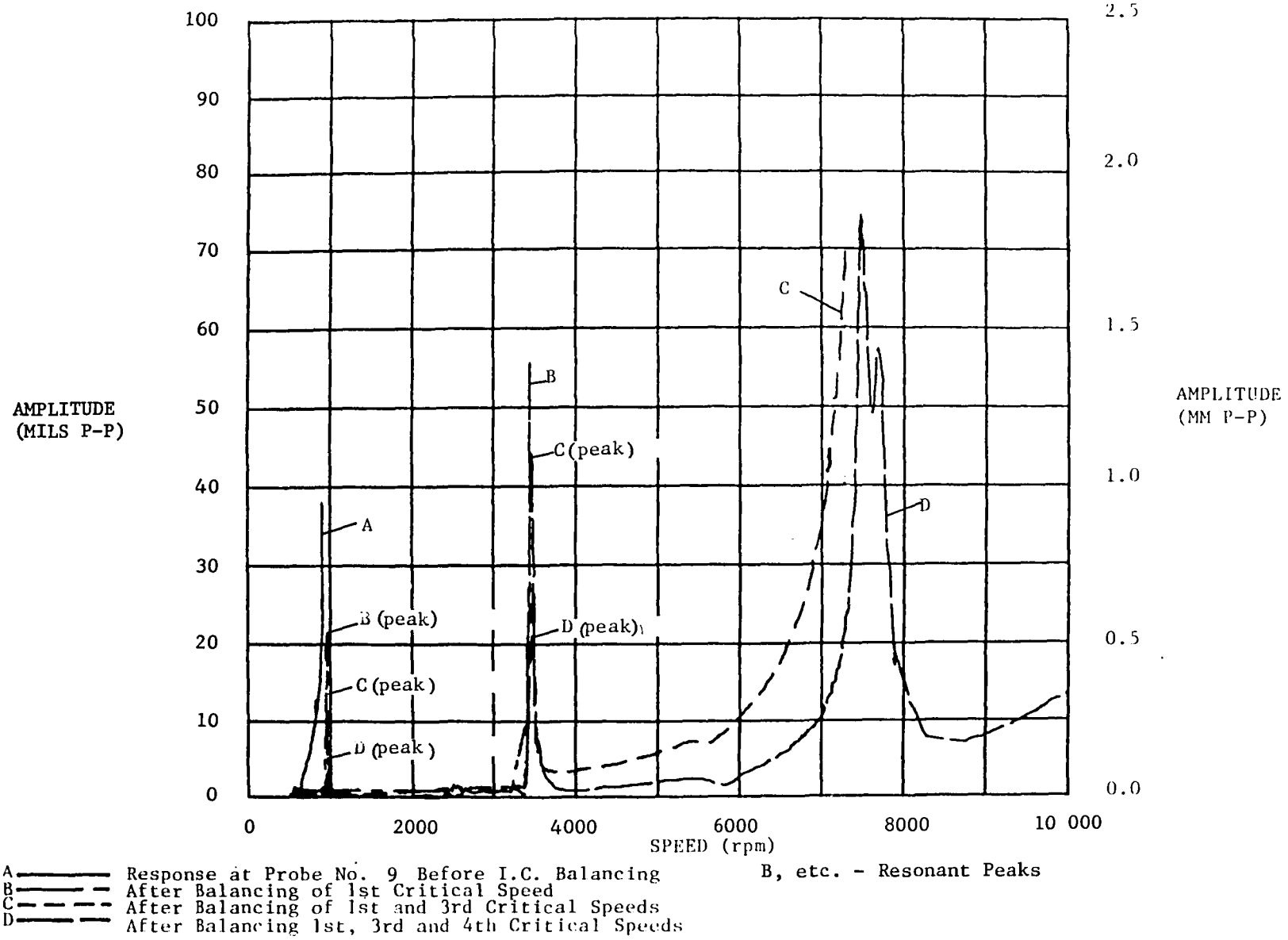

Fig. X.6 Response at Probe No. 9 During Influence Coefficient Balancing

placement probe locations for the balanced test shaft is presented in Figure X.7. For the response at probe Number 3 (see Figure VII.19 for probe identification numbers), separate phase plane plots are shown for each of the critical speeds in Figures X.8 through X.10.

MODAL BALANCING

A modified modal balancing procedure was used to balance the test shaft after most of the correction weights installed during the influence coefficient balancing had been removed in order to produce a moderately unbalanced test shaft. At the beginning of the modal balancing tests, the test shaft could not be run above approximately 921 rpm.

The procedure for the modified modal balancing of the first critical speed of the test shaft was no different from the influence coefficient balancing procedure described earlier in this section of the report. The same single displacement probe and single balancing plane, located near the center of the shaft, were used for the first critical speed and for the influence coefficient balancing. Data for the modified modal balancing was taken at 901 rpm. Several features of the influence coefficient balancing technique were used during the modified modal balancing. One of these was the use of two trial weight runs for each balancing plane, with the trial weight location shifted 180° from one run to the next. Also, for the modified modal balancing of the third and fourth critical speeds, balancing data was taken from several displacement probes and a least squares minimization analysis was used to calculate the correction weight sets, such that the response at all of these displacement probes would be minimized. An existing influence coefficient balancing program was used for the acquisition of balancing data, the calculation of influence coefficients and, under certain circumstances, the calculation of correction weights during the modified modal balancing.

Balancing data was taken for the first critical speed, as described above, and a correction weight was calculated. This correction weight was installed and the response amplitude at the balancing speed was reduced by about 97 percent. The first critical speed was easily negotiated and well controlled.

The procedure used for the third critical speed differed significantly from that used during influence coefficient balancing. Balancing planes 2 and 6, located approximately at the quarter points of the test shaft, were used. The first step was to determine the sensitivities of the test shaft near the first critical speed to unbalances at planes 2 and 6. Trial weight runs were conducted for planes 2 and 6, while response data was taken at 924 rpm and 944 rpm. The data taken at 944 rpm was not consistent due to time variation of the response at speeds very near the first critical speed (approximately 947 rpm). The sensitivities of the response of the test shaft, however, to unbalances located in planes 2 and 6, based on the data taken at 924 rpm, were essentially equal. Therefore, equal weights placed in planes 2 and 6, 180° apart, would be expected to have little or no effect on the response at the first critical speed, while significantly affecting the third critical response. Consequently, a modal trial weight set, based on such a pair of weights, was used for taking balancing data at the third critical speed. As expected, this trial weight set had no noticeable effect on response of the test shaft at the first critical speed. The trial weight set was treated as a single weight in the balancing calculations, and a correction weight set was calculated using standard influence coefficient techniques with data taken at

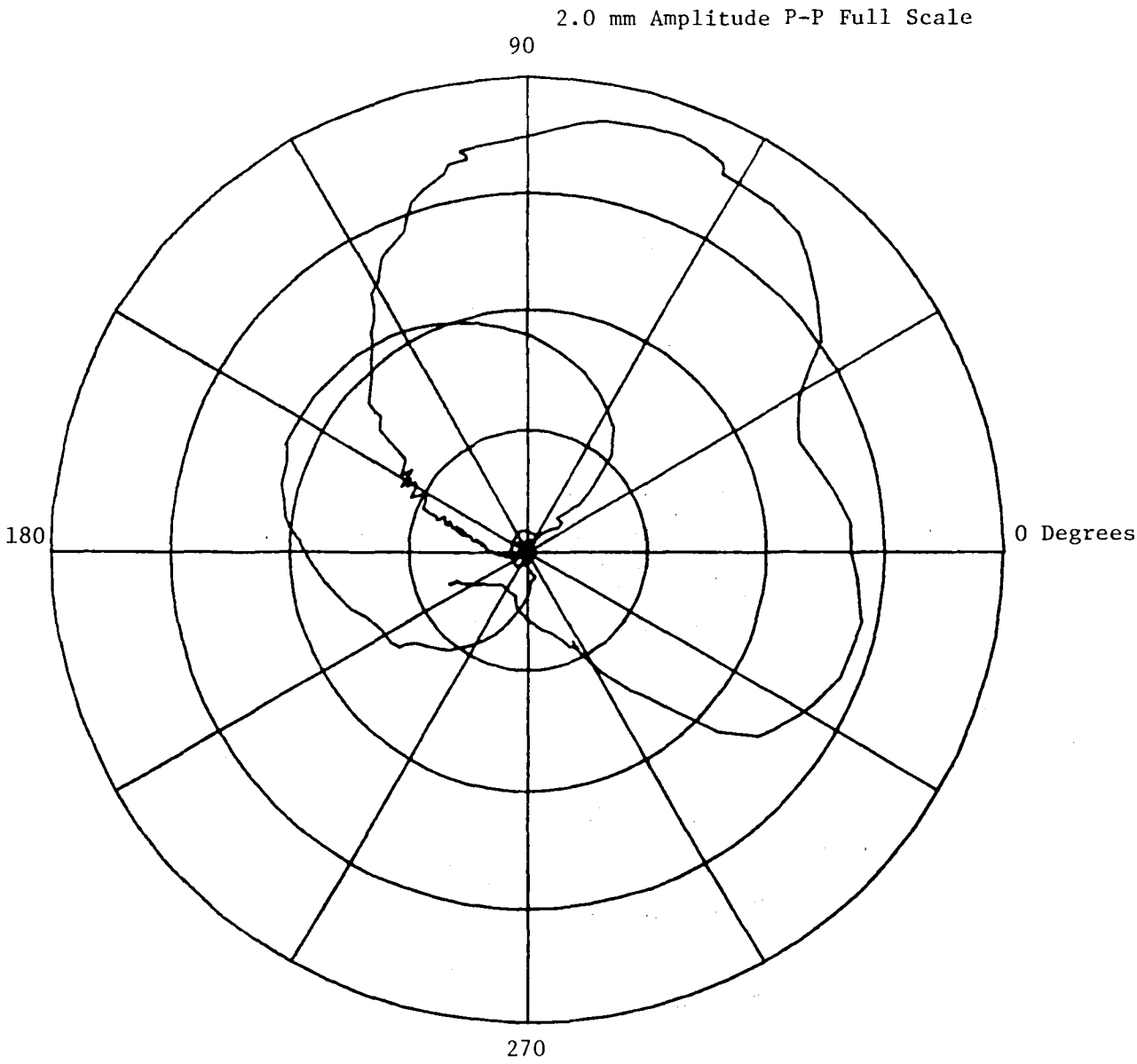

Fig. X.7 Phase Plane Plot for Probe No. 9 After Balancing of 1st, 3rd, and 4th Critical Speed (Influence Coefficient Balancing)

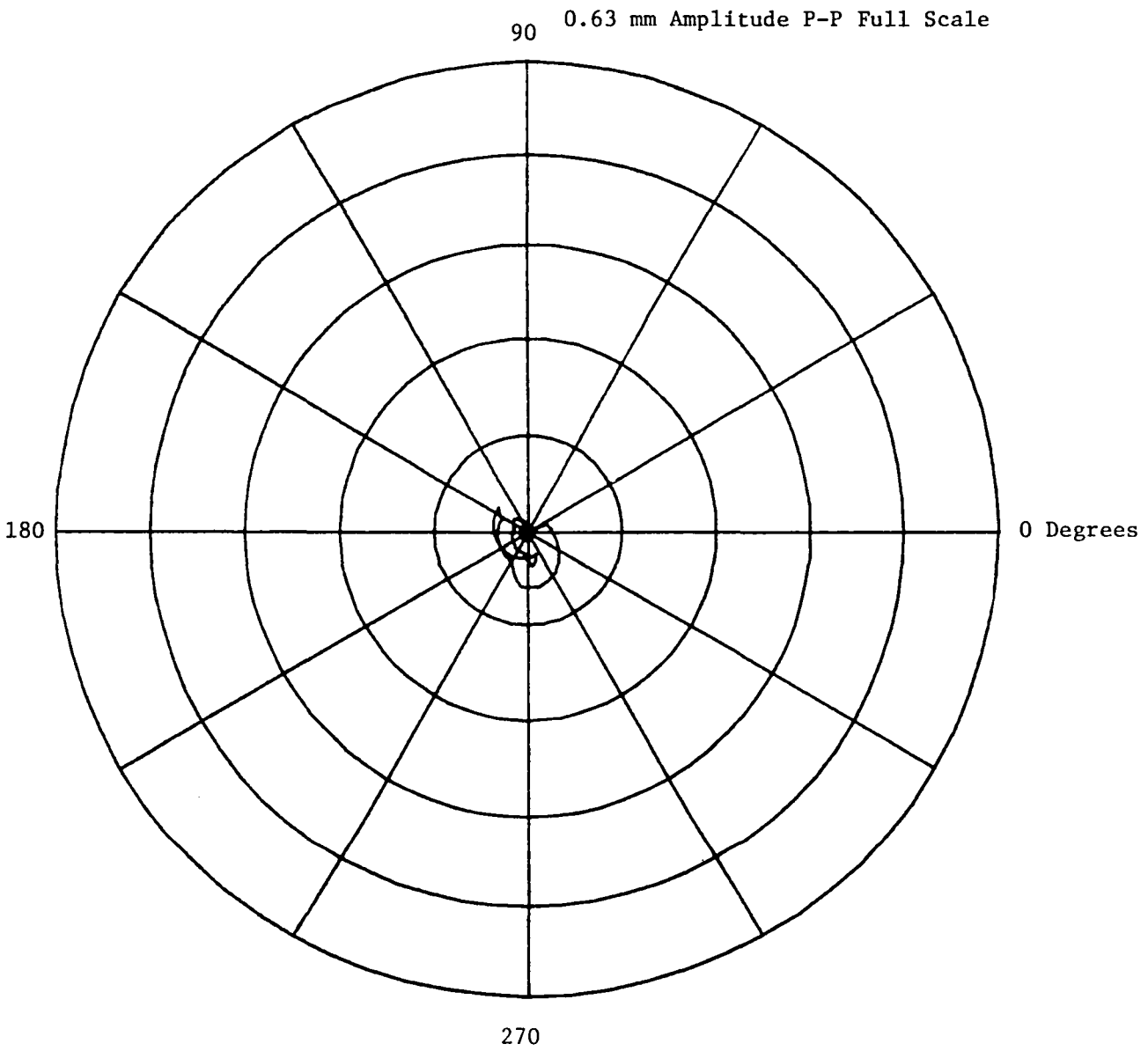

Fig. X.8 Phase Plane Plot for Probe No. 2 at First Critical Speed After Balancing 1st, 3rd, and 4th Critical Speeds (Influence Coefficient Balancing)

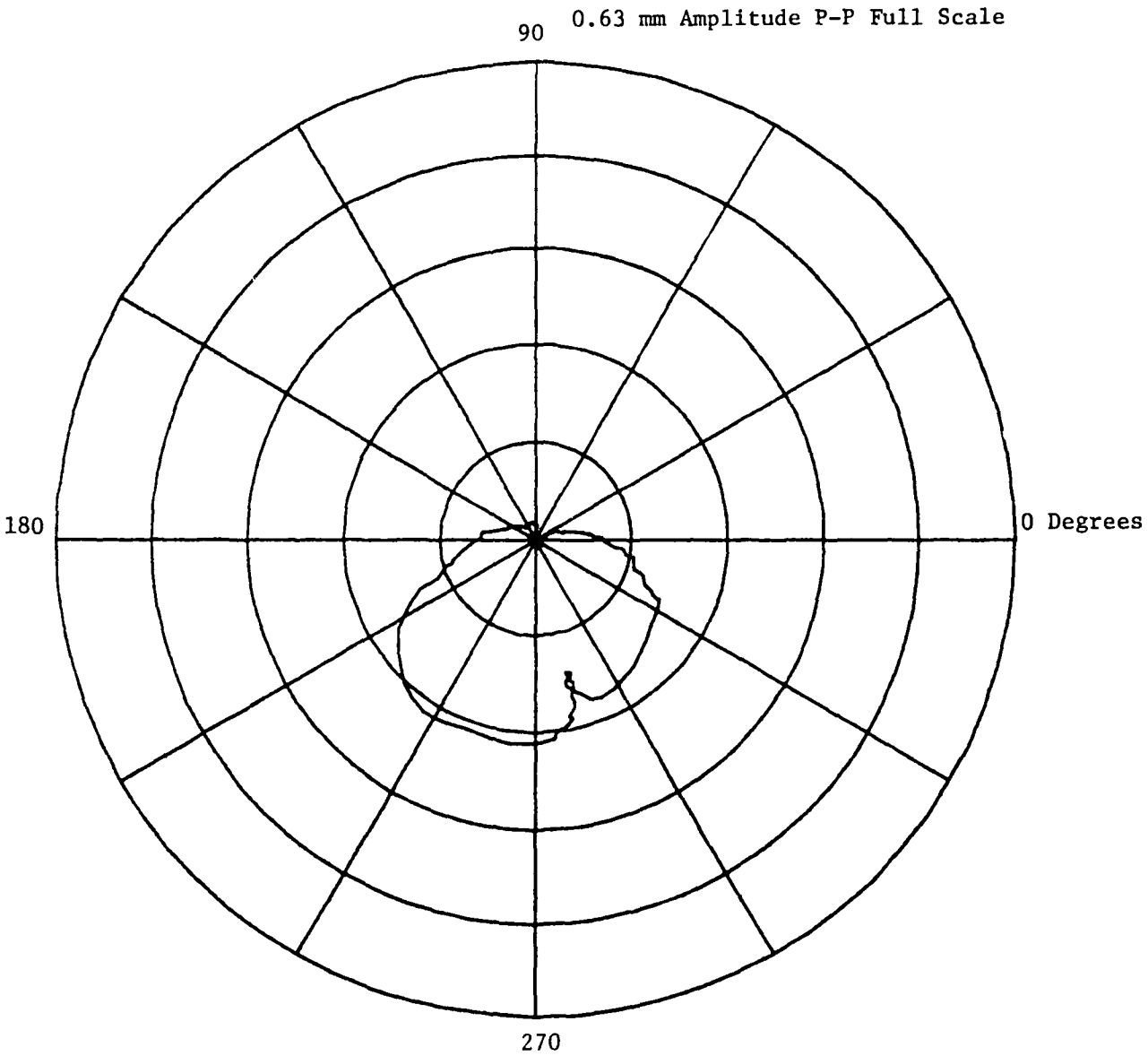

Fig. X.9 Phase Plane Plot for Probe No. 2 at Third Critical Speed After Balancing 1st, 3rd, and 4th Critical Speeds (Influence Coefficient Balancing)

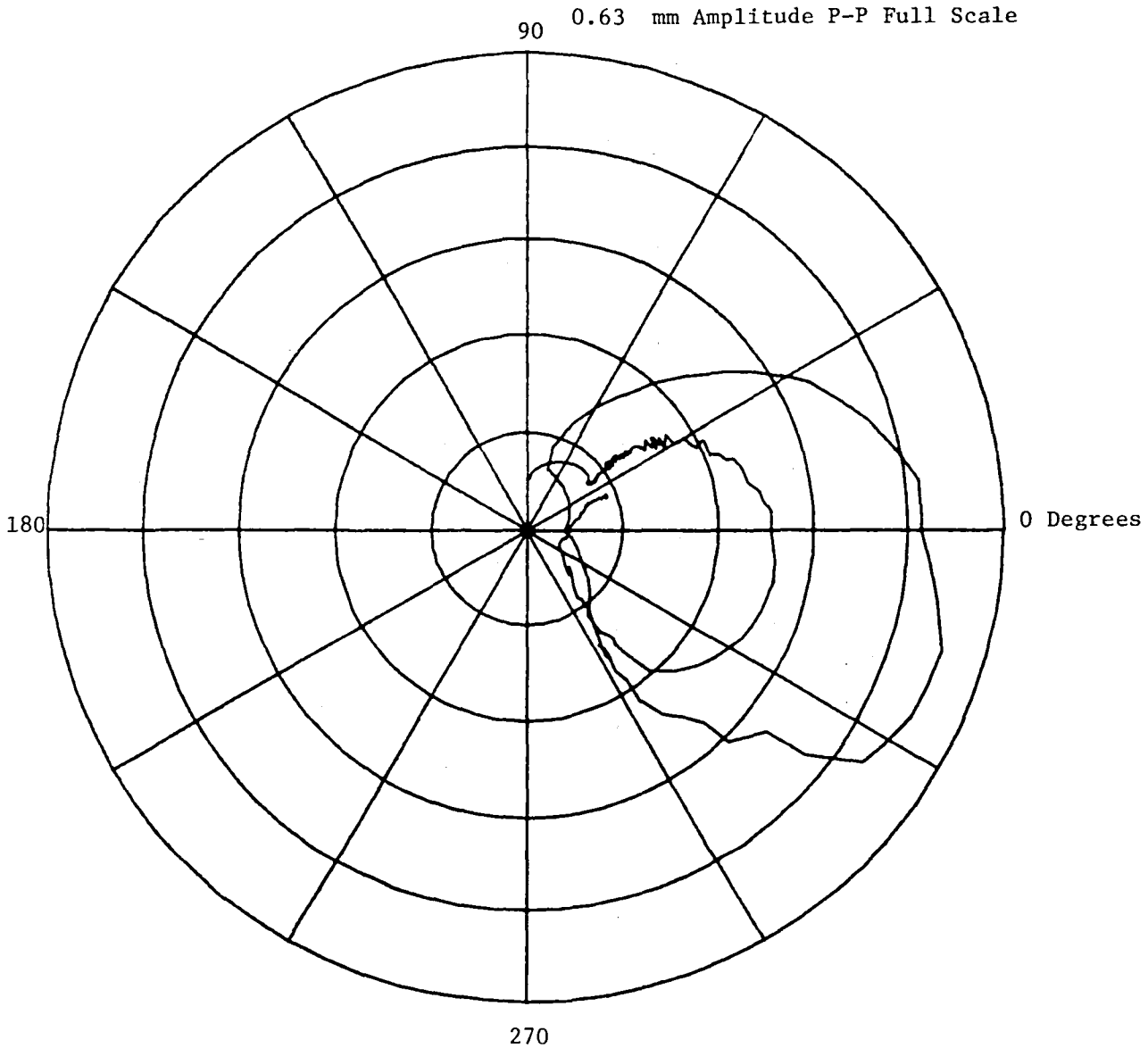

Fig. X.10 Phase Plane Plot for Probe No. 2 at Fourth Critical Speed After Balancing 1st, 3rd, and 4th Critical Speeds (Influence Coefficient Balancing)

3200 rpm. Since there was no effect at the first critical speed, it was not necessary to take balancing data at the first critical speed. The balancing data for the third critical speed was taken from the two displacement probes adjacent to planes 2 and 6. Two sequential modal correction weight sets were added and a great reduction in amplitude resulted. The third critical speed was easily negotiated with no noticeable effect on amplitudes of the first critical speed. Examination of the resulting test shaft response data indicated that some response to the fourth critical speed was left at 3200 rpm, while virtually no response to the third critical speed remained. The use of two displacement probes and least squares minimization of the balancing data, during the balancing of the third critical speed, permitted the separation of the modes of response during the calculation of the correction weights. Had a single displacement probe been used, the correction weight would have been calculated such that the response at the displacement probe would have been reduced to zero. This would have resulted in equal and opposite responses to the third and fourth critical speeds, at the balancing speeds, and a less effectively balanced third critical speed. Using the modified modal balancing technique, the third critical speed was very well balanced.

The procedure for modified modal balancing of the fourth critical speed was similar to that for the third critical speed. In this case, three balancing planes were used, planes 2, 4, and 6, and sensitivities for each of these planes at the first and third critical speeds were determined from trial weight data taken at 917 rpm and 3200 rpm. Based on these sensitivities, the modal trial weight set used for balancing the fourth critical speed was composed of 1 gram weights in planes 2 and 6, on the same side of the test shaft; and a 1.4 gram weight in plane 4 on the opposite side of the test shaft. Balancing data for the fourth critical speed, using this modal trial weight set, was taken at 6400 rpm. Three probes, adjacent to planes 2, 4, and 6, were used for balancing data. The two trial-weight-per-plane feature of influence coefficient balancing was used by first installing the plane 2 and 6 trial weights at 0° and the plane 4 trial weight at 180°, and by taking balancing data. Then, the plane 2 and 6 trial weights were moved to 180°, while the plane 4 trial weight was moved to 0°, and, again, balancing data was taken. The effect of the summation of these three trial weights at the fourth critical speed was equivalent to a trial weight an order of magnitude larger than that used for the fourth critical speed balancing runs during the influence coefficient balancing operation. Consequently, the modal trial weight set had a much more significant effect on the response near the fourth critical speed. As intended, the modal trial weight set for the fourth critical speed had almost no effect on the response at the first and third critical speeds.

A relatively large correction weight set was calculated for balancing the fourth critical speed, a total of about 30 grams; this modal correction weight set was installed. Subsequently, the response of the test shaft at the first critical speed was slightly worse than before the addition of this correction weight set. The response at the third critical speed was apparently unaffected, while the response at the fourth critical speed was reduced by more than 94 percent. The fourth critical speed was easily negotiated after the addition of this single modal correction weight set.

In an attempt to offset the effect of this correction weight set on the response of the first critical speed, a trim balance correction weight was calculated for the first critical speed with data taken at 901 rpm. This correction weight

was installed and resulted in considerable improvement at the first critical speed, no effect at the third critical speed, and a slight improvement at the fourth critical speed. Thus, using the modified modal balancing technique, the test shaft was successfully balanced through the first four flexural critical speeds.

Plots of synchronous amplitude, as a function of rotational speed, for a number of displacement probes are presented in Figures X.11 through X.16. These plots show the response of the test shaft at various stages of the modified balancing procedure. A phase plane plot of the response at one of the displacement probe locations for the balanced test shaft is presented in Figure X.17. For the response at probe No. 3, separate phase plane plots are shown for each of the critical speeds in Figures X.18 through X.20.

DAMPER BEHAVIOR

During the operation of the test rig, the amplitude of vibration of the test shaft damper was observed to grow to a maximum at speeds which were apparently not related to the critical speeds of the test shaft. Examination of two of the synchronous response plots for the test shaft damper, presented in Figures X.21 and X.22, reveals apparent resonances at about 4100 rpm and 5700 rpm. These resonances appear to be critical speeds of the damper shaft and are quite well damped, as would be expected. The damper amplitudes at these resonances are very small when compared to the amplitude of vibration of the test shaft. It is not surprising, therefore, that the test shaft did not appear to respond to the damper resonances. It should be noted that some advantage may be gained from the appearance of such damper resonances. If a damper can be designed to have intentional resonances which coincide with the critical speeds of a test shaft, then significant damper amplitudes at the test shaft critical speeds will be ensured. The result is a "tuned" damper.

OPERATION TO 12,000 RPM

After a subsequent disassembly and reassembly of the test rig, the test shaft was again balanced through four flexural critical speeds. The test rig was run to over 12,000 rpm; this was the first time it had been run to more than 10,000 rpm. At 12,000 rpm there was substantial synchronous growth of the response to the fifth critical speed. There was also a very large subsynchronous response of the first and fourth critical speeds. In fact, the subsynchronous response of the first critical speed, while running at 12,000 rpm, was such that the test rig could not be run higher in speed. It is possible that subsynchronous response of the first critical speed was due to internal damping, similar to that observed with the undamped test rig. If this is the case, then the effect of the added damping was to raise the threshold of this instability from just over the first critical speed to almost 13 times the first critical speed, which was indeed a substantial improvement. The subsynchronous response of the fourth critical speed was most significant at a rotational speed of about 11,800 rpm, as illustrated by the frequency spectrum plot at the top of Figure XI.7. However, at a rotational speed of 12,000 rpm, the subsynchronous response of the first critical speed became predominant, while that of the fourth critical speed had become much less significant, as illustrated by the frequency spectrum plot presented at the bottom Figure XI.7. In any case, it was demonstrated that the test rig could be run to more than 11,000 rpm with no large synchronous or nonsynchronous response of the test shaft.

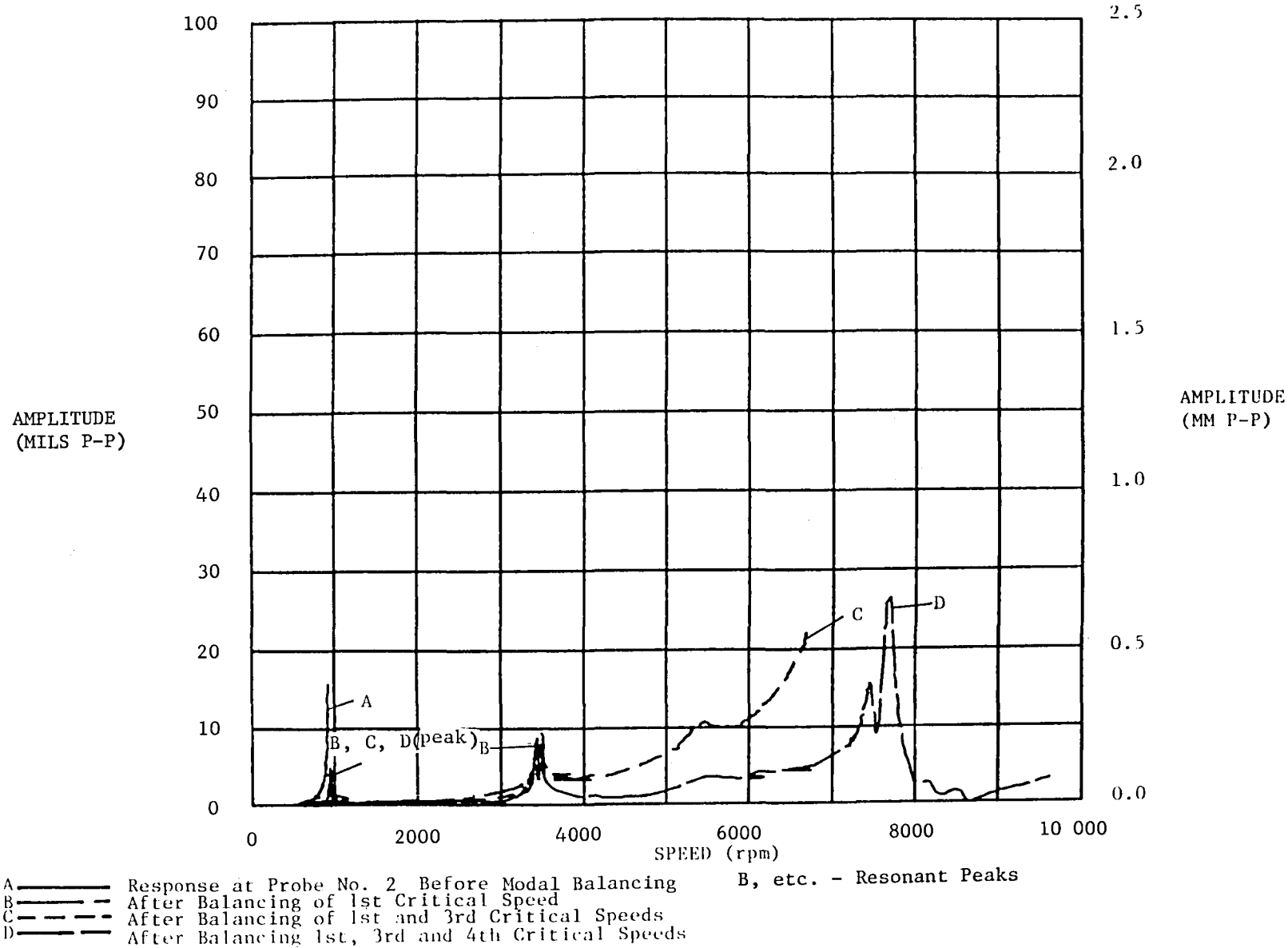

Fig. X.11 Response at Probe No. 2 During Modal Balancing

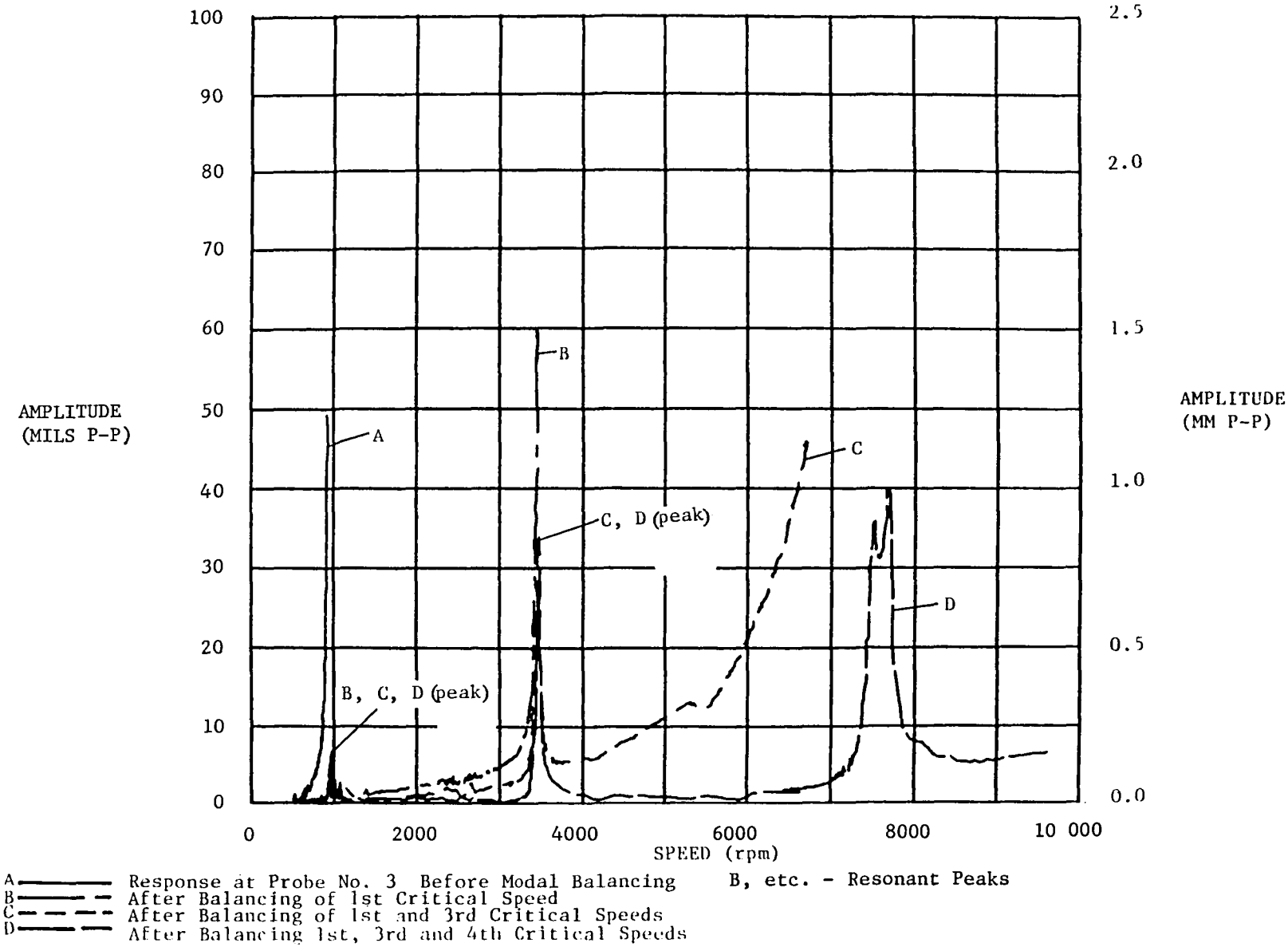

Fig. X.12 Response at Probe No. 3 During Modal Balancing

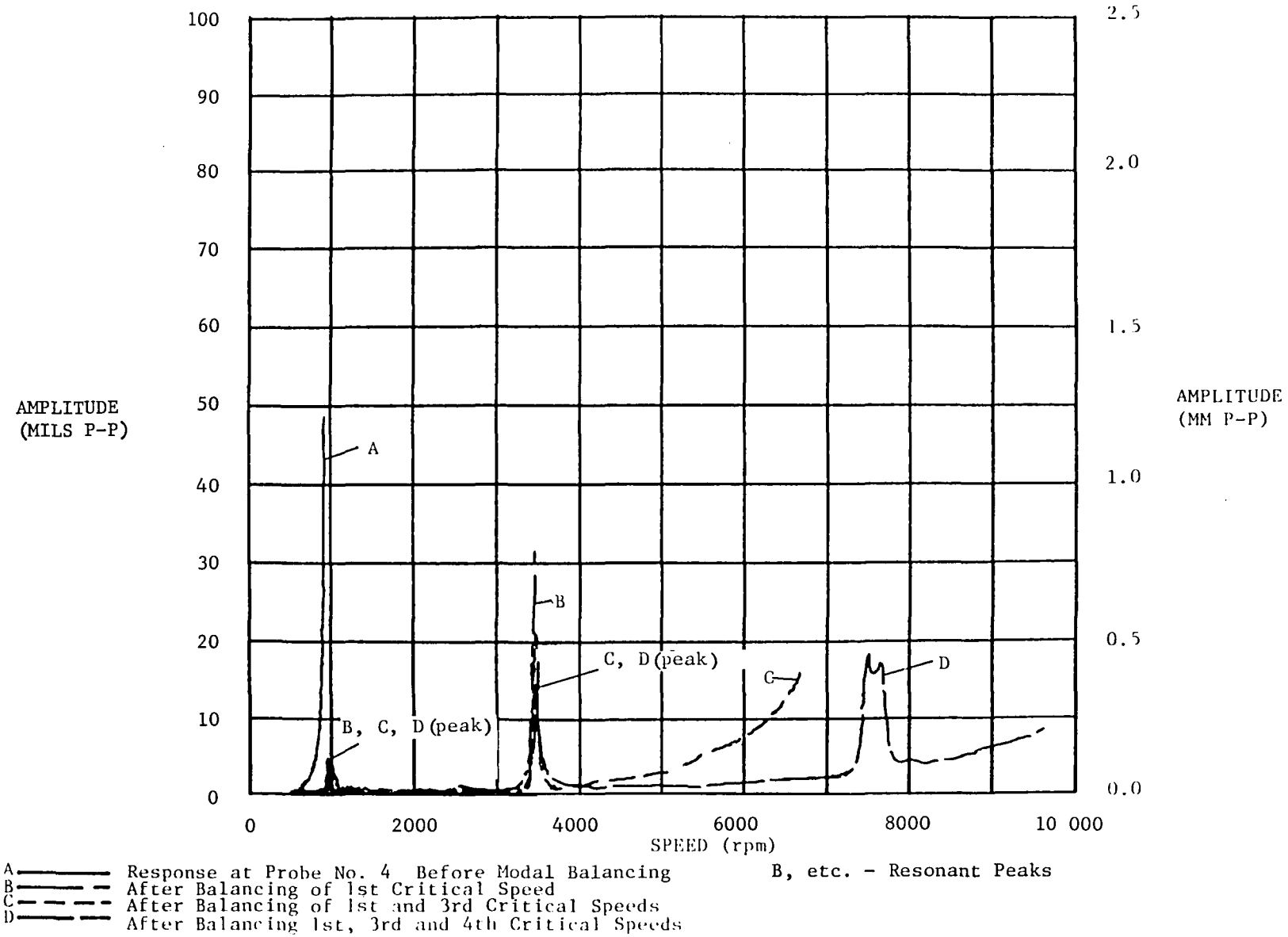

Fig. X.13 Response at Probe No. 4 During Modal Balancing

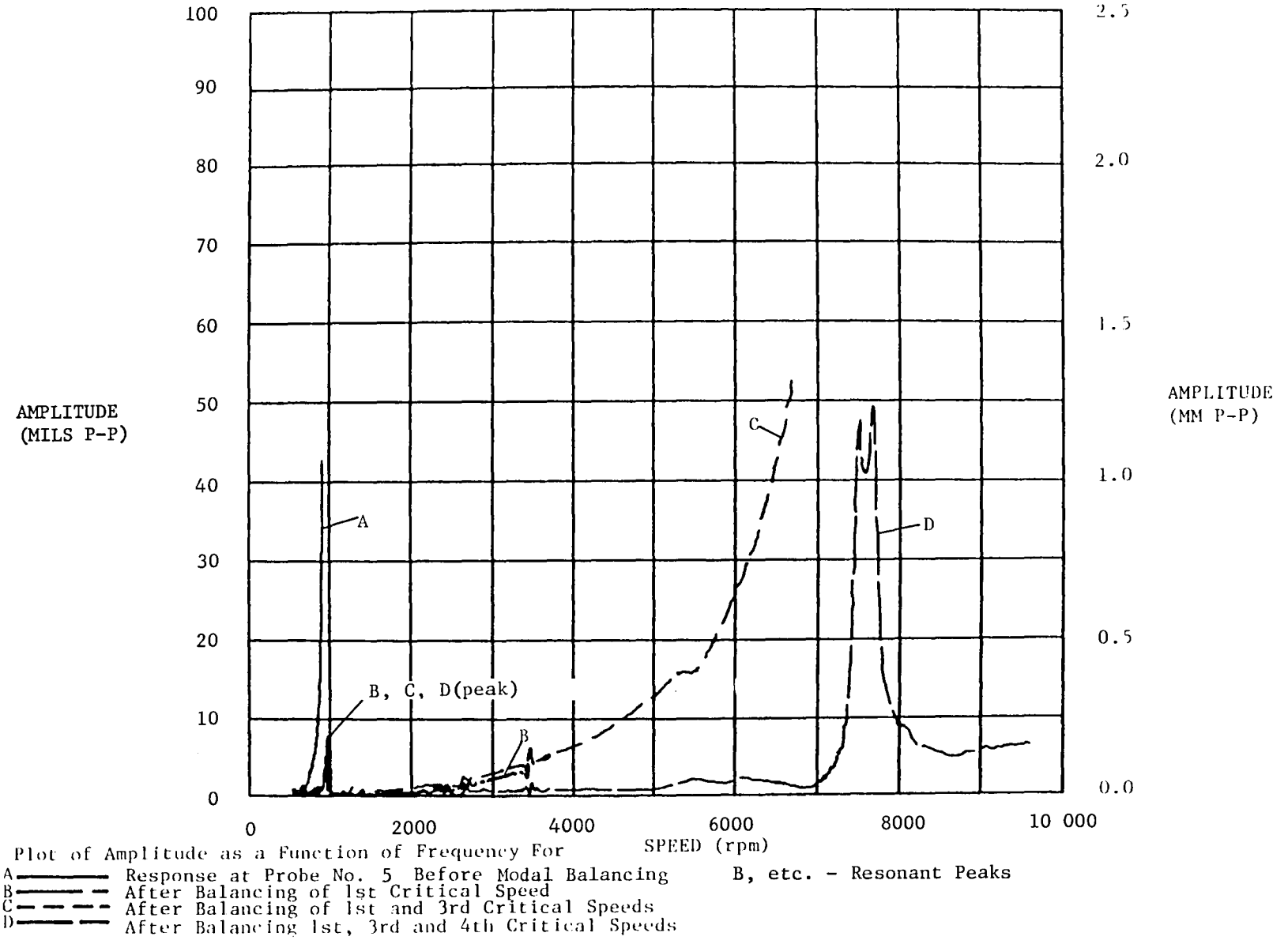

Fig. X.14 Response at Probe No. 5 During Modal Balancing

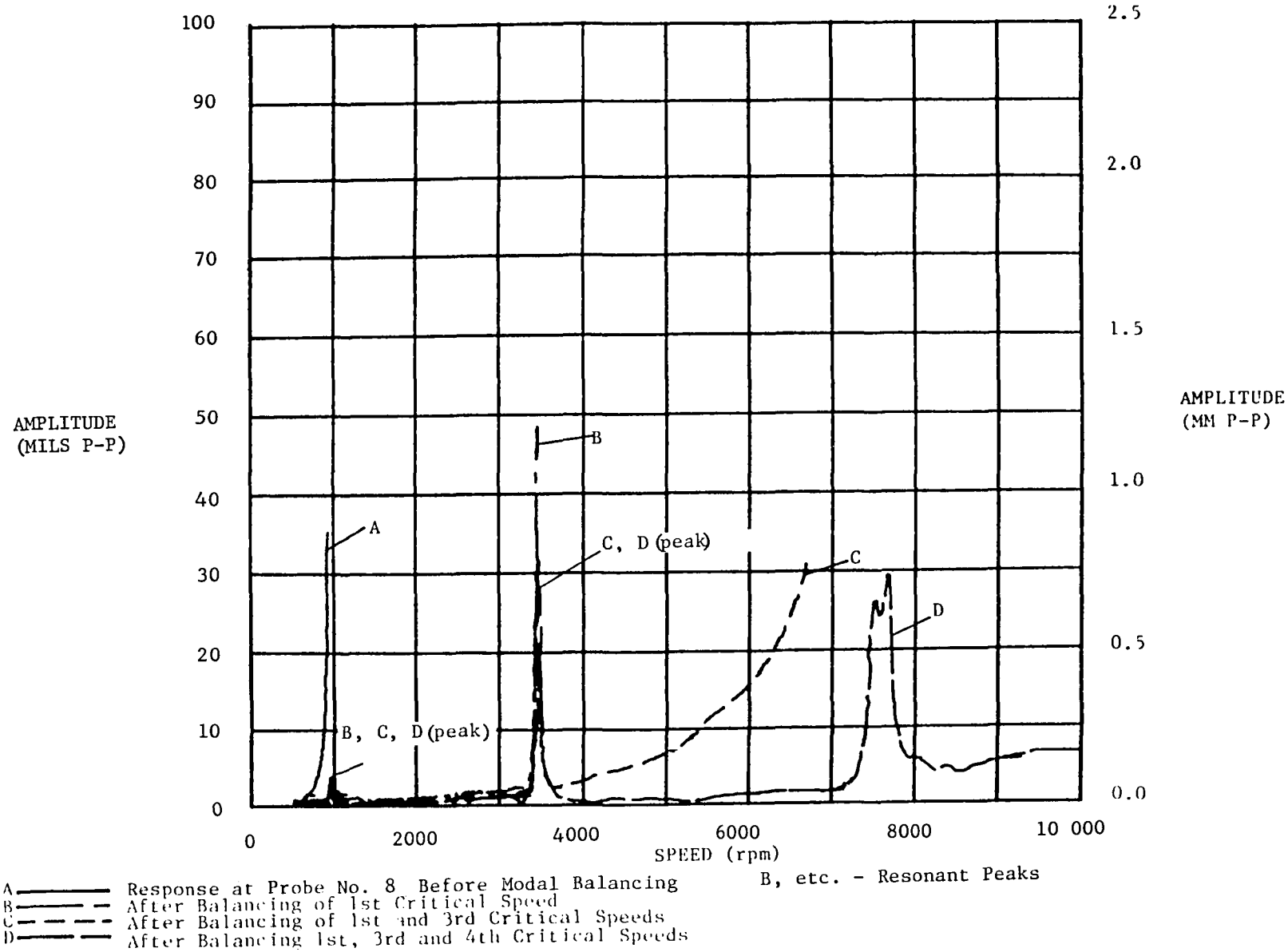

Fig. X.15 Response at Probe No. 8 During Modal Balancing

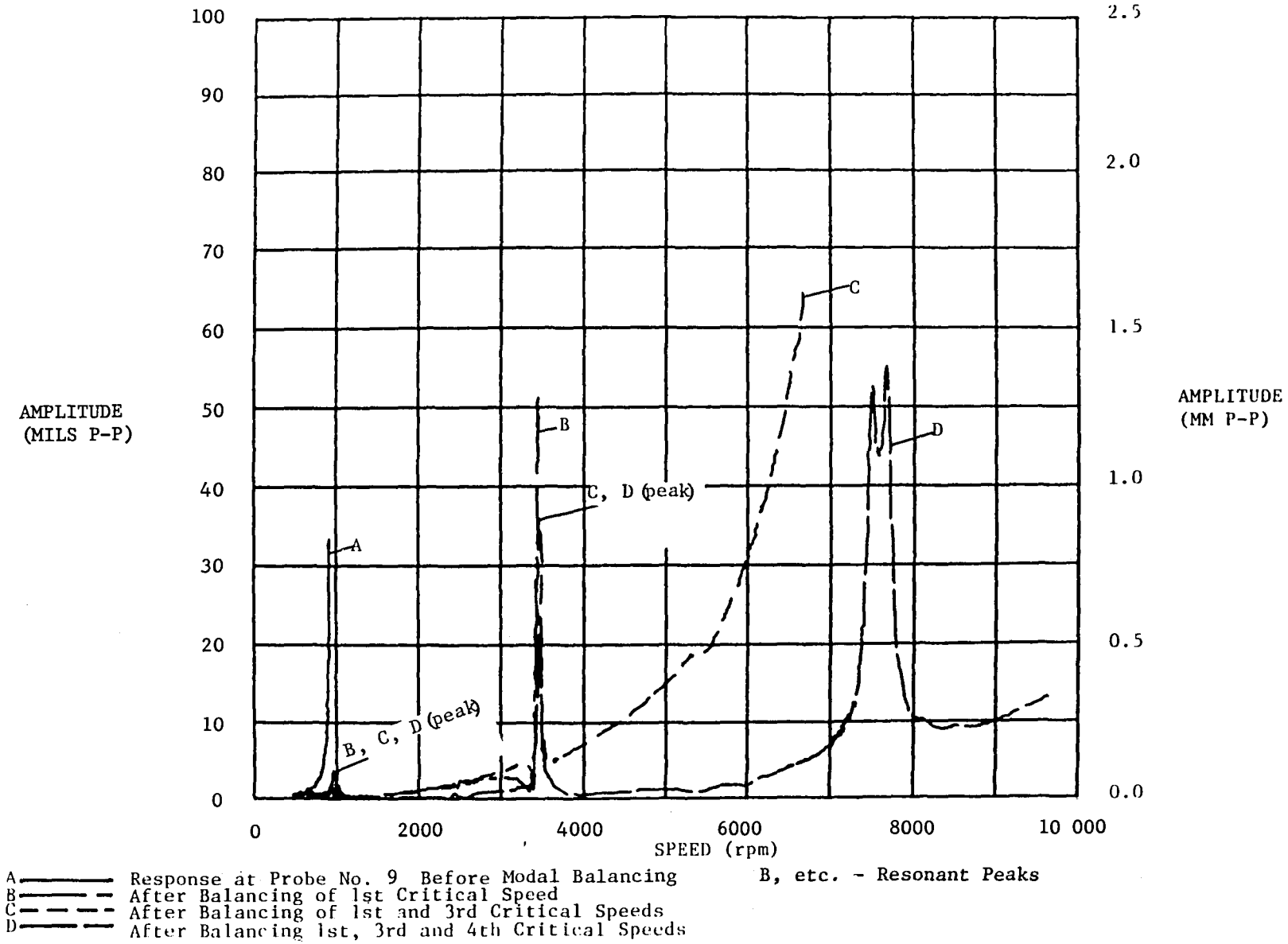

Fig. X.16 Response at Probe No. 9 During Modal Balancing

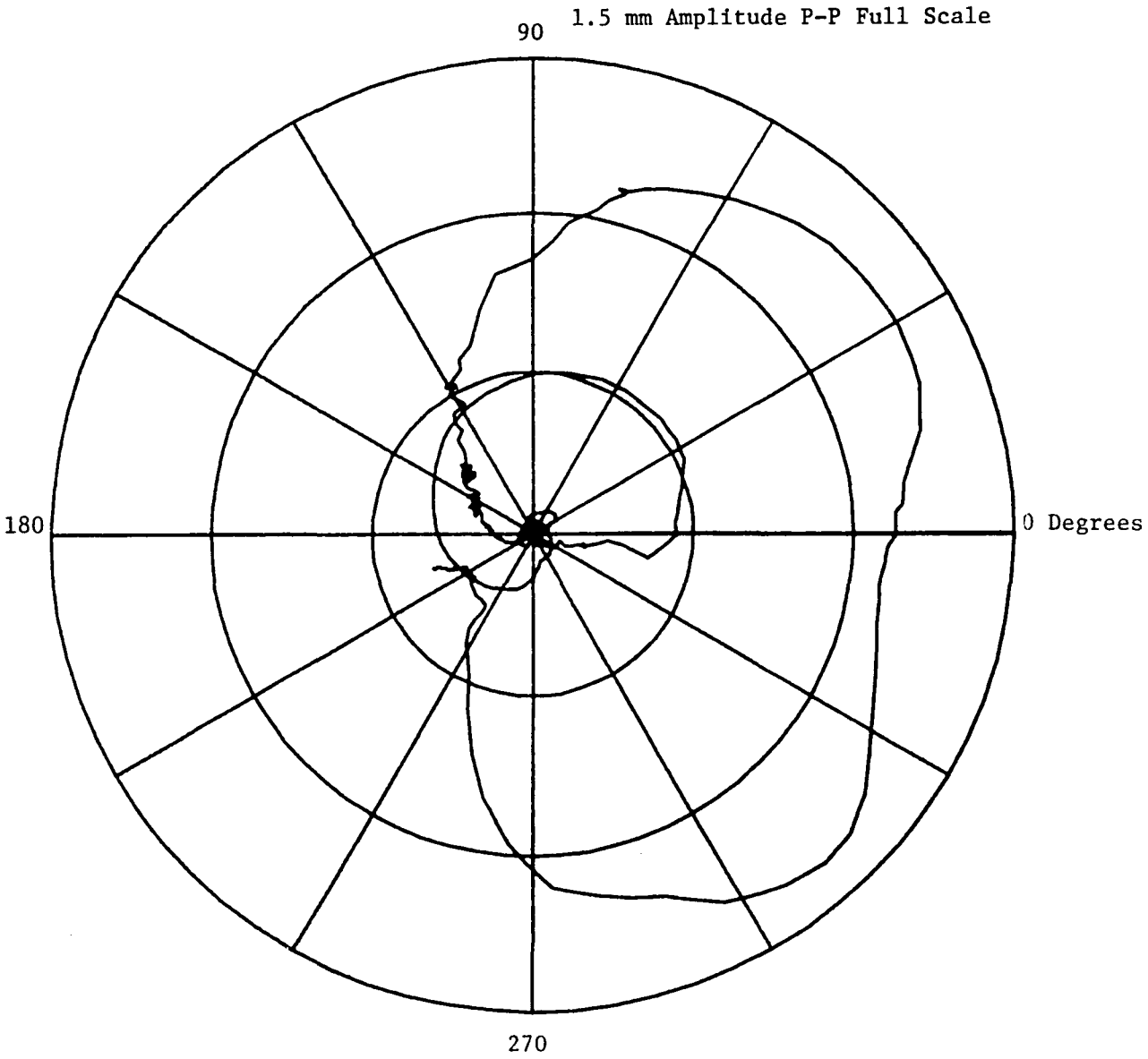

Fig. X.17 Phase Plane Plot For Probe No. 9 After Balancing of 1st, 3rd and 4th Critical Speed (Modal Balancing)

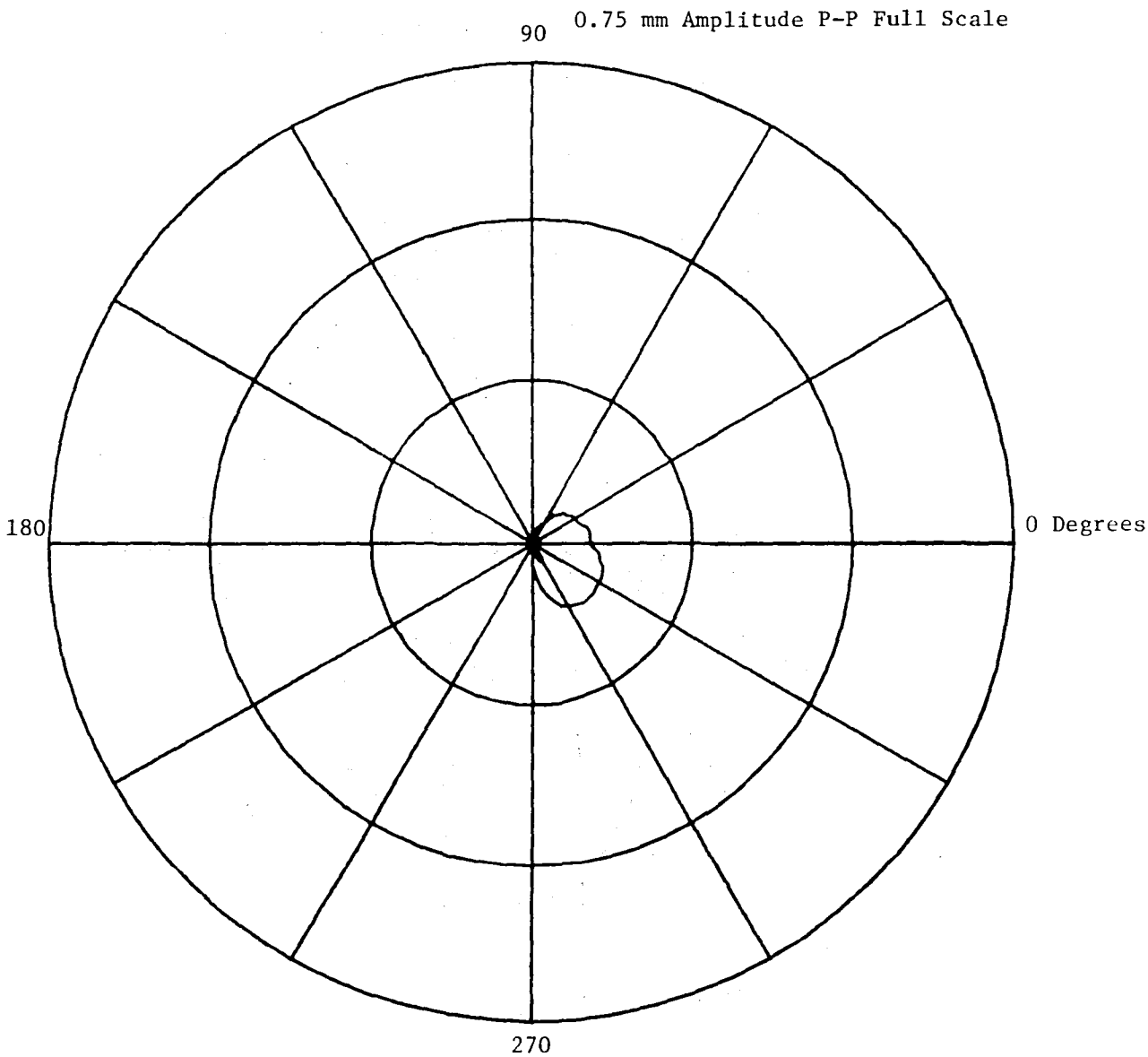

Fig. X.18 Phase Plane Plot For Probe No. 3 at First Critical Speed After Balancing of 1st, 3rd and 4th Critical Speed (Modal Balancing)

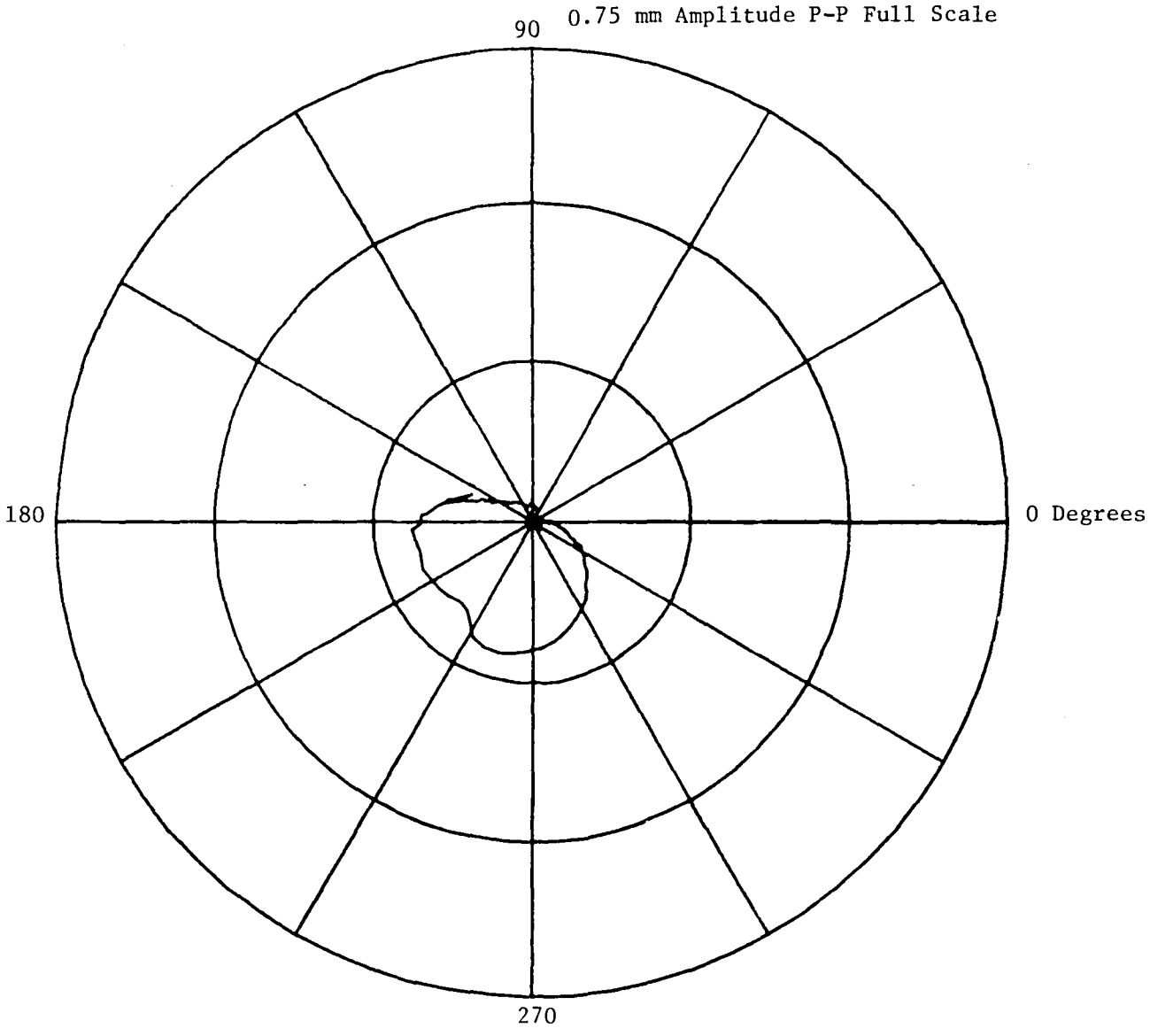

Fig. X.19 Phase Plane Plot For Probe No. 3 at Third Critical Speed After Balancing of 1st, 3rd and 4th Critical Speed (Modal Balancing)

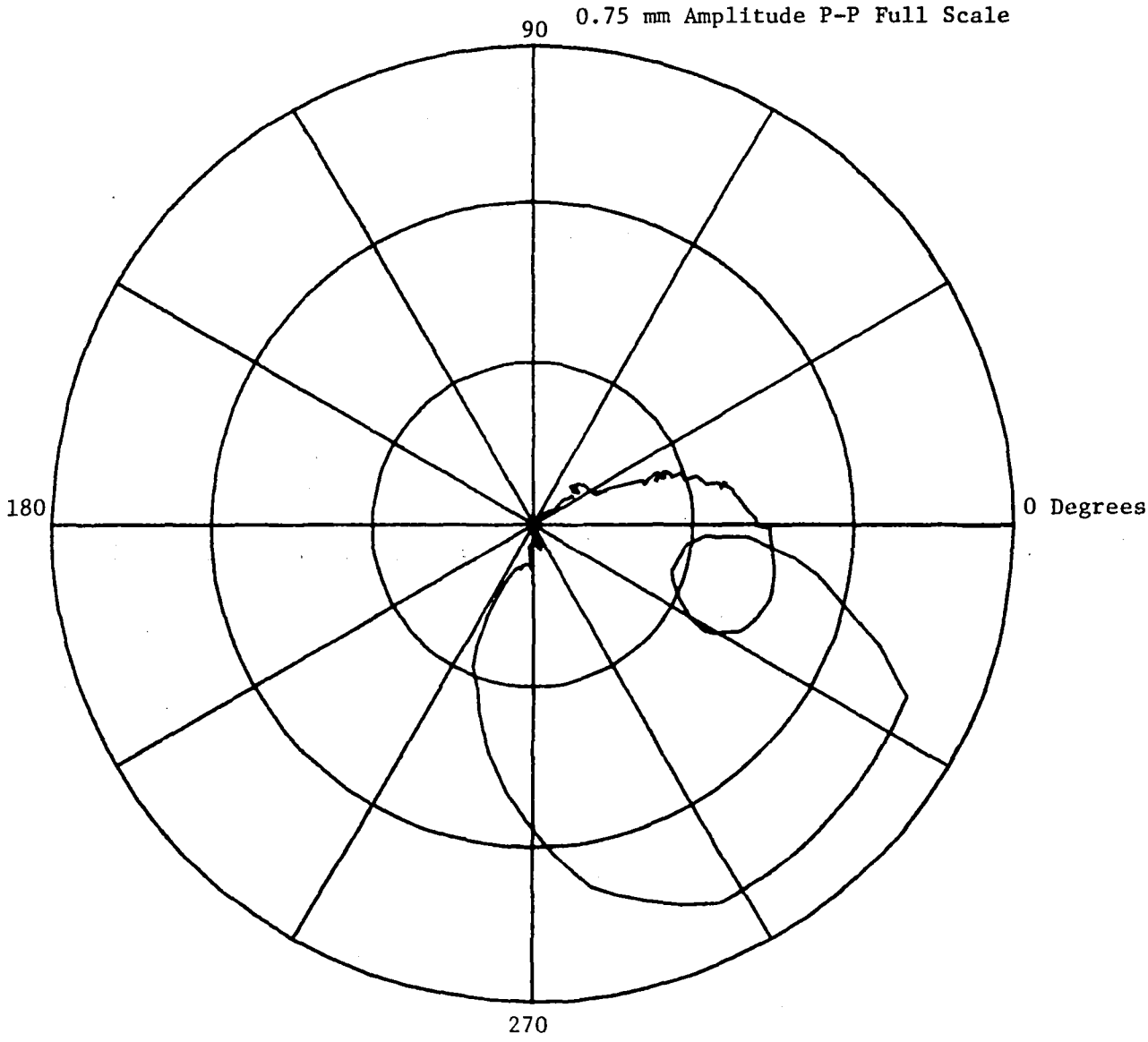

Fig. X.20 Phase Plane Plot For Probe No. 3 At Fourth Critical Speed After Balancing of 1st, 3rd and 4th Critical Speed (Modal Balancing)

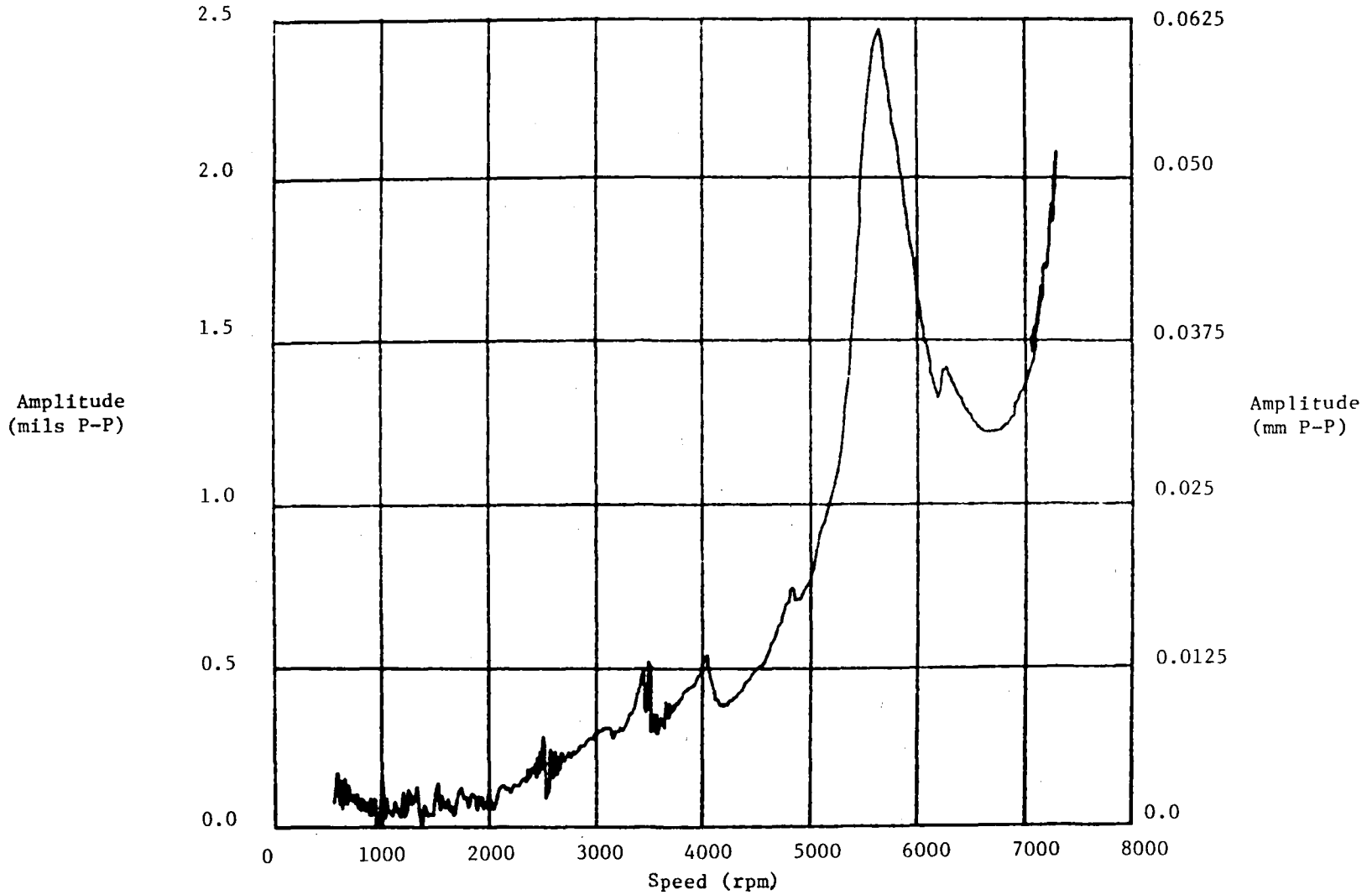

Fig. X.21 Plot of Amplitude as a Function of Frequency for Probe No. 10 After Balancing of 1st and 3rd Critical Speeds (Illustrating Damper Resonance)

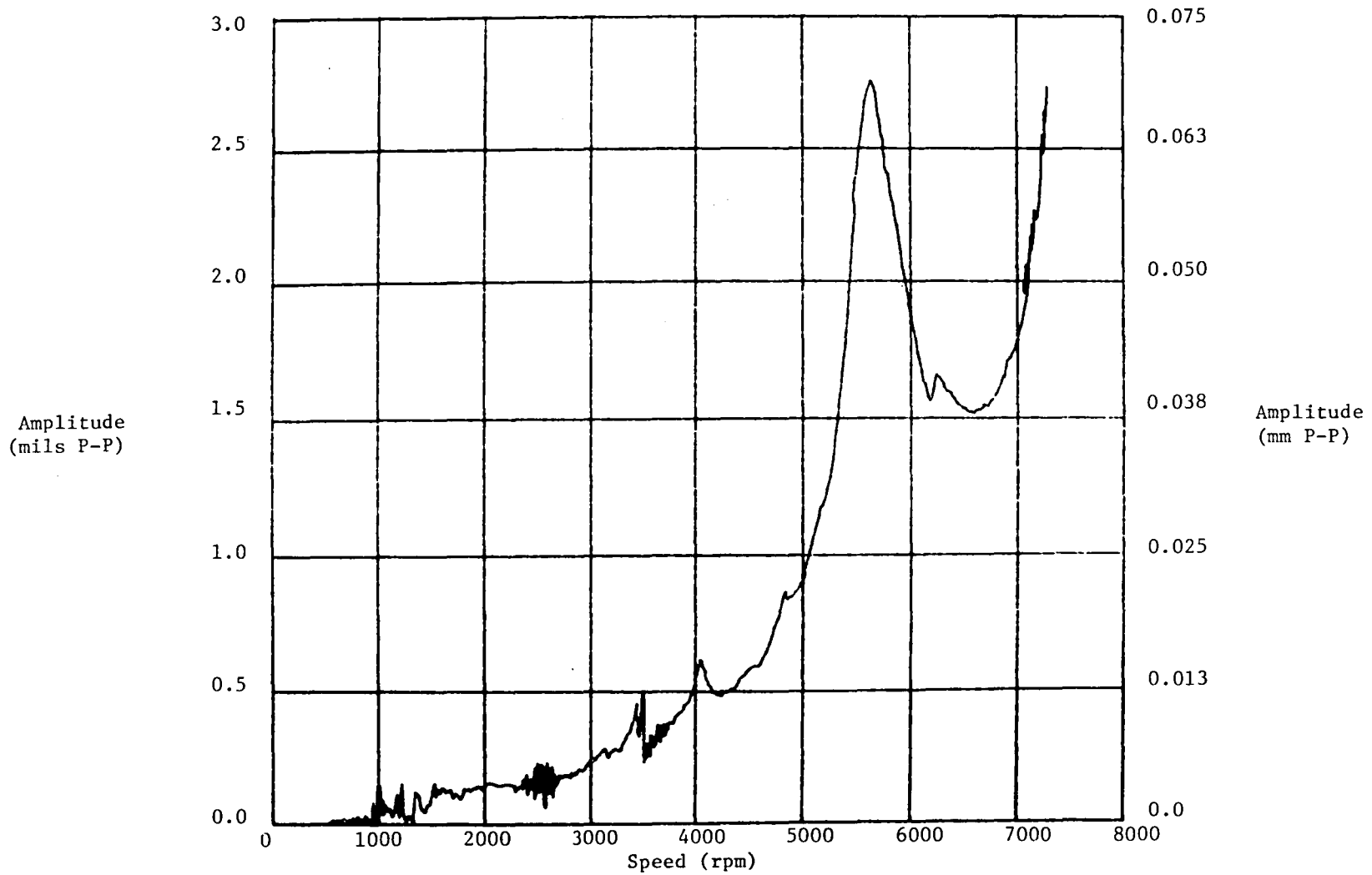

Fig. X.22 Plot of Amplitude as a Function of Frequency for Probe No. 11 After Balancing 1st and 3rd Critical Speeds (Illustrating Damper Resonance)

Plots of synchronous test shaft response, as a function of speed, for several of the displacement probes for the run up to 12,000 rpm are presented in Figures X.23 through X.31. Phase plane plots for a few of these probes are presented in Figures X.32 through X.35.

It is notable that amplitudes between resonances were unexpectedly high during this run to 12,000 rpm. While no definite explanation exists, it is suspected that these high amplitudes are related to a mechanical problem which culminated in seizure of coupling hub and end cap of the drive end high-speed spindle. Design clearance was low and some slight shift of parts had occured. No serious damage occurred and the parts were repaired.

COMPARISON BETWEEN MEASUREMENT AND PREDICTION

There was satisfactory agreement between the predicted and measured critical speeds. The first critical speed was predicted to be about 853 rpm, and was actually about 947 rpm. Predictions for the higher critical speeds were even closer. The third critical speed was predicted to occur at 3383 rpm, and actually occurred at 3470 rpm, which is an error of less than 3 percent. The fourth critical speed was predicted to occur at 7619 rpm, and as measured, there was a double peak at the fourth critical speed, the first occurring at 7480 rpm, and the second at about 7640 rpm, both within 2 percent of prediction.

Values of log decrement have been calculated from the test shaft response data from several displacement probes for the first, third, and fourth critical speeds, for comparison with the predicted values of log decrement. The log decrement was calculated as the damping ratio times 2π. The damping ratio is equal to the reciprocal of the product of the rotational frequency and the change in the phase angle for a unit change of rotational frequency at the peak of a critical speed. The phase angle is measured in radians and the rotational frequency in any convenient units for this calculation. Results are presented in Table 2, based on the data from probe Number 2 taken during the run to 10,000 rpm after the completion of the influence coefficient balancing procedure. These results are fairly typical for data taken from other probes and runs. The measured log decrement for the first critical speed was 0.098, as compared to the predicted value of about 0.07. For the third critical speed, the measured value of log decrement was 0.106, as compared to the predicted value of 0.12. The log decrements measured for the two peaks of the fourth critical speed were 0.104 and 0.090, as compared to the predicted value of 0.13. Therefore, the measured log decrement for the first critical speed was slightly higher than the predicted value, while those for the third and fourth critical speeds were slightly lower than the corresponding predicted values. Considering the sensitivity to damper support stiffness and damping of the predicted values of log decrement, at least part of the discrepancy between the predicted and measured values of log decrement could be attributed to the actual stiffness or damping (or both) being slightly lower than the design values.

In summary, good agreement was achieved between analytical predictions and test results for the supercritical shaft test rig.

EFFECT OF TORQUE

Following the operational checkout of the torquing system, the effects of torque upon the response characteristics of the test shaft were investigated.

TABLE 2

COMPARISON OF PREDICTIONS AND MEASUREMENT

FOR LOG DECREMENT AND CRITICAL SPEED

Critical Speed	Quantity	Predicted	Measured
1	Critical Speed	853 rpm	940 rpm
	Log Decrement	0.07	0.098
2	Critical Speed	(Critically Damped)	(Critically Damped)
	Log Decrement		
3	Critical Speed	3383	3470
	Log Decrement	0.12	0.106
4	Critical Speed	7619	7500
	Log Decrement	0.13	0.104
	Critical Speed	-	7670
	Log Decrement	-	0.090

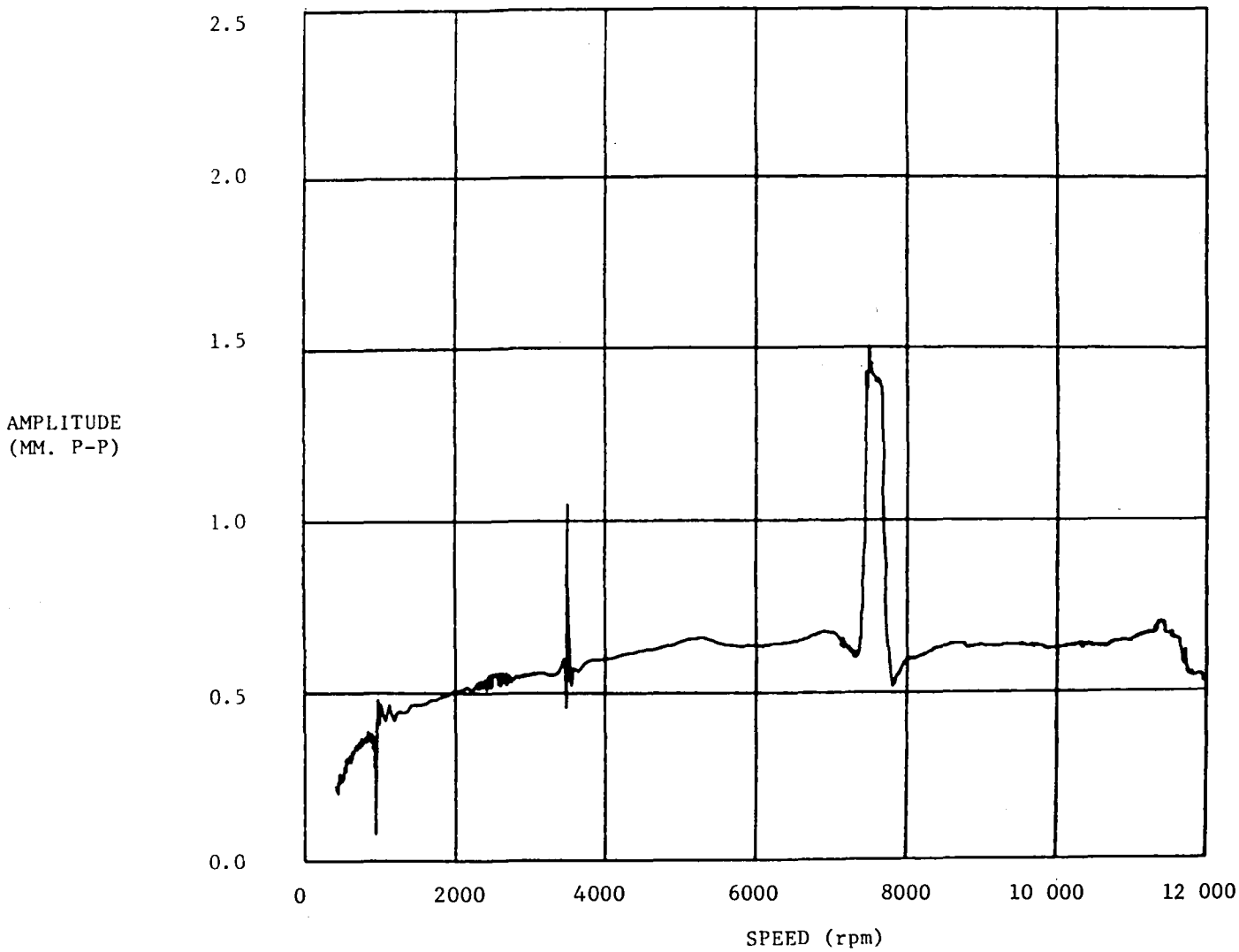

Fig. X.23 Plot of Amplitude as a Function of Frequency for Synchronous Response at Probe No. 3 to 12000 rpm (No Torque)

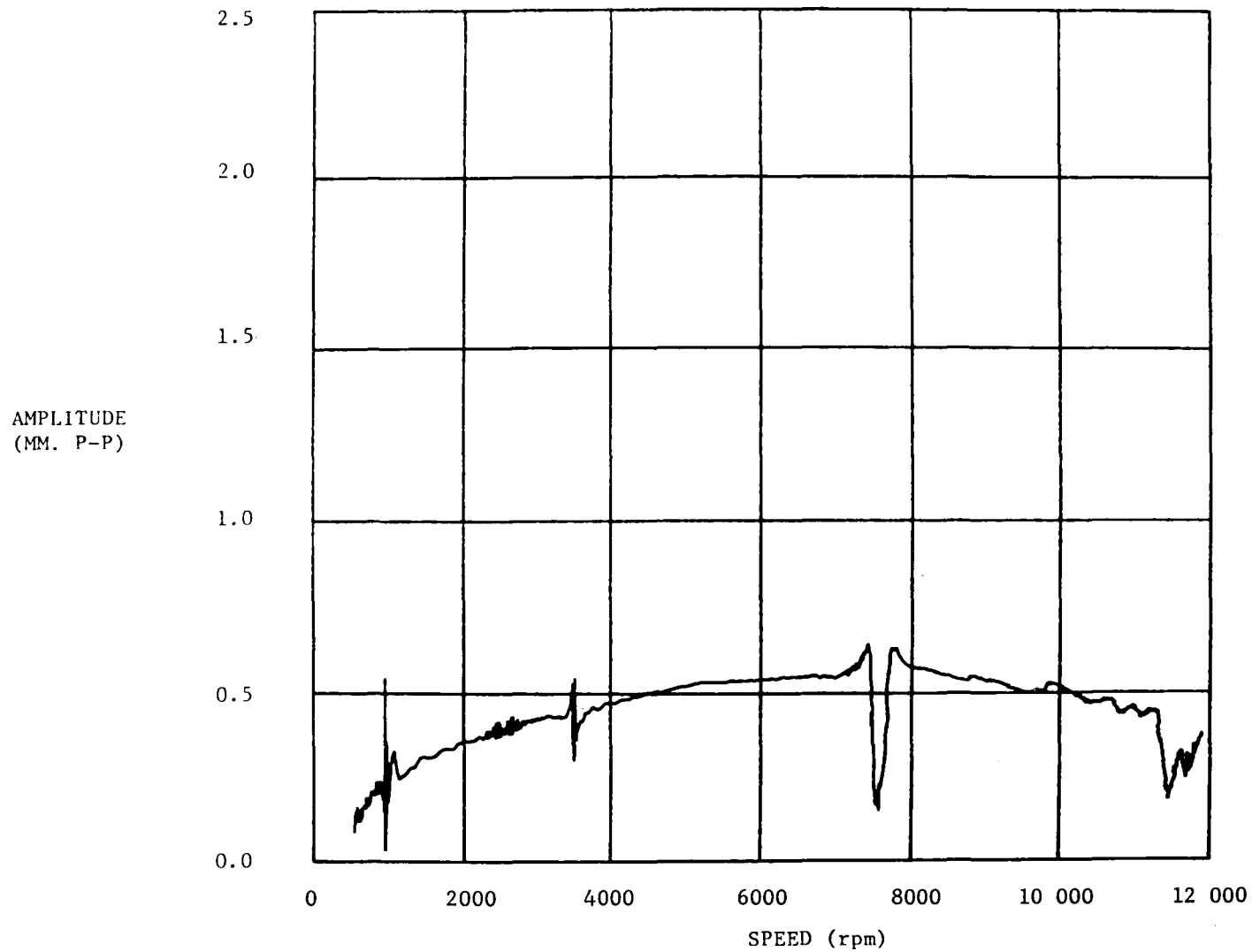

Fig. X.24 Plot of Amplitude as a Function of Frequency for Synchronous Response at Probe No. 4 to 12000 rpm (No Torque)

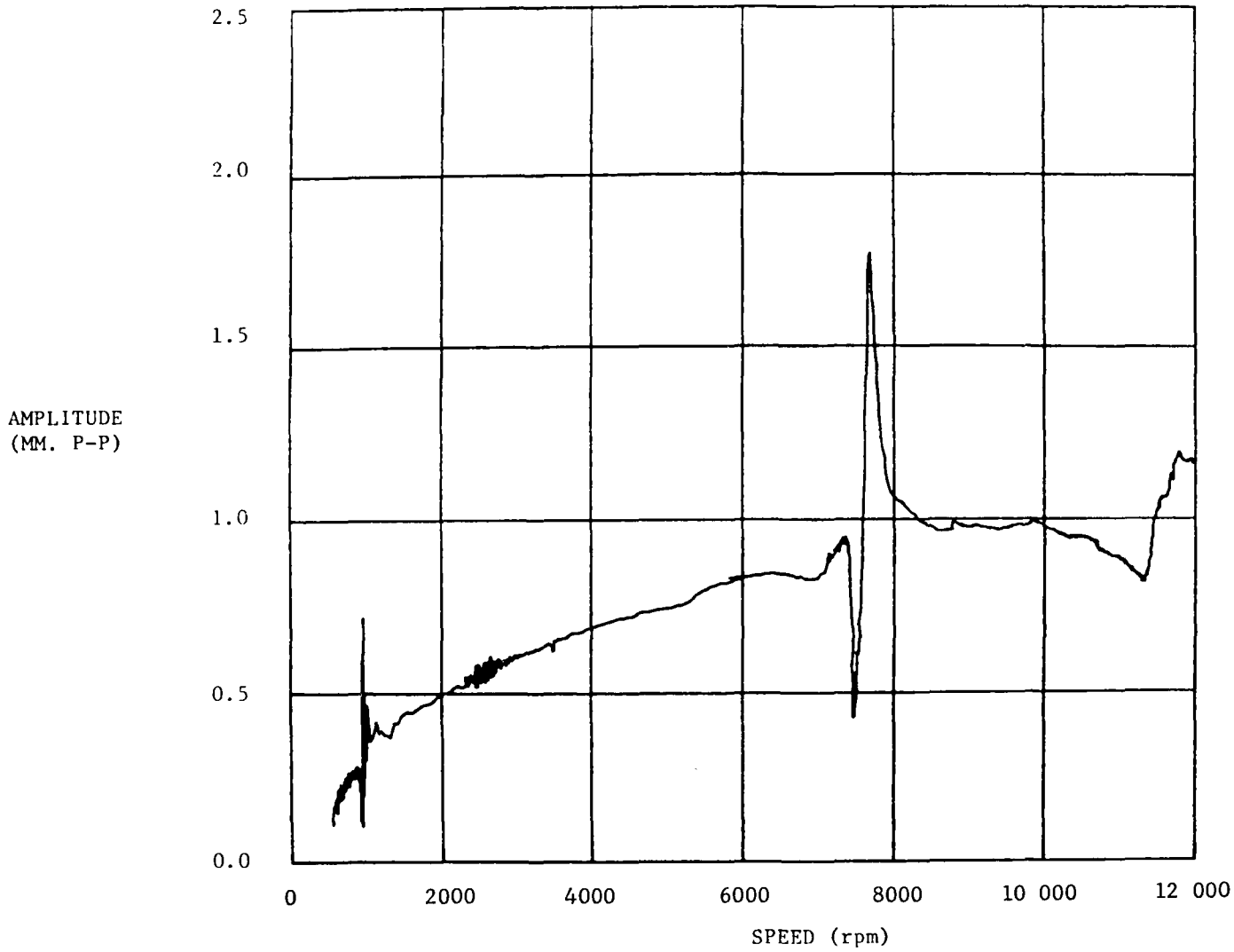

Fig. X.25 Plot of Amplitude as a Function of Frequency for Synchronous Response at Probe No. 5 to 12000 rpm (No Torque)

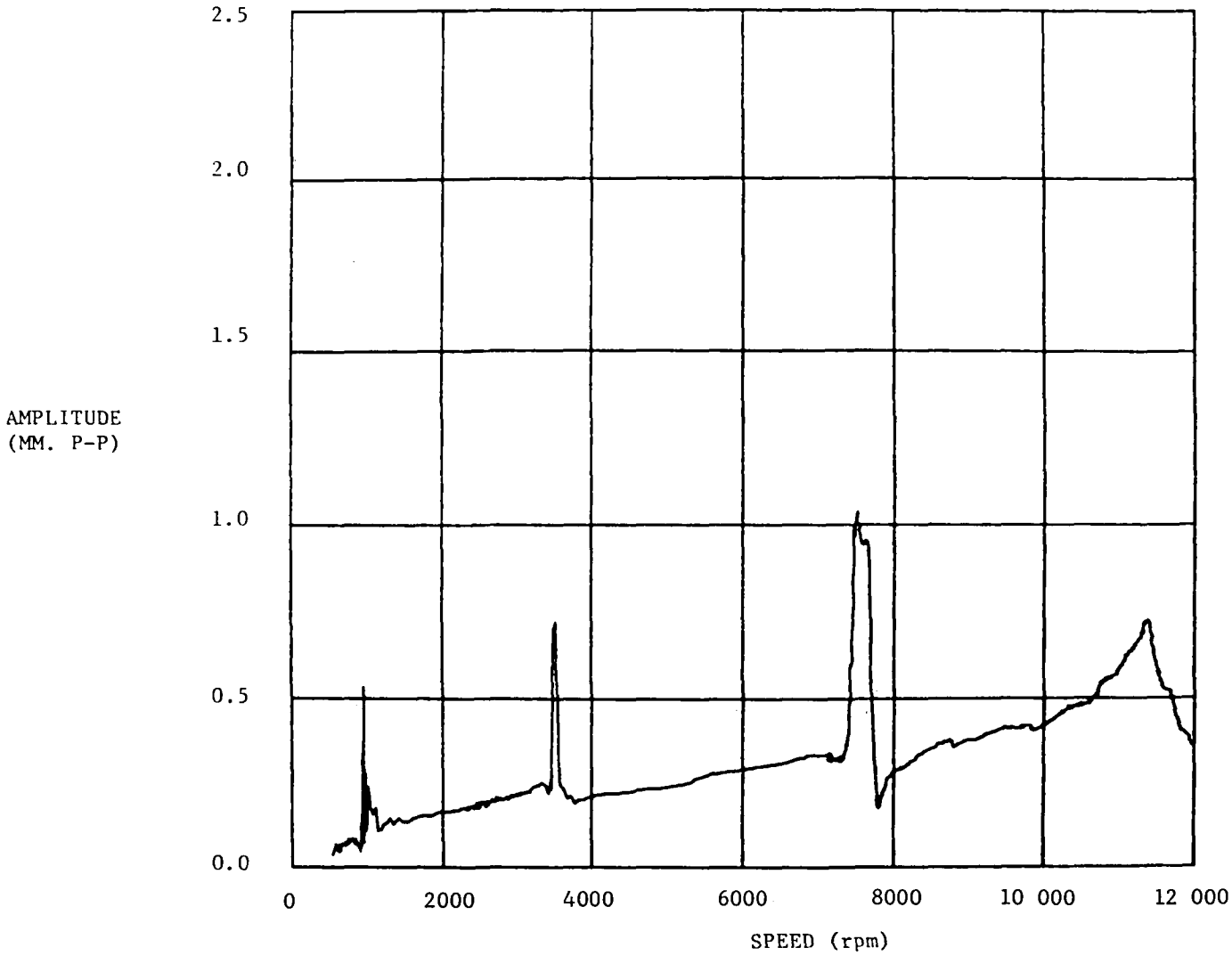

Fig. X.26 Plot of Amplitude as a Function of Frequency for Synchronous Response at Probe No. 5 to 12000 rpm (No Torque)

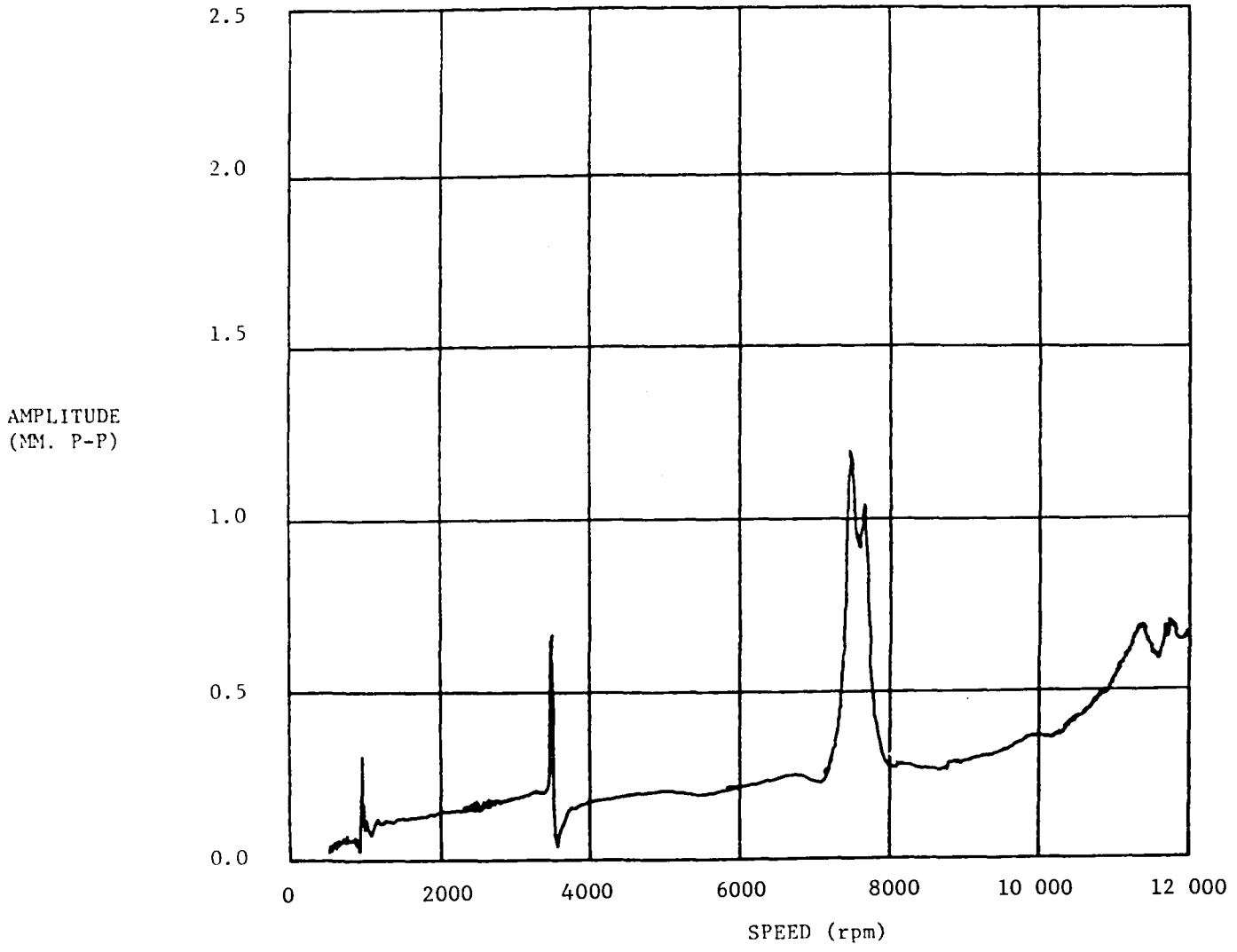

Fig. X.27 Plot of Amplitude as a Function of Frequency for Synchronous Response at Probe No. 9 to 12000 rpm (No Torque)

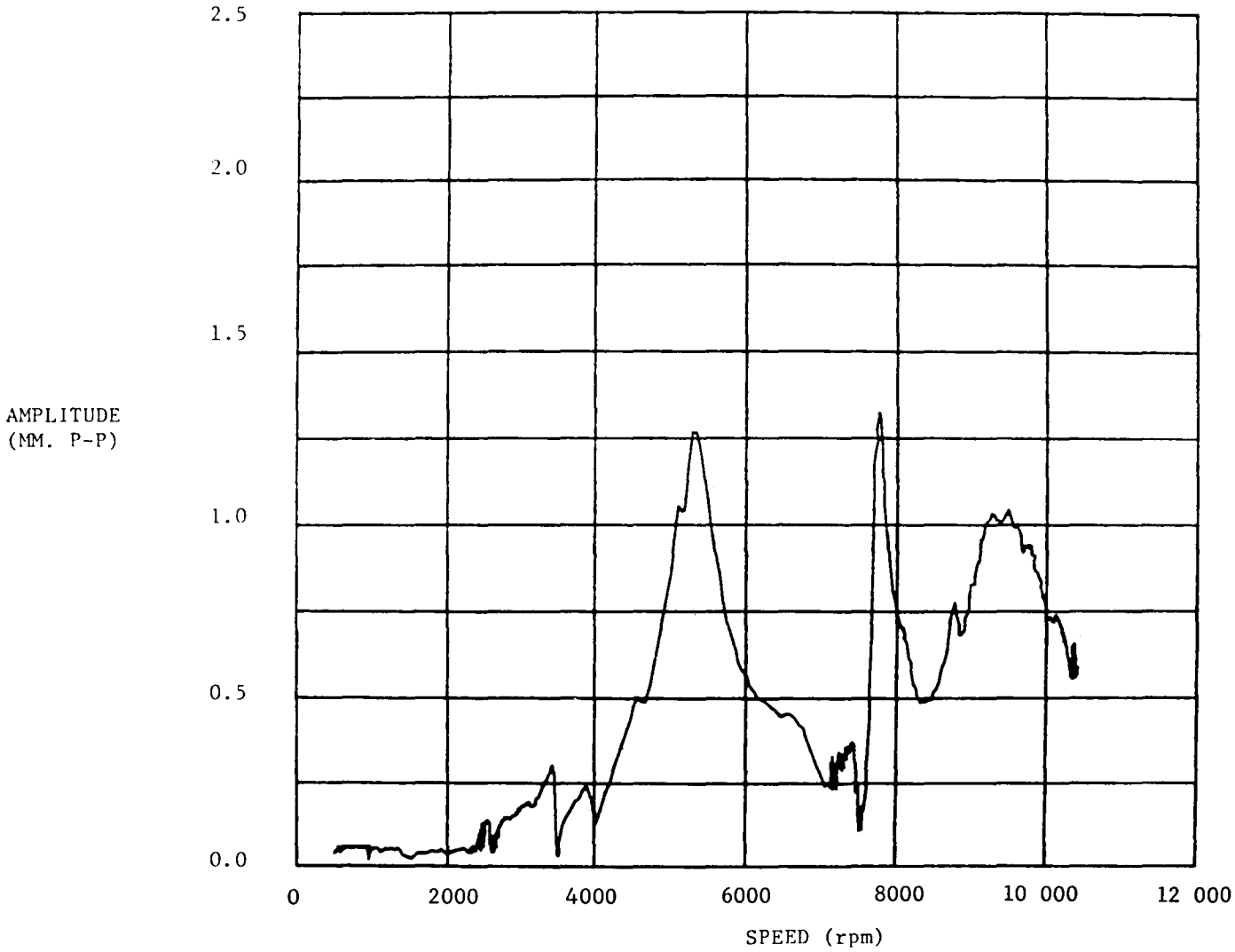

Fig. X.28 Plot of Amplitude as a Function of Frequency for Synchronous Response at Probe No. 11 to 12000 rpm (No Torque)

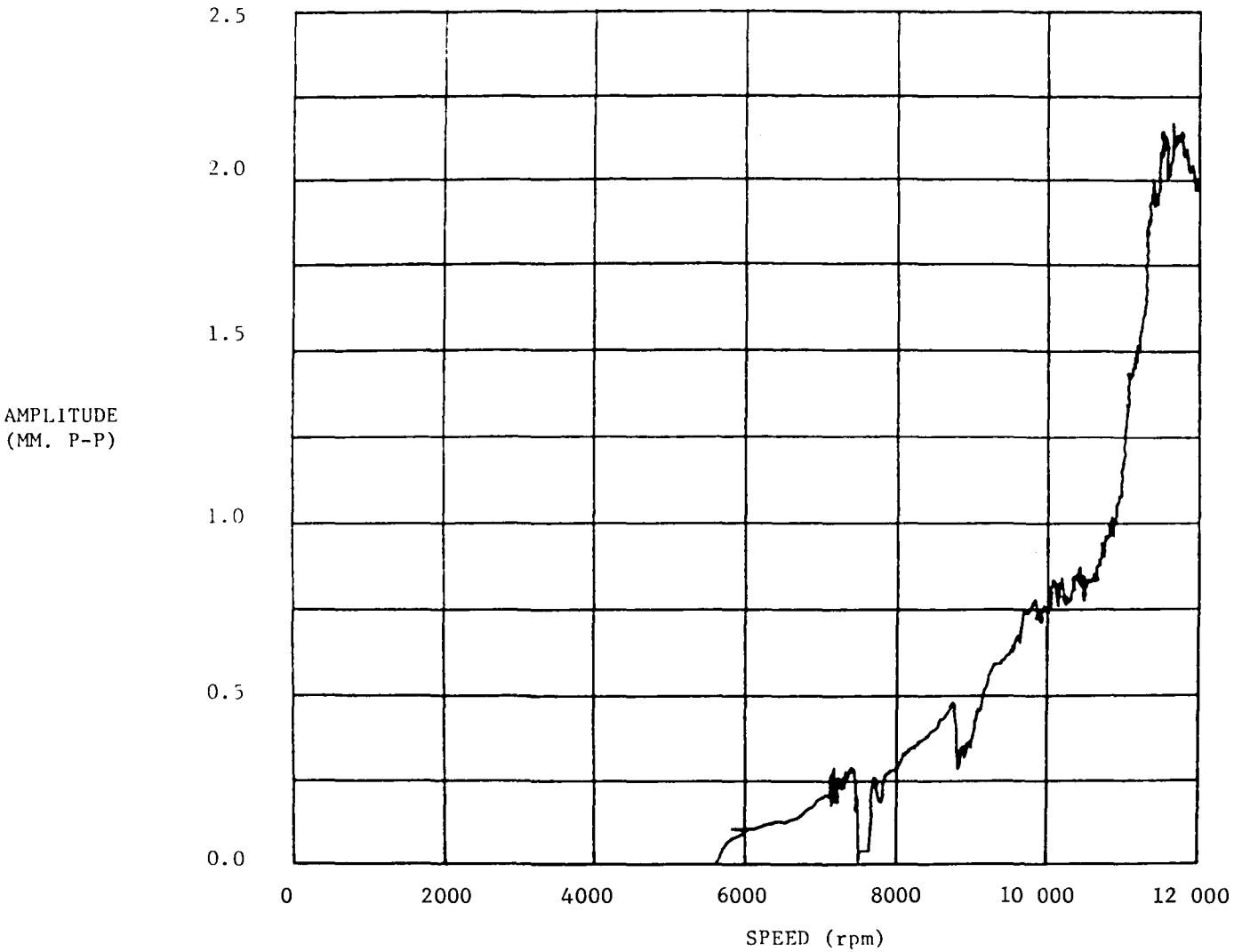

Fig. X.29 Plot of Amplitude as a Function of Frequency for Synchronous Response at Probe No. 12 to 12000 rpm (No Torque)

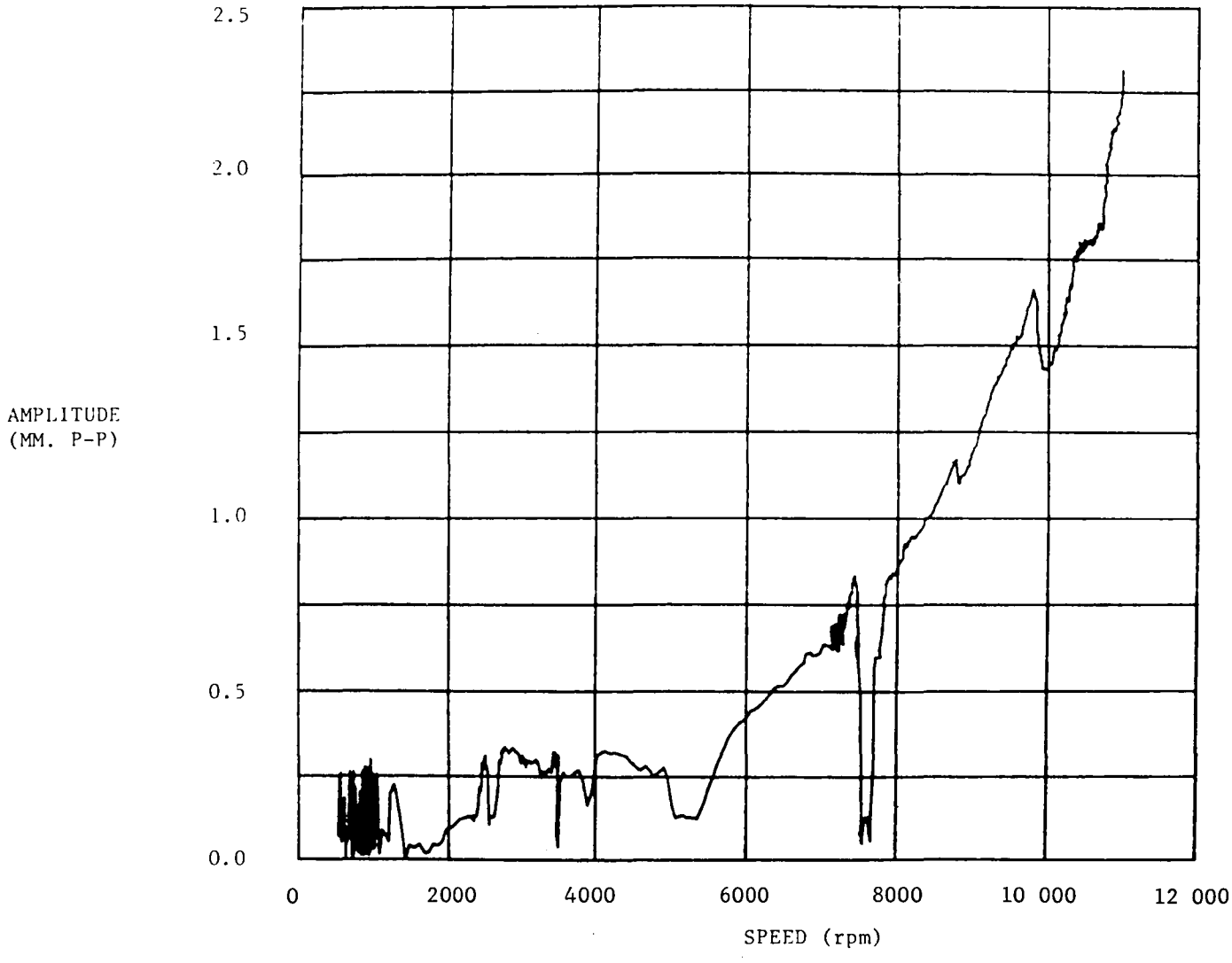

Fig. X.30 Plot of Amplitude as a Function of Frequency for Synchronous Response at Probe No. 13 to 12000 rpm (No Torque)

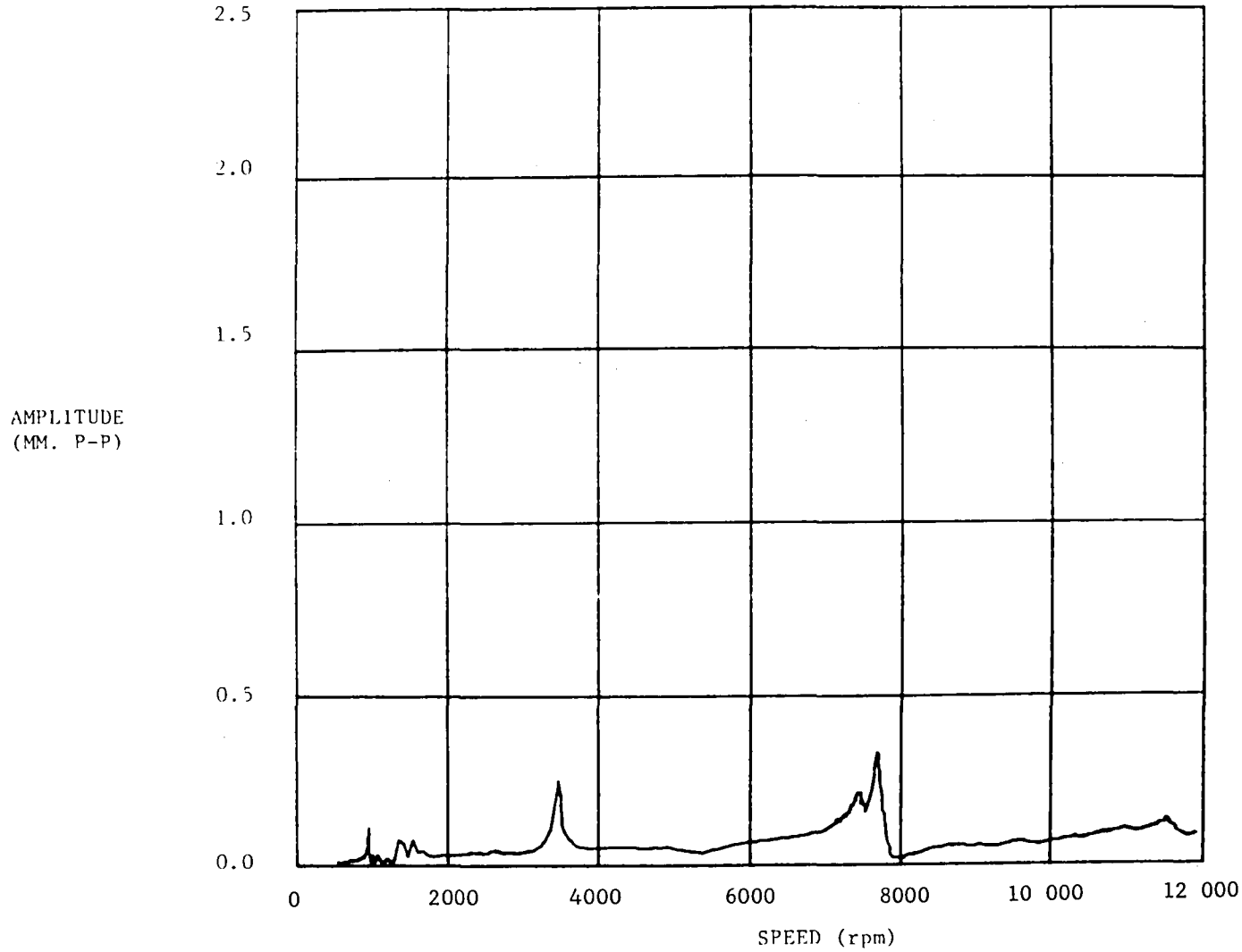

Fig. X.31 Plot of Amplitude as a Function of Frequency for Synchronous Response at Probe No. 15 to 12000 rpm (No Torque)

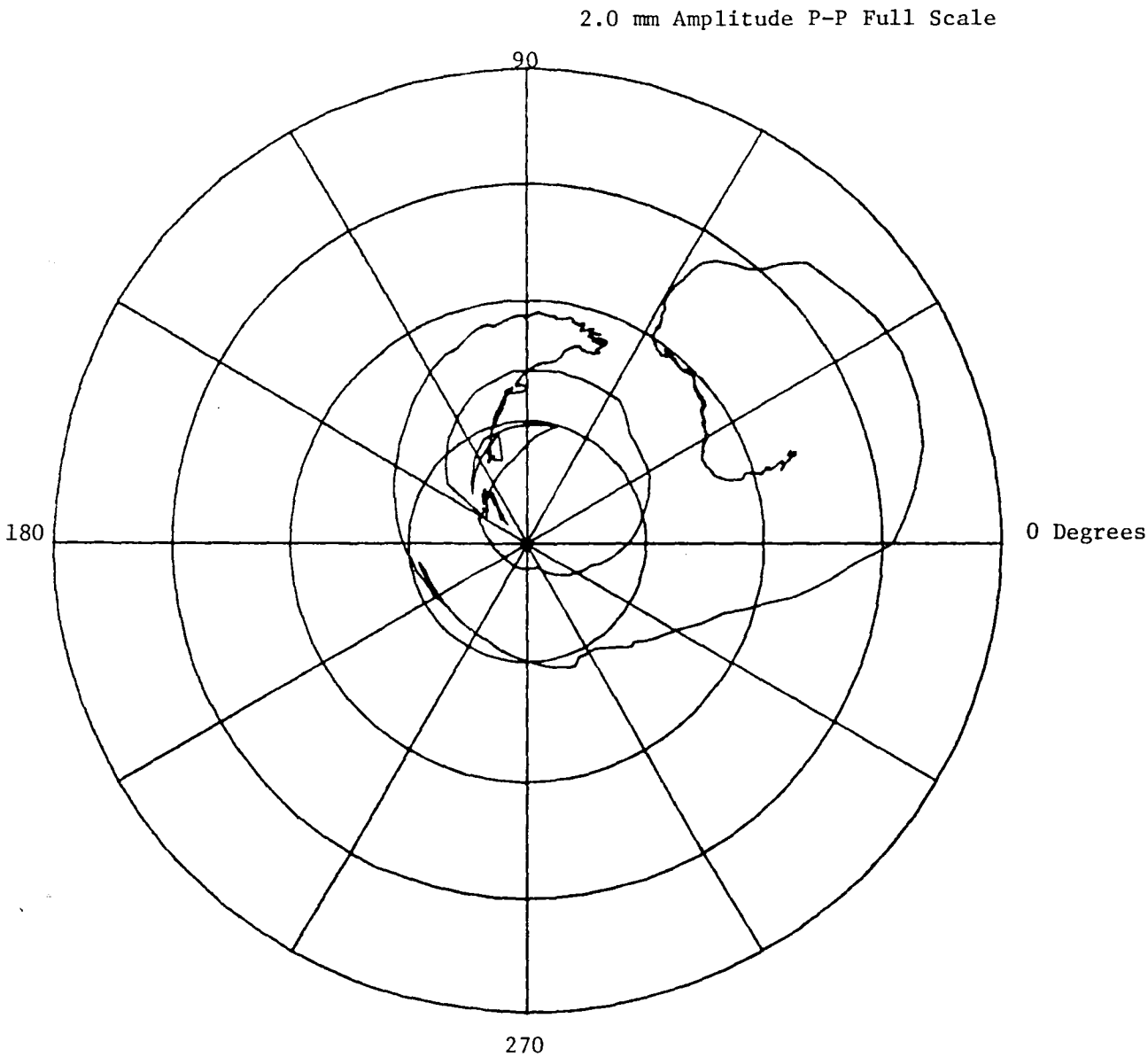

Fig. X.32 Phase Plane Plot for Synchronous Response at Probe No. 5 to 12000 rpm (No Torque)

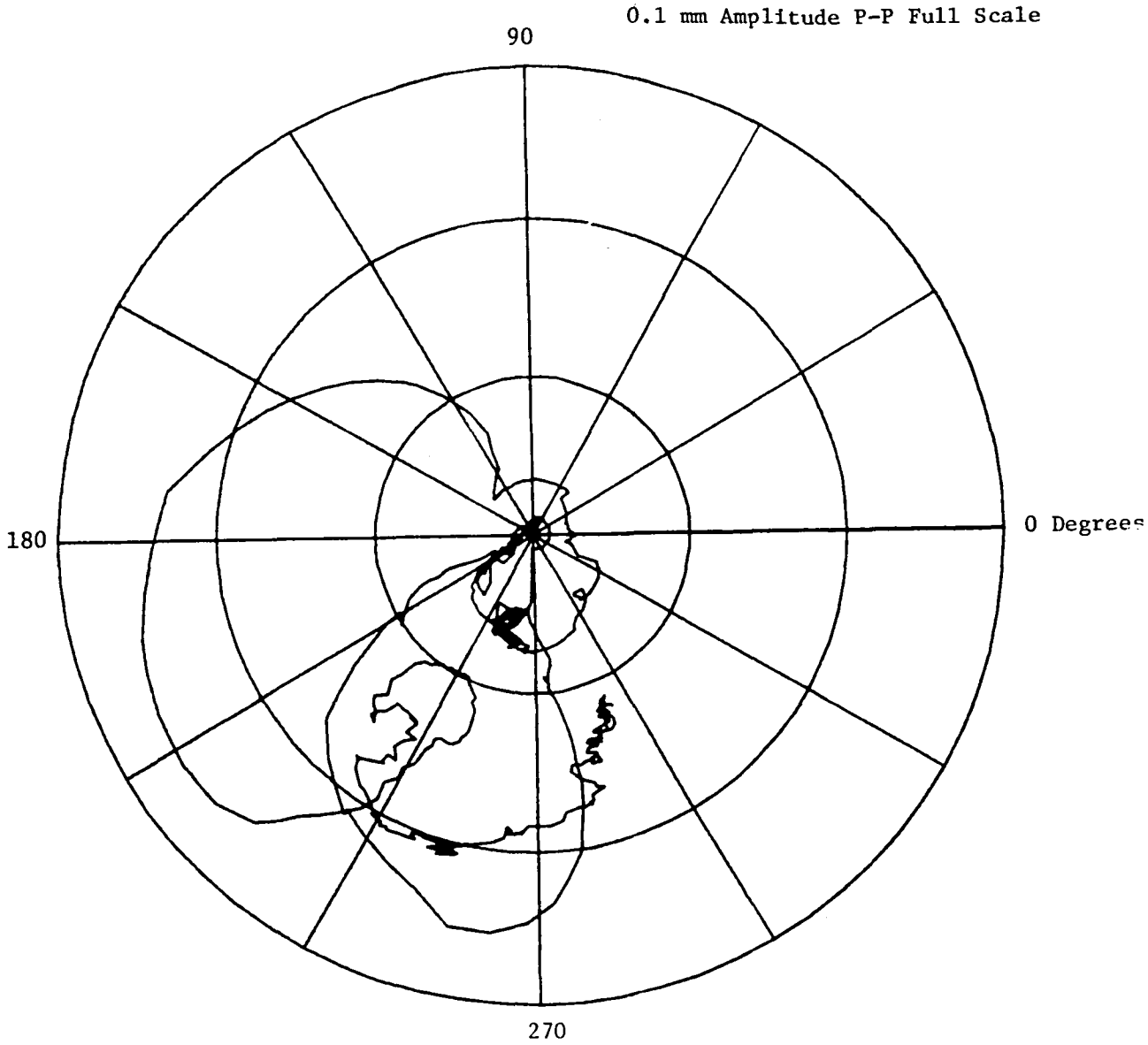

Fig. X.33 Phase Plane Plot for Synchronous Response at Probe No. 11 to 12000 rpm (No Torque)

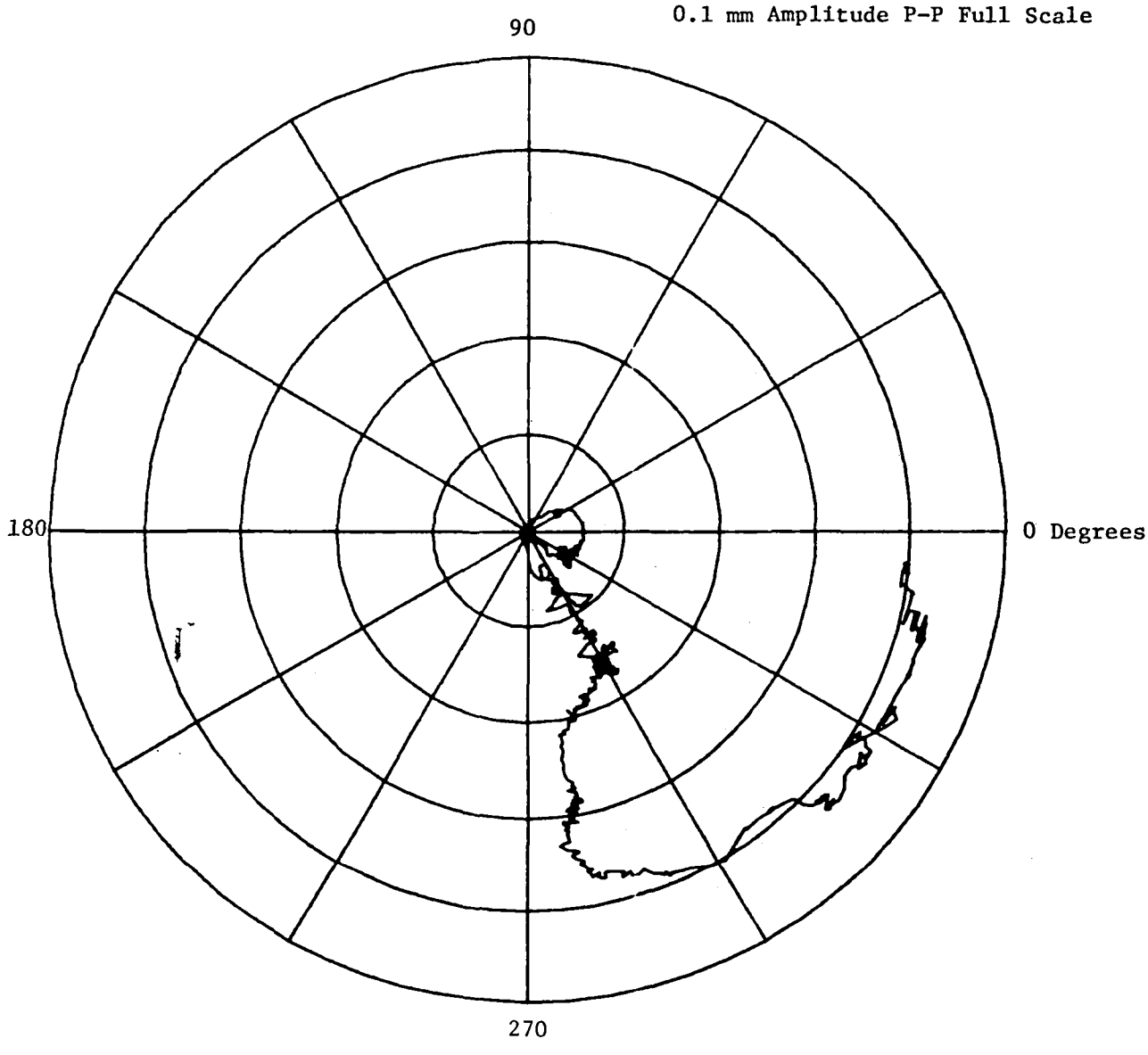

Fig. X.34 Phase Plane Plot for Synchronous Response at Probe No. 12 to 12000 rpm (No Torque)

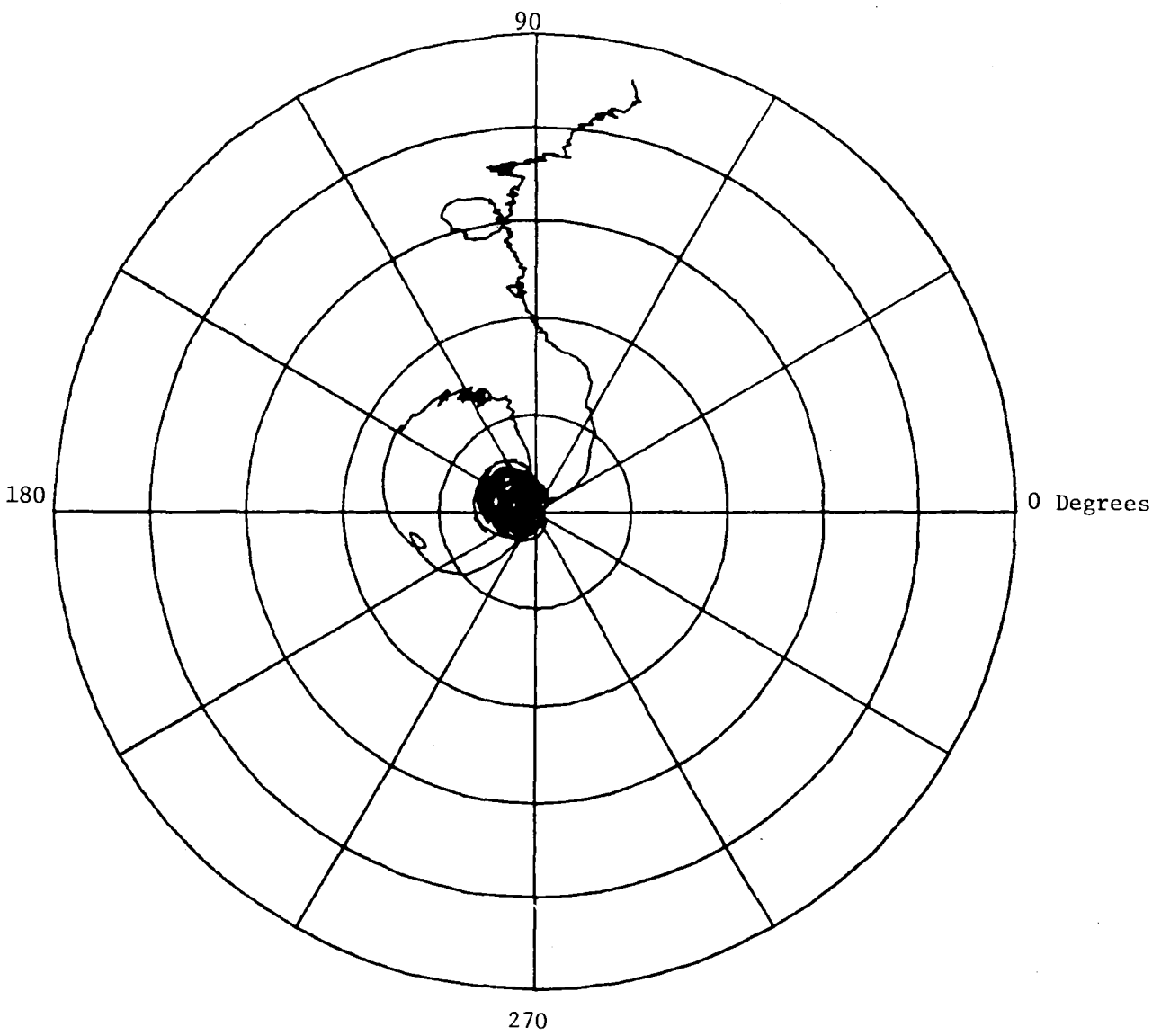

Fig. X.35 Phase Plane Plot for Synchronous Response at Probe No. 13 to 12000 rpm (No Torque)

As a reference condition, the test shaft was run once through without torque. There was some significant degradation in the response at the first critical speed, as compared to the balance condition of the shaft at the end of the balancing tests. The response at the third and fourth critical speeds was essentially unchanged. A one-plane balance of the first critical speed was conducted with no torque applied. The influence coefficients which had been used during the modal balancing of the first critical speed were used for this balancing run. The resulting response at the first critical speed was significantly improved, while the response at the third critical speed was unaffected; but at the fourth critical speed it was somewhat worse. The test shaft seemed more sensitive to unbalance than it had been during the balancing tests. While being run up to the fourth critical speed after this last balancing run, the test shaft rubbed the displacement probes in the center of the shaft. The two probes located vertically and horizontally in the center of the shaft were damaged and had to be replaced. In addition, the response of the test shaft was changed and aggravated at the first and fourth critical speeds.

Another trim balance run was conducted for the first critical speed. The response was improved and the first critical speed was negotiated. However, this correction weight made the fourth critical speed even worse, and the test shaft still appeared to be more sensitive to unbalance than it had been during the balancing tests. An attempted trim balance of the fourth critical speed produced inconsistent results and led to speculation that the test shaft damper might not be operating properly.

At this point, the test shaft damper was carefully examined and damper oil was discovered on the outside of the damper housing. The pressure in the damper had also fallen, indicating that the damper was no longer sealed. A crack was found in the copper tubing below the sight glass of the damper. This section of copper tubing was replaced and it was refilled. The damper was apparently no longer leaking oil; however, it was still not possible to obtain the proper pressure. Another careful examination of the damper revealed a crack in the pipe nipple which supplies air to the damper bladder; it was replaced and proper pressurization of the damper was achieved.

The test rig was run again after the repair of the damper and great improvement was seen in the response at the first critical speed. The fourth critical speed was also improved, but it was still not negotiable. One modified modal balancing run was attempted at the fourth critical speed. As a result, the response at the first and third critical speeds was slightly worse and the response at the fourth critical speed was much better, but still not negotiable. Therefore, it was decided to remove the modal trim set and perform initial investigations of torque effects of the first and third critical speeds only.

The torque tests were begun with a reference run without torque. The high pressure solenoid was disengaged in order to release the torque, but the torque sensor indicated that there was actually a torque of about 34 N-m (300 in.-lb) applied to the test shaft, apparently built in during the assembly of the four square test rig. Approximately 900 N-m (8000 in.-lb) of torque was then applied to the test shaft and the test rig was run again to over 7000 rpm. The application of torque did not seem to have any significant effect upon the speeds at which the first and third critical speeds occurred. The response, however, at the first and third critical speeds deteriorated, more so at the first critical speed than at the third. When the test shaft torque was reduced to 450 N-m

(4000 in.-lb) there was no noticeable effect on the speeds at which the first and third critical speeds occurred, but the amplitude at the first and third critical speeds was between those without any torque applied and those with 900 N-m (8000 in.-lb) of torque. The response at the first critical speed again appeared more sensitive to torque than at the third. When the torque was reduced to about 225 N-m (2000 in.-lb), the response at the first critical speed was not significantly different than it had been with 450 N-m (4000 in.-lb) of torque applied; but the response at the third critical speed was slightly reduced from that with 450 N-m (4000 in.-lb). The test rig was then run essentially without torque, by reducing the control air pressure to the torquing system to zero, while leaving the high pressure solenoid engaged. According to the torque sensor, a torque of about 62 N-m (550 in.-lb) was actually being applied to the test shaft. The response at both the first and third critical speeds appeared to be just slightly higher than with only 34 N-m (300 in.-lb) of applied torque, but lower than with 225 N-m (2000 in.-lb) of applied torque. The high pressure solenoid was then released so that the torque was reduced to about 34 N-m (300 in.-lb) and the test rig was run again. The results agreed very favorably with the previous results for the same condition. Response plots for several of the test shaft displacement probes, demonstrating the effect of applied torque on the test shaft response, are presented in Figures X.36 to X.40.

It was not possible to make accurate quantitative comparisons of the response at the critical speeds under varying levels of torque, because of the high sensitivity of response at the critical speeds to the acceleration rate of the test rig as the critical speeds were being negotiated. However, some definite trends that were observed concerning the response at the first and third critical speeds with varying levels of torque applied to the test shaft are as follows:

- Increasing the level of torque resulted in increasing the response at both the first and third critical speeds.
- The first critical speed was significantly more sensitive to changing levels of torque than the third.
- There was no noticeable change in the speed at which the first and third critical speeds occurred with changes in torque.

The changes in the response of the test shaft with changes in torque load were attributed to a change in the unbalance configuration of the test shaft, caused by twisting of the test shaft. Calculations indicate an expected twist in the test shaft of about 7.6 degrees from end to end for a 900 N-m (8000 in.-lb) applied torque. This twist could be expected to result in a significant change in the net effect of local unbalance vectors, since the unbalance of the test shaft is distributed along the shaft, while the balancing corrections (particularly for the first critical speed) are in (or near) the center of the shaft.

Measurement of Shaft Twist

A series of tests was conducted to determine what the actual twist in the shaft would be with an applied torque. These tests involved taking data from all shaft displacement probes at a speed well below the first critical speed under various levels of torque. The speed chosen for these tests was 770 rpm because this was enough below the first critical speed that the test shaft did not

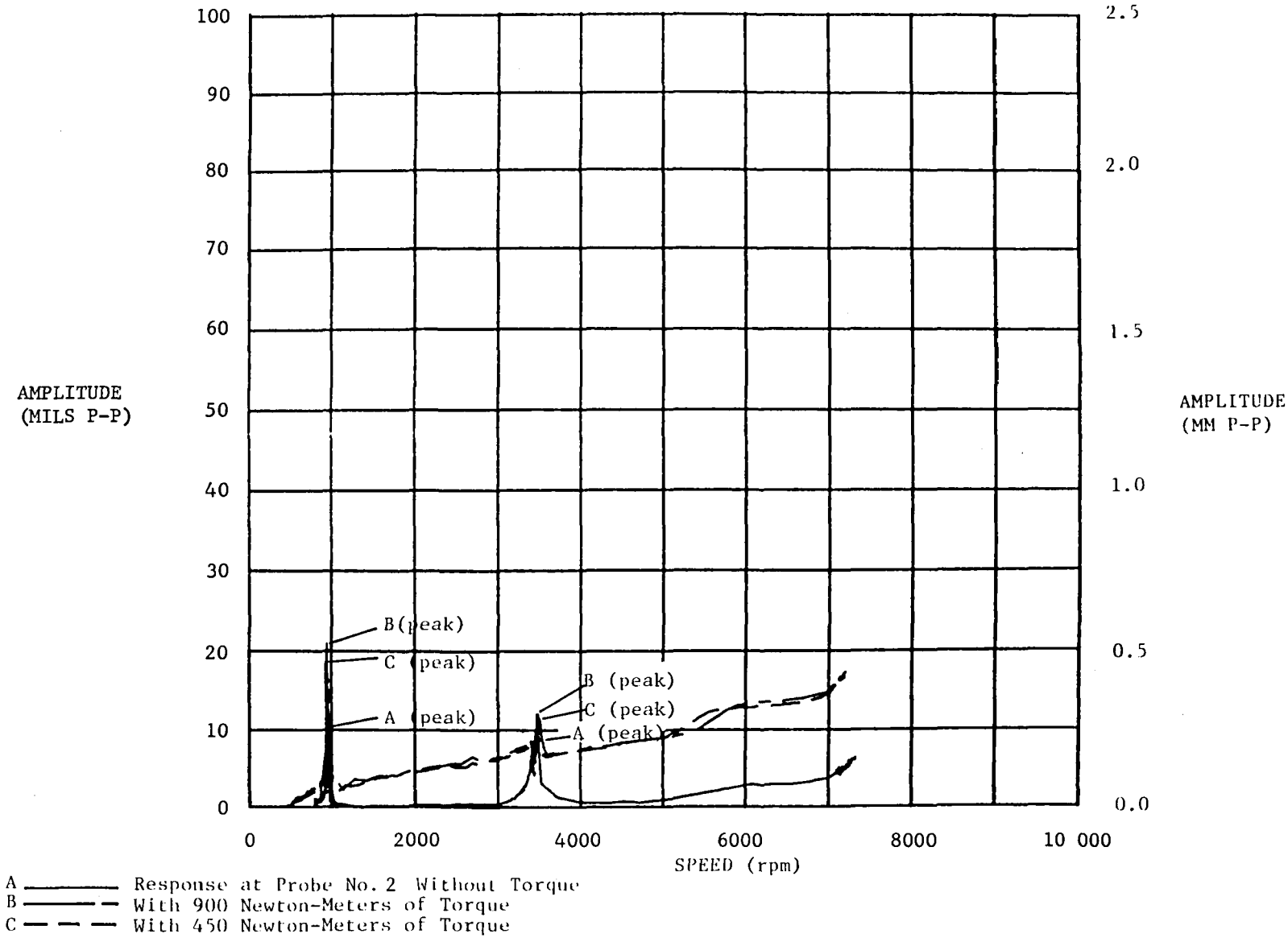

Fig. X.36 Plot of Amplitude as a Function of Frequency for Probe No. 2 (Torque Tests)

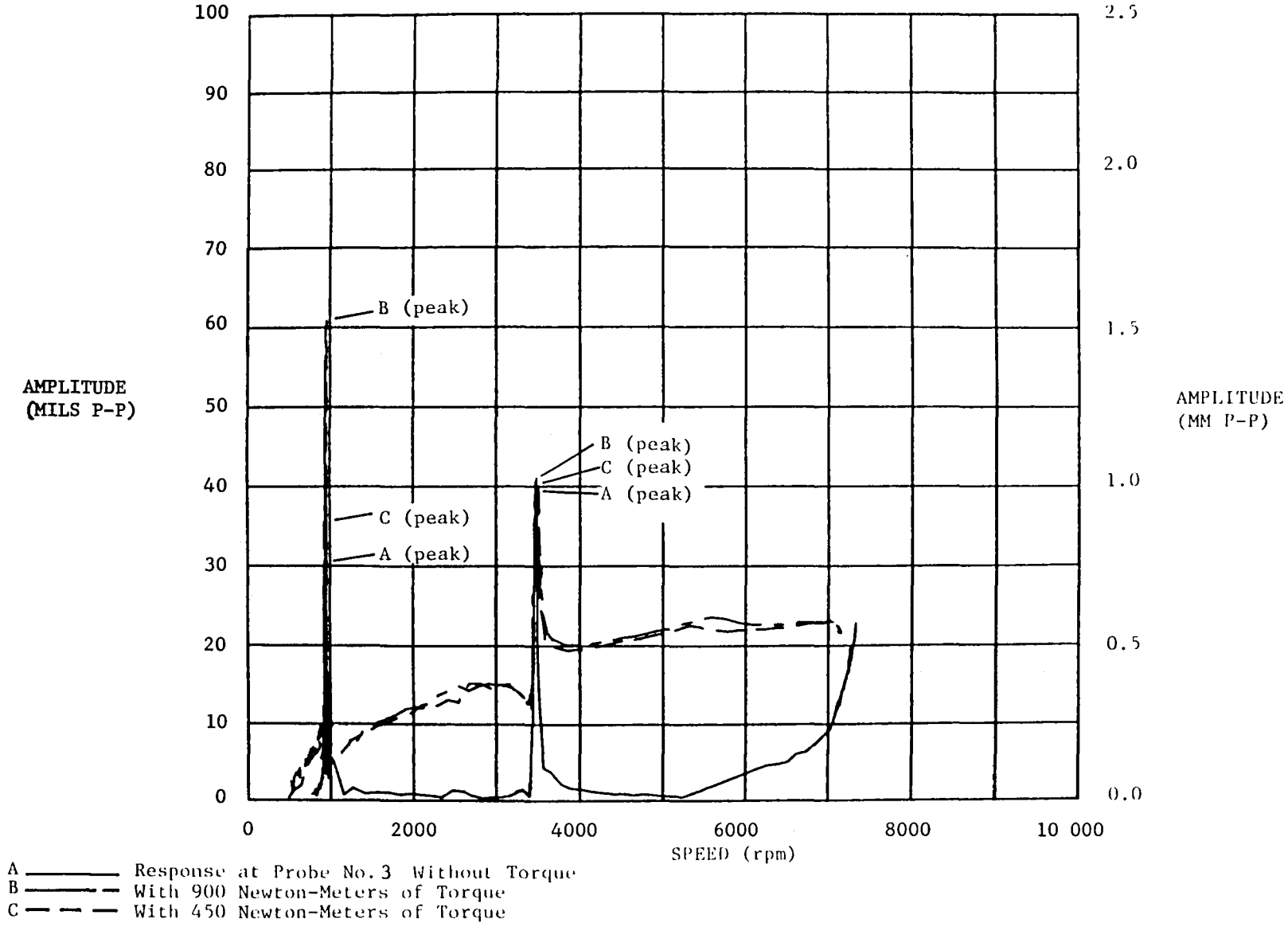

Fig. X.37 Plot of Amplitude as a Function of Frequency for Probe No. 3 (Torque Tests)

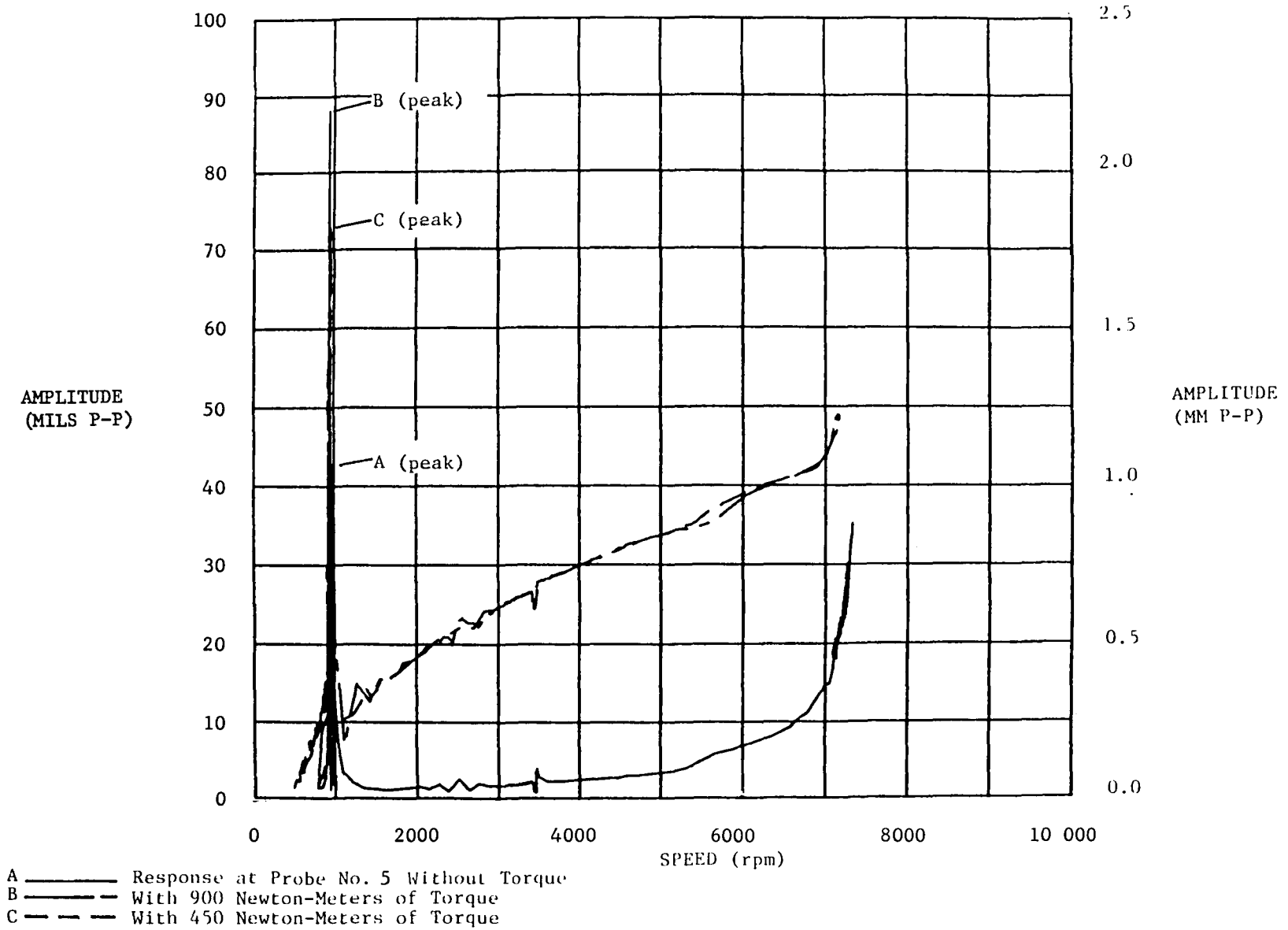

Fig. X.38 Plot of Amplitude as a Function of Frequency for Probe No. 5 (Torque Tests)

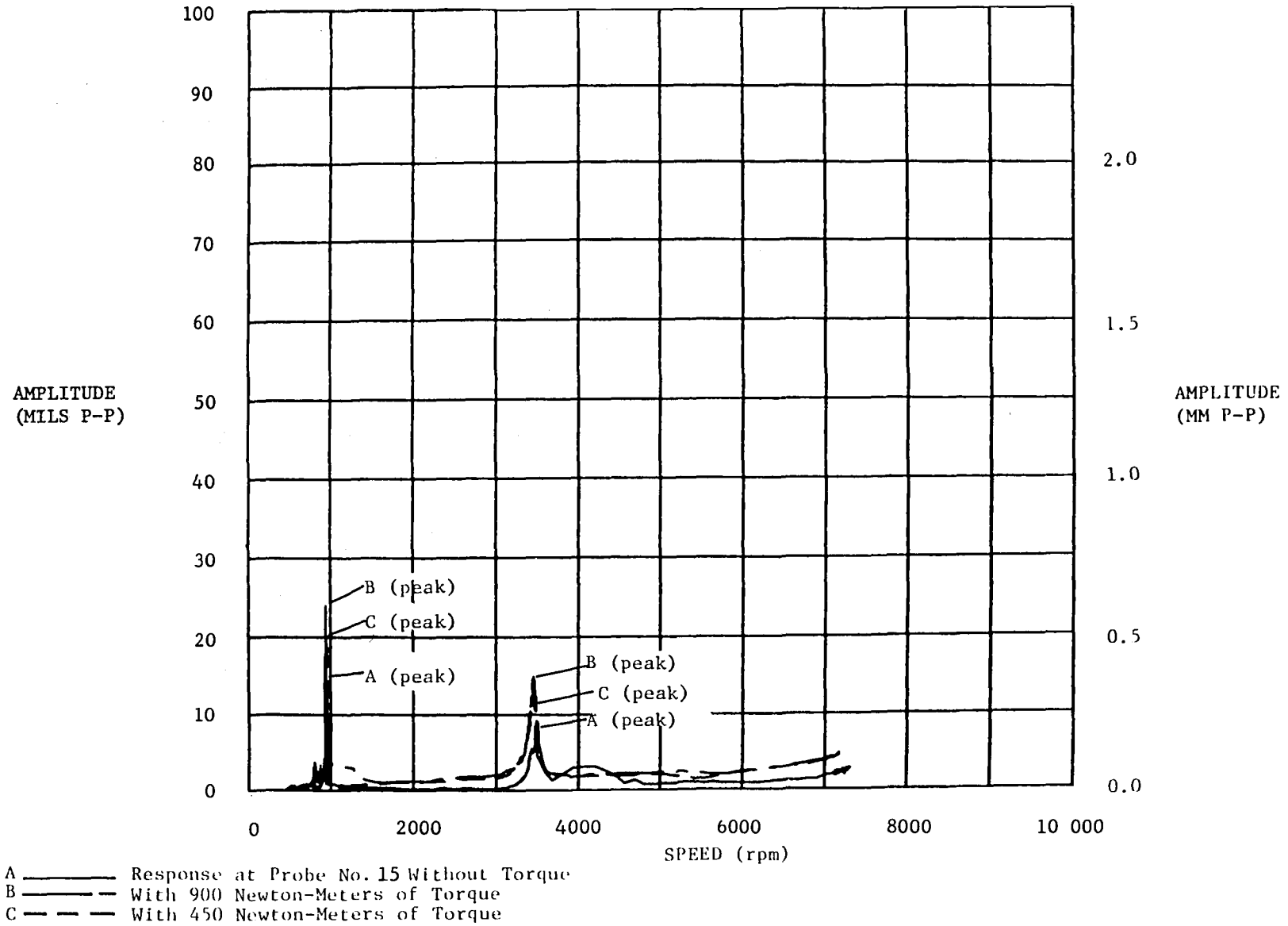

Fig. X. 39 Plot of Amplitude as a Function of Frequency for Probe No. 15 (Torque Tests)

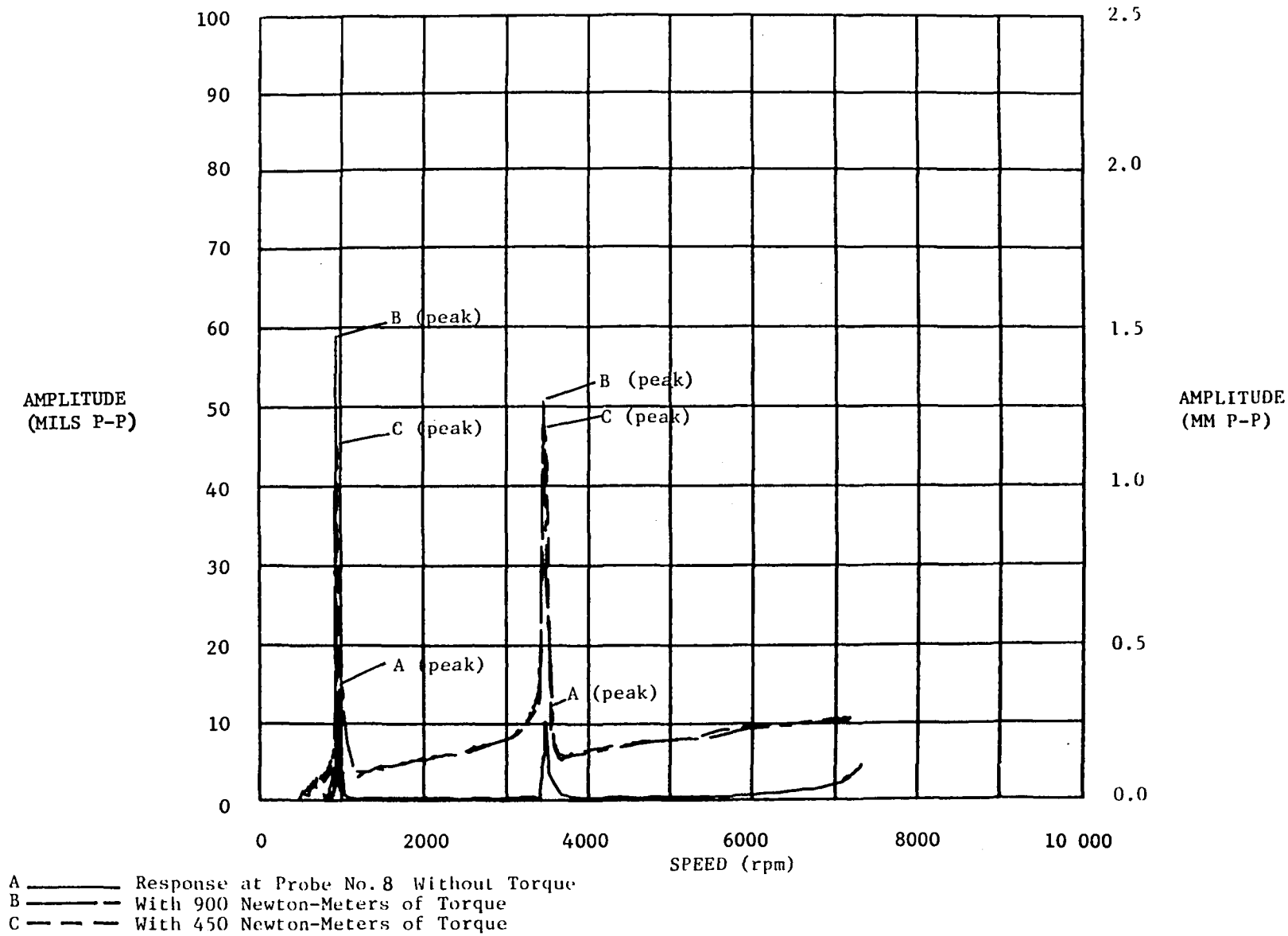

Fig. X.40 Plot of Amplitude as a Function of Frequency for Probe No. 8 (Torque Tests)

exhibit any significant response to the first critical speed. Also this speed was high enough that it was possible to get steady readings from the displacement probes. The results of these tests are presented in Table 3. Initially, the test rig was run with no torque, with the high pressure solenoid disengaged (actually about 34 N-m (300 in.-lb) of residual torque). Data was taken from all the test shaft displacement probes. About 900 N-m (8000 in.-lb) of torque was then applied to the test shaft and data was again taken. Some angle shift was noted all along the shaft, although there was significantly more angle shift at the far end of the shaft than at the near end where the drive end spindle was attached. This angle shift is indicated as a change in the phase angle of the displacement probe signal relative to the phase reference signal described above. The high pressure solenoid was disengaged and data was taken with only 34 N-m (300 in.-lb) of residual torque. A constant angle shift was seen along the entire shaft as compared to the first "no torque" run; that is, the angle shift was the same along the whole length of the shaft, indicating that the angle shift was probably due to clearance in the gears which had been taken up when the torque was applied.

About 450 N-m (4000 in.-lb) of torque was applied and data was again taken. Angle shifts qualitatively similar to those for the 900 N-m (8000 in.-lb) torque case were observed, but their magnitudes were only about half of those observed when 900 N-m (8000 in.-lb) of torque was applied. The torque was then reduced to 225 N-m (2000 in.-lb), and data was taken, and the results were quite consistent. The angle shifts were, again, similar to those observed with higher torques, but the overall angle shifts were proportionately smaller. The control air pressure was then reduced to zero, reducing the torque to about 56 N-m (500 in.-lb) and data was taken. There was still a small angle shift with a similar distribution as when higher torques were applied, but the angle shift was much smaller than for the higher torques. The high pressure solenoid was released, reducing the torque to about 34 N-m (300 in.-lb), and data was taken. The three degree angle shift, as compared to the first "no torque" run, still appeared, but there was essentially no distributed angle shift. This data was a good repeat of the second "no torque" run. The results of these tests indicated that there was indeed a significant twist in the shaft due to the application of torque. It was also apparent that the twist in the shaft was roughly proportional to the level of torque being applied.

Balancing Under Torque

A test was conducted to balance the test shaft while applying a torque load. A balancing run was conducted for the first critical speed, using the probe and plane located near the center of the test shaft, and balancing at a speed of 901 rpm. The test shaft was run under 900 N-m (8000 in.-lb) of torque load. Trial weight runs were conducted to calculate new influence coefficients, and from these influence coefficients, to calculate a correction weight. A single correction weight set was applied and the response at the balancing speed, with the torque applied, was reduced from 0.36 mm (14 mils) to 0.04 mm (1.7 mils). The first critical speed was easily negotiated with a full applied torque. It was found to be no more difficult to balance the test shaft with applied torque than it had been without applied torque.

The torque was released and the test shaft was run again. The first critical speed was still negotiable without any applied torque. However, the response at the first critical speed was 0.08 mm (3.3 mils) in the opposite direction, which was clearly worse than it had been under torque. Again, this was

TABLE 3

EFFECT OF TORQUE ON TWIST OF SHAFT

ANGLE OF SHIFT (DEGREES)

Torque	Probe #						
N-m	2	3	4	5	7	8	15
34 Reference Case	0	0	0	0	0	0	0
900	4.1	4.9	7.7	7.1	10.9	12.4	13.6
34	2.5	1.5	2.6	1.9	3.1	3.3	4.0
450	4.2	3.5	5.6	5.8	6.6	9.9	10.5
225	3.0	2.4	4.4	3.4	5.9	6.8	6.0
56	3.1	2.0	3.7	2.1	4.6	4.2	4.9
34	4.1	2.4	4.0	2.8	3.9	4.6	4.9

apparently due to a change in the unbalance configuration of the test shaft. Data was taken at 901 rpm without torque to estimate the effect of the applied torque in terms of relative unbalance. The data that was taken indicated that releasing the torque was roughly equivalent to applying 0.3 grams of unbalance at the plane nearest the center of the shaft. The influence coefficients for the test shaft near the first critical speed were not affected by the application of torque, within the range of experimental error.

XI. NONSYNCHRONOUS VIBRATIONS

A flexible shaft is prone to a number of vibration phenomena which occur at frequencies other than those synchronous with rotational speed. Those observed with the present test shaft include:

- Two-per-rev excitation of the first critical speed
- Two-per-rev excitation of higher critical speeds
- Subsynchronous forced excitation of first and third critical speeds by damper bearing cage rotational frequency.
- Subsynchronous self-excitation of the first critical speed.

Two-per-rev excitation of the first critical speed can be seen clearly by reference to Figure XI.1. In this figure, plots of amplitude versus frequency for various operating speeds below the first critical are presented. The first spectrum corresponds to an operating speed of 480 rpm, which is very close to half the first critical speed, and distinct peaks may be seen in the spectrum, both at running speed and at twice running speed, which is very close to the first critical speed. Both peaks are of similar amplitude and at higher speeds, 800 rpm and 900 rpm, the running speed and shaft critical peaks are lower than when running at half the first critical speed.

Figure XI.2 provides relevant supplementary data on the two-per-rev excitation of the first critical speed. Six shaft orbits are presented in this figure and the three in the left hand column correspond to operation at 800 rpm, while the three in the right correspond to operation at 484 rpm, which is close to half the first critical speed. Orbits are presented for different probes; in the left hand column, the distinctive four lobe orbits associated with this shaft system may be observed. In the right hand column, there is a distinct increase in amplitude and change in phase of orbital vibrations, which would be observed when a critical is being excited.

The specific cause of the two-per-rev excitation occurring at 480 rpm has not been proven. The most likely candidate is considered to be flexural asymmetry in the shaft which would inevitably be present as a result of manufacturing imperfections and would be almost certain to excite a lightly damped first critical speed. The other possibility is the effect of misalignment in the couplings which is frequently associated with two-per-rev excitations.

In addition to two-per-rev excitation of the first critical speed, there was a distinct two-per-rev excitation of the third critical speed. This may be seen in Figures XI.3 and XI.4. In Figure XI.3, the frequency corresponding to two-per-rev is just a little lower than the third critical speed and at both excitation frequency and critical speed frequency, response is relatively small, certainly less than the one-per-rev amplitude. In Figure XI.4, the two-per-rev and the third critical frequency are the same. Here there is a very distinct peak and its amplitude is almost exactly the same as the one-per-rev amplitude. The source of this two-per-rev excitation is a little harder to attribute to the gravity effect since the third mode is an even mode with a mode shape approximately like a full sine wave. Here, perhaps, the effects of coupling misalignment are a more likely cause.

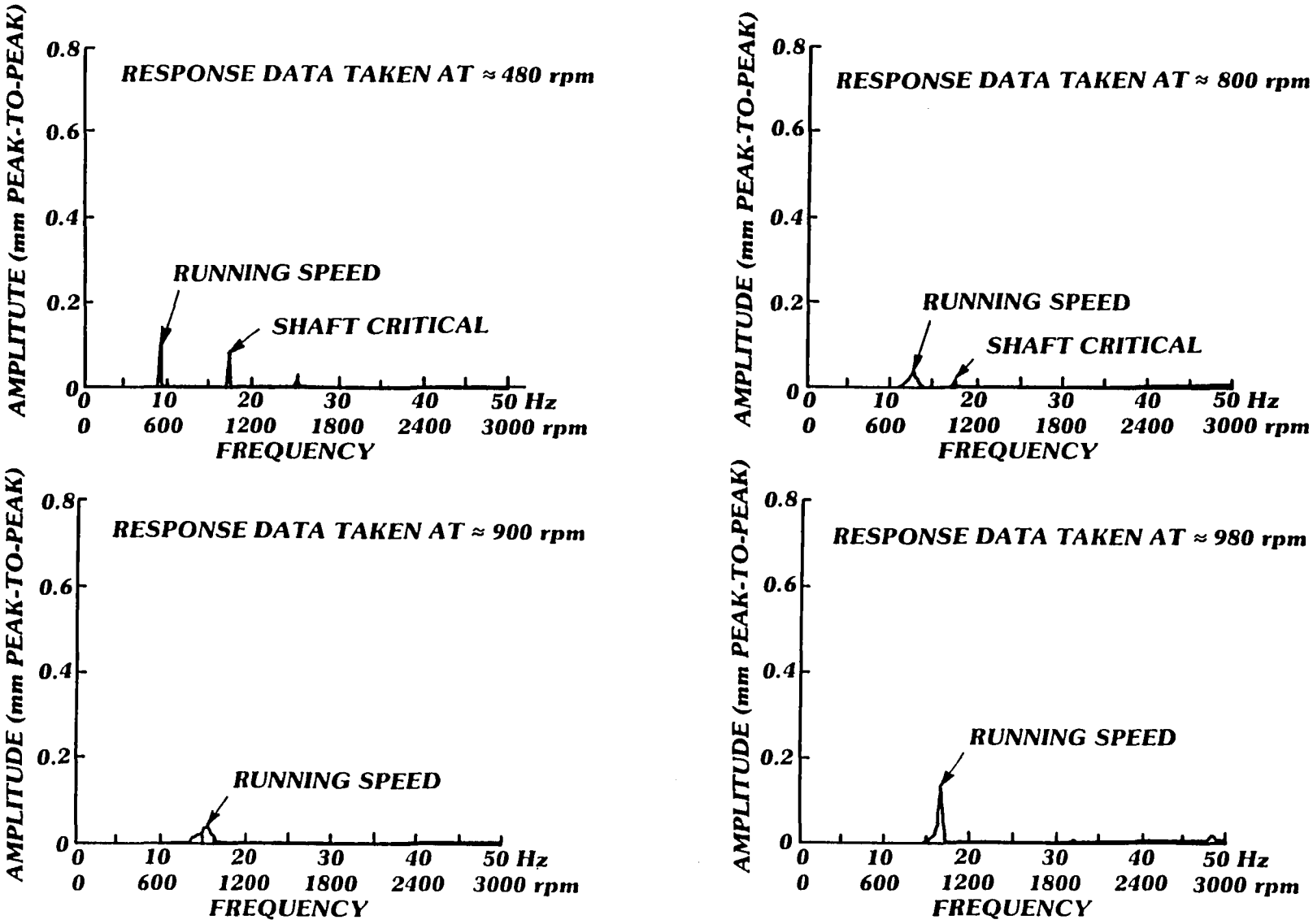

Fig. XI.1 Frequency Spectrum Plots of Test Shaft Vibration with No Damper

(NOTE: This Figure is a reprint of Fig. VIII.6)

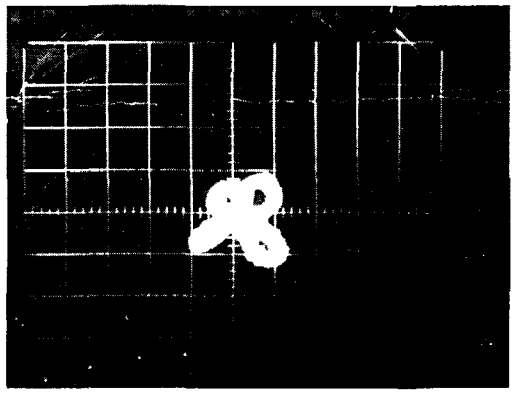

1 Vert., # 2 Horz., 800 rpm

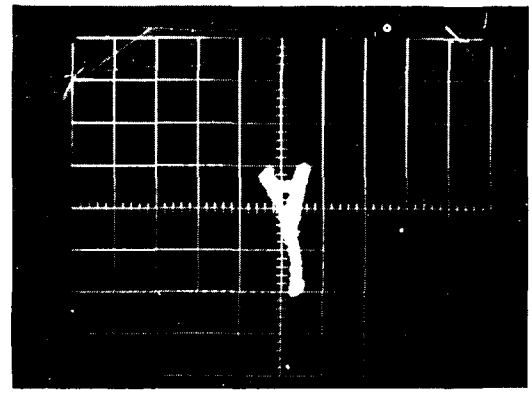

8 Vert., #15 Horz., 484 rpm

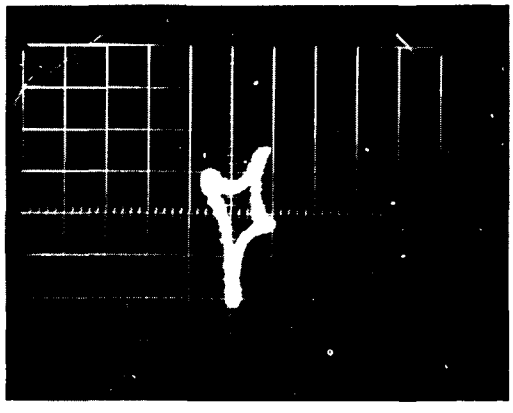

5 Vert., # 6 Horz., 800 rpm

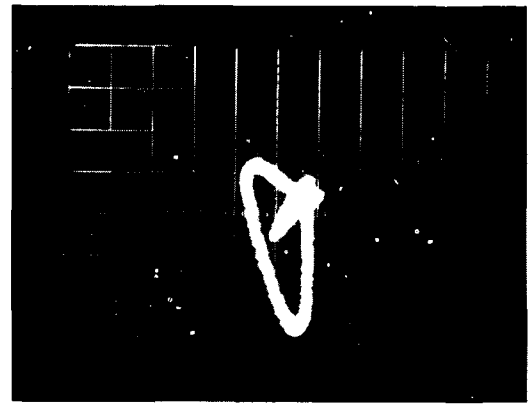

5 Vert., # 6 Horz., 484 rpm

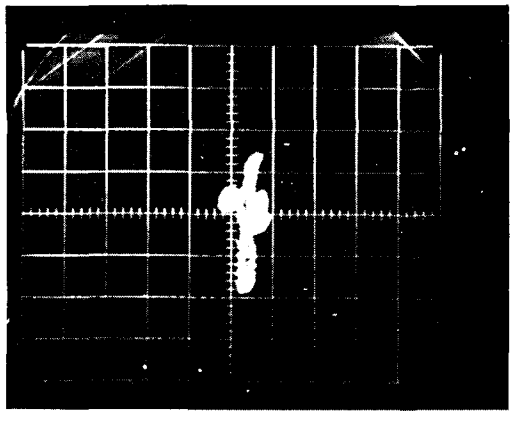

8 Vert., #15 Horz., 800 rpm

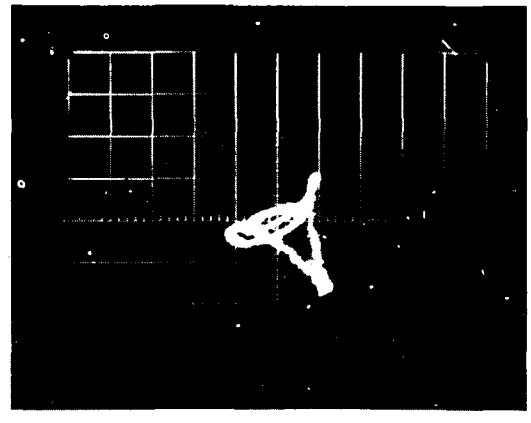

#1 Vert., # 2 Horz., 484 rpm

Fig. XI.2 Photographs of Undamped Test Shaft Orbits

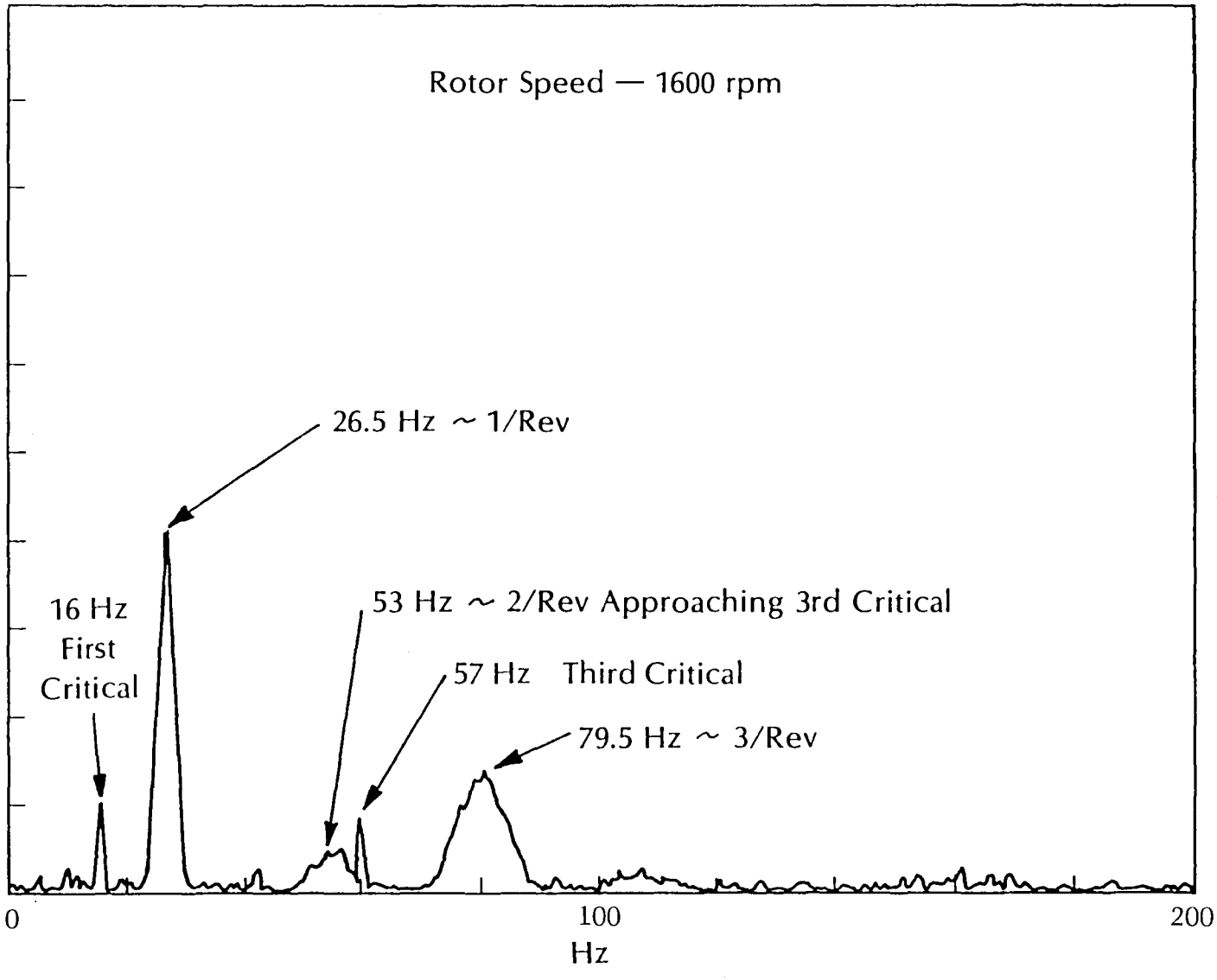

Fig. XI.3 2/Rev Approaching 3rd Critical

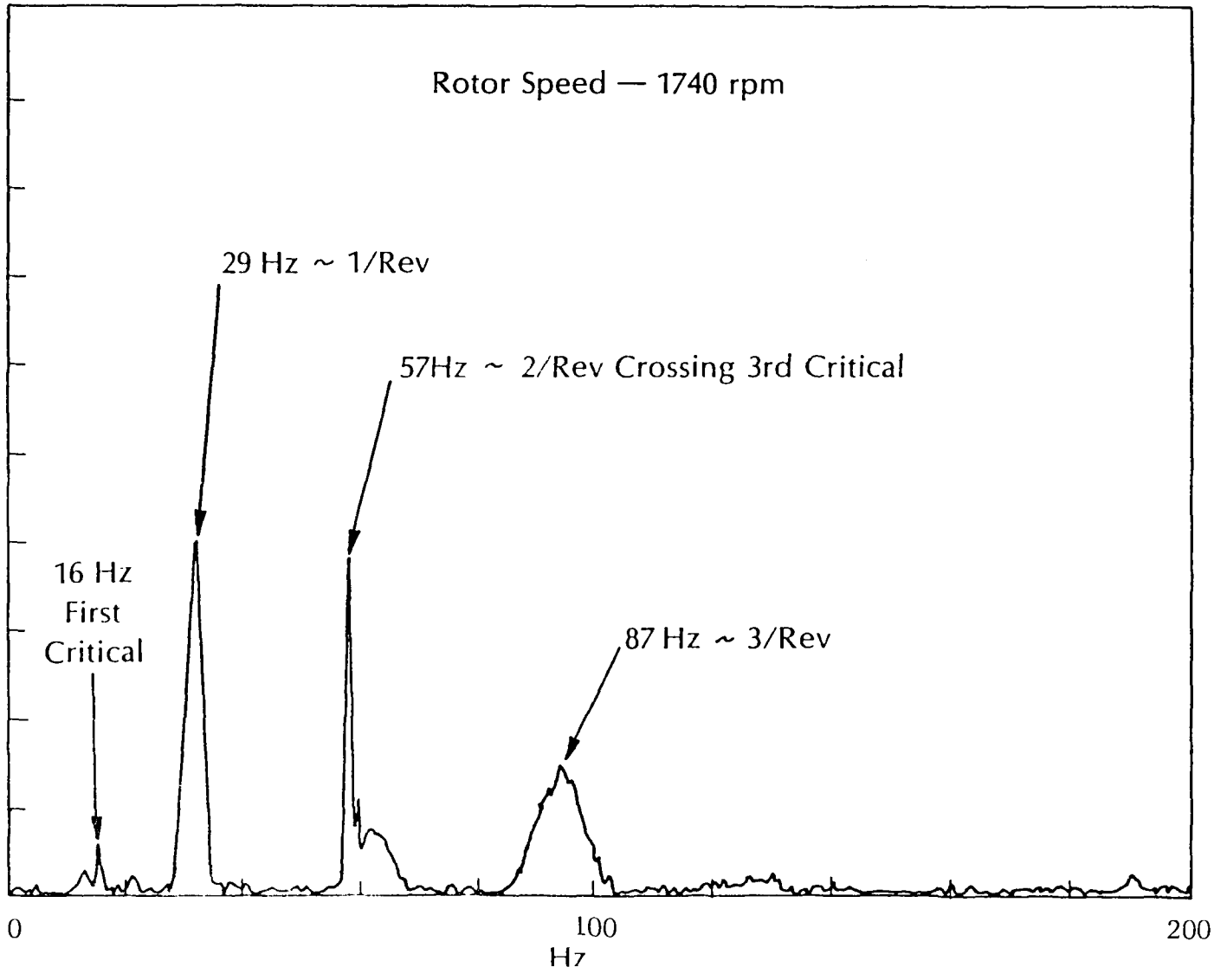

Fig. XI.4 2/Rev Exciting 3rd Critical

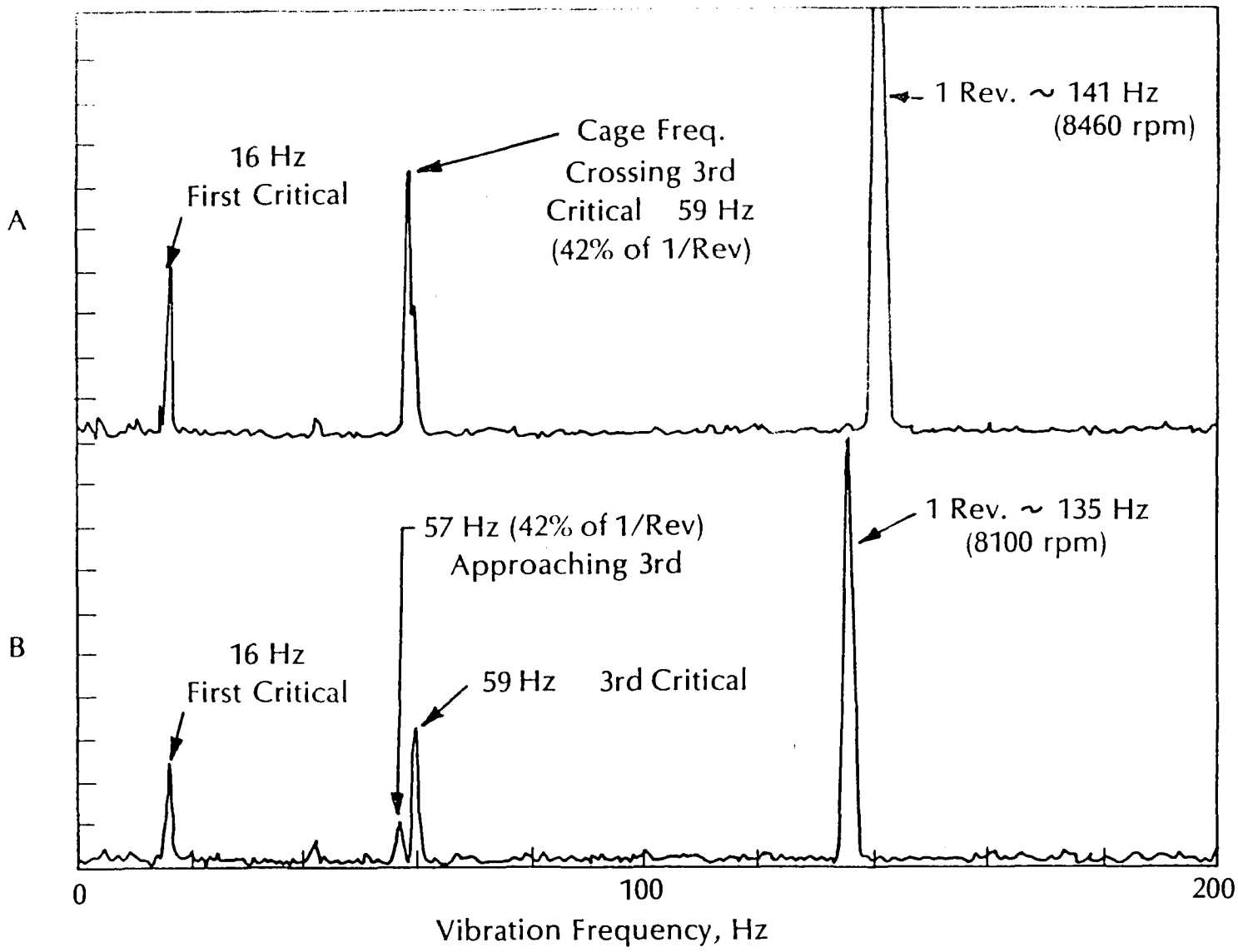

Fig. XI.5 Cage Frequency Excitation of 3rd Critical

The effects of cage excitation may be seen in Figure XI.5. In this case, an excitation frequency equal to 42 percent of synchronous is in the region of the third critical speed. In the lower of the two spectra, it is at a frequency 2 Hz below the third critical and in the upper spectrum, the cage frequency and the third critical frequency are at the same frequency, with a significant increase in vibration amplitude. The ratio of cage excitation frequency to running speed is calculated to be 42 percent, accounting for bearing parameters: ball diameter, race diameters, race curvature ratios, and contact angles.

Subsynchronous self-excited vibrations at the first natural frequency can be seen in Figures XI.6 and XI.7. Figure XI.6 shows four frequency spectra when the hard-mounted test shaft was running at speeds close to, and a little above, the first critical speed. In the first spectrum, the running speed in the shaft critical are at the same frequency and a very large peak response to unbalance is seen. In the second and third frames, distinct separation between the running speed excitation and vibrations at the shaft critical can be seen, and, in both cases, the shaft critical has a significantly higher amplitude than the response at running speed. In the fourth frame, the subsynchronous vibrations have grown to the extent that their amplitude is almost the same as that during peak amplitude negotiation of the first critical.

In Figure XI.7, two vibration spectra corresponding to rig operation in the region of 12,000 rpm may be seen. These were for the rig with the squeeze-film damper in operation. In the upper frame, which was at a slightly lower speed than in the lower frame, the amplitude of vibration at the first critical frequency is small and of little importance. In the lower frame, which corresponds to a slightly higher speed, vibrations at the first critical frequency have grown very large, and are significantly higher than the synchronous vibrations at the running speed.

All these nonsynchronous vibrations are of significant amplitude. Their presence in the vibrations spectra for a supercritical power transmission shaft at various speeds in the operating range, indicates that very careful observations of the entire vibration spectra should be made in any supercritical power transmission shaft application.

The various sources of excitation should be further quantified and the conditions which will lead to larger or smaller excitation forces should be identified. In addition, methods of designing effective control of these vibrations, either at their source or by vibration energy removal, should be developed and a basis for their optimization established.

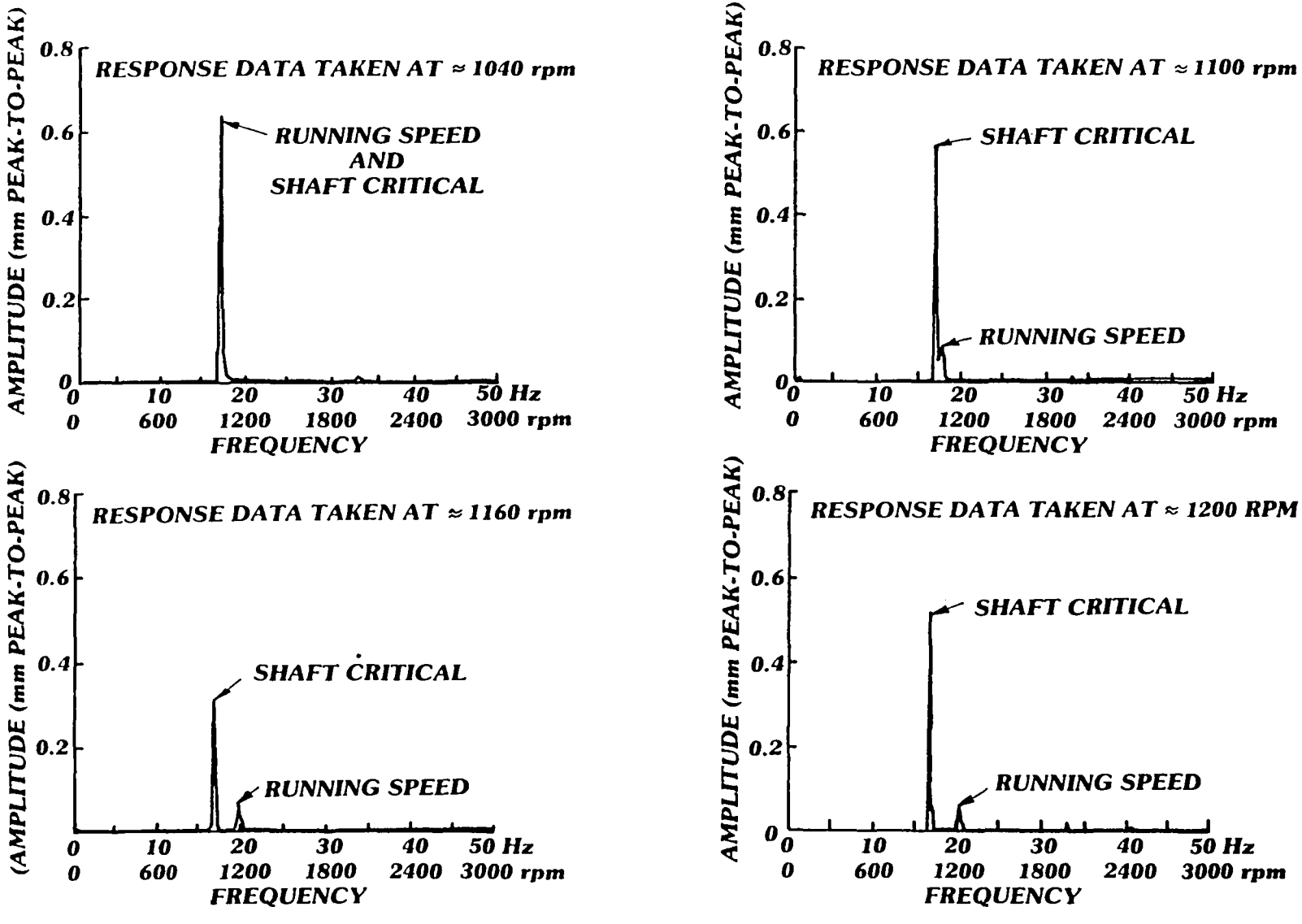

Fig. XI.6 Frequency Spectrum Plot of Test Shaft Vibration with No Damper Running Above First Critical Speed

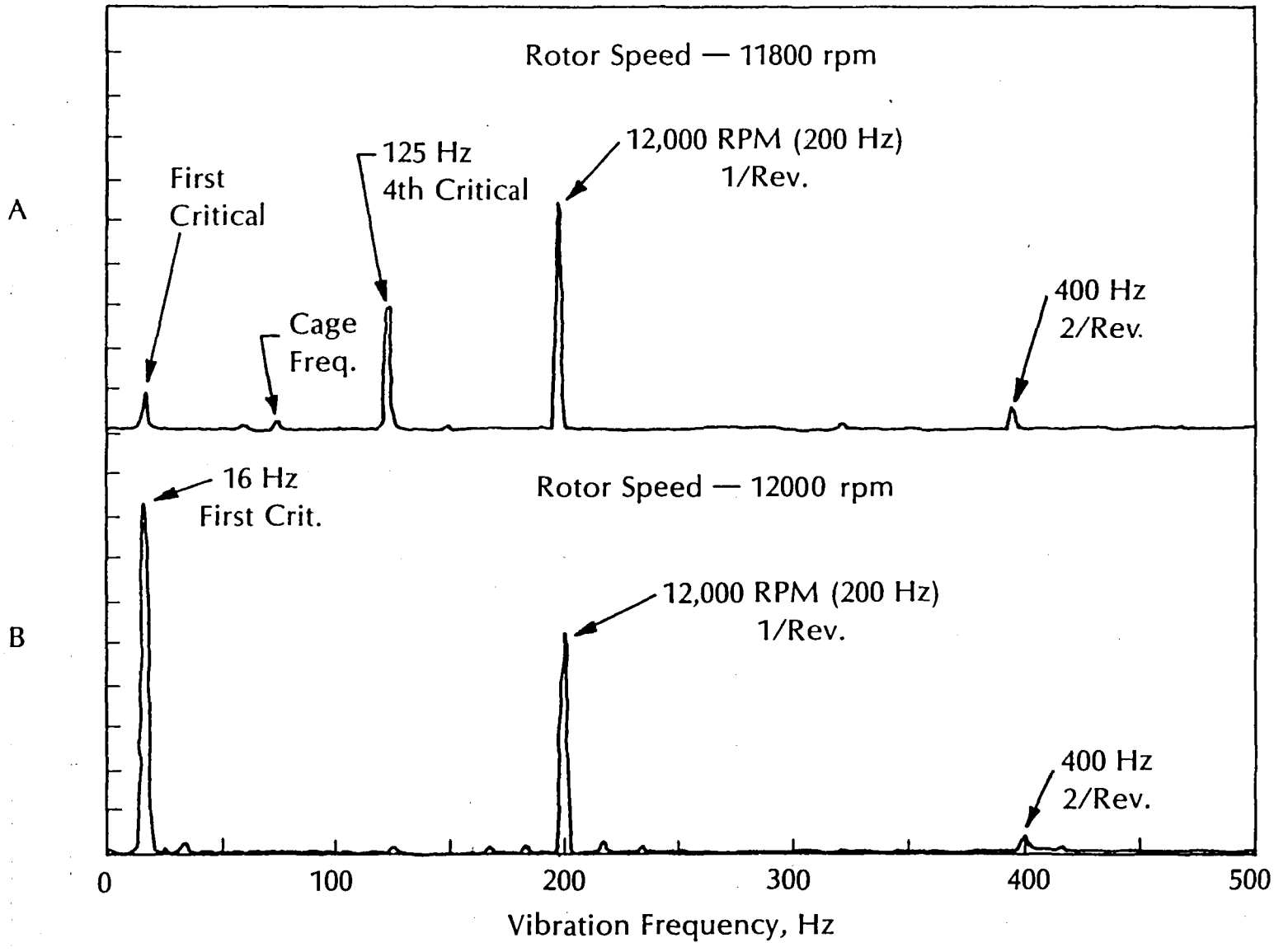

Fig. XI.7 Rig Vibration Spectra Near 12000 rpm

REFERENCES

1. Dubensky, R.G., Mellor, Jr., C.C., and Voorhees, J.E., "Design Criteria for High-Speed Power-Transmission Shafts, Part I", to WPAFB, Technical Documentary Report No. ASD-TDR-62-728, Part I, Contract No. AF33(616)-8290 (August, 1962).

2. Close, D.A., Day, J.B., Meacham, H.C., and Voorhees, J.E., "Design Criteria for Supercritical Shaft Systems, Part II", Technical Documentary Report No. ASD-TDR-62-728, Part II, Contract No. AF 33(657)-10330, SA/2(64-2637) (December, 1964).

3. "Design Manual - Supercritical-Speed Power-Transmission Shafts", prepared for U.S. Army Transportation Research Command and U.S. Air Force Research and Technology Division by Battelle Memorial Institute, December, 1964.

4. Prause, R.H., Meacham, H.C., and Voorhees, J.E., "The Design and Evaluation of a Supercritical-Speed Helicopter Power-Transmission Shaft", J. Eng. Ind., Trans. ASME, Vol. 89, pp. 719-728, 1967.

5. Baier, Robert J., "Flight Test Evaluation of a Supercritical-Speed Shaft", Final Report D210-10082-1, prepared by the Boeing Company - Vertol Division for the U.S. Army Aviation Materiel Laboratories, Ft. Eustis, VA, under Contract CA44-177-AMC-353(t) (also issued as USAAVLABS Technical Report 70-50), 1970.

6. Smalley, A.J., Darlow, M.S., Mehta, R.K., "The Dynamic Characteristics of O-Rings", J. of Mechanical Design, Trans. ASME, Vol. 100, No. 1, pp. 132-138, 1978.

7. Mohan, S., Hahn, E.J., "Design of Squeeze Film Damper Supports for Rigid Rotors". J. Engineering for Industry, Vol. 96, pp. 976-982, 1974.

8. Thomsen, K.K., Andersen, H., "Experimental Investigation of a Simple Squeeze Film Damper", Journal of Engineering for Industry, Vol. 96, pp. 427-430, May 1974.

9. Gunter, E.J., "Influence of Flexibly Mounted Rolling Element Bearings on Rotor Response Part I, Linear Analysis", Journal of Lubrication Technology, Trans. ASME, Vol. 92, No. 1, pp. 59-75, Jan. 1970.

10. Holmes, R., "Research Note: The Non-Linear Performance of Squeeze-Film Bearings", Journal of Mechanical Engineering Science, Vol. 14, No. 1, 1972.

11. Little, R.M., "The Application of Linear Programming Techniques to Balancing Flexible Rotors", Ph.D. Thesis, School of Engineering and Applied Science, University of Virginia, August 1971.

12. Badgley, R.H., Tessarzik, J.M., "Balancing of High-Speed Interconnect Shafting for Operation Above Multiple Bending Critical Speeds", Technical paper presented at 30th Annual National Forum of the American Helicopter Society, Washington, D.C., May 1974.

1. Report No.	2. Government Accession No.	3. Recipient's Catalog No.
NASA CR-3155		

4. Title and Subtitle	5. Report Date
DESIGN AND APPLICATION OF A TEST RIG FOR SUPER-CRITICAL POWER TRANSMISSION SHAFTS	August 1979
	6. Performing Organization Code

7. Author(s)	8. Performing Organization Report No.
M. Darlow and A. Smalley	MTI 78TR41
	10. Work Unit No.

9. Performing Organization Name and Address	11. Contract or Grant No.
Mechanical Technology Incorporated 968 Albany-Shaker Road Latham, New York 12110	NAS 3-16824
	13. Type of Report and Period Covered
12. Sponsoring Agency Name and Address	Contractor Report
National Aeronautics and Space Administration Washington, D.C. 20546	14. Sponsoring Agency Code

15. Supplementary Notes

Final report, Project manager, David P. Fleming, Fluid System Components Division, NASA Lewis Research Center, Cleveland, Ohio 44135.

16. Abstract

This report describes the design, assembly, operational check-out and application of a test facility for testing supercritical power transmission shafts under realistic conditions of size, speed and torque. Alternative balancing methods and alternative damping mechanisms are demonstrated and compared. The influence of torque upon the unbalance distribution is studied, and its effect on synchronous vibrations is investigated. The feasibility of operating supercritical power transmission shafting is demonstrated, but the need for careful control, by balancing and damping, of synchronous and nonsynchronous vibrations is made clear. The facility has been demonstrated to be valuable for shaft system development programs and studies for both advanced and current-production hardware.

17. Key Words (Suggested by Author(s))	18. Distribution Statement
Supercritical shaft; Balancing; Damping; Helicopter; Power transmission	Unclassified - unlimited STAR Category 37

19. Security Classif. (of this report)	20. Security Classif. (of this page)	21. No. of Pages	22. Price*
Unclassified	Unclassified	166	A08

* For sale by the National Technical Information Service, Springfield, Virginia 22161

NASA-Langley, 1979